TEXT FLY WITHIN THE BOOK ONLY

UNIVERSAL
LIBRARY

INTERNATIONAL SERIES OF MONOGRAPHS ON

EARTH SCIENCES

EDITOR DR. EARL INGERSON
U.S. Geological Survey, Washington 25, D.C.

VOLUME 1

CONTRIBUTIONS IN GEOPHYSICS

In Honor of Beno Gutenberg

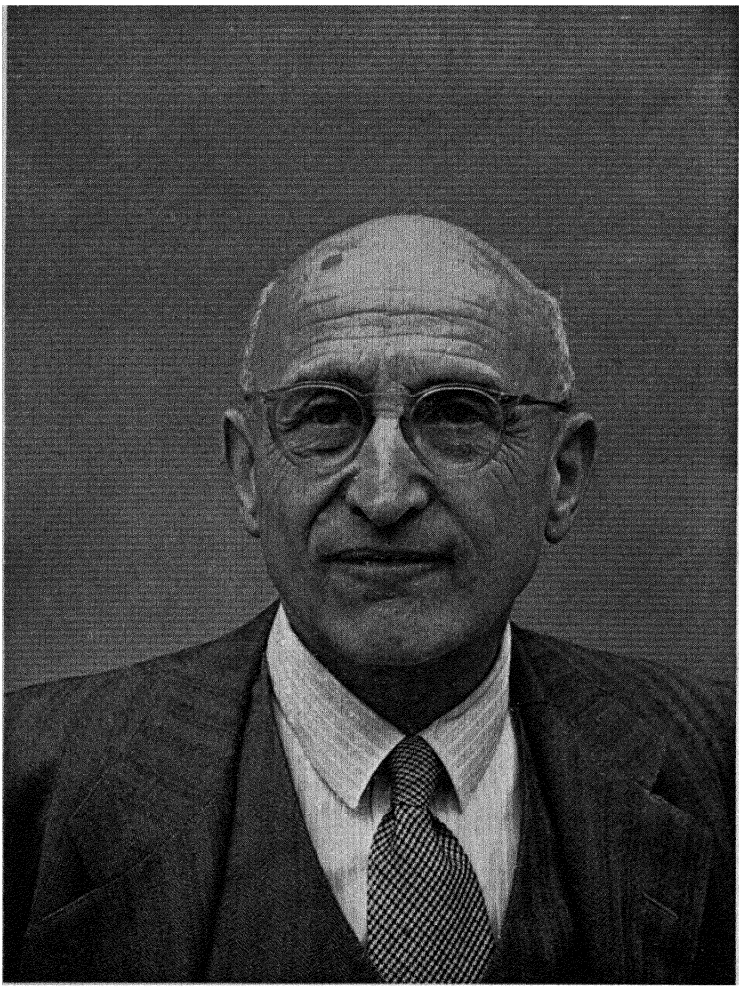

Beno Gutenberg

CONTRIBUTIONS IN GEOPHYSICS

In Honor of Beno Gutenberg

Editors

HUGO BENIOFF
Professor of Seismology
California Institute of Technology

MAURICE EWING
Professor of Geology
Columbia University

BENJAMIN F. HOWELL, JR.
Professor of Geophysics
The Pennsylvania State University

FRANK PRESS
Professor of Geophysics
California Institute of Technology

PERGAMON PRESS

LONDON · NEW YORK

PARIS · LOS ANGELES

1958

PERGAMON PRESS LTD.
4 *and* 5 *Fitzroy Square, London W.*1
PERGAMON PRESS INC.
122 *East* 55*th Street, New York* 22, *N.Y.*
P.O. Box 47715, *Los Angeles, California*
PERGAMON PRESS S.A.R.L.
24 *Rue des Écoles, Paris V*e

Library of Congress Card No. 58–8073

Printed in Great Britain by Page Bros. (Norwich) Ltd.

CONTENTS

PREFACE

THIS volume of papers has been assembled to pay due honor to Beno Gutenberg in recognition of his outstanding contributions to geophysics both as a research man and a teacher of researchers. Our knowledge of the earth would be far less than it is today if it had not been for Gutenberg's persistent search for understanding of geophysical phenomena. Publication of this volume is planned to approximate to the time of Dr. Gutenberg's retirement, because of age, as Director of the Seismological Laboratory of the California Institute of Technology. As a testimonial to the importance of his leadership, a few representatives of his many friends, his colleagues, fellow scientists, and his former students were invited to contribute to this volume. The diverse nature of the topics chosen is a measure of the breadth of Gutenberg's interests. The wide geographic distribution of the contributors' homes indicates the range of his influence.

The papers themselves give a picture of the status of geophysical research today. They are typical of the scholarly work which Gutenberg has inspired by his example and enthusiasm. Their presentation here is not only a tribute to the man in whose honor they were written, but a proof that his lifetime of devotion to teaching and research has built a firm foundation on which his fellow geophysicists will continue with him to expand the frontiers of knowledge.

THE EDITORS

BIOGRAPHICAL NOTE

DR. BENO GUTENBERG was born on 4 June 1889 in Darmstadt, Germany. He received his Ph.D. in geophysics from Göettingen University in 1911, and an honorary Ph.D. from Uppsala in 1955. He was employed by the International Association of Seismology in their Central Offices in Strassburg until 1918. In 1924 he was placed in charge of the Seismic Station at the University of Frankfurt. He was a professor at Frankfurt from 1926–1930, at which time he moved to Pasadena, California, where he was appointed Professor of Geophysics and Meteorology at the California Institute of Technology. He was Director of the Seismological Laboratory of that institution from 1947 until his retirement from that position in 1957. In 1955 he was William Smith Lecturer for the Geological Society of London.

He has written several hundred scientific papers in many areas of geophysics, and is the author or editor of several books. The greatest part of his work has been in seismology and physics of the earth's interior, but his works cover also propagation of sound waves in and structure of the atmosphere, post-glacial uplift, and elasticity and plasticity of rocks.

Dr. Gutenberg is recipient of the Charles Lagrange Prize, Classe des Sciences and the Prix de Physique du Globe (1952) from the Royal Academy of Belgium, and the Bowie Medal (1953) from the American Geophysical Union. He is a member of the National Research Council and the National Academy of Science of the United States. He was President of the Seismological Society of America from 1945–1947 and of the International Association of Seismology and Physics of the Earth's Interior from 1951–1954. He is also a fellow or member of the American Association for the Advancement of Science, Geological Society of America, American Physical Society, American Geophysical Union, American Association of Petroleum Geologists, Royal Astronomical Society, American Meteorological Society, Society of Exploration Geophysicists, Washington Academy of Sciences, Geological Society of London, Academy Lincei of Rome, Royal Swedish Academy of Sciences, Finnish Academy of Sciences and Letters, Royal Society of New Zealand (honorary), and the Finnish Geographical Society (honorary).

1

THE ENERGIES OF SEISMIC BODY WAVES AND SURFACE WAVES

MARKUS BÅTH

ENERGY computations by means of body waves and surface waves for a number of shallow-focus earthquakes have given the following results.

(1) The energy ratio E/E_{LR} decreases with increasing magnitude according to the formula

$$\log (E/E_{LR}) = 5.34 - 0.56\, M_S$$

This is explained by the influence of the linear dimensions of the source on the development of surface waves.

(2) The following energy formula is deduced

$$\log E = 12.24 + 1.44\, M_S$$

in very good agreement with GUTENBERG and RICHTER's (1956b) latest results, obtained by completely different methods and different material.

(3) The energy ratio $E_S/E_P = 1.5 \pm 0.4$ is independent of magnitude and of epicentral distance.

(4) The extinction is very strong for the body waves and it may account for a factor of approximately 20 in the total energy. The extinction is mainly due to scattering within the crust in the focal region, increases with decreasing wave length, and is larger for transverse than for longitudinal waves. The usually assumed extinction along the total wave path in the mantle amounts approximately to 10–15 per cent of the crustal extinction. The large extinction of the high frequencies in the focal region constitutes the most serious difficulty in energy determinations from body waves.

UP to now three different earthquake magnitude scales have been in current use, i.e.

M_L determined according to the original definition by RICHTER for local shocks in California;

M_B calculated from the ratio of amplitude over period for body waves (P, PP, S) for distant earthquakes of any depth;
M_S calculated from the amplitudes of surface waves for shallow distant earthquakes.

In order to avoid confusion I use the same notation for the magnitudes as GUTENBERG and RICHTER (1956b); index S in M_S refers to surface waves, in all other cases to S waves. As the three scales are inconsistent with each other, GUTENBERG and RICHTER (1956b) defined a 'unified magnitude' m with the following relations to M_L, M_B, and M_S:

$$m = 1.7 + 0.8\,M_L - 0.01\,M_L^2 \tag{1}$$

$$m = M_B \text{ (without correction)} \tag{2}$$

$$m = M_S - 0.37\,(M_S - 6.76) \tag{3}$$

The following equation by the same authors expresses the most reliable connection hitherto between the total energy E (in ergs) of the seismic waves and the 'unified magnitude' m

$$\log E = 5.8 + 2.4\,m \tag{4}$$

All logarithms in this paper are to the base 10. Inserting into Eq. (4) the expressions (1)–(3) we obtain

$$\log E = 9.9 + 1.92\,M_L - 0.024\,M_L^2 \tag{5}$$

$$\log E = 5.8 + 2.4\;\; M_B \tag{6}$$

$$\log E = 11.8 + 1.5\;\; M_S \tag{7}$$

The present author (BÅTH, 1955a) has derived a relation between E and M by performing an integration over the Rayleigh-wave phase for 27 earthquakes recorded at the seismic station at Kiruna and covering the magnitude range 5.3–7.8. The resulting formula reads

$$\log E = (7.2 \pm 0.5) + (2.0 \pm 0.07)\,M + \log (x/2) \tag{8}$$

where x denotes the ratio of the total seismic wave energy and the energy of the Rayleigh waves, i.e.

$$x = E/E_{LR} \tag{9}$$

In the paper mentioned $x = 2$ was believed to be a likely value, but I also remarked that 'if future investigations will give some more reliable value of x for shallow-focus earthquakes, this can be put into this formula, and the result of our investigation is still valid'. 'Even if x should have a systematic variation with M for shallow-focus earthquakes, our Eq. (8) is valid'. The following development has shown that the last supposition was true.

The magnitude M in Eq. (8) is equivalent to M_S. Therefore, equating the expressions for $\log E$ in Eqs. (7) and (8), we find that

$$\log x = 4.9 - 0.5\, M_S \tag{10}$$

A few values of x computed from this equation are given in the following table:

M_S	x
5.0	250
5.5	140
6.0	80
6.5	45
7.0	25
7.5	14
8.0	8

The result that x decreases with increasing M seems to be likely for reasons outlined below. However, at first sight the variation of x with M obtained here may seem to be too rapid; furthermore, the numerical values of x may seem to be too large. Equation (10) has been obtained by a combination of (7) and (8), i.e. two formulas obtained by completely different methods and by the use of totally different material. It is therefore desirable to investigate the dependence of x on M by using a homogeneous material. In the following the results of such an investigation will be given.

For a number of shallow-focus earthquakes the total energy of

P and S waves (E_P, E_S respectively) have been estimated by integration over the respective wave trains and using the following formula

$$E_{P,S} = 8\pi^3\rho \left[h^2 + 4r_0(r_0 - h) \sin^2\frac{\Delta}{2}\right] \int c\left(\frac{A}{T}\right)^2 dt \qquad (11)$$

where ρ = density = 2.7 g/cm^3, h = focal depth = 20 km, r_0 = the earth's radius = 6370 km, Δ = epicentral distance, c = wave velocity = 6.0 km/sec for P waves and 3.4 km/sec for S waves, A = ground amplitude, T = wave period, t = time. For derivation see e.g. BULLEN (1947, p. 231). When every crest and trough is measured, the formula (11) simplifies as follows, assuming a constant period T along the wave train

$$E_{P,S} = 4\pi^3\rho \left[h^2 + 4r_0(r_0 - h) \sin^2\frac{\Delta}{2}\right] \frac{c}{T} \Sigma A^2 \qquad (12)$$

where the summation is extended over the wave trains and includes all three components, i.e.

$$\Sigma A^2 = \Sigma A_N^2 + \Sigma A_E^2 + \Sigma A_Z^2$$

Equation (11) assumes spherically symmetrical energy radiation from the focus; this limitation will be discussed below. A further limitation is that the extinction is not taken into account in (11); the extinction has a very large influence, which will also be discussed below. The effect of the free surface is also neglected, but this effect is to sufficient approximation cancelled already in the derivation of the simple formula (11).

Equation (11) has been applied to fifteen shallow-focus earthquakes, recorded by the Galitzin instruments at the Kiruna seismograph station. The earthquakes measured were selected among the earthquakes for which I have earlier determined the energy of the Rayleigh waves (see Table 1 in BÅTH, 1955a). Of the earthquakes listed there, only those could be used, for which the P and S phases were measurable. Table 1 in this paper contains our present results, arranged in order of increasing M_S. The total energy E is given by the relation

$$E = E_P + E_S \qquad (13)$$

E_S includes the energy both of SV and SH. It is obvious that E_{LR} or the energy of any other waves should not be included in this sum. Only longitudinal and transverse body waves are generated by the earthquake, and the surface waves are in their turn created from the body waves by a complicated process. The surface waves therefore derive their energy from the body waves. The energy E_{LR} of the Rayleigh waves, given in Table 1, has been taken over from my earlier paper. For earthquake No. 6 the P waves were not measurable due to microseisms, and for earthquake No. 14 no S waves could be distinguished on the records. In these two cases the values of E_P and E_S respectively have been calculated by using the mean ratio E_S/E_P, derived from the other observations.

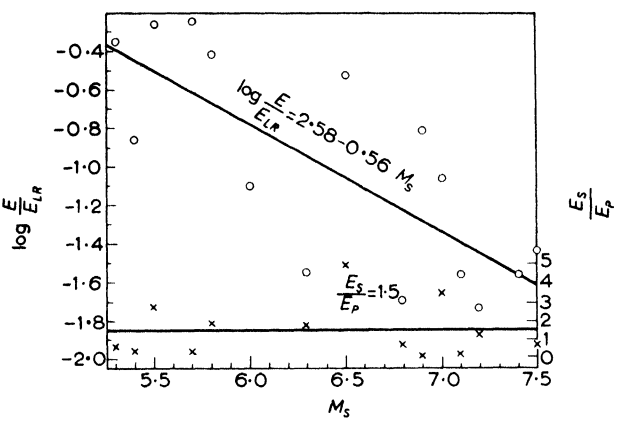

FIG. 1. Log (E/E_{LR}) ○ and E_S/E_P × plotted against magnitude M_S.

In Fig. 1 $\log x$ is plotted against M_S. The straight line in Fig. 1 corresponds to the least-square solution, which is

$$\log x = (2.58 \pm 0.85) - (0.56 \pm 0.13)\, M_S + C \qquad (14)$$

where the mean errors are given and C is a constant, due to the extinction and other effects. JEFFREYS (1923) carried out similar energy computations for the Pamir earthquake of 1911 (magnitude $= 7\frac{3}{4}$). His results lead to a value of $\log x = -1.3$, which within the error limits agrees very well with my formula (14).

As $E > E_{LR}$, it follows from the definition of x in Eq. (9), that

TABLE 1

No.	Date	Origin time (GMT) h m s	Epicenter Lat. deg.	Epicenter Long. deg.	Δ Kiruna deg.	M_S	E_P (erg $\times 10^{18}$)	E_S (erg $\times 10^{18}$)	E_S/E_P	log E	log E_{LR}	log x
1	Jul. 23, 1953	01 05 44	26¼ N	65 E	50	5.3	0.038	0.025	0.66	16.80	17.15	−0.35
2	Jul. 22, 1953	12 52 12	42 N	143½ E	63	5.4	0.045	0.019	0.42	16.81	17.67	−0.86
3	Jun. 7, 1953	12 23 56	20 N	70 W	72	5.5	0.151	0.413	2.74	17.75	18.01	−0.26
4	Feb. 23, 1953	00 46 08	29½ N	81 E	52	5.7	0.256	0.092	0.36	17.54	17.79	−0.25
5	Jun. 16, 1953	09 53 06	31 N	141 E	73	5.8	0.678	1.277	1.88	18.29	18.71	−0.42
6	Oct. 13, 1953	08 53 45	30 N	113½ W	78	6.0	(0.173)	0.253	—	(17.63)	18.74	(−1.11)
7	Jul. 9, 1953	19 02 06	40¼ N	78½ E	42	6.3	0.087	0.154	1.77	17.38	18.93	−1.55
8	May 31, 1953	19 58 35	20 N	70½ W	71	6.5	7.269	35.684	4.91	19.63	20.16	−0.53
9	Sep. 23, 1953	02 14 36	50½ N	156 E	57	6.8	4.841	3.272	0.68	18.91	20.61	−1.70
10	Dec. 25, 1953	01 51 29	53 N	159¾ E	56	6.9	66.016	3.173	0.05	19.84	20.66	−0.82
11	Nov. 26, 1953	08 14 12	34 N	141 E	69	7.0	9.956	33.873	3.40	19.64	20.71	−1.07
12	Jan. 13, 1952	04 03 37	22 N	124⅓ E	75	7.1	19.141	4.992	0.26	19.38	20.95	−1.57
13	May 19, 1952	18 32 21	42¼ N	143½ E	63	7.2	11.780	14.742	1.25	19.42	21.16	−1.74
14	Dec. 12, 1953	17 31 23	3¾ S	80¾ W	98	7.4	43.046	(62.847)	—	(20.02)	21.58	(−1.56)
15	Jul. 21, 1952	11 52 14	35 N	119 W	73	7.5	144.672	94.726	0.65	20.38	21.82	−1.44

$x > 1$ and $\log x > 0$ for all values of M_S. However, all our values of $\log x$ are negative, which is primarily due to the fact that the extinction of the body waves was neglected in Eq. (11). The surface waves derive their energy from the body waves. It is likely that only the body waves with an upward direction from the focus are able to create surface waves, those with a downward direction not. This means that $x = E/E_{LR} \geqslant 2$ even for the largest earthquakes. The condition $x = 2$ or $\log x = 0.3$ for $M_S = 9$ gives $C = 2.76$. Inserting this value of C into (14) we obtain

$$\log x = 5.34 - 0.56\, M_S \tag{15}$$

It is evident that the agreement with Eq. (10) is good. The discrepancies are completely within the limits of error. The second decimals given here are naturally only of use for calculations. By a combination of the measurements on surface waves by BÅTH (1955a) and his own measurements on S waves, SOLOVJEV (1956) has also found that E_{LR}/E_S increases with increasing M_S. However, the rate of increase of this ratio found by SOLOVJEV is less than what is obtained from the closely agreeing formulas (15) and (10). For selected values of M_S Eq. (15) gives the following values of x, to be compared with similar computations made above using Eq. (10).

M_S	x
5.0	347
5.5	182
6.0	96
6.5	50
7.0	26
7.5	14
8.0	7

Combining Eqs. (15) and (8), using also two decimals in Eq. (8), we obtain the following energy formula

$$\log E = 12.24 + 1.44\, M_S \tag{16}$$

to be compared with (7). It is evident that these two energy formulas

obtained by different methods and different material, agree very well within the limits of error. The following table gives a numerical comparison between the two formulas.

M_S	log E Eq. (7)	log E Eq. (16)
5.0	19.30	19.44
5.5	20.05	20.16
6.0	20.80	20.88
6.5	21.55	21.60
7.0	22.30	22.32
7.5	23.05	23.04
8.0	23.80	23.76

Within the magnitude range considered (5.0–8.0) the agreement is extremely good.

The older energy formula $\log E = 12 + 1.8\,M$, which has been used by many authors, gives the energy 50–400 times as large as Eq. (7) for the magnitude range 5.0–8.0. It is interesting to note that the error in the old formula does not lie so much in the constant term as in the factor of M.

At the same time as this paper further develops the energy formula, earlier given by me (BÅTH, 1955a), it has also given independent confirmation of the correctness of GUTENBERG and RICHTER's (1956b) new energy formula (7). Indirectly the other energy formulas (5) and (6) are also confirmed. The transformation from (7) to (6) depends on the relations (2) and (3). Of these equations (2) is a definition and (3) has been obtained independently by me with very good numerical agreement (BÅTH, 1955b). The energy formula (6) has therefore also been confirmed by this investigation. In fact, substituting m for M_S in (16) by means of (3) we find that

$$\log E = 6.5 + 2.3\,m \tag{17}$$

This agrees within error limits with (4). GUTENBERG and RICHTER (1956b) emphasize that the constant term 5.8 in (4) is not accurately fixed, and that log E calculated from (4) may be in error by as much as one unit. The agreement between the Eqs. (4) and (17) is in fact

much better than is to be expected from this statement, which is obvious from the following values.

m	log E Eq. (4)	log E Eq. (17)
5	17.8	18.0
6	20.2	20.3
7	22.6	22.6
8	25.0	24.9

The present investigation has also yielded estimates of the energy ratio E_S/E_P; see Table 1. The mean value with its standard error from thirteen observations is $E_S/E_P = 1.5 \pm 0.4$. This result should be compared with earlier findings of GUTENBERG (1945a, 1945b), that longitudinal and transverse waves receive approximately the same energy at the source. More recently, however, GUTENBERG and RICHTER (1956a) assume the energy in P waves to be only half that in the S waves. The large scatter of our observations is natural, because of the assumption of spherical symmetry in Eq. (11). Plotting E_S/E_P against M_S we find this energy ratio to be constant, independent of magnitude (see Fig. 1). A least-square solution gives $E_S/E_P = 1.605 - 0.022\ M_S$, which is a completely insignificant deviation from the constant mean value just given. Plotting E_S/E_P against Δ, we also find the ratio to be independent of epicentral distance, although earthquakes within the same area tend to give similar values of E_S/E_P. This is explained from the earthquake mechanism to be discussed below.

With the numerical results now at hand, I will proceed to discussions of the various problems involved.

The decrease of the energy ratio $x = E/E_{LR}$ with increasing magnitude has been directly verified quantitatively. This effect is explained by the influence of the linear extensions of the focal region on the development of surface waves (both with regard to the amplitudes and to the length of the wave train). In large earthquakes the hypocentral region extends both to the earth's surface and large distances in a horizontal direction. For an earthquake smaller than about magnitude 5, the fault plane usually does not reach the earth's surface. For still smaller shocks the hypocentral region is very

limited and buried within the earth, and the surface waves are then only poorly developed. The consequence is that with increasing magnitude the energy in the surface waves increases more rapidly than the total energy of the earthquake. It has been attempted to explain this phenomenon by the factor exp $\{-c(h/\lambda)\}$, where $c =$ a constant, $h =$ focal depth, and $\lambda =$ wave length, appearing in the expression for the amplitudes of the surface waves. This explanation works well for the range between normal depth (around 20 km) and 100 km (see BÅTH, 1952), whereas for our present problem, concerning the depth range 0–30 km, it is insufficient as an explanation. In other words, the variation of x with M_S is far too rapid to be explained by this factor alone. In an earlier paper (BÅTH, 1952) I determined this factor numerically with the result that

$$M_S = 0.0082\, h + c_1 \tag{18}$$

if h is expressed in km and $c_1 =$ constant for a given shock at a given epicentral distance. Inserting this into

$$\log E_{LR} = 6.9 + 2.0\, M_S \tag{8a}$$

and noting that E is independent of h within the depth range 0–30 km, we find

$$\log x = -0.0164\, h + c_2 \tag{19}$$

where c_2 is a constant under the same conditions as c_1 is a constant. Equation (19) gives

$$(x)_{h=0} : (x)_{h=20} = 2.1$$

and

$$(x)_{h=0} : (x)_{h=30} = 3.1,$$

i.e. values incapable of explaining the rapid variation of x with M_S found above. We have here compared the values of x for a given shock, i.e. for a given M_S, but occurring at different depths. If we interpret the phenomenon as just a depth effect, then x should be

independent of M_S for a given depth. Even if reasonable assumptions are made with regard to λ for shocks of various magnitudes, this does not improve the results. It is evident that this phenomenon, which is closely connected with the generation of surface waves, is too complicated to be explained by the factor exp $\{-c(h/\lambda)\}$, as far as the depth interval 0–30 km is concerned.

As the next problem I wish to discuss the influence of the earthquake mechanism. Equation (11) for $E_{P,S}$ presupposes equal radiation in all directions from the focus of the energy of the body waves. It is now well known that this is far from the truth. For a point on the extension of a fault no P and no S are observed, whereas for a point on the normal to a fault, no P but a maximum amplitude of S is obtained. As a consequence the energy ratio E_S/E_P obtained at a single station for a given shock does not give the energy ratio between transverse and longitudinal waves at the source. In order to determine the energy ratio E_S/E_P for a given shock it is necessary to use the records at a number of stations in all directions from the epicenter. If, in addition, a fault-plane solution has been made for the earthquake, this will be of great help. In the present investigation a number of earthquakes in widely different regions of the world have been used. In this case the effects of the mechanisms of the different shocks to a large extent cancel each other in the mean values. This is true for the relations (14) and (15) and for the mean value of E_S/E_P, which may therefore be considered as representative. But in both cases the relatively large scatter of the individual observations is easily explained by the non-symmetrical energy radiation from the source. The existence of wave guides in the lithosphere and the asthenosphere is another reason for unsymmetrical energy radiation. In the future I hope it will be possible to extend the present investigation to a much larger material with still more reliable mean relations and mean values as a result.

Equation (14) above is a mean relation for all earthquakes used. I have tried to see if different relations would be obtained for foci in continental and in oceanic regions. This is difficult, partly because of the small material, partly because the crustal structure cannot be assigned with certainty in several cases, especially as many shocks occur near the margins between continental and oceanic structures. Still, the indications seem to be quite clear. Of five oceanic cases there are four above the mean line (Nos. 3, 5, 8, 11) and only one

below (No. 12). Of ten continental cases there are four above the mean line (Nos. 1, 4, 10, 15), five below (Nos. 2, 6, 7, 9, 13), and one on the line (No. 14). Separating the oceanic and continental cases from each other, the following approximate relations are obtained.

For oceanic earthquakes:

$$\log x = 2.58 - 0.56\, M_S + 0.3 \tag{14a}$$

and for continental earthquakes:

$$\log x = 2.58 - 0.56\, M_S - 0.2 \tag{14b}$$

leaving out the additional constant. The difference of 0.5 in $\log x$ for oceanic and continental earthquakes corresponds to a factor of 3 in the total energy. This is explained by the existence of wave guides in the continental crust.

The necessary increase of $\log x$ for continental earthquakes, i.e. 2.96 comparing (14b) with (15), corresponds to a factor of about 900 in the computed total energy. Part of this is due to local conditions at the station (ground, instruments). The correction of the magnitudes computed from body waves at Kiruna is + 0.3 in the mean (BÅTH, 1955b). This makes a factor of 5 in the energy, considering Eq. (4) or (17). A factor of 3, already mentioned, is ascribed to the effect of continental low-velocity layers, comparing Eqs. (14a) and (14b). The last-mentioned factor of 3 is only a rough mean value for the magnitude range considered.

Part of the remaining factor of 60 is due to the fact that the waves measured have an energy spectrum. Our knowledge of the spectra of P and S at distant stations is very incomplete. A series of instruments with different response curves would be needed for the construction of an energy spectrum. Therefore only assumptions can so far be made as to the spectrum. S waves are usually not recorded on the short-period instruments. We assume that the energy E_S measured in the medium- and long-period range represents the total energy of S at a distant station. For P waves, however, we have also clear records on short-period instruments (periods of P around 1 sec) with energies at least comparable to those measured on the long-period instruments. For more detailed discussion of this see BÅTH

(1955b). Only the long-period part of P was measured in order to get values comparable with S within the same general period range. In view of the uncertainty of the energy spectrum at a distant station, we make two reasonable assumptions:

(a) The total energy of P at a distant station is 10 times the energy of long-period P. With the ratio $E_S/E_P = 1.5$ (for the long periods), we find that this assumption increases the total energy by a factor of 4.6.

(b) The total energy of P at a distant station is 5 times the energy of long-period P. Then the total energy is increased by a factor of 2.6.

The remaining part of the factor 60, i.e. in round numbers (a) $60 : 5 = 12$, (b) $60 : 3 = 20$, is explained by the extinction in the focal region. Starting from the expression (14b) for continental earthquakes we find, in summary, that the required increase of the total energy is given by a factor of 900, which in round numbers, can be split up as follows

$$900 = 5 \times 3 \times (5 \text{ to } 3) \times (12 \text{ to } 20),$$

where the factors are in turn due to local effects at the station, channel effects in the continental crust, the energy spectral distribution, and the extinction primarily in the focal region. The extinction varies with the wave length, and the values given here represent an over-all effect for all wave lengths. The exact values of the third and fourth factors are difficult to fix owing to our ignorance of the energy spectrum, but their product (60) is more reliable.

In my earlier computations of the energy of Rayleigh waves (BÅTH, 1955a) the extinction was taken into account. For the surface waves this is possible with sufficient accuracy. For body waves, however, the extinction is a much more difficult problem. In our Eq. (11) no account was taken of the extinction, and its effect was afterwards corrected for by the condition that $\log x \geqslant 2$. As already indicated the extinction is responsible for a factor of about 20 in the total energy. It is very probable that practically all of this large extinction takes place within a few degrees distance of the source and mainly among the short periods. The extinction of the body waves is not evenly distributed along the whole path as for the surface waves,

and it is therefore not right to correct for the extinction for the body waves in a similar way as for the surface waves. For the body waves the extinction outside the nearest few degrees of the source is probably quite small.

A factor e^{kD}, taking account of the extinction in the mantle, can easily be evaluated, using GUTENBERG's (1945a) value of $k = 0.00012$ km^{-1}; D is the length of the whole path. We find the following values:

D km	e^{kD}
4000	1.6
5000	1.8
6000	2.0
7000	2.2
8000	2.5
9000	2.8
10000	3.2

These factors are included in the factor of about 20 mentioned above, and it is evident that the usual extinction along the whole path through the mantle can account for only about 10–15 per cent of the total extinction.

The extinction, here found to be responsible for a factor of approximately 20 in the energy, may be compared with other estimates. JEFFREYS' calculations (1952, pp. 40, 107) show that this amount is not unreasonable. An application of JEFFREYS' theory to a P wave of 0.1 sec period (considering the predominance of short periods in the focal region) shows that the extinction factor e^{kD} is equal to 20 already in a distance of 3.0 km; for an S wave of the same period the required distance is only about half as long. Comparison should also be made with KAWASUMI (1952), who found that the energy passing a sphere of 100 km radius around the source is about one-thirtieth of the energy emitted from the hypocenter. Compare also the estimates of GUTENBERG and RICHTER (1956b, p. 13), which agree as far as order of magnitude is concerned.

The properties of the body-wave extinction can be summarized in the following three rules.

(1) The extinction is mainly due to scattering within the crust;

discontinuities in the earth as well as local station conditions contribute.

(2) The extinction (scattering) increases with decreasing wave length.

(3) The extinction (scattering) is larger for the transverse than for the longitudinal waves.

These rules are supported by a variety of observations. The body waves of deep earthquakes have higher frequencies than those of shallow earthquakes. PP has usually longer periods than P, and PP is often missing from records of short-period instruments. The reason is certainly the extinction of the shorter periods of PP, passing twice through the crust at the reflexion. The same is true for pP in many cases. MOONEY (1951) has reported observations of P and pP, which indicate high absorption in the crustal and near-crustal layers. The crust is heterogeneous, and the irregularities are of such mean size as to produce very effective scattering of the higher frequencies. The effective propagation of crustal channel waves occurs only for higher periods, above about 2 sec. The increase of the extinction with decreasing wave length is a general phenomenon for wave motions, although the exact dependence on the wave length may be different in different cases. Rule 3 above is evident from a comparison of the records of short-period seismographs of near-by and of distant earthquakes. A record of a near-by earthquake has much larger amplitudes in the S phase, especially of Sg, than in the P phase. But in a short-period record of a distant earthquake there is only a P phase, and usually no trace of an S phase. An explanation for this difference in the extinction of longitudinal and transverse waves remains to be given.

The consequence of the extinction for the energy determination is that no absolute values of the energy released can be obtained from P and S waves alone. The extinction must also be determined and taken into account. For this reason more reliable values of the energy can be obtained by measuring the surface waves, for which the extinction can fairly easily be accounted for; the draw-back with the use of the surface waves is the variation of E/E_{LR} with magnitude, but this relation is now known and can be taken into account.

As our present measurements were made only on long-period records (Galitzin), the energy ratios E_S/E_P refer to the medium- and long-period part of the spectrum. The mean ratio E_S/E_P is therefore

representative, if this part of the energy spectrum constitutes the same proportion of the total original energy for longitudinal as for transverse waves.

Finally, I wish to acknowledge the privilege I have had for several years in discussing these and similar seismological problems with Professor Beno Gutenberg and his colleagues at the Seismological Laboratory in Pasadena both by correspondence and during my visits there.

REFERENCES

BÅTH, M. (1952) Earthquake magnitude determination from the vertical component of surface waves, *Trans. Amer. Geophys. Un.* **33** (No. 1), 81–90.

—— (1955a) The relation between magnitude and energy of earthquakes, *Trans. Amer. Geophys. Un.* **36** (No. 5), 861–865.

—— (1955b) The problem of earthquake magnitude determination, *Ass. Séism. Phys. l'Intérieur Terre* **19**, 5–93.

BULLEN, K. E. (1947) *An Introduction to the Theory of Seismology*, Cambridge University Press.

GUTENBERG, B. (1945a) Amplitudes of P, PP, and S and magnitude of shallow earthquakes, *Bull. Seism. Soc. Amer.* **35** (No. 2), 57–69.

—— (1945b) Magnitude determination for deep-focus earthquakes, *Bull. Seism. Soc. Amer.* **35** (No. 3), 117–130.

—— and RICHTER, C. F. (1956a) Earthquake magnitude, intensity, energy, and acceleration (Second paper), *Bull. Seism. Soc. Amer.* **46** (No. 2), 105–145.

—— —— (1956b) Magnitude and energy of earthquakes, *Ann. Geofis.* **9** (No. 1), 1–15.

JEFFREYS, H. (1923) The Pamir earthquake of 18 February 1911, in relation to the depths of earthquake foci, *Mon. Not. Roy. Astr. Soc., Geophys. Suppl.* **1**, 22–31.

—— (1952) *The Earth*, 3rd ed. Cambridge University Press.

KAWASUMI, H. (1952) On the energy law of occurrence of Japanese earthquakes, *Bull. Earthquake Res. Inst.* **30**, Pt. 4, 319–323.

MOONEY, H. M. (1951) A study of the energy content of the seismic waves P and pP, *Bull. Seism. Soc. Amer.* **41** (No. 1), 13–30.

SOLOVJEV, S. L. (1956) On the relation between earthquake energy and magnitude (in Russian), *Izv. Akad. Nauk SSSR, Geophys. Ser.* No. 3, 357–359.

2

ENERGY IN EARTHQUAKES AS COMPUTED FROM GEODETIC OBSERVATIONS

PERRY BYERLY AND JOHN DENOYER

Geodetic observations

THREE western United States earthquakes which have produced notable fault breaks have occurred in areas where geodetic observations had been made before the faulting and immediately thereafter. These shocks were the San Francisco (California) earthquake of 1906, the Imperial Valley (California) earthquake of 1940, and the Dixie Valley–Fairview Peak (Nevada) earthquake of 1954.

In the case of the last of these we were indeed fortunate, for the United States Coast and Geodetic Survey had set up triangulation points in the summer of 1954. The shock occurred on 16 December and the Survey reoccupied the stations in the spring of 1955. Therefore the change in position of the stations represents almost wholly the fling at the time of the faulting. In the case of the 1906 earthquake the triangulation before the faulting had been made many years earlier and so corrections for added strain accumulated between the early surveys and the day of faulting must be made. In each case the stations were reoccupied by the Coast and Geodetic Survey shortly after the earthquake.

The method of this paper is to compute the shear strain energy (about to be relieved) in the earth just before the faulting or its equivalent, the work done at the time of faulting. It may be that there is additional strain which is not relieved and perhaps some dilatational energy was relieved although such appears to have been small.

The assumption is made that the deformation of strain at the earth's surface persisted unaltered to the depth to which the fault broke and no deeper, i.e. that a horizontal surface at this depth was effectively lubricated.

For these three earthquakes the horizontal displacements occurring at the time of the shock or those due to strain (about to be relieved) just before the shock may be represented by the empirical equation

$$v = \frac{2M}{\pi} \cot^{-1} ax \tag{1}$$

where the plane of the fault is the yz plane, the z axis pointing down dip and the y axis is horizontal. The xz plane bisects the fault plane. The displacement v is in the direction of the y axis; M is the maximum value of v. The fit of this equation is the kind of fit to which we are accustomed in seismology as is shown in Figs. 1, 2, 3.

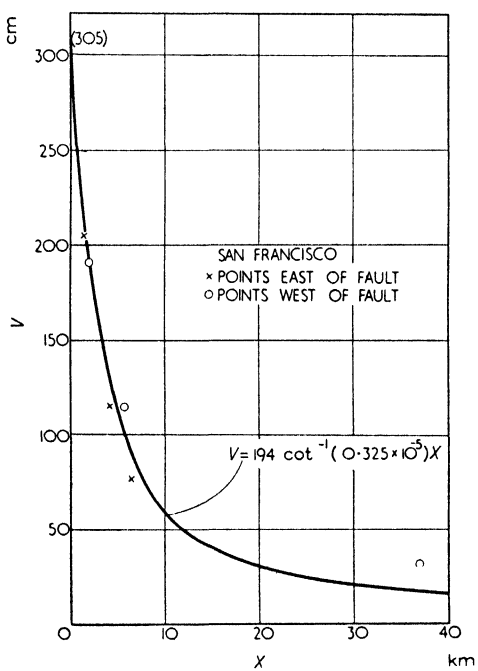

FIG. 1.

In the California earthquakes the displacement was almost wholly horizontal; in the Nevada shock there was also considerable vertical displacement.

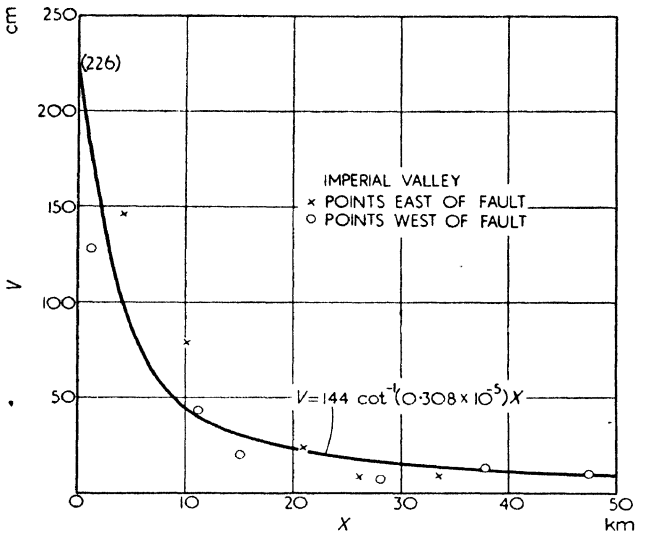
cm
250
200
150
100
50
V
(226)
IMPERIAL VALLEY
× POINTS EAST OF FAULT
○ POINTS WEST OF FAULT
V=144 cot⁻¹(0·308×10⁻⁵)X
0
10
20
30
40
50
X
km

FIG. 2.

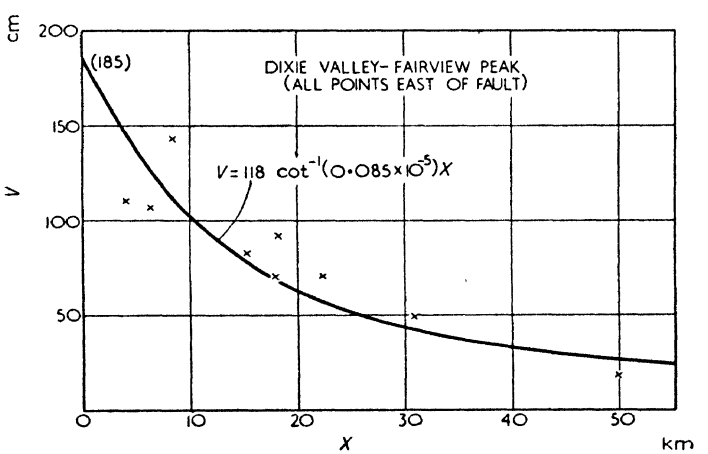
cm
200
150
100
50
V
(185)
DIXIE VALLEY–FAIRVIEW PEAK
(ALL POINTS EAST OF FAULT)
V=118 cot⁻¹(0·085×10⁻⁵)X
0
10
20
30
40
50
X
km

FIG. 3.

The shear strain energy relieved by the horizontal motion is, for one side of the fault

$$E = \int_0^D dz 2 \int_0^L dy \int_0^\infty \frac{\mu}{2} \left(\frac{\partial v}{\partial x}\right)^2 dx \tag{2}$$

Here D is the depth of fault break, $2L$ is the length of the fault break, and μ is the rigidity.

The work done along one side of the fault at the time of breaking may be expressed as

$$W = \frac{1}{2} \int_0^D dz 2 \int_0^L dy \int_{v(0,y)}^0 \mu_0 \left(\frac{\partial v}{\partial x}\right)_{x=0} dv \tag{3}$$

The two expressions (for E and W) should be equal according to the Elastic Rebound Theory (REID, 1910).

They do not check if μ is a constant unless $\partial v/\partial x = (\partial v/\partial x)_{x=0}$ BENIOFF (1951) has pointed out that the curvature of the lines of displacement v versus x in Fig. 1 suggests that the rigidity along the fault must be less than that at a distance from it. Continued breaking in the fault zone suggests it perhaps.

The expressions for W and E become equal if we take

$$\mu = \mu_0 \left(\frac{\partial v}{\partial x}\right)_{x=0} \frac{1}{\partial v/\partial x} = \mu_0 (1 + \alpha^2 x^2) \tag{4}$$

We then have

$$E = W = \frac{\mu_0}{2} \int_0^D dz 2 \int_0^L dy \int_0^\infty \left(\frac{2M}{\pi}\right)^2 \frac{\alpha^2}{1 + \alpha^2 x^2} dx$$

$$= \frac{2\mu_0 DLM^2 \alpha}{\pi} \tag{5}$$

We are aware that pure elasticians may feel that the computation of strain energy by Eq. (2) is not justifiable when μ is a function of x. However the use of the equivalent Eq. (3) should not be open to such criticism.

The total energy will be obtained by applying Eq. (5) to both

sides of the fault. We may also treat the case in which the displacement along the fault dies off linearly from its center, putting

$$v = \frac{2M}{\pi}\left(1 - \frac{|y|}{L}\right)\cot^{-1}\alpha x \tag{6}$$

This leads to

$$E = W = \frac{2\mu_0 DLM^2\alpha}{3\pi} \tag{7}$$

for the work done along one side of the fault. Here M is now the maximum value of v at the middle of the fault break. The difference in energy computed by Eq. (5) and (7) is not great since in (5) one would use a value of M which was a mean.

In Eq. (4) we have arbitrarily taken $\mu = 3 \times 10^{11}$ at that distance from the fault where $\partial v/\partial x$ has dropped to one-tenth its value at the fault. Thus $\mu_0 = 3 \times 10^{10}$.

The depth of fault break

The most difficult term to evaluate in Eqs. (5) or (7) is D, the depth of fault break. We may follow the line of attack used by REID (1910) in the study of the 1906 earthquake, but with considerable alterations. Referring to Fig. 4 we express the energy density along the earth's surface as a function of the length of the fault, the depth of break, and the distance, x, from the fault. We assume Lambert's Law, i.e. the energy emitted from an element of fault surface varies as $\cos\theta$. We also assume that the displacement along the fault was a linear function of the distance from the middle of the fault, so that the energy was proportional to $(L - |y|)^2$. The equation is considerably simplified when the term $L - |y|$ is omitted, i.e. the displacement is taken as constant along the fault.

Next we consider a fault which is not vertical (the Dixie Valley–Fairview Peak shocks). For this case we do not require the displacement to die off from the center but let it be constant along the fault. The diagram, integral, and solutions are given in Figs. 5 and 6. Figs. 5 and 6 refer to the energy per unit surface area, E, corresponding respectively to the regions on the foot wall side (i.e. to the left) and the hanging wall side (i.e. to the right) of the fault. The y

axis is parallel to the fault outcrop and the z axis is in the direction of dip. The x axis passes through the point where the energy density is to be computed. The xz plane bisects the fault plane. Q is the

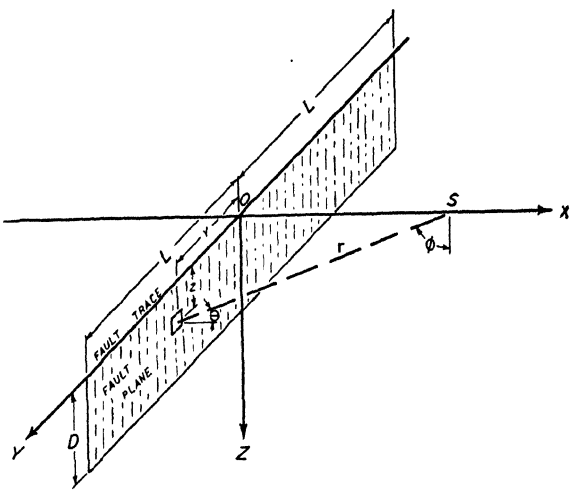

$$E = 2\int_0^D\int_0^L \frac{A(L-y)^2 \cos\theta \cos\phi \, dy\, dz}{r^2} = 2\int_0^D\int_0^L \frac{A(L-y)^2 x\, dy\, dz}{(x^2+y^2+z^2)^2}$$

$$E = AL^2\left\{\tan^{-1}\frac{L}{X} - \frac{X}{\sqrt{X^2+D^2}}\tan^{-1}\frac{L}{\sqrt{X^2+D^2}} - \frac{X^2}{L^2}\tan^{-1}\frac{L}{\sqrt{X^2+L^2}} + \frac{X\sqrt{X^2+D^2}}{L^2}\tan^{-1}\frac{L}{\sqrt{X^2+L^2+D^2}} + \frac{X}{L}\log_e\frac{X^2(X^2+L^2+D^2)}{(X^2+L^2)(X^2+D^2)}\right\}$$

FIG. 4.

distance from the origin to the surface of the earth—the fault trace and D' the dimension of the fault break measured down dip.

The formula in Fig. 6 degenerates to

$$E = A\left[\tan^{-1}\frac{L}{x} - \frac{x}{\sqrt{(x^2+D^2)}}\tan^{-1}\frac{L}{\sqrt{(x^2+D^2)}}\right] \qquad (8)$$

for a vertical fault.

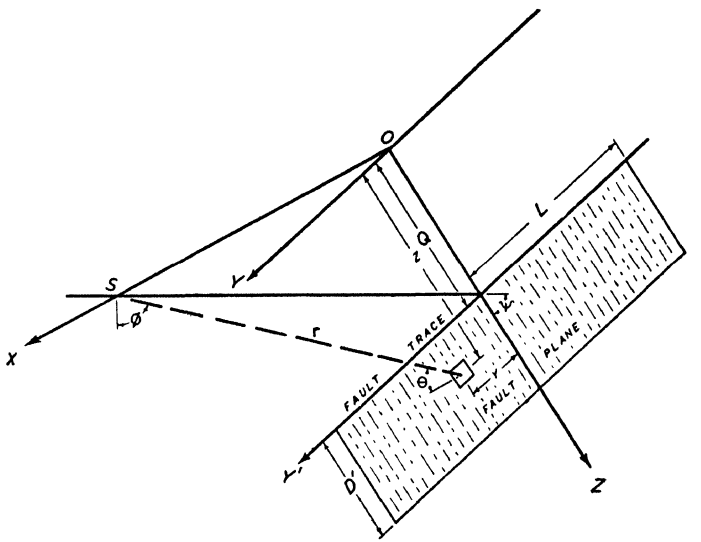

$$E = 2\int_{Q}^{D'+Q}\int_{0}^{L} \frac{A\cos\theta\cos\phi\,dy\,dz}{r^2} = 2\int_{Q}^{D'+Q}\int_{0}^{L} \frac{Ax}{(x^2+y^2+z^2)^{\frac{5}{2}}}(z\sin\Psi - x\cos\Psi)\,dy\,dz$$

$$E = A\left\{\tan^{-1}\left(\frac{L}{x}\sin\Psi\right) - \frac{D'\cos\Psi + x\csc\Psi}{\sqrt{x^2\csc^2\Psi + 2D'x\cot\Psi + D'^2}}\tan^{-1}\frac{L}{\sqrt{x^2\csc^2\Psi + 2D'x\cot\Psi + D'^2}}\right.$$

$$\left. - \frac{L\cos\Psi}{\sqrt{x^2+L^2}}\left(\tan^{-1}\frac{D'+x\cot\Psi}{\sqrt{x^2+L^2}} - \tan^{-1}\frac{x\cot\Psi}{\sqrt{x^2+L^2}}\right)\right\}$$

FIG. 5.

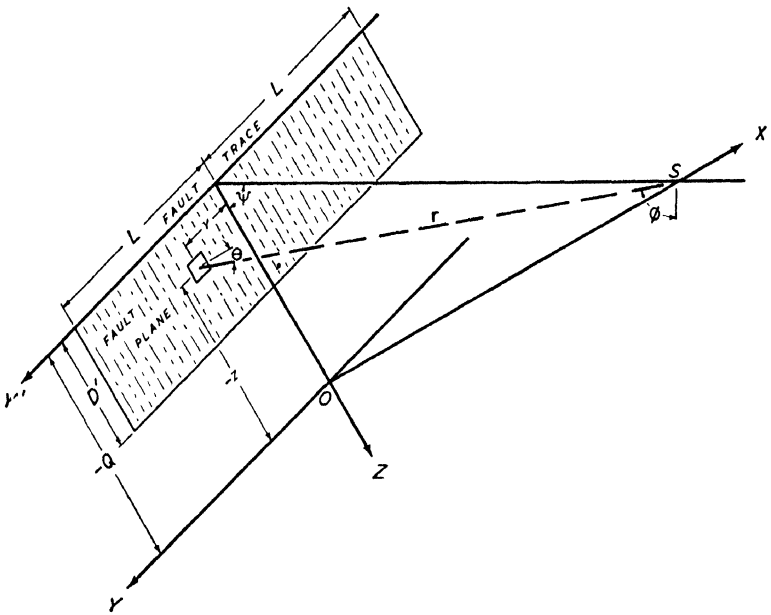

$$E = 2\int_{-Q}^{D'-Q}\int_{0}^{L}\frac{A\cos\theta\cos\phi\,dy\,dz}{r^2} = 2\int_{-Q}^{D'-Q}\int_{0}^{L}\frac{Ax}{(x^2+y^2+z^2)^2}(z\sin\Psi + x\cos\Psi)\,dy\,dz$$

$$E = A\left\{\tan^{-1}\left(\frac{L}{X}\sin\Psi\right) + \frac{D'\cos\Psi - x\csc\Psi}{\sqrt{x^2\csc^2\Psi - 2D'x\cot\Psi + D'^2}}\tan^{-1}\frac{L}{\sqrt{x^2\csc^2\Psi - 2D'x\cot\Psi + D'^2}}\right.$$

$$\left. + \frac{L\cos\Psi}{\sqrt{x^2+L^2}}\left(\tan^{-1}\frac{D'-x\cot\Psi}{\sqrt{x^2+L^2}} + \tan^{-1}\frac{x\cot\Psi}{\sqrt{x^2+L^2}}\right)\right\}$$

FIG. 6.

The next requirement is to correlate the value of E with field observations. The observations are the intensities of the earthquake as a function of distance from the middle of the fault break. First, from the isoseismals we get as best we can the intensities as a function of distance from the fault, measuring perpendicularly from the center of the fault. For the vertical fault this is along the x axis. For the fault dipping at an angle it is x cosec Ψ.

We can take from Gutenberg and Richter or from NEUMANN (1954).

$$\log_{10} a = \frac{I}{3} + C \tag{9}$$

We bear in mind the uncertainties of this relationship (HERSHBERGER, 1956). In formula (9) a is the maximum acceleration and I the Modified Mercalli Intensity.

Now we consider that the energy density on the surface at any point as proportional the square of the velocity of vibration so that

$$E \propto \left(\frac{2\pi}{T}\right)^2 A^2$$

A being the amplitude; whereas for the acceleration

$$a^2 \propto \left(\frac{2\pi}{T}\right)^4 A^2 \propto \left(\frac{2\pi}{T}\right)^2 E$$

So

$$\frac{E_0}{E_x} = \frac{\log^{-1}\left\{\frac{2}{3}(I_0 - I_x)\right\}}{(T_x/T_0)^2} \tag{10}$$

where the subscript zero refers to values at the fault trace and the subscript x to values at a distance x.

So Eq. (10) combined with the equations for energy in Figs. 4 or 5 and 6 gives a relation between depth of fault break and intensity as a function of parameter D.

Method of computing D

We then plot as a continuous curve on Figs. 7 and 8 the values of E_0/E_x computed from the right hand member of the equation in Fig. 4 for a vertical fault. For the dipping fault we plot in Fig. 9

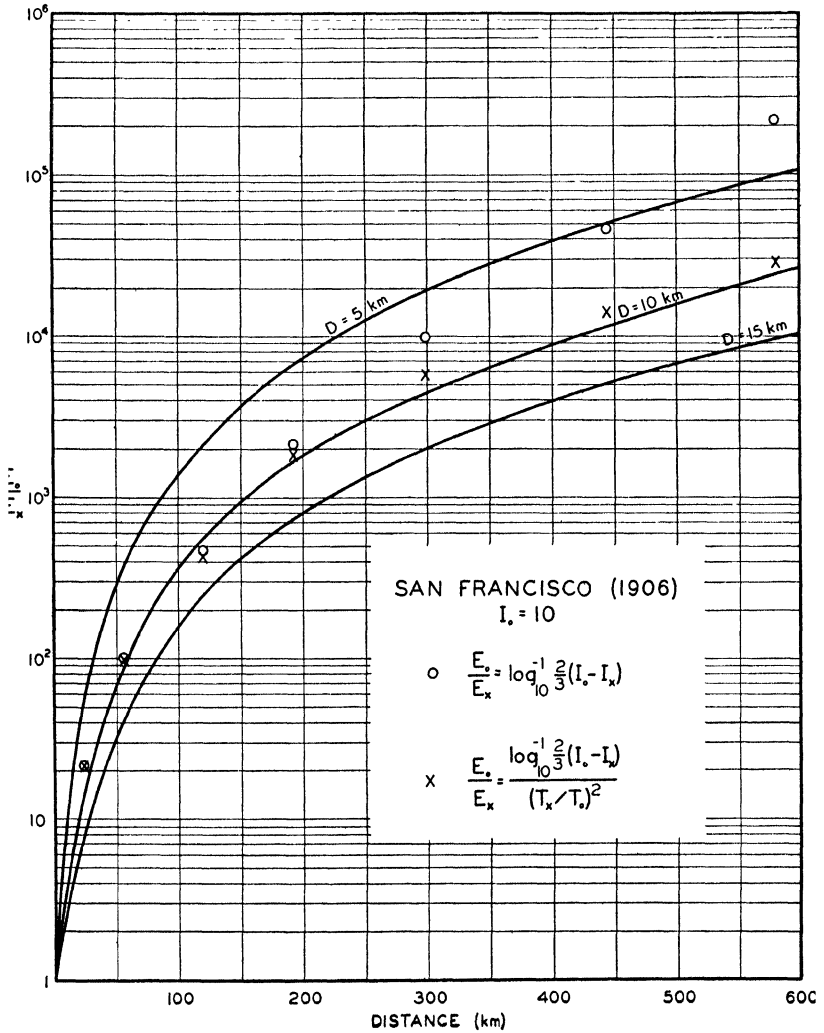

FIG. 7.

the values of E_0/E_x computed from equations in Figs. 5 and 6. These are plotted against distance with D as a parameter.

Then we plot the points from the right hand side of Eq. (10) to

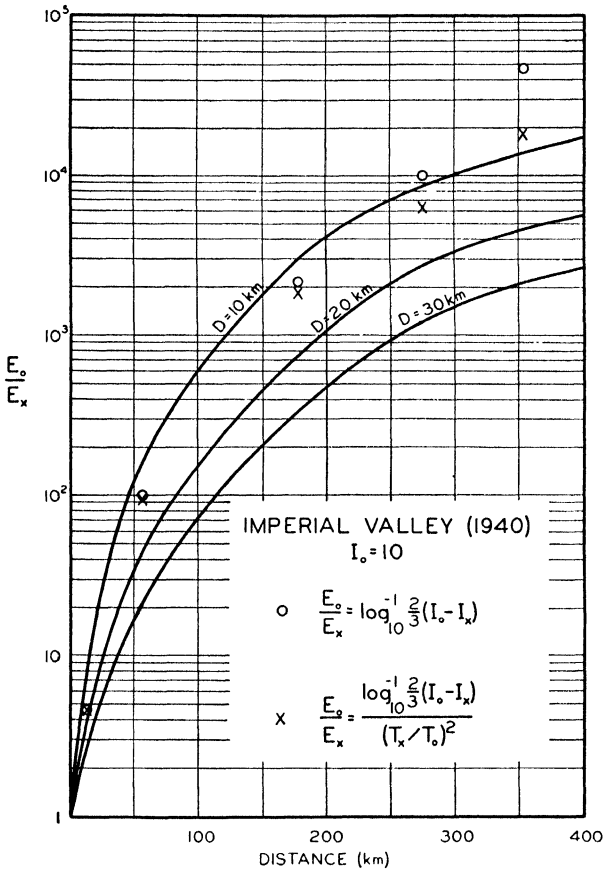

FIG. 8.

see how they fit. In the case of Fig. 7 (1906 'quake) we found that we could obtain a fit if we took

$$\log_{10} \frac{T_x}{T_0} = 1.3 \times 10^{-6}\, x^2 \qquad (11)$$

where x is measured in kilometers. This involves a change in T_x/T_0 from 1 to 2.94 in 600 km. It is not our thought that this is a change in period of a wave but that it merely states that the maximum

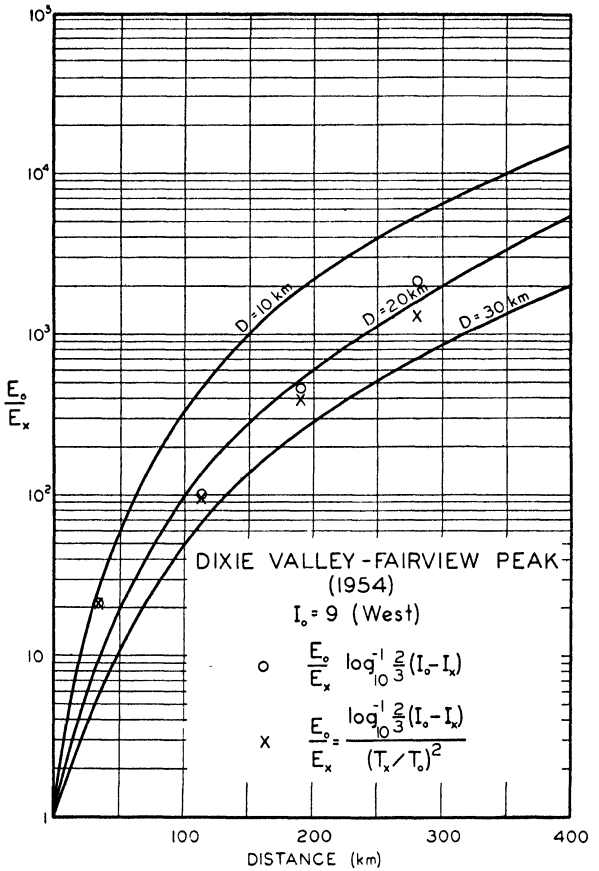

FIG. 9(a).

acceleration is carried by a longer wave at greater distance due to greater dissipation of shorter waves. Equation (11) should not be used at distances greater than 600 km. Since Eq. (11) also was found satisfactory for the other two shocks it was adopted.

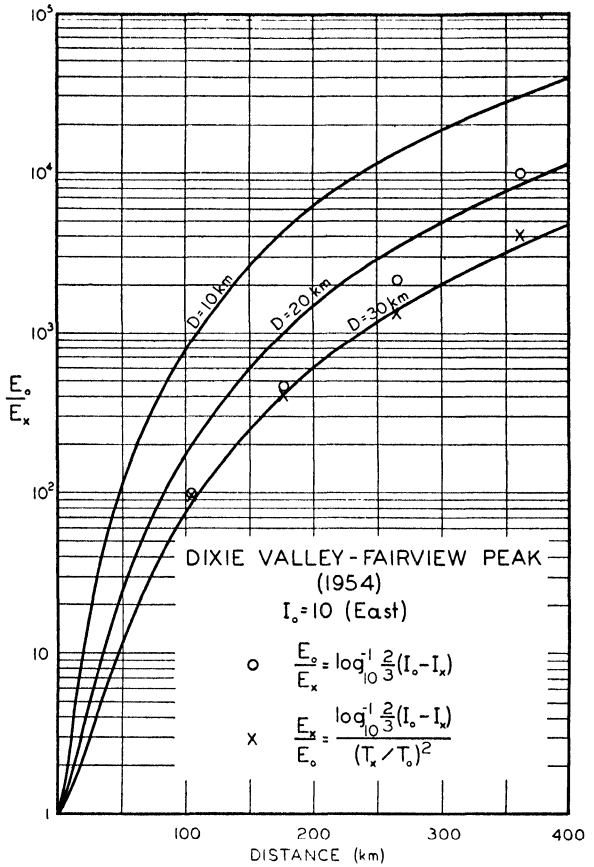

FIG. 9(b).

The earthquake of 1906

The length of fault break was taken as 436 km. In order to get the depth of fault break for this earthquake we measured intensity as a function of distance east of the fault break. To the west was the Pacific Ocean. We used the isoseismals from the Report of the State Earthquake Investigation Commission. A difficulty was the anomalous effect of the deep sediments in the Great Valley as contrasted with the firm foundation of the Coast Ranges and the Sierra Nevada. So we took our line just north of the Golden Gate to avoid too great an

effect of the Coast Ranges. The intensities were given in the Rossi-Forel scale but we feel that an effort to change to Modified Mercalli is unwarranted. The intensities as a function of distance are given in Table 1.

TABLE 1

x (km)	I	x (km)	I
0	10	193	5
24	8	298	4
56	7	443	3
120	6	580	2

Following the procedure outlined above, we plot Fig. 7 and conclude 10 km for the value of D. Now Harry Fielding Reid got 8 km by a similar method but refused to accept it as too shallow, adopting 20 km.

ROCHESTER in a Master's thesis written at the University of Toronto has theoretically concluded a formula from dislocation theory which at the earth's surface is identical with our empirical formula (1). However his value of α is the reciprocal of the depth of fault break and gives only 3 km as the depth of break! The value of 10 km was distasteful to us, but the rapid die off of intensity from the fault seems to demand a shallow break. To get a depth of 20 km we would have to reduce the intensity at the fault to 9, which we hesitate to do.

REID (1910) gives the horizontal shift of triangulation stations of the Coast and Geodetic Survey between early surveys (about 25 years before 1906) and the positions just after the shock. We need to correct for the slow drift of strain accumulation in order to find the values of v which were relieved at the time of the shock.

This is accomplished as follows: the changes in position given by REID were based on a fixed base line some 60 km east of the fault.

The observed displacements will be the sum of a slow drift and a fling at the time of the shock or

$$t_1 C_x + v_x = S_x \tag{12}$$

Here t_1 is the time between the surveys, C_x is the velocity of drift of a point at distance x from the fault, v_x its fling and S_x its measured displacement.

For points east of the fault (toward the base line) the fling of point x may also be expressed as

$$v_{xe} = -t_2 C_x \tag{13}$$

where t_2 is the total time of accumulation of strain. For points west of the fault

$$v_{xw} = 2M - t_2 C_x \tag{14}$$

where $2M$ is the maximum displacement on the fault at the time of the break.

The velocity C_x may be eliminated between Eqs. (12) and (13) and between (12) and (14), giving

$$v_{xe} = \frac{S_x t_2}{t_2 - t_1} \tag{15}$$

$$v_{xw} = \frac{S_x t_2 - 2Mt_1}{t_2 - t_1} \tag{16}$$

For the 1906 earthquake, surveys were conducted during 1874–1892 and from 1906–1907. Averages of the observed displacements at various distances from the fault were given by REID. If we assign as did Reid

t_1 = 25 years (time between surveys)
t_2 = 100 years (total time for the accumulation of strain)
$2M$ = 610 cm (maximum displacement)

the fling at the time of the earthquake can be estimated.

Table 2 summarizes the data as averaged by REID and our addition to it is the last column. The fling corresponding to each distance is added in the last column.

TABLE 2

No. of points	Distance from fault (km) East	West	Displacement (cm) South	North	Fling v (cm) South	North
10	1.5		154		205	
3	4.2		86		115	
1	6.4		58		77	
12		2.0		295		191
7		5.8		238		115
1		37.0		178		32

We note that the maximum rate of drift, about 20 ft/100 years or 2.4 in. year, agrees well with WHITTEN's (1949) 2 in./year obtained from more recent observations.

The corrected values of v are plotted as a function of x in Fig. 1. These are near the center of the fault.

So with M and a evaluated (Fig. 1) the energy relieved (or work done) is computed by Eq. (7). We find $E = 0.9 \times 10^{23}$ ergs. The values of the constants are given in Table 3.

The Imperial Valley earthquake of 1940

In Fig. 10 are presented movements of triangulation stations on either side of the 1940 fault break as taken from a map prepared by C. A. Whitten of the Coast and Geodetic Survey.

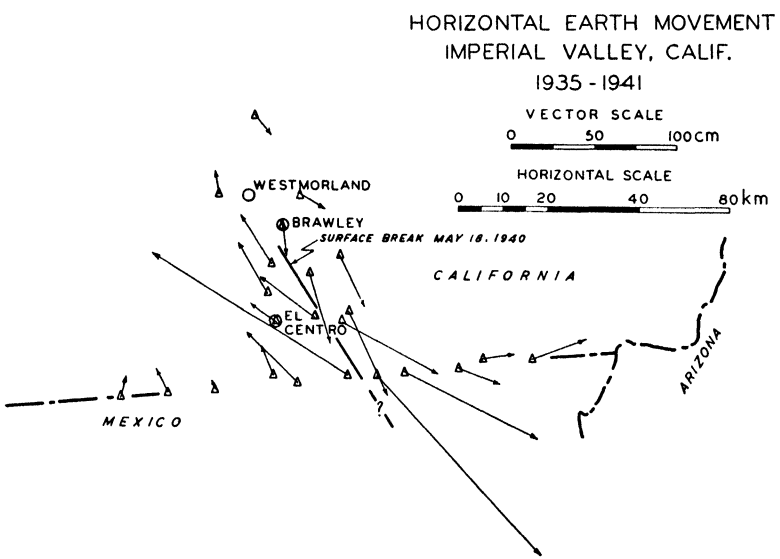

FIG. 10.

For this earthquake the survey before the fault break was made in 1935 (in the region near the center of the fault where we used the observations) and the later one in 1941. The only data for rate of drift would have been the changes between 1941 and a later survey in 1954, both after the shock (WHITTEN, 1956). The rates so computed for points well west of the fault are so large that if we take them as

applicable between 1935 and 1940 we find the fling at a distance west to be south instead of north. The displacement along the fault was the normal California west side north, the maximum being 14 ft or better. These displacements were in alluvium which makes the matter troublesome.

So we made no corrections for elastic drift during the 6 years between the first survey and the earthquake. Fig. 2 shows the values of v as a function of x and the equations of type (1).

From the isoseismals of this shock as published by F. P. ULRICH (1941) we get the intensity as a function of distance along a line perpendicular to the center of the fault and from Eq. (10) compute E_0/E_x using again Eq. (11) for period change. This gives us the points plotted as crosses in Fig. 8. The points are compared with the curves drawn from the equation in Fig. 5 with D as a parameter and we choose $D = 12$ km. The value of L is taken as 80 km. There was a break in the United States about 40 km in length. Since the maximum fault displacement was near the border we add 40 km in Mexico although the trace was not completely observed in that country.

In Fig. 2 the values of v are plotted as a function of x. A curve is drawn and the equation is given on the figure. Equation (7) then gives us an energy of 9.6×10^{21} ergs (see Table 2).

The Nevada earthquake of 16 December 1954

Two earthquakes about 4 min apart occurred in the early morning of 16 December 1954 in the Dixie Valley–Fairview Peak region of west-central Nevada. Faulting was conspicuous over a north–south zone some 80 km long. There were two major faults but also a number of others. The great fault on the eastern flank of Fairview Peak was probably the most conspicuous. However, that on the western side of Dixie Valley was hardly less remarkable. The scarps caused by the faulting indicated largely vertical movement, but in places large horizontal displacement was observed. However some of the vertical scarps seemed partially due to settling of soil on the valley side. CARL ROMNEY (1955) performed an analysis of the first motion of the first of the two shocks, Fairview Peak, and concluded that the fault dipped 60° to the east and that the horizontal motion was about twice the vertical. The results of triangulation and leveling confirm this. The full report of this earthquake is to appear

in a group of papers to be published in the Bulletin of the Seismological Society of America.

The isoseismal map of these earthquakes was prepared by the United States Coast and Geodetic Survey. The faulting was at the extreme west of the inner isoseismal, in agreement with a fault dipping east. In Fig. 9 are plotted E_0/E_x to the east and to the west of the fault. The points are computed from Eqs. (10) and (11) using $I_0 = 10$ to the east and 9 to the west. The solid lines are drawn from the equations from Figs. 5 and 6. We selected 27 km the value of D' now measured down dip. However for computing the energy in horizontal strain we used Eq. (5) and a depth $D = 23$ km.

The shift of triangulation stations at the time of this shock was presented by WHITTEN (1956).

The displacements to the east of the fault are fitted to an Eq. of type (1) in Fig. 3. The displacements west of the fault die off very quickly with distance and seem erratic. We cannot use them with our formula. Perhaps this is because of the Fallon–Stillwater earthquakes (BYERLY *et al.*, 1956) which centered some 40 miles east of the Fairview Peak–Dixie area in July and August 1954. This was during the period that the original triangulation surveys were being made.

Therefore we compute the energy of the horizontal component of the strain to the east of the fault as $E = 0.5 \times 10^{22}$ ergs. Perhaps it should be multiplied by two to care for the western side. The leveling observations made along the highway across the fault by the State of Nevada indicate the major changes to be east of the fault, a lowering of the highway. Across the fault the change in level was as much as 180 cm. However, the observations suggest a settling down of the alluvium in many cases. A law of the type of Eq. (1) does not fit these vertical displacements.

We can fall back on Romney's conclusion that the vertical down dip displacement at depth was about one-half the horizontal. We might then increase the energy to 1×10^{22}–1.5×10^{22} ergs.

Conclusion

We have computed the depth of fault break and the strain energy released for three earthquakes in which there was surface faulting. The results are as follows where D is the depth of breaking below the surface and E is the energy.

TABLE 3

Earthquake	L (km)	D (km)	α	M (cm)	E (ergs)
San Francisco (1906)	218	10	0.325×10^{-5}	305	0.9×10^{23}
Imperial Valley (1940)	40	12	0.308×10^{-5}	226	9.6×10^{21}
Fairview Peak (1954)	40	23	0.085×10^{-5}	185	1 to 1.5×10^{22}

REFERENCES

BENIOFF, H. (1951) Mechanism of earthquake generation, *Bull. Geol. Soc. Amer.* **62**, 1526.

BYERLY, P., SLEMMONS, D. B., TOCHER, D., STEINBRUGGE, K. V., MORAN, D. F. and CLOUD, W. K. (1956) The Fallon–Stillwater earthquakes of July 6, 1954 and August 23, 1954, *Bull. Seism. Soc. Amer.* **46** (No. 1), 1–40.

HERSHBERGER, J. (1956) A comparison of earthquake accelerations with intensity ratings, *Bull. Seism. Soc. Amer.* **46** (No. 4), 317–320.

NEUMANN, F. (1954) *Earthquake Intensity and Ground Motion.* University of Washington Press, Seattle.

REID, H. F. (1911) *Elastic Rebound Theory.* University of California Publications, *Bull. Dept. Geol. Sci.* **6**, 413–444.

—— (1910) *The California Earthquake of April* 18, 1906. Vol. 2, The Mechanics of the Earthquake. The Carnegie Institution of Washington.

ROCHESTER, M. G. The Application of Dislocation Theory to Fracture of the Earth's Crust. Manuscript on file in the library of the University of Toronto.

ROMNEY, C. F. (1955) The Dixie Valley–Fairview Peak Earthquakes of December 16, 1954. Doctor's Thesis, University of California.

ULRICH, F. P. (1941) The Imperial Valley earthquakes of 1940, *Bull. Seism. Soc. Amer.* **31** (No. 1), 13–31.

WHITTEN, C. A. (1949) Horizontal earth movement in California, *J. Coast and Geodetic Survey*, No. 2, 84–88 (April).

—— (1956) Crustal movements in California and Nevada, *Trans. Amer. Geophys. Un.* **37** (No. 4), 393–398.

3

THE VARIATION OF AMPLITUDE AND ENERGY WITH DEPTH IN LOVE WAVES

ROBERT STONELEY

THE variation of the amplitude of surface elastic waves with distance from a free surface is of interest both in seismology and in the vibration of roads and solid structures. The present paper investigates numerically the variation of amplitude for Love waves propagated in a solid having two uniform surface layers, of equal thicknesses, underlain by a very great depth of uniform material. The densities and rigidities of the three media are taken to represent an ultrabasic rock, of great thickness, with surface layers of granitic and basaltic rock in which the granitic layer is the outermost. The relative amplitudes of the vibration have been computed for eight different depths in respect of thirteen different values of the wave-velocity, covering the whole permissible range of wave velocities.

The potential energy and kinetic energy in each of the three media are calculated in two representative cases, namely relatively short waves and relatively long waves. As might be expected, in the former case most of the energy, whether potential or kinetic, is confined to the granitic layer, while, in the latter case, most of the energy is located in the ultrabasic material with the remainder divided about equally between the two surface layers.

1. Introduction

When a long train of surface elastic waves is propagated in a direction parallel to the surface of a layered structure in which the medium furthest from the free surface is uniform and effectively of infinite thickness (this will be called 'the lowest medium'), the amplitude of the motion at great depth will depend exponentially on the distance from the boundary of the lowest medium. For Love waves, the amplitude is proportional to a negative exponential function; for Rayleigh waves the amplitudes of the horizontal and vertical components are each proportional to the sum of two negative exponential functions.

The numerical evaluation of the variation of amplitude with depth is of some practical interest. When seismographs are installed in borings the amplitudes of earthquake waves may be measured directly, and the same considerations apply to microseisms and to the recordings of explosions. By means of the well-known reciprocal theorem these amplitudes may be discussed in relation to the surface amplitude and the depth of focus. There is, too, an obvious application to the problem of road vibration. The problem was discussed for Rayleigh waves in a single surface layer by A. W. LEE (1932); for Rayleigh waves in a double surface layer the computation of the variation of amplitude is very heavy, and has recently been carried out with the aid of the SEAC electronic computer at the National Bureau of Standards, Washington, D.C. See R. STONELEY and U. HOCHSTRASSER (1957).

2. The dependence of amplitude on depth in Love waves

For Love waves in a double surface layer the amplitude in any one of the three media can be expressed in explicit form (STONELEY, 1950) and the extension to three or more surface layers is straightforward. In the problem of two surface layers the free surface is taken as $z = -T_1$, the junction of the two surface layers as $z = 0$, and the junction of the inner layer and the subjacent material as $z = T_2$. These two layers, from the free surface downwards, are distinguished by suffixes 1, 2, respectively, while the subjacent material, extending from $z = T_2$ to $z = +\infty$, is denoted by the suffix 3. The rigidity and the density are written as μ, ρ, with appropriate suffixes. The velocity β of distortional waves in any medium is given by $\beta^2 = \mu/\rho$.

Then for a wave of wave length $2\pi/\kappa$ and wave velocity c propagated in the x direction in any homogeneous medium the displacement is

$$(0, V(z), 0) \exp i\kappa(x - ct) \tag{1}$$

where $V(z)$ satisfies

$$\frac{d^2V}{dz^2} + \kappa^2\left(\frac{c^2}{\beta^2} - 1\right)V = 0 \tag{2}$$

The boundary conditions are that the traction across the free

surface vanishes, and that the displacement and stress are continuous across the interfaces. The condition that the energy per wave length is finite rules out solutions for $V(z)$ in region 3 that contain either a positive exponential or a periodic function. Then writing

$$s_1 = \kappa\left(\frac{c^2}{\beta_1^2} - 1\right)^{\frac{1}{2}}\ ;\ s_2 = \kappa\left(\frac{c^2}{\beta_2^2} - 1\right)^{\frac{1}{2}}\ ;\ p_2 = \kappa\left(1 - \frac{c^2}{\beta_2^2}\right)^{\frac{1}{2}}\ ;$$

$$p_3 = \kappa\left(1 - \frac{c^2}{\beta_3^2}\right)^{\frac{1}{2}}, \tag{3}$$

and using s_2 or p_2 according as c is greater or less than β_2, it is found that suitable expressions for $V(z)$ are:

$$\left.\begin{aligned} V_1 &= M\cos s_1(z + T_1),\\ V_2 &= M\{\cos s_1T_1\cos s_2z - (\mu_1s_1/\mu_2s_2)\sin s_1T_1 \\ &\qquad \sin s_2z\}\\ V_3 &= M\exp\{-p_3(z - T_2)\}\,.\,\{\cos s_1T_1\cos s_2T_2 \\ &\qquad - (\mu_1s_1/\mu_2s_2)\sin s_1T_1\sin s_2T_2\} \end{aligned}\right\}\ \beta_1 < \beta_2 < c < \beta_3 \tag{4}$$

$$\left.\begin{aligned} V_1 &= M\cos s_1(z + T)\\ V_2 &= M\{\cos s_1T_1\cosh p_2z - (\mu_1s_1/\mu_2p_2)\sin s_1T_1 \\ &\qquad \sinh p_2z\}\\ V_3 &= M\exp\{-p_3(z - T_2)\}\,.\,\{\cos s_1T\cosh p_2T_2 \\ &\qquad - (\mu_1s_1/\mu_2p_2)\sin s_1T_1\sinh p_2T\} \end{aligned}\right\}\ \beta_1 < c < \beta_2 < \beta_3 \tag{5}$$

where M is a constant.
For the intermediate case $\beta_1 < c = \beta_2 < \beta_3$,

$s_2 = p_2 = 0$, while now $s_1/\kappa = (\beta_2^2/\beta_1^2 - 1)^{\frac{1}{2}}$,

giving

$$V_1 = M\cos s_1(z + T_1),$$

$$V_2 = M\{\cos s_1T_1 - (\mu_1s_1z/\mu_2)\sin s_1T_1\},$$

$$V_3 = M\exp\{-p_3(z - T_2)\}\,.\,\{\cos s_1T_1 - (\mu_1s_1T_2/\mu_2)\sin s_1T_1\}. \tag{6}$$

The equation giving c as a function of κ can be obtained at once for any one of the three cases by writing $\mu_2 dV_2/dz = \mu_3 dV_3/dz$ at $z = T_2$. These three forms are given, of course, in the paper already cited.

3. Computation of the amplitude

In view of the amount of arithmetic involved, as well as the time spent in looking-out and interpolating the trigonometric functions required, it appears sufficient to take one illustrative model. For $T_1 = T_2 = T$ with media 1, 2, 3 corresponding respectively to granitic, basic and ultrabasic rock, solutions of the wave velocity equation are already available (STONELEY, 1948). Computations of $V(z)$ with $M = 1$ have been effected for values of c/β_2 at intervals of 0.02 from 0.92 to 1.16 for the values of z equal to $-T$, $-\frac{1}{2}T$, 0, $\frac{1}{2}T$, T, $\frac{3}{2}T$, $2T$ and $3T$, that is to say, at the discontinuities, the median planes of the surface layers, and at three depths in the

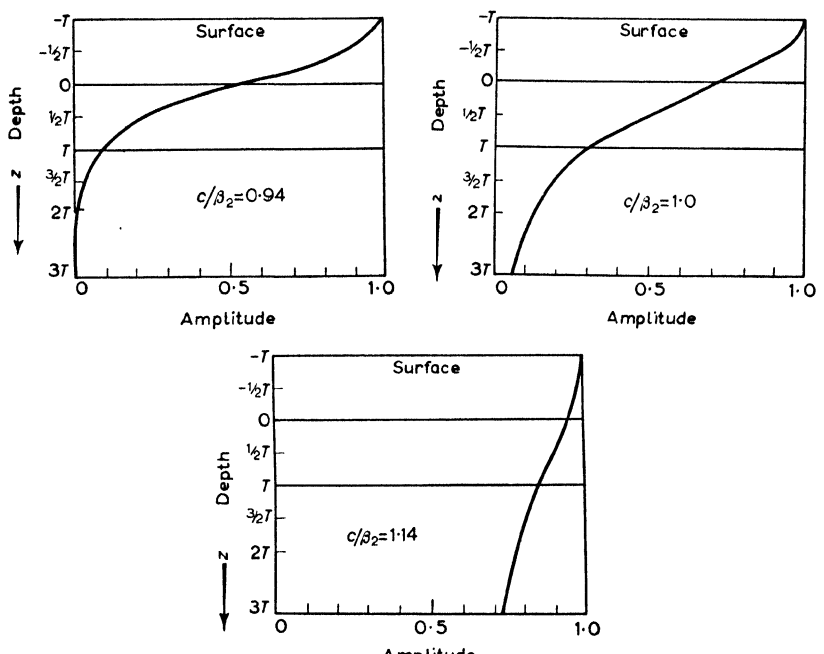

FIG. 1(a). Variation of amplitude with depth; surface waves of short period. (b). Variation of amplitude with depth; surface waves of medium period. (c). Variation of amplitude with depth; surface waves of long period.

ultrabasic material. The densities and rigidities in C.G.S. units are $\rho_1 = 2.65$; $\rho_2 = 2.85$; $\rho_3 = 3.4$; $\mu_1 = 2.997 \times 10^{11}$; $\mu_2 = 3.989 \times 10^{11}$; $\mu_3 = 6.469 \times 10^{11}$.

The relative amplitudes corresponding to the various depths are given in Table 1, with the appropriate value of κT at the bottom of each column. Some examples of the variation of amplitude with depth are shown graphically in Fig. 1.

TABLE 1

Relative amplitudes as functions of depth and wave velocity

c/β_2 / z	0.92	0.94	0.96	0.98	1.00	1.02	1.04
$-T$	1.0	1.0	1.0	1.0	1.0	1.0	1.0
$-\frac{1}{2}T$	0.83094	0.87213	0.89663	0.91324	0.92587	0.93604	0.94557
0	0.38092	0.52123	0.60791	0.66802	0.71447	0.75344	0.78822
$\frac{1}{2}T$	0.12550	0.26371	0.36495	0.44438	0.51079	0.56966	0.62524
T	0.02545	0.09178	0.16529	0.23823	0.30712	0.37616	0.44574
$\frac{3}{2}T$	0.00481	0.03411	0.08251	0.14199	0.20404	0.27200	0.34451
$2T$	0.00091	0.01268	0.04119	0.08357	0.13555	0.19668	0.26627
$3T$	0.00032	0.00175	0.01027	0.02932	0.05983	0.10283	0.15906
κT	5.42221	3.34585	2.44815	1.93334	1.59034	1.33833	1.13950

c/β_2 / z	1.06	1.08	1.10	1.12	1.14	1.16
$-T$	1.0	1.0	1.0	1.0	1.0	1.0
$-\frac{1}{2}T$	0.95413	0.96237	0.97055	0.97889	0.98763	0.99701
0	0.82075	0.85232	0.88393	0.91646	0.95083	0.98807
$\frac{1}{2}T$	0.67891	0.73259	0.78779	0.84882	0.90846	0.97760
T	0.51723	0.59213	0.67198	0.75877	0.85501	0.97406
$\frac{3}{2}T$	0.42232	0.50671	0.59933	0.70252	0.81952	0.96475
$2T$	0.34483	0.43362	0.53454	0.65044	0.78550	0.95554
$3T$	0.22989	0.31755	0.42522	0.55757	0.72163	0.93736
κT	0.97322	0.82661	0.69002	0.55394	0.40381	0.18956

4. The energy distribution

In an elastic wave the mean energy per wave length is half potential and half kinetic. This result holds only for the system as a whole,

and not for the energies in, say, a column of given constant cross section terminated by the planes $z = Z_1$ and $z = Z_2$. This will appear in the numerical illustrations. Accordingly it is necessary to consider separately the distributions of potential energy E_p and kinetic energy E_k, which may conveniently be specified per unit area of a plane parallel to $z = 0$.

Since the average value of $\sin^2 \kappa(x - ct)$ or $\cos^2 \kappa(x - ct)$ over a wave length is $\frac{1}{2}$, the average values of E_p and E_k per unit column are:

$$E_p = \tfrac{1}{4} \int_{Z_1}^{Z_2} \mu \left\{ \left(\frac{dV}{dz} \right)^2 + \kappa^2 V^2 \right\} dz \tag{7}$$

$$E_k = \tfrac{1}{4} \int_{Z_1}^{Z_2} \rho \kappa^2 c^2 V^2 dz = \tfrac{1}{4} \int_{Z_1}^{Z_2} \mu \kappa^2 (c^2/\beta^2) V^2 dz \tag{8}$$

in which V, μ and β are functions of z, while κ and c are constant for the integrations. In the present problem μ and β are constant in any one layer.

From Table 1, the energies per unit depth at any level could be found by the use of interpolation formulas, or alternatively direct from Eqs. (4), (5), (6) for $V(z)$. By way of illustration, the values of E_p and E_k for the three media, per unit column, have been found by direct substitution in Eqs. (7) and (8) and integrating between the appropriate limits. Two rather extreme cases have been considered, $c/\beta_2 = 0.94$, corresponding to relatively short waves of wave length 1.88 T, and $c/\beta_2 = 1.14$, corresponding to long waves of wave length 15.56 T.

The details of the integration and evaluation are rather long and not of sufficient interest to reproduce here; the trigonometrical and hyperbolic functions (such as $\cos s_1 T$ and $\sinh p_2 T$) have already been evaluated in the course of compiling Table 1. The energies in the media are exhibited in Table 2, in which the unit is $\frac{1}{4}\kappa^2 T \times 10^{11}$ ergs, where T is expressed in cm and κ in cm^{-1}.

The difference in the two cases is striking. In the former, corresponding to short waves, some 85 per cent of the energy is located in the granitic layer, and only about 0.5 per cent in the ultrabasic material (medium 3). For long waves the distribution is reversed: more than three-quarters of the energy is in medium 3, while the

remainder is shared in roughly equal proportions between the surface layers 1 and 2. It may be noted that the equality of E_p and E_k affords, in both cases, a stringent test of the accuracy of the

TABLE 2

$c/\beta_2 = 0.94$

Medium	E_p	Percentage	E_k	Percentage
1	2.2295	83.09	2.3512	87.63
2	0.4351	16.21	0.3231	12.04
3	0.0188	0.70	0.0089	0.33
Sum	2.6834	100.00	2.6832	100.00

$c/\beta_2 = 1.14$

Medium	E_p	Percentage	E_k	Percentage
1	2.9589	8.3153	4.6634	13.1054
2	3.5100	9.8641	4.2646	11.9847
3	29.1148	81.8206	26.6557	74.9099
Sum	35.5837	100.0000	35.5837	100.0000

computation, and indeed of the accuracy of the solutions of the wave velocity equation on which this work is based.

5. Acknowledgments

This work was carried out during the tenure of a Visiting Professorship at American University, Washington, D.C., for which funds were provided by the Office of Naval Research. I am indebted to the California Institute of Technology for the award of a Visiting Research Fellowship in Geophysics.

My special thanks are due to Professor BENO GUTENBERG for allowing me to carry out this research in the Department of Geology and Geophysics at Pasadena, and to Professor C. HEWITT DIX for the computational facilities afforded to me.

REFERENCES

LEE, A. W. (1932) The effect of geological structure on microseismic disturbance, *Mon. Not. Roy. Astr. Soc., Geophys. Suppl.* **3**, 83–105.

STONELEY, R. (1948) The continental layers of Europe, *Bull. Seism. Soc. Amer.* **38**, 268.

—— (1950) The effect of a low velocity internal stratum on surface elastic waves, *Mon. Not. Roy. Astr. Soc., Geophys. Suppl.* **6**, 28–35, eq. (3).

STONELEY, R. and HOCHSTRASSER, U. (1957). The attenuation of Rayleigh waves with depth in a medium with two surface layers, *Mon. Not. Roy. Astr. Soc., Geophys. Suppl.* **7**, 279-288.

4

ABOUT SOME PHENOMENA PRECEDING AND FOLLOWING THE SEISMIC MOVEMENTS IN THE ZONE CHARACTERIZED BY HIGH SEISMICITY

PIETRO CALOI

THE existence of strict ties between slow movements of the earth's crust and shocks in the zone of high seismicity is shown. The direction of the movement (positive or negative) in the strained region is the same as the initial direction (compression or dilatation) of the longitudinal wave of the following shock. A local shock can remove an obstacle which obstructed fault-block rotation, which in fact can follow such a shock immediately.

Tilt-meters record tilting movements associated with distant or near earthquakes.

Wide alpine zones periodically are affected by tilt-storms, which can last several days.

1

SOME significant examples of strict relations between seismic phenomena and slow angular changes of the apparent vertical, noted in highly seismic zones, have been described in previous works (CALOI, 1953; CALOI and SPADEA, 1955 a and b). The tilt and seismographic observations obtained in the zone near Tolmezzo during the seismic period which occurred during the first half of October 1954 are particularly interesting.

For the past several years a seismic station, with an instrument of small period (about 1 sec) and making a mechanical record, has been working at Tolmezzo. A pair of tilt-meters for recording the local changes of the apparent vertical are in operation near Tolmezzo at a distance of about 3 km from the seismic station in tunnels driven into the rock on the opposite sides of a creep surface.

These tilt-meters have already given us valuable evidence about the connection between slow movements of the earth's crust and

sudden breakings. The one which occurred in the Autumn of 1954 is one of the most important. After 22 September, the instruments began to record a gradual tilt, at first north-eastward, then decidedly north-westward. The tilt in this direction was particularly active from 3 to 8 October; then it turned north-eastward. Fig. 1 shows a synthesis of the deviations recorded in the mentioned time, reproduced in its components in Fig. 2.

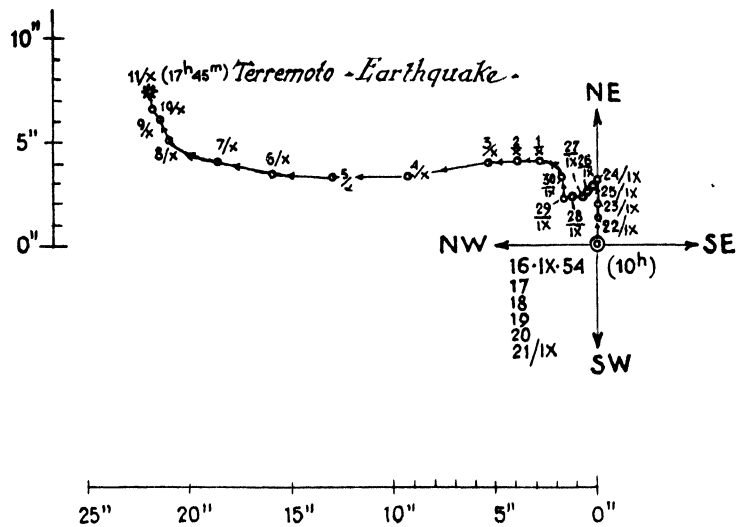

FIG. 1. Tilt variation from 16 September 1954 to 11 October 1954.

Following the latter change of direction the principal shock of the concomitant seismic period occurred. It greatly frightened the inhabitants of that region during the night of 11 October. Fig. 3 shows the macroseismic observations of this shock, which damaged the instruments of the seismic station at Tolmezzo, at a focal distance of about 10 km.

With the data of seven stations (Tolmezzo, Pieve di Cadore, Trieste, Padova, Salò, Zurigo and Neuchâtel) we have obtained the following values for the epicentral co-ordinates and for the initial time:

$$\phi = 46^\circ\ 20'\ \text{N} \quad \text{geographic}$$
$$\lambda = 13^\circ\ 06'\ \text{E}$$
$$H = 17^h\ 45^m\ 25^s$$

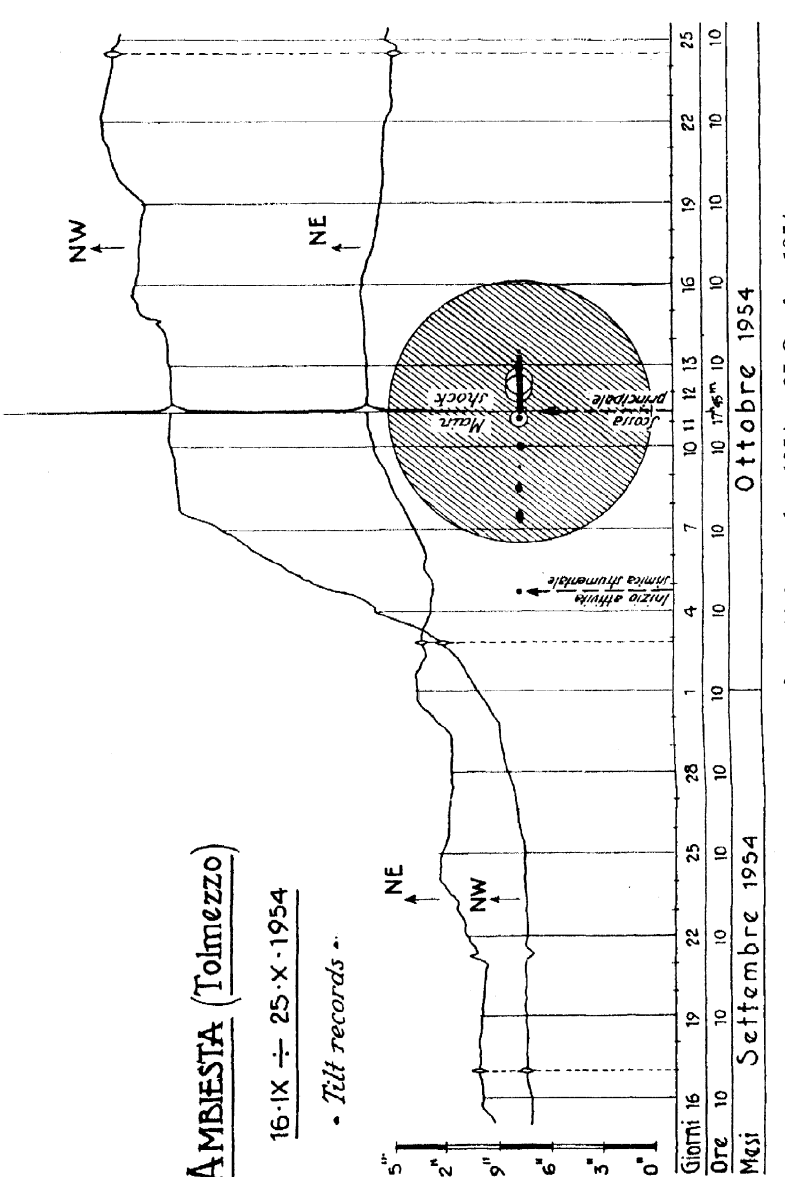

FIG. 2. Tilt records at Tolmezzo from 16 September 1954 to 25 October 1954.

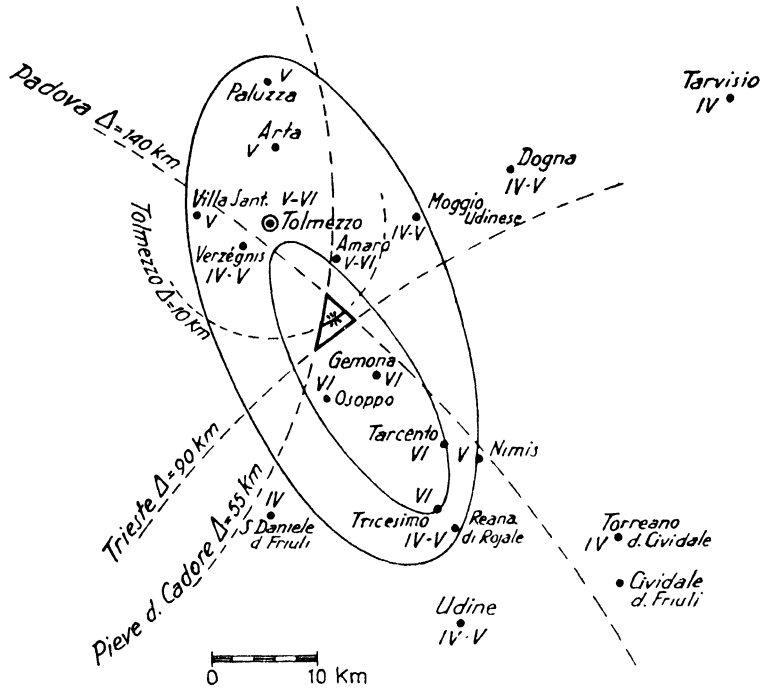

FIG. 3. Earthquake of 11 October 1954: macroseismic observations.

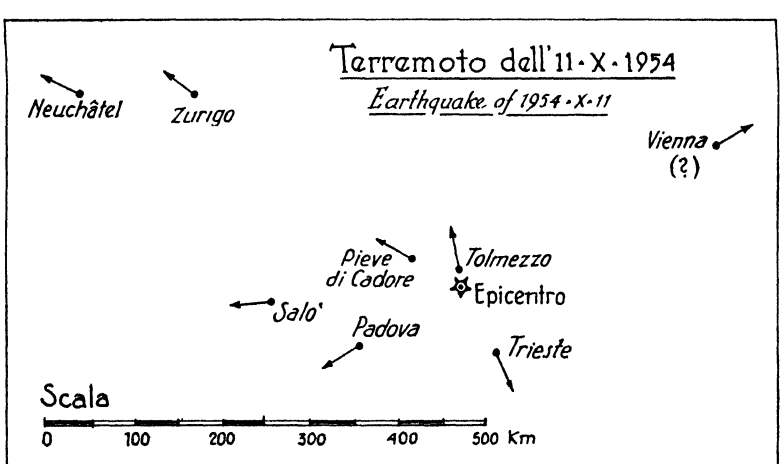

FIG. 4. Earthquake of 11 October 1954: direction of Pg-waves at some seismological stations around the epicenter.

The depth of focus is 5–10 km, and the magnitude has a value of 3.5. Fig. 4 shows the superficial distribution of the directions of the initial longitudinal movements.

Although the record obtained at Vienna has an uncertain beginning, so that it is impossible to ascertain if the compression area closes around the epicenter, the earthquake doubtless can be attributed to a sudden vertical uplift. In any case, we have to observe that compressions have characterized the zone near Tolmezzo (Ambiesta) where the tilt-meters work.

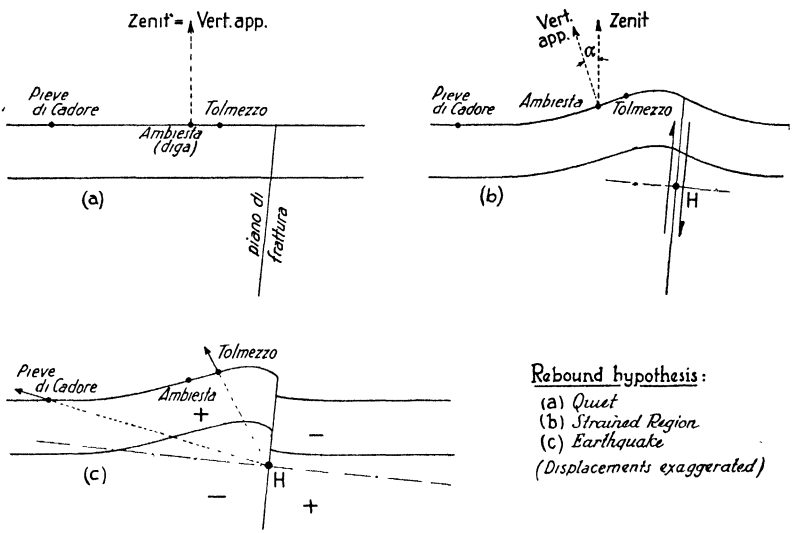

FIG. 5. Earthquake of 11 October 1954: hypothesis of faulting origin.

Now, as Figs. 1 and 2 clearly show, some days before the principal shock the tilt-meters showed tilts north-westward and north-eastward, as if the ground was lifting lightly south-eastward and south-westward. This coincides with the direction of the initial movement of the earthquake. Therefore, the principal shock was preceded by a slow lifting movement in the epicentral zone (at least in the south-east side, if it was caused by a fracture). This movement was sudden and always in the same positive direction after having passed the breaking point of the material. About this, one should recall K. E. BULLEN's recent research. He finds that the zone where the material

is near the breaking point in an earthquake of great intensity is equal to a volume of a sphere with a radius of 25 km (BULLEN, 1955). Keeping in mind the uncertainties about the values of these distances, it is possible that this volume reaches that of a sphere with a radius of 50 km.

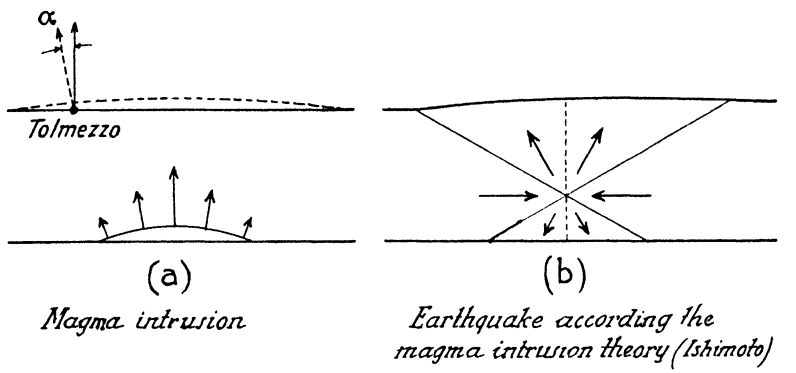

FIG. 6. Earthquake of 11 October 1954: hypothesis of magma intrusion origin.

The great nearness of the tilt-stations to the epicentral zone (about 5 km) puts them in the 'strained region' of BULLEN's concept. In other words, at least in the zone north-west of the epicenter, in the focal region the pattern of the strains had to be of type *b* of Fig. 5, as the tilt records show. On reaching the breaking point with such a situation, we had to expect the records to show compressions in the above mentioned zone, as occurred exactly (Fig. 4).

The interpretation of the observed facts is even more clear, if this is possible, adopting Ishimoto's hypothesis on the cause of earthquakes (ISHIMOTO, 1933). As is well known, he maintained that earthquakes are caused by magma intrusions in the earth's crust ('magma intrusion' theory). As the crust is deformed, the rocks flow in warm viscous currents, which focus the deforming energy in the overlying part of the earth's crust. According to Kawasumi's elaboration of this hypothesis, when the axis of the nodal cone is vertical, in a circular zone around the epicenter only compressions will occur (KAWASUMI, 1934). About this, I remark that almost all earthquakes of the Appennine region fit this mechanism. Therefore, it is probable that the earthquakes are not restricted to faultings, as

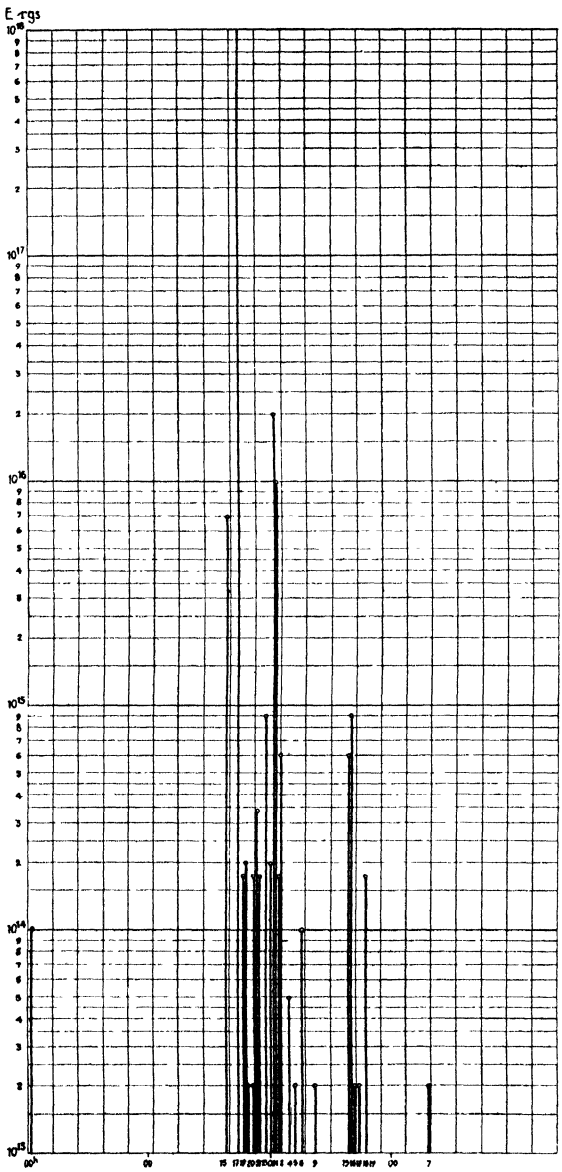

FIG. 7. Earthquakes of 10 to 13 October 1954: energy of main shock, foreshocks and aftershocks.

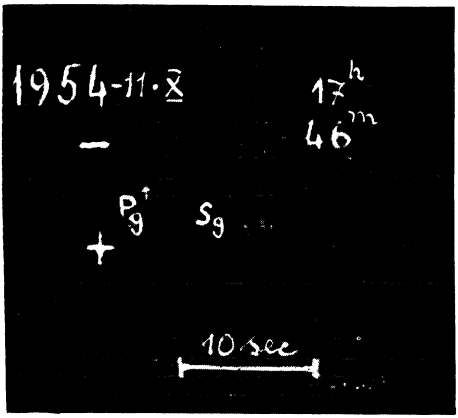

FIG. 8. The record of principal shock at Pieve di Cadore (Δ = 55 km; vertical comp.).

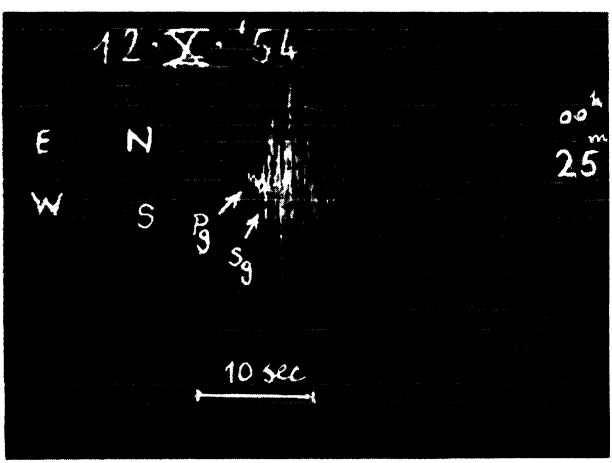

FIG. 9. The main of aftershocks sequence at Tolmezzo (Δ = 10 km; EW comp.).

many think today, but they occur also as suggested by ISHIMOTO, studied by KAWASUMI, and as recently restated with some change by T. MATUZAWA (1953) and K. KASAHARA (1956).

We could also explain the earthquake we are examining clearly in accordance with ISHIMOTO's and KASAHARA's theory, if the beginning at Vienna were a compression. The variation of the apparent vertical which preceded the earthquake would be explained once more by the rising observed in the 'strained region' (Fig. 6(a)), and then proved by the compressions around the epicenter (Fig. 6(b)).

Independent of these considerations, in the case we are examining the connection between slow movements of the earth's crust and seismic activity appears to be intimate and unquestionable. In succession, the tilt north-westward was accentuating as if determined by a pressure of the ground from the slowly rising south-eastern area, while as has been stated above, the first, lightest shocks were being recorded from the seismographs at Tolmezzo. The shocks, which were noted only from the instruments and not by the inhabitants, became increasingly frequent as the stresses increased in the slowly moving zone until the fracturing occurred on 11 October at $17^h\ 45^m$. Then an almost uninterrupted succession of independent small instrumental shocks followed, relieving other stresses in the strata involved in the earthquake. Fig. 2 shows a schematic description of the phenomenon as it occurred. The shocks recorded at Tolmezzo (9 before the principal shock, and 24 in the 36 hr following it) are represented by small circles with radii proportional to the intensity (by a circle of radius 22 mm is represented an energy of about 10^{18} ergs), while two lines marked 'NE' and 'NW' represent the tilt-records synthetized in Fig. 1. Because of the low sensitivity of the seismographs at Tolmezzo, we have to suppose that the real number of potentially recordable shocks preceding and following the principal shock was greater than observed.

It is worth pointing out once more that the seismic activity begins with the accentuation of the slow ground tilt, showed by the tiltmeters. Fig. 7 shows a condensed description of energy spread from these shocks, calculated by the well-known methods. Fig. 8 shows the record of the principal shock obtained at Pieve di Cadore; Fig. 9 the main aftershock at Tolmezzo. The example described is a significant proof of the strict connection between gradual movements of the earth's layers under the action of the stresses working in them

and the sudden faultings (earthquakes) caused by these stresses. Another similar seismic period occurred in this zone a few months previous to the case just described and since the tilt-meters began

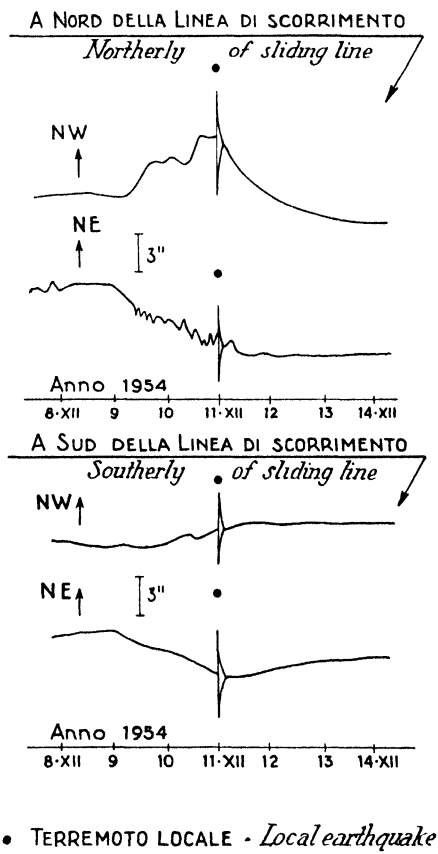

FIG. 10. Tilt records northerly and southerly of sliding surface. After the small local earthquake the northern side of fault slides slowly in the direction of SE.

to work. It appears that in both cases the earthquakes were recorded in the slow initial phase of the deformation. Of course, we don't draw hazardous inferences from this, but we remark the particular interest of the phenomenon.

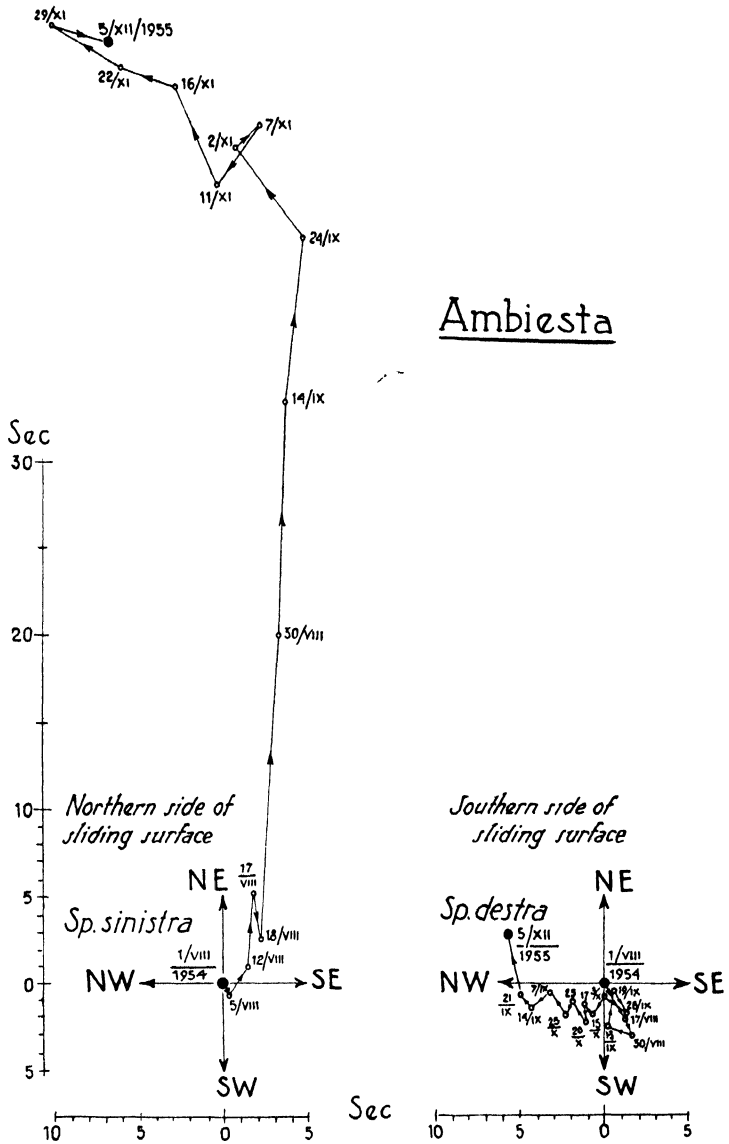

FIG. 11. Tilting movements of opposite side of sliding surface from 1 August 1954 to 5 December 1954.

2

When these slow movements involve the zone near Ambiesta where the tilt-meters work, cases no less significant than those already mentioned can occur. For example, examine what occurred from 8 to 16 December 1954. Especially on the NE border of the breaking line, on either side of which two tilt-stations work, after 9 December an increasing restlessness was observed with quick and irregular deviations superposed on changes respectively in the NE and SE direction. This precedes the local shock occurred in the zone about 13^h of 11 December.

Soon after the shock, the tilt line loses every accidentality, becoming smooth as if the continual working preceding the sudden faulting were finished (Fig. 10). While both of the NE–SW components of tilt are almost parallel, and the SE–NW component operating on the SW side of the fault does not show anything unusual, the SE–NW component on the opposite side of the fault shows a sudden change in direction at the time of the earthquake. There is a noticeable deviation south-eastward during 5 or 6 days, as if the earthquake shock had removed an obstacle opposing motion in that direction.

Sometimes the tilt represents movements of simple uplift of one block, rather than movements of parallel rotation of both blocks along the fault. During the months August and December of 1955 there was a characteristic example (Fig. 11). At this time the seismic station at Tolmezzo recorded a series of small instrumental shocks, an example of which is shown in Fig. 12. In this case, it seems that the energy connected with the changes is much less than in the case of parallel rotation of the two fault blocks.

3

The significance of systematic tilt-records obtained during recent years in the Oriental Alps zone, where some tilt-stations work in chambers inside deep tunnels, is not limited to what has been mentioned above. From the beginning of the work (1948) we obtained records caused by earthquakes with near or distant origin. The records from local earthquakes are similar to those described in Figs. 2 and 10. Resonance phenomena (the tilt-meters have periods of 10–12 sec) are not a sufficient explanation of the remarkable recorded amplitudes of which Fig. 13 is an example. The static

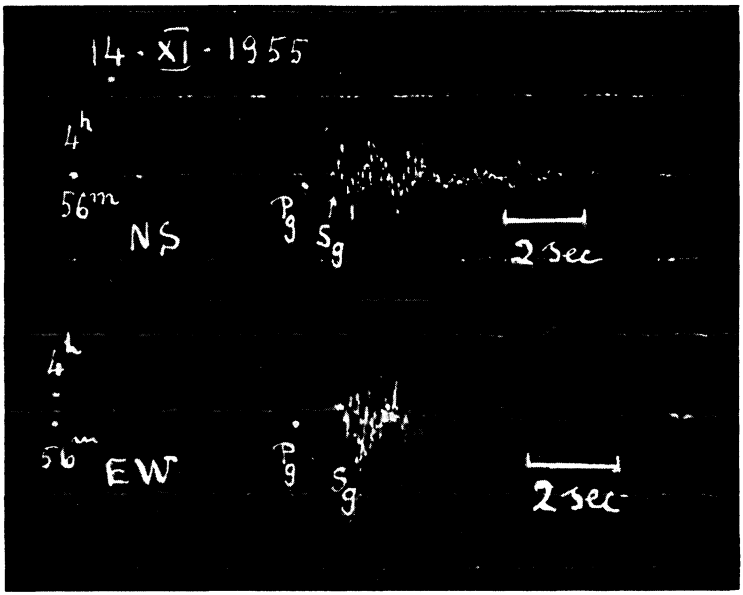

FIG. 12. One of small local shocks at Tolmezzo during October and November 1955.

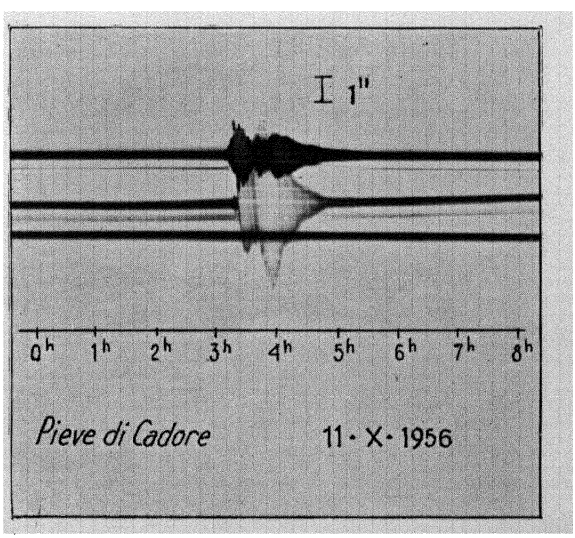

FIG. 13. Tilt-records of Curili earthquake of 11 October 1956, at Pieve di Cadore.

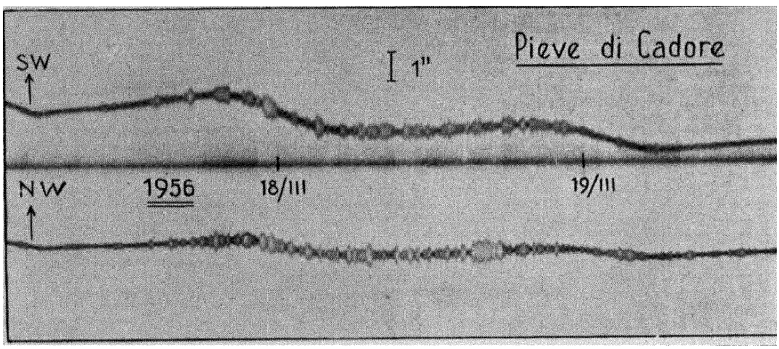

FIG. 15. Tilt-storm at Pieve di Cadore (17 to 20 March 1956).

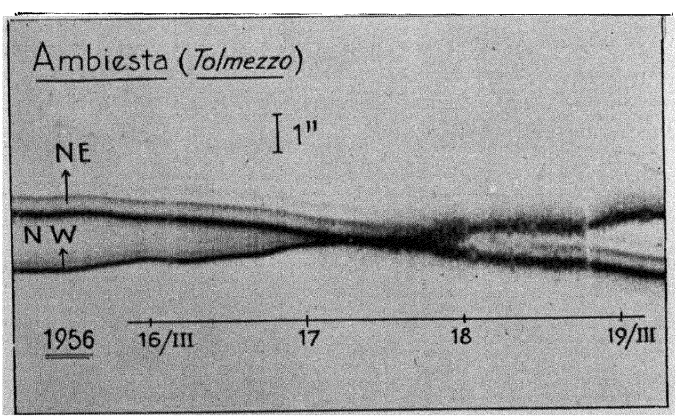

FIG. 16. Tilt-storm at Tolmezzo (17 to 20 March 1956).

magnification of instruments for the displacements involved here is 15 only. There must be some protracted undulatory phenomenon to explain the observations.

Another phenomenon of remarkable interest is recorded periodically from the above-mentioned tilt-stations: that of 'tilt-storms'. This has been mentioned already in a report in 1953 (CALOI, 1953).

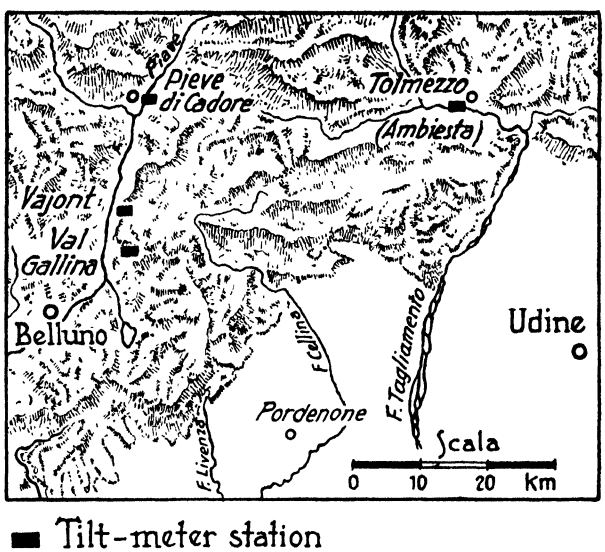

FIG. 14. Tilt-meter stations in Cadore and Carnia.

Suddenly, all stations of the mountain group, with normal climatic and meteorological conditions, begin to record quick oscillations which continue several days with alternate phases. Examine for example the tilt-storm recorded in the Oriental Alps during the second half of March 1956. All the zone included between the extreme tilt-stations (from Pieve valley to Tagliamento valley) is troubled by quick undulatory movements which continue for several days (Figs. 14, 15 and 16). I do not yet know the cause of this phenomenon, but I shall attempt to explain it after further study.

REFERENCES

BULLEN, K. E. (1955) On the size of the strained region prior to an extreme earthquake, *Bull. Seism. Soc. Amer.* **45** (No. 1), Jan.

CALOI, P. (1953) Osservazioni sismiche e clinografiche presso grandi dighe di sbarramento, *Ann. Geofis.* **VI** (No. 3).

—— and SPADEA, M. C. (1955a) Prime indicazioni di registrazioni clinografiche ottenute in una zona ad elevata sismicità, *Ann. Geofis.* **VIII** (No. 1).

—— —— (1955b) Relazioni fra lente variazioni d'inclinazione e moti sismici in zona ad elevata sismicità, *R.C. Accad. Lincei*, series VIII, **XVIII**, March.

ISHIMOTO, M. (1933) La deformation de la croute terrestre et la production des ondes sismiques au foyer, *Bull. Earthq. Res. Inst. Tokyo* **XI**.

KASAHARA, K. (1956) Strain energy in the visco-elastic crust, *Bull. Earthq. Res. Inst.* **XXXIV**, 157.

KAWASUMI, H. (1934) Study on the propagation of seismic waves, *Bull. Earthq. Res. Inst.* **XII**, 690.

MATUZAWA, T. (1953) Feldtheorie der Erdbeben, *Bull. Earthq. Res. Inst.* **XXXI**, 179.

5

ZUR MECHANIK UND DYNAMIK DER ERDBEBEN

WILHELM HILLER

DIE Frage nach der Mechanik und Dynamik der Erdbeben kann man, was das Endziel anbelangt, weitgehend in die geologische Richtung der Erdbebenforschung einreihen. In ihr kann man drei grosse Gesichtspunkte herausstellen, die zugleich auch in grossen Zügen die zeitliche Entwicklung dieser Forschung charakterisieren:

1. Die geographische Verteilung der Hauptbebengebiete

Die Erdbebengeographie hat schon in ihren ersten Entwürfen gezeigt, dass die Hauptbebengebiete an ganz bestimmte Zonen der Erde gebunden sind. Im Laufe der Jahrzehnte wurde dieses Bild bis zum heutigen Tage vervollständigt und verfeinert, wozu einerseits die Erweiterung des Stationsnetzes auf der ganzen Erde samt Steigerung der Empfindlichkeit und Zuverlässigkeit der Beobachtungsinstrumente und andererseits die Einführung der 'Magnitude' durch B. GUTENBERG und C. F. RICHTER beigetragen haben. Das Buch von B. GUTENBERG und C. F. RICHTER über 'Seismicity of the earth and associated phenomena', das heute unentbehrlich in der Hand eines jeden Seismologen ist, enthält den neuesten Stand dieses Zweigs der Erdbebenforschung.

Das Bild der geographischen Verteilung der wichtigsten Erdbebenherde ist allgemein bekannt; darüber soll hier im einzelnen nicht gesprochen werden. Nur auf den einen grossen Gesichtspunkt soll nochmals hingewiesen werden: Die Hauptbebengebiete sind aufs engste gebunden an verhältnismässig junge geologische Grossereignisse, die Entstehung der jungen Faltengebirge und Tiefseegräben. Wir dürfen daraus die Schlussfolgerung ziehen, dass diese jungen Gebilde auch heute noch nicht abgeschlossen sind, sondern dass in ihrem Bereich die alten Kräfte noch weiterwirken, wenn

auch teilweise in abgeschwächtem Masse. Die Bindung der Erdbebenherde an die tektonischen Störungen, die bei der Bildung der Faltengebirge und Tiefseegräben entstanden sind, ist sehr eng. Soweit genügend ins einzelne gehende Beobachtungen vorliegen, kann man feststellen, dass die Bebenherde unmittelbar mit den bekannten tektonischen Störungen zusammenfallen. Dies ist z.B. im südwestdeutschen Erdbebengebiet, wo die Tektonik in der Hauptsache als Folge der Alpenauffaltung entstanden ist und wo bei dem vorhandenen dichten Stationsnetz die Herde der einzelnen Beben mit grosser Genauigkeit bestimmt werden können, ganz streng der Fall.

2. Der mechanische Vorgang im Herd

Wenn man weiss, was bei einem Erdbeben im Herd mechanisch vor sich gegangen ist, so kennt man die Natur des Bebens (tektonisches oder vulkanisches Beben oder Einsturzbeben) und hat damit auch schon zuverlässige Anhaltspunkte für seine Ursache. In seiner eingehenden Monographie 'Die mitteleuropäischen Beben vom 16 November 1911 und vom 20 Juli 1913' hat B. GUTENBERG schon auf die Richtung der ersten Bodenbewegung für die Pg- und die Pn-Welle an den verschiedenen Stationen rings um den Erdbebenherd hingewiesen. Aber erst von etwa 1930 an haben verschiedene Seismologen damit begonnen, aus der azimutalen Verteilung der Richtung der ersten Bodenbewegung (Kompression oder Dilatation) systematisch Schlussfolgerungen auf den mechanischen Vorgang im Herd zu ziehen.

Anfangs wurde diese Methode nur auf herdnah gelegene Beobachtungsstationen (bis etwa 500 km Entfernung) angewendet. Dabei hat man den Vorteil, dass mit der Pg-Welle, die vom Herd aus nach oben abgeht, und mit der Pn-Welle, die vom Herd aus nach unten abgeht, der mechanische Vorgang im Herd vollräumig erfasst wird. Ausserdem ist in diesem Fall die praktische Anwendung der Methode recht übersichtlich und häufig auch recht einfach. Bei einem gewöhnlichen Scherungsbruch gehen in räumlich quadrantenförmiger Anordnung vom Herd Kompressions- und Dilatationswellen ab. Man hat also diese vom Herd ausgehende einfache Anordnung von Kompression und Dilatation nur geometrisch oder modellmässig mit der Erdoberfläche zum Schnitt zu bringen und erhält so je nach der räumlichen Orientierung des Scherungsbruchs

im Herd wechselnde Bilder in der Verteilung von Kompression und Dilatation an der Erdoberfläche. Je nach der räumlichen Orientierung des Scherungsbruchs sind diese Verteilungsbilder an der Erdoberfläche einfach oder aber auch recht verwickelt. Für einen horizontalen Scherungsbruch entlang einer vertikalen bzw. horizontalen Fläche oder für einen vertikalen Scherungsbruch entlang einer vertikalen Fläche ist das Verteilungsbild einfach; recht verwickelt wird es aber für einen beliebig schräg orientierten Scherungsbruch. Bei der praktischen Anwendung dieses Verfahrens ist es am zweckmässigsten, für die wichtigsten Orientierungen eines Scherungsbruchs modellmässig die Verteilungsbilder von Kompression und Dilatation für Pg und Pn abzuleiten und das nach den Seismogrammen gefundene damit zu vergleichen.

Neuerdings wird die Methode mit Erfolg auch auf Fernbeben-Seismogramme (in erster Linie unter Benützung der P-, PcP-, PP- und PKP-Wellen und bei Tiefherdbeben noch zusätzlich der pP- und pPKP-Wellen) angewendet, wobei die Krümmung der Erdoberfläche und die Krümmung der Wellenstrahlen auf ihrem Weg durch das Erdinnere entsprechend berücksichtigt werden müssen. Der mechanische Vorgang im Herd wird aber in diesem Fall nicht ganz so vollräumig erfasst wie aus Nahbebenregistrierungen.

Die weltweite Anwendung dieser Methode auf die verschiedenen Herdgebiete ist augenblicklich noch in vollem Gang, sodass sich ein abschliessendes Bild vorerst noch nicht geben lässt. Soweit aber für einzelne Herdgebiete schon umfangreiche Beobachtungen und Auswertungen vorliegen, kann man feststellen, dass der mechanische Vorgang im Herd weitgehend mit der Tektonik der betreffenden Gegend übereinstimmt. Nicht nur die Lage der Bebenherde (wie im 1. Abschnitt ausgeführt), sondern auch der Herdmechanismus spricht dafür, dass wir die heutigen Erdbeben im grossen und ganzen als eine unveränderte Fortsetzung schon lange im Gang befindlicher tektonischer Vorgänge zu betrachten haben. Für Herdgegenden, deren Tektonik uns noch nicht bekannt ist und sich durch direkte Beobachtungen nur schwierig oder vielleicht überhaupt nicht erschliessen lässt, haben wir durch Ermittlung des mechanischen Vorgangs in den Bebenherden die Möglichkeit, deren Tektonik in grossen Zügen kennenzulernen.

Die Anwendung der Methode der azimutalen Verteilung von Kompression und Dilatation auf mitteltiefe und tiefe Beben (mit

Herdtiefen bis zu etwa 700 km) hat eindeutig gezeigt, dass auch bei diesen Beben scherungsbruchartige Vorgänge im Herd stattfinden, dass also in den Erdgebieten, in denen tiefe Beben auftreten, die tektonischen Störungen sehr tief reichen. In diesen besonders stark gestörten Zonen sammeln sich die gegenseitigen Spannungen rascher an, als sie durch die sicher vorhandene Fliessfähigkeit des Materials ausgeglichen werden können. Die weiteren Studien über den Herdmechanismus bei tiefen Beben werden uns noch aufschlussreiche Einblicke in den Ablauf der Tektonik in den verschiedenen Niveaus von der Erdoberfläche bis zur Tiefe von etwa 700 km geben.

3. Die Verkoppelung von Erdbeben bzw. Herdgebieten im Zusammenhang mit der Dynamik der Erdbeben

In den beiden vorangegangenen Abschnitten wurden in grossen Zügen einige Gedanken über die Mechanik der Erdbeben ausgesprochen. In gewissem Sinn leiten sie aber auch schon zur Frage der Dynamik der Erdbeben über. Kennen wir den Herdmechanismus, so können wir etwas über die lokale oder vielleicht auch regionale Ursache des Bebens aussagen. Offen bleibt aber zunächst immer noch die Frage, woher nun letzten Endes die Kräfte dazu kommen. Diese Frage soll hier in kleinem Ausschnitt und nur von *einer* Seite her beleuchtet werden, nämlich auf Grund der vielfach vermuteten und wohl auch vorhandenen Verkoppelung von Erdbeben.

Jedem Seismologen, der über Jahrzehnte laufend die Seismogramme seiner Stationen auswertet, fällt immer wieder auf, dass der zeitliche Ablauf der seismischen Aktivität sowohl kleinräumig in den einzelnen Herdgebieten als auch grossräumig auf der ganzen Erde nicht gleichmässig erfolgt, sondern dass ruhigere Zeitabschnitte mit lebhafteren abwechseln. Ein regelmässiger periodischer Rhythmus, der klein- oder grossräumig über längere Zeit anhält, ist aber nicht festzustellen und doch scheint ein gewisser Rhythmus vorhanden zu sein. Kleinräumig ist es so, dass in einem gewissen, in sich mehr oder weniger geschlossenen Herdgebiet nach längerer oder kürzerer Ruhe die verschiedenen Einzelherde nacheinander oder sogar hin- und herwechselnd ansprechen. Aehnliches ist grossräumig oder gar für die ganze Erde für die verschiedenen Herdgebiete gelegentlich zu beobachten. Diese Frage der Verkoppelung von

Erdbeben ist in regionaler Ausdehnung schon mehrfach untersucht und dargestellt worden.

Ein Fall interessanter kleinräumiger Verkoppelung war in den Jahren 1933 bis 1936 an den Beben in Südwestdeutschland zu beobachten. In Südwestdeutschland haben wir verschiedene Herdgebiete, die eng an tektonische Störungen gebunden sind: Das in diesem Jahrhundert aktivste Herdgebiet ist die Zollernalb (Ebingen-Balingen-Hechingen) im Bereich des Zollerngrabens und seiner Randstörungen. Südlich davon, in Oberschwaben und im Bereich des Bodensees, liegt ein weiteres Herdgebiet, das mit den zahlreichen dort vorhandenen Verwerfungen und Grabenbrüchen in Zusammenhang steht. Ein ausgedehntes Herdgebiet liegt im ganzen Bereich des Rheintalgrabens, mit Herden im Rheintal zwischen Schwarzwald und Vogesen und mit Herden an den zahlreichen Randstörungen des Schwarzwalds. In den Jahren 1933 bis 1936 ereigneten sich im südwestdeutschen Raum rund 60 Beben. Den Anfang dieser Reihe bildete das Rastatter Beben am 8 Februar 1933 mit zahlreichen schwächeren Nachbeben am gleichen und an den folgenden Tagen. Annähernd die Hälfte der Beben in diesem Zeitraum ging von der Zollernalb aus. Besonders zu erwähnen sind noch die Beben im westlichen Bodenseegebiet am 31 Januar 1935 und an den folgenden Tagen, das Oberschwäbische Beben am 27 Juni 1935 mit einem Nachbeben am 28 Juni und schliesslich ein Doppelbeben im nördlichen Schwarzwald (Gebiet der Hornisgrinde) am 30 Dezember 1935. Der zeitliche Ablauf aller Beben dieser Reihe war so, dass die einzelnen Herdgebiete nicht für sich allein, sondern in häufigem Wechsel hin und her ansprachen. Aehnliches, nur nicht in dieser Häufigkeit und Mannigfaltigkeit, war auch in anderen Zeitabschnitten zu beobachten. Man ersieht daraus ganz deutlich, dass wohl irgendeine kräftemässige Verkoppelung unter den einzelnen Herdgebieten vorhanden ist; welcher Art diese Verkoppelung im einzelnen ist, lässt sich freilich vorläufig noch in keiner Weise sagen, da es sich hier offensichtlich um ein sehr verwickeltes Wechselspiel der Kräfte handelt. Die gegenseitigen Entfernungen zwischen den einzelnen Herdgebieten mit diesem Kräftespiel betragen etwa 60 bis 120 km. Die vertikale Erstreckung des Bandes, in dem dieses Kräftespiel vor sich geht, dürfte wohl etwa von derselben Grössenordnung sein, also rund 100 km, auch wenn die Herdtiefe der einzelnen Beben wesentlich geringer ist (etwa 8–15 km).

Die Verkoppelung der Beben in diesem verhältnismässig kleinen Raum ist auch leicht zu verstehen; denn er ist ein Teilgebiet des ganzen alpinen Raums. Die gemeinsame Ursache für die Tektonik und die heutigen Erdbeben in diesem Raum ist die Alpenauffaltung. Eine Antwort auf die Frage, woher die Kräfte für die Alpenauffaltung kommen, ist damit allerdings nicht gegeben.

Vielleicht erhalten wir aber für diese Frage einen Hinweis aus der grossräumigen Verkoppelung der Erdbeben; denn der grossräumige zeitliche Ablauf der seismischen Aktivität lässt für gewisse Zeitabschnitte ähnliche Zusammenhänge, also Verkoppelung im grossen vermuten. Als bemerkenswertes Beispiel dafür wird der zeitliche Ablauf der seismischen Aktivität auf der ganzen Erde im Zeitabschnitt November 1955 bis Februar 1956 gewählt. Der vorangegangene Monat (Oktober 1955) und der darauffolgende Monat (März 1956) zeigen im wesentlichen dasselbe Bild wie die ausgewählten vier Monate. Zur weitgehenden Ausschaltung von weniger bedeutenden lokalen oder kleinregionalen Einflüssen und Bebenursachen wurden für die Betrachtung nur die starken Beben mit einer Magnitude von 6 und mehr ausgewählt. Die Gesamtzahl der so ausgewählten Beben beträgt für die ganze Erde in diesen vier Monaten 56 Beben, die in der beigegebenen Tabelle nach Datum, Herdzeit H (MGZ) in Stunde und Minute, Herdkoordinaten in geographischer Breite B und Länge L, Herdtiefe h in km (ein Strich bedeutet etwa normale Herdtiefe), Magnitude M und allgemeiner Bezeichnung der Herdlage aufgeführt sind. Die Auswahl der Beben erfolgte nach den 'epicenter cards' des USCGS in Washington und nach den monatlichen Bulletins des Bureau Central International de Séismologie in Strasbourg.

Von diesen 56 Beben hatten 49 ihren Herd im pazifischen Raum; die seismische Aktivität der ganzen Erde hatte sich also in diesen vier Monaten zum weitaus grössten Teil auf den pazifischen Raum konzentriert. Es lag daher nahe, einmal den zeitlichen und räumlichen Ablauf der Aktivität im pazifischen Grossraum während dieser Zeitspanne für sich zu betrachten. Deshalb sind die restlichen 7 Beben, deren Herd ausserhalb dieses Raums liegt, bei den fortlaufenden Bebennummern in der Tabelle nicht mitgezählt. In Abb. 1 sind im oberen Teil die einzelnen Herdlagen mit der entsprechenden Nummer eingetragen (wo eine starke Häufung der Herde vorhanden ist, konnte nicht jeder Herd ganz genau richtig liegend eingezeichnet

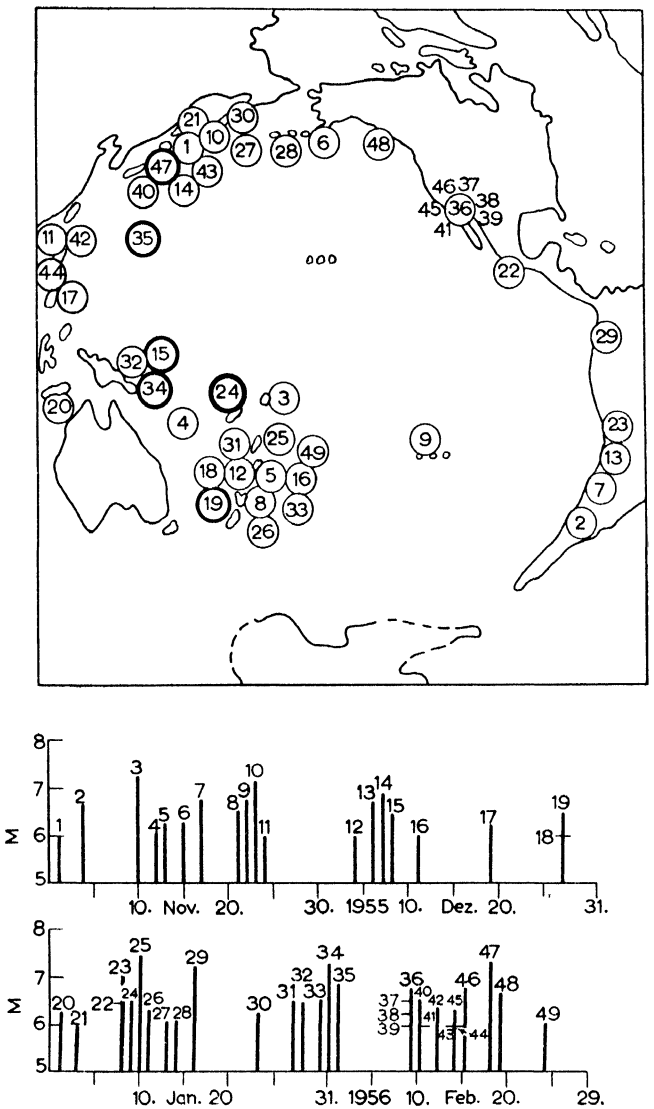

Abb. 1. Zeitlicher und räumlicher Ablauf der seismischen Aktivität (mit Bebenmagnitude $\geqslant 6$) im pazifischen Raum in den Monaten November 1955 bis Februar 1956.

Beben mit Magnitude 6 *und mehr, November* 1955 *bis Februar* 1956

Nr.	Datum	*H*	*B*	*L*	*h* (km)	*M*	Herdlage
			November 1955				
1	1	23 : 46	40 N	144 E	—	6	Nähe der Ostküste von Hondo, Japan
2	4	22 : 44	39 S	69 W	100	6.75	Provinz Mendoza, Argentinien
3	10	01 : 44	15 S	174 W	100	7.25–7.5	Samoa-Inseln
4	12	15 : 45	17 S	167 E	—	ca.6	Gegend der Neuen Hebriden
5	13	23 : 07	33 S	179 W	100	6.25	Gegend der Kermadek-Inseln
6	15	10 : 07	55 N	155 W	—	6.25–6.5	Südküste von Alaska
7	17	06 : 53	26 S	69 W	—	6.75	Nord-Chile
8	21	21 : 04	38 S	178 E	—	6.5	Nähe der Ostküste der Nordinsel von Neu-Seeland
9	22	03 : 24	24 S	123 W	—	6.75	Pazifik, Paumotu-Inseln
10	23	06 : 29	50 N	157 E	—	7–7.25	Südküste von Kamtschatka
11	24	04 : 51	19 N	120 E	—	ca.6	Nähe der Nordküste von Luzon, Philippinen
			Dezember 1955				
12	4	02 : 01	35 S	179 W	—	6	Gegend der Kermadek-Inseln
13	6	04 : 31	20 S	70 W	—	6.75	Nord-Chile
14	7	15 : 03	26 N	142 E	—	6.75–7	Bonin-Inseln
15	8	17 : 36	4 S	152 E	500	ca.6.5	Gegend von Neu-Britannien
16	11	11 : 12	—	—	—	ca.6	Gegend der Kermadek-Inseln
	14	10 : 52	22 N	93 E	—	6.25–6.75	Grenzgebiet von Pakistan und Burma
17	19	03 : 14	8 N	127 E	—	6–6.5	Nähe der Ostküste von Mindanao
18	27	02 : 28	26 S	177 W	200	ca.6	Gegend der Kermadek-Inseln
19	27	17 : 21	32 S	180	400	6.5	Kermadek-Inseln
			Januar 1956				
20	1	23 : 08	7 S	130 E	150	6–6.5	Gegend der Insel Timor
21	3	15 : 41	48 N	155 E	—	6	Kurilen
22	8	07 : 11	17 N	99 W	—	6.5	Mexiko
23	8	20 : 54	19 S	70 W	—	ca.7	Nord-Chile
24	9	12 : 06	23 S	179 E	650	6.5	Fidschi-Inseln
25	10	08 : 52	25 S	176 W	—	7.5	Gegend der Tonga-Inseln
26	11	05 : 40	39 S	175 E	180	6.25	Nordinsel von Neu-Seeland

	11	06 : 10	8 N	94 E	—	6–6.5	Nikobaren
27	13	03 : 28	—	—	—	ca.6	Nähe der Ostküste von Kamtschatka
28	14	14 : 09	51 N	173 W	—	ca.6	Aleuten
29	16	23 : 37	1/2 S	80 W	—	7–7.5	Nähe der Küste von Ecuador
	21	17 : 36	23 N	94 E	—	ca.6	Grenzgebiet von Assam und Burma
30	23	03 : 47	55 N	162 E	—	6–6.5	Nähe der Ostküste von Kamtschatka
31	27	13 : 39	26 S	176 W	—	6–7	Gegend der Tonga-Inseln
32	28	07 : 43	4 S	151 E	100	6.5	Neu-Britannien
33	30	08 : 43	38 S	177 E	—	6–6.75	Nähe der Nordküste der Nordinsel von Neu-Seeland
34	31	09 : 17	4 S	152 E	400	7–7.25	Neu-Irland
			Februar 1956				
35	1	13 : 42	19 N	145 E	350	6.75–7	Marianen
	1	15 : 11	39 N	16 E	200	6–6.25	Tyrrhen. Meer
36	9	14 : 32	32 N	116 W	—	6.75–7	Kalifornien
37	9	15 : 24	32 N	116 W	—	6.5	Kalifornien
38	9	16 : 30	32 N	116 W	—	6.25	Kalifornien
39	9	18 : 49	32 N	116 W	—	6	Kalifornien
40	10	00 : 03	37 N	142 E	—	6.5	Nähe der Küste von Hondo, Japan
41	10	18 : 13	31 N	116 W	—	6	Kalifornien
42	12	11 : 49	19 N	120 E	—	6.25–6.5	Nähe der NW-Küste von Luzon, Philippinen
43	14	00 : 53	35 N	140 E	—	ca.6	Nähe von Tokyo, Japan
44	14	12 : 35	17 N	120 E	—	ca.6	Nähe der Westküste von Luzon, Philippinen
45	14	18 : 33	31 N	116 W	—	6–6.5	Kalifornien
46	15	01 : 20	31 N	116 W	—	6.5–6.75	Kalifornien
47	18	07 : 34	30 N	138 E	450	7.25–7.5	Nähe der Südküste von Hondo, Japan
48	19	02 : 18	52 N	131 W	—	6.5–6.75	Königin Charlotte-Inseln
	20	20 : 31	40 N	30 E	—	5.5–6.5	West-Türkei
49	24	09 : 19	33 S	180	—	ca.6	Gegend der Kermadek-Inseln
	29	20 : 51	24 N	95 E	—	ca.6	Grenzgebiet von Burma und Indien
	29	21 : 26	24 N	95 E	—	ca.6	Grenzgebiet von Burma und Indien

werden). Beben mit Herdtiefen von 300 km und mehr sind durch einen dickeren Kreis gekennzeichnet. Im unteren Teil der Abbildung ist der zeitliche Ablauf zusammen mit der Magnitude M der einzelnen Beben dargestellt. Verfolgt man nun den zeitlichen und räumlichen Ablauf, so erkennt man, dass ein häufiges Springen der einzelnen Herde in oft kurzen Zeitabständen auf grosse Entfernungen vorkommt. Bei dieser vorläufig summarischen und nur grossräumigen Betrachtung werden die wenigen tiefen Beben absichtlich nicht gesondert gewertet. Von den 48 vorkommenden Uebergängen von Herd zu Herd fallen 21 auf Entfernungen, die etwa der Gesamtausdehnung des Pazifiks entsprechen, und 17 auf Entfernungen, die annähernd der halben Ausdehnung des Pazifiks entsprechen.

Man kann nun dieses häufige Hin- und Herspringen der Erdbebenauslösungen im ganzen pazifischen Raum als reinen Zufall ansehen. Wenn aber 38 von 48 Uebergängen, also rund 80%, grossräumig innerhalb verhältnismässig kurzer Zeit stattfinden, so kann man auch vermuten, dass dies mehr als nur ein Zufall ist, dass hier vielmehr eine grossräumige Verkoppelung der Beben über den ganzen pazifischen Raum vorliegt. Dieser Raum entspricht etwa einem Viertel der gesamten Erdoberfläche. Wenn wir annehmen, dass die Verkoppelung der Beben über einen solch grossen Raum tatsächlich vorhanden ist, so zwingt sich uns daraus eine gewisse Schlussfolgerung auf. Man kann sich vorstellen, dass bei kleinräumiger Verkoppelung der Erdbeben die Fortleitung der Kräfte und Spannungen als Kräftespiel in oberflächennahen Schichten von wenigen Hundert Kilometer Dicke stattfindet, das Band mit dem Wechselspiel der Kräfte also nicht besonders dick ist. Wenn aber das Kräftespiel mindestens über ein Viertel der Erdoberfläche gehen soll, so sträubt man sich schon allein gefühlsmässig gegen eine derartige Vorstellung. Vielmehr drängt sich einem der Gedanke auf, dass dann an dem Wechselspiel nicht nur ein Band, sondern ein grösserer Raum beteiligt ist, der beträchtlich in die Tiefe des Erdinnern hineinreicht, also den ganzen Erdmantel oder gar noch den Erdkern umfasst. Dieser Gedanke kann nun gleich in der Weise erweitert werden, dass Erdmantel und Erdkern nicht nur an der Fortleitung der Kräfte beteiligt sind, sondern dass hier die Kräfte überhaupt entstehen. Wir hätten demnach die eigentliche Energiequelle der Erdbeben im tiefen Innern der Erde

zu suchen, wie dies in Abb. 2 für den Zeitabschnitt November 1955 bis Februar 1956 schematisch dargestellt ist.

Wenn diese Vorstellung richtig ist, müssten wir dem Erdinnern noch eine gewisse Dynamik, wohl in Form von langsam verlaufenden Strömungen, zuschreiben. Im allgemeinen betrachtet man

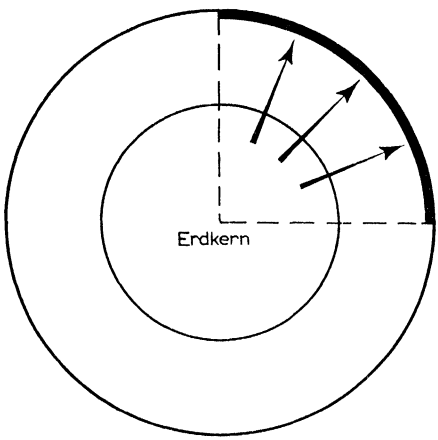

ABB. 2. Schematische Darstellung der Energielieferung aus dem Erdinnern für die in Abb. 1 betrachteten Erdbeben.

ja bisher das Erdinnere als in Ruhe, als vollkommen im Gleichgewichtszustand befindlich. Diese Vorstellung müsste dann etwas abgeändert werden. Für gewisse Betrachtungen und Darstellungen kann die seitherige statische Vorstellung über das Erdinnere auch weiterhin beibehalten werden, so z.B. für die mittlere Verteilung der Dichte, des Drucks und der elastischen Konstanten im Erdinnern. Genau genommen hätten wir aber im Erdinnern langsam wechselndes Gleichgewicht zwischen Schwerkraft und Bewegungskräften, also eine Art stationären Gleichgewichts. Möglicherweise kommen die Kräfte für die Strömungen im Erdinnern aus dem Erdkern, was zur Folge hätte, dass die äussere Begrenzung des Erdkerns ebenfalls in leichter Bewegung ist. Die äussere Begrenzung des Erdkerns würde demnach kleine Unregelmässigkeiten aufweisen, was durch eine Untersuchung, die einer meiner Schüler kürzlich mit Hilfe der am Erdkern reflektierten PcP- und ScS-Wellen durchgeführt hat, im grossen und ganzen bestätigt erscheint. Dazu

sei noch erwähnt, dass seit einigen Jahren auch die Erdmagnetiker zur Erklärung der magnetischen Säkularvariation an derartige Strömungen im tiefen Erdinnern denken.

Die dynamischen Vorgänge, die sich uns an der Erdoberfläche in Form von Tektonik, Gebirgsbildungen, Vulkanismus und Erdbeben offenbaren, dürften also teilweise oder vielleicht zum grössten Teil ihre Ursache und ihre Energiequelle im tiefen Erdinnern haben. In dem oben betrachteten Zeitabschnitt um das Ende des Jahres 1955 und den Anfang des Jahres 1956 konzentrierte sich die seismische Aktivität gerade auf den ganzen pazifischen Raum, was zusammen mit Beobachtungen anderer Art darauf hinweist, dass der Pazifik neben den anderen grossen Ozeanen und den Kontinenten auf der Erde eine gewisse einheitliche Sonderstellung einnimmt. Im Gesamtablauf über lange Zeit beschränken sich die Strömungen im tiefen Erdinnern natürlich nicht nur in der Richtung nach dem Pazifik, sondern finden auch nach anderen Richtungen statt. Man kann sich aber vorstellen, dass in gewissen Zeitabschnitten bald die eine, bald eine andere Richtung bevorzugt wird, um auf diese Weise die Gesamtseismizität der Erde erklären zu können. Es handelt sich dabei ohne Zweifel um sehr verwickelte Wechselbeziehungen zwischen den Kräften und Vorgängen im Erdinnern einerseits und den Erscheinungen an der Erdoberfläche andererseits, in die sicher auch noch zeitliche Verzögerungen eingehen.

Die hier gemachten Ausführungen sollen ein Versuch und ein Hinweis sein, zur Erklärung der Hauptenergiequelle der Erdbeben mit allen Begleiterscheinungen mehr an das tiefe Erdinnere zu denken, als dies seither im allgemeinen getan wird.

6

DIRECTION OF DISPLACEMENT IN WESTERN PACIFIC EARTHQUAKES*

JOHN H. HODGSON

IN AN earlier paper it was shown that fault plane solutions for earthquakes associated with a particular geographic feature have null vectors which lie parallel to the strike of that feature. MCINTYRE and CHRISTIE have suggested that this demands either (1) that the fault strikes be parallel to the feature or (2) that the displacement be perpendicular to the feature.

Solutions based on *P* only are ambiguous. It is shown that, in both the northwest and southwest Pacific, published solutions support MCINTYRE's conclusion but do not select between the two possibilities. KOGAN has produced 21 solutions for earthquakes in the northwest Pacific. These solutions, which have been made available by SCHEIDEGGER, use *S*, and so are unambiguous. In no case do they support possibility (1) above. The displacements tend to be parallel to the northern Marianas; elsewhere they are nearly perpendicular to the associated feature as suggested in (2).

With this as a guide, it is possible to select from the two possible planes obtained in solutions published earlier that which gives displacement most nearly perpendicular to the feature. There is good agreement between the displacements so selected and KOGAN'S solutions. Displacements are inclined to the normals to the geographic features at angles of 15°–30°; the sign of the angle is consistent over most arcs but varies from arc to arc. An exception is the New Hebrides arc, for which the sign of the angle is opposite at the two ends of the arc.

It is concluded that the data support MCINTYRE and that, while possibility (2) is favored, possibility (1) cannot be eliminated, particularly in the southwest Pacific.

Introduction

For the past several years the writer has been applying BYERLY's method to determine the direction of faulting in large earthquakes.

* Published by permission of the Deputy Minister, Department of Mines and Technical Surveys, Ottawa, Canada.

A recent paper (HODGSON, 1957), hereafter referred to as Paper 1, reviewed this program and provided a summary of all solutions carried out by BYERLY's method. These solutions were based on the *P* waves only, so that in each case a pair of planes are defined rather than a single plane, and there is no indication which of these represents the fault. The intersection of these planes is, however, a uniquely defined line which has been called the 'null vector'. It was shown that the null vectors tend to lie parallel to planes having the strike of the associated geographic feature. It was pointed out that this implied a correlation with geology and suggested a high degree of consistency in the method, but no attempt was made to interpret the significance of the null vector.

In a discussion of Paper 1, MCINTYRE and CHRISTIE (1957) suggested that the null vector is identical with an axis widely used by structural geologists—the *B*-kinematic axis. From the known properties of this axis, and from the demonstrated properties of the null vector, McIntyre and Christie argued that either the displacements occurring during faulting should be perpendicular to the associated geographic feature, or that the fault strikes should be parallel to the feature. They regarded the latter as the more probable, and showed that the fault plane solutions in the New Zealand–Kermadec–Tonga arc may best be interpreted to support this conclusion.

Investigation is hampered by the ambiguity of solutions made by BYERLY's method. Fortunately a large volume of Russian fault plane literature has become available in English through the efforts of SCHEIDEGGER (1957), who has reviewed the methods used and has summarized the results in tabular form. The Russians have made extensive use of the *S* phases, which has enabled them to distinguish the fault plane from the auxiliary plane. Most of the Russian studies have dealt with swarms of small earthquakes within the boundaries of the Soviet Union, but one paper (KOGAN, 1954) gives fault plane solutions for a number of large earthquakes in the northwest Pacific. Since these solutions each provide a uniquely defined fault plane, the direction of displacement may be unambiguously determined.

It is the purpose of this paper to examine the direction of the faults and of the displacements in KOGAN's solutions, and to compare these with the directions of the associated geographic features. The results will be used as a guide in analysing displacements in other

available solutions of the western Pacific. The data to be discussed have been obtained from two tables, the first that in which SCHEIDEGGER (1957) summarizes the Russian solutions, the second Table 1 of Paper 1. Both these tables give the amount and direction of dip of the two planes. In the case of the Russian data, it is known which of these represents the auxiliary plane; in the case of Paper 1 a selection must be made. Since the auxiliary plane is, by definition, normal to the displacement, the trend of the displacement may be obtained immediately by reversing the dip direction of the auxiliary plane, and its plunge may be obtained by subtracting the dip of that plane from 90°.

Presentation and discussion of the data

Northwestern Pacific. Russian solutions. The earthquakes for which KOGAN has presented solutions are listed in Table 1, in which

TABLE 1

Earthquakes analysed by Kogan (1954) *as presented by Scheidegger* (1957)

Designation	Date	ϕ	λ	h
		°N	°E	
A	25 May 1950	12.5	142.5	0.01R
B	26 May 1950	18.5	145	0.03R
C	15 Feb. 1948	19	145	0.03R
D	6 Feb. 1948	19.5	146	0.03R
E	5 Jun. 1950	21	143.5	0.04R
F	15 Dec. 1948	22	143	0.03R
G	2 Jan. 1949	22.5	143.5	0.01R
H	13 Jul. 1950	27.5	141	0.08R
I	11 Jul. 1951	28.5	141.5	0.07R
J	16 Apr. 1951	30.5	138.5	0.07R
K	14 Jul. 1949	31	142	0.06R
L	26 Aug. 1948	33	138	0.01R
M	11 Jul. 1949	34	134	0.00R
N	28 May 1952	34	135.5	0.05R
O	21 May 1949	34	140	0.00R
P	4 Mar. 1952	41.5	141.5	0.00R
Q	9 Mar. 1952	41.5	143	0.00R
R	7 Mar. 1952	42	145	0.01R
S	10 Aug. 1951	45.5	143	0.05R
T	23 Feb. 1950	48	148	0.06R
U	23 Mar. 1948	50	157.5	0.03R

they have been assigned letters, A to U. The epicenters have been arranged by latitude, from south to north. Where a number of epicenters have the same latitude they have been arranged by longitude, from west to east.

Not all of KOGAN's solutions have been used. His results were originally presented on a map, in which the strikes and dips of the faults and the directions of displacement were indicated by symbols. The scale of the published map was so small that it was difficult to extract accurate data. As a result, many of the solutions listed by SCHEIDEGGER do not obey the orthogonality criterion, despite the fact that the Russians take account of this requirement in making

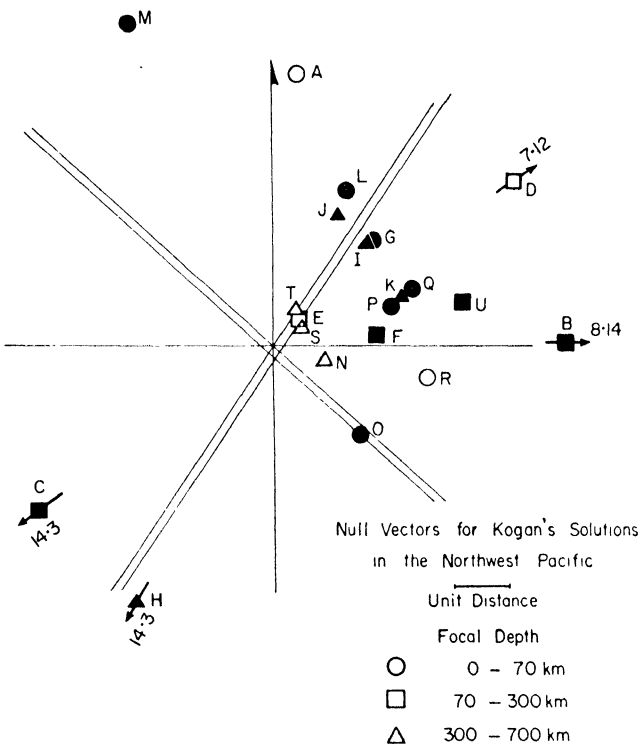

FIG. 1. Null vector diagram for KOGAN's solutions in the northwest Pacific. Open symbols indicate solutions which do not satisfy the orthogonality criterion. The diagonal bands are those defined by the null vectors discussed in Paper 1.

their solutions. Those solutions which fail very badly in this respect have been discarded in the present study.

The null vectors from KOGAN'S solutions have been plotted in Fig. 1, using the projection developed in Paper 1. Solid symbols have been used to indicate solutions which obey the orthogonality criterion satisfactorily, open symbols to indicate those which failed

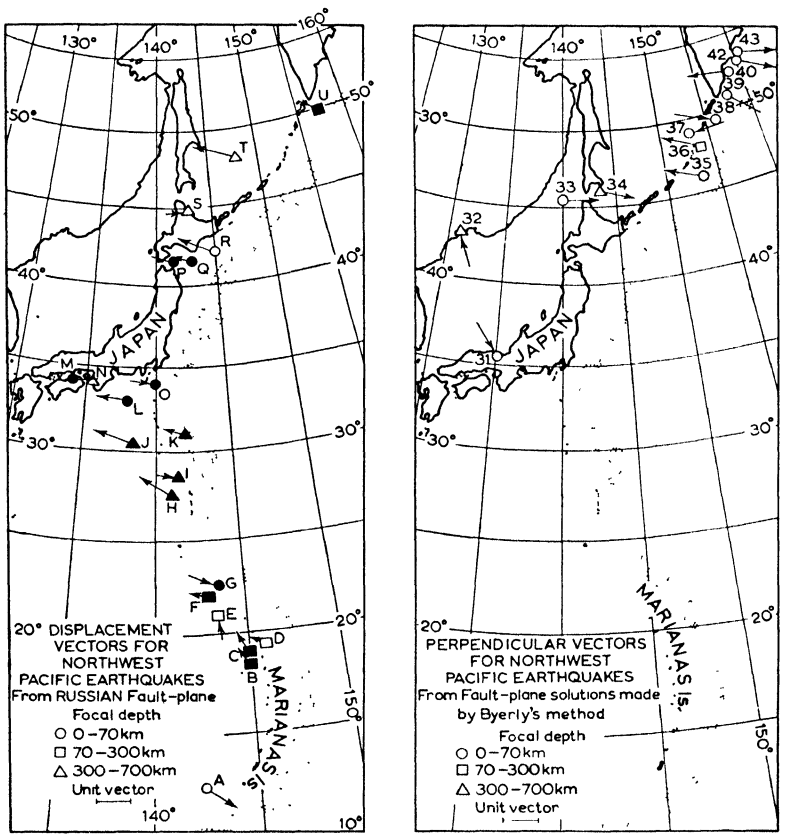

FIG. 2. Displacement directions in the northwest Pacific (a) from KOGAN and (b) from HODGSON. The vectors are the horizontal projections of unit vectors drawn in the direction of displacement and do not represent absolute displacement. They have been drawn on the hanging-wall side of the fault and indicate the direction in which it moved. Shaded areas represent ocean deeps.

to obey the criterion but not so badly as to demand discard. Superimposed on the diagram are the two bands defined by the null vectors listed in Paper 1. Eleven out of thirteen null vectors listed in that earlier study lay within these bands. It is clear that KOGAN's solutions do not adhere to the same pattern, nor indeed to any pattern, except that there is a tendency for the points to cluster in the northeast quadrant. This must not be regarded as a criticism of the Russian solutions, but rather as an indication that the properties of the null vector are open to question. It will be seen later that the Russian solutions do have their own type of self-consistency.

The epicenters for which KOGAN has supplied solutions have been plotted in Fig. 2a. Open and closed symbols have the same meaning here as in Fig. 1. The map gives some indication that in the Marianas the displacements tend to be parallel to the arc, but the data are scarcely sufficient to permit of a firm generalization. In other areas they are nearly perpendicular to the geographic feature. Table 2 provides a more careful examination of this, for it compares the direction of the displacement and the strike direction of the faults with the direction of the normal to the geographic feature. The signs assigned to the angular differences are explained in Fig. 3.

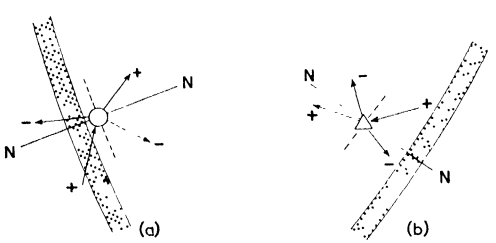

FIG. 3. Two examples, corresponding (a) to a northwest striking arc and (b) to a northeast striking arc, showing how signs have been assigned to the angle between the displacements and the normal. Four possible positions of a displacement vector have been shown in each case and the sign of each has been indicated. A positive sign corresponds to a counter-clockwise rotation from the normal.

The directions listed in Table 2 for the normals to the geographic feature may be open to question in some cases. Their determination is not difficult where the feature is a simple island arc or ocean deep, but it becomes very arbitrary where two arcs intersect. For epicenters

TABLE 2

Direction of displacement and of faulting in the northwest Pacific from Kogan's solutions

(Derived from SCHEIDEGGER 1957)

Earthquake	Direction of normal to geographic feature	Direction of displacement	Difference between displacement and normal to feature	Strike direction of fault	Difference between strike and normal to feature	Fault type
			Epicentres south of the Japanese mainland			
A	N 13° W	S 54° E	+41°	N 36° W	+23°	Dextral strike–slip
B	S 83° W	N 32° W	−65°	N 88° W	− 9°	Thrust
C	S 75° W	N 26° W	−79°	N 54° E	+21°	Gravity
D	S 75° W	N 75° W	−30°	N 55° E	+20°	Gravity
E	S 56° W	S 6° E	+62°	N 13° E	+43°	Sinistral strike–slip
F	S 53° W	N 76° W	−51°	N 89° E	−36°	Gravity
G	S 50° W	N 65° W	−65°	N 57° E	− 7°	Thrust, with strong dextral strike–slip
H	N 89° W	N 57° W	−32°	N 21° E	+70°	Dextral strike–slip
I	S 75° W	N 80° W	−25°	N 54° E	+21°	Thrust, with strong dextral strike–slip
J	S 82° W	N 71° W	−27°	N 70° E	+12°	Sinistral strike–slip
K	S 85° W	N 73° W	−22°	N 76° E	+ 9°	Thrust
L	S 78° W	N 83° W	−19°	N 37° E	+41°	Gravity, with strong sinistral strike–slip
O	S 80° W	N 82° W	−18°	N 52° W	−48°	Thrust
			Japan and the Kuriles			
M	N 24° W	N 81° E	+75°	N 28° W	+ 4°	Dip–slip, sense unknown
N	N 23° W	N 54° W	+31°	N 70° W	+47°	Dextral strike–slip with strong thrust component
P	N 64° W	N 72° W	+ 8°	N 79° E	+37°	Dip–slip, sense unknown
Q	N 62° W	N 71° W	+ 9°	N 75° E	+43°	Gravity
R	N 60° W	N 63° W	+ 3°	N 79° W	+19°	Dip–slip, sense unknown
S	N 42° W	S 88° W	+50°	N 69° E	+69°	Dextral strike–slip
T	N 50° W	N 69° W	+19°	N 85° W	+35°	Sinistral strike–slip
U	N 50° W	N 52° W	+ 2°	N 84° E	+46°	Thrust

M and N, for example, the normal has been taken to the main Japanese islands. These epicenters might very well be associated instead with the chain of small islands stretching south from Japan along longitude 140° E.

The mean angle between the normal and the displacement for the earthquakes of the northern Marianas (epicentres B to G) is $-68° \pm 15°$*. The mean displacement thus makes an angle of 22° with the arc, which confirms the visual observation that it is more nearly tangential than normal to the feature in this area. The single solution at the south end of the Marianas arc suggests displacement perpendicular to the arc, but this earthquake is indicated by an open symbol and the direction must not be depended upon too closely. The fault strikes are inclined to the normal at an average angle of $23° \pm 7°$; this value is obtained by considering only the absolute value of the angle. The algebraic mean direction is inclined to the normal at $+5° \pm 14°$.

On the basis of such data as are available it must be concluded that in the Marianas neither do the faults strike in the direction of the feature, nor are the displacements perpendicular to the feature.

Epicenters H to O (omitting M and N which have been assigned to the Japanese arc) are associated with the Bonins and with that chain of islands running south from the Japanese mainland. For this series the mean angle between the normal and the displacement is $-24° \pm 2°$, the mean angle between the fault strikes and the normals has an absolute value of $34° \pm 12°$, and the algebraic mean of the faults is inclined to the normal at $+18° \pm 19°$. As in the Marianas there is no support for the idea that the fault strikes should be parallel to the feature. The displacement direction has become much more nearly normal to the feature; there is again a negative angle but of a much smaller amount.

Earthquakes M, N, and P to U are associated with the main Japan–Kurile arc. For this arc the mean angle between the normals and the displacement vectors is $+25° \pm 10°$. It is not clear that epicenters M and N should be included with this set; if they are eliminated the angle becomes $+15° \pm 8°$. Here again the displacement is normal rather than tangential to the geographic feature. It may be significant that the angle is consistently positive for this

* The uncertainty is the standard deviation of the mean. This convention will be followed throughout the paper.

section, whereas it was negative for those areas south of the Japanese mainland. The angles between the strike of the faults and the normal all have a positive sign, so that the algebraic and the absolute mean are the same— $+ 38° \pm 8°$. The Japan–Kurile arc provides another case in which the displacements tend to be perpendicular to the feature.

In each of the three areas considered, the mean absolute angle between the fault strikes and the normals had about the same value, the average being 32°. In the two arcs south of the Japanese mainland both positive and negative angles were developed, so that the mean strike direction approached that of the normal; in the Japan–Kurile arc only the positive system was formed.

The relatively small standard deviations of both displacements and strike directions inspire confidence in the Russian results, even though they do not give a null vector symmetry. These results lead to the following conclusions:

(1) In the northern Marianas the displacements are inclined to the arc at small angles; elsewhere the displacements are inclined to the normal to the arc at small angles.

(2) There is a strong indication that the sign of these angles is consistent over an arc.

(3) The strikes of the faults are inclined to the normal at an average angle of 32°. In the Japan–Kurile arc all the fault strikes are inclined in the same direction to the normal; in the other areas considered the fault strikes are inclined both positively and negatively to the normal so that the algebraic mean approaches the normal.

Solutions by Byerly's method. Paper 1 lists thirteen earthquakes in the northwest Pacific for which solutions have been obtained, all of them associated with the Japan–Kurile feature. Each of these solutions presents two possible positions of the fault plane, and, since most of the solutions represent strike–slip faulting on steeply dipping planes, the two planes are approximately at right angles in most cases. Therefore if it is possible in a particular case to select a plane which gives displacement perpendicular to the feature, it would be equally possible to select the other plane of the pair and so obtain displacements parallel to the feature. Indeed, by selecting first a normal displacement and then a tangential one, one might obtain a random system of displacements.

However, if the Russian data may be regarded as sufficient to indicate a general trend, they lead to the selection of that plane which gives displacement most nearly normal to the feature. Displacements so selected have been plotted in Fig. 2b, the identifying numbers being those assigned in Paper 1. The data have been summarized in Table 3. It should be noted in passing that the

TABLE 3

Direction of displacement and of faulting in the northwest Pacific from solutions by Byerly's method

(Selected to give displacement normal to the features)

Earthquake	Direction of normal to geographic feature	Direction of displacement	Difference between displacement and normal to feature	Strike direction of fault	Difference between strike and normal to feature	Fault type
31	N 22° W	N 35° W	+13°	N 29° W	+ 7°	Sinistral strike–slip
32	N 22° W	S 23° E	+ 1°	N 6° W	−16°	Sinistral strike–slip
33	N 49° W	N 89° E	+32°	N 85° W	+36°	Dextral strike–slip
34	N 47° W	S 76° E	+29°	N 67° W	+20°	Dextral strike–slip
35	N 49° W	N 69° W	+20°	N 71° W	+22°	Sinistral strike–slip
36	N 54° W	N 65° W	+11°	N 67° W	+13°	Sinistral strike–slip
37	N 55° W	N 84° E	+41°	N 89° E	+36°	Sinistral strike–slip
38	N 51° W	N 66° W	+15°	N 58° W	+ 7°	Sinistral strike–slip
39	N 51° W	S 43° E	− 8°	N 43° W	− 8°	Dextral strike–slip
40	N 56° W	N 80° W	+24°	N 85° W	+29°	Sinistral strike–slip
41	N 56° W	N 82° E	+42°	N 82° E	+42°	Dextral strike–slip
42	N 52° W	S 52° E	+ 8°	N 54° W	+ 2°	Dextral strike–slip
43	N 55° W	S 74° E	+19°	N 70° W	+15°	Dextral strike–slip

displacement plotted for epicenter 31, the Tango earthquake, was that actually observed. This is additional confirmation that displacement in Japan is normal to the arc.

Table 3 shows that the directions of displacement so selected vary from the direction of the normal to the geographic feature by a mean angle of $+ 20° \pm 4°$. Admitting that the possibility of tangential or random displacement cannot be ruled out, this agrees very well, both in magnitude and sign, with the Russian results. The corresponding fault strikes make an absolute angle with the normal

of 19° ± 4°, and have an algebraic mean direction inclined to the normal at an angle of + 16° ± 6°. This is very nearly the angle made by the displacement, and reflects the fact that, since faulting is principally strike–slip on steeply dipping planes, the fault strike is controlling the direction of displacement.

It will be recalled that the null vector diagram for the northwest Pacific (Fig. 17, Paper 1) suggested two tectonic directions rather than the single one used here. The second direction trended N 48° W and was defined by epicenters 33, 34, 37, 41, and 43. If these epicenters are eliminated from Table 3 the mean displacement from the normal becomes + 10° ± 4°, the absolute angle between the faults and the normal becomes 13° ± 4°, and the algebraic value of this angle is + 7° ± 6°.

The five earthquakes eliminated from Table 3 have been reconsidered in Table 4. Displacements have been selected to be as nearly

TABLE 4

Direction of displacement and of faulting in the northwest Pacific from solutions by Byerly's method

(Selected to give displacement normal to N 48° W)

Earthquake	Normal to direction indicated by null vector diagram	Direction of displacement	Difference between displacement and normal to feature	Strike direction of fault	Difference between strike and normal to feature	Fault type
33	N 42° E	S 5° W	+37°	N 1° W	+41°	Sinistral strike–slip
34	N 42° E	S 24° W	+18°	N 15° E	+27°	Sinistral strike–slip
37	N 42° E	S 1° E	+43°	N 6° W	+48°	Dextral strike–slip
41	N 42° E	S 8° E	+50°	N 9° W	+50°	Sinistral strike–slip
43	N 42° E	S 21° W	+21°	N 17° E	+25°	Sinistral strike–slip

as possible normal to N 48° W. They make an average angle with the normal of + 34° ± 8°. The fault strikes all make a positive angle with the normal, so that their mean absolute and algebraic angles are the same, + 38° ± 8°. The alternative system of faults yields a mean angle to the normal of + 56° ± 8°. All of these angles lie so close to 45° that it is impossible to decide whether they are

normal or parallel to the postulated feature. The data supporting the direction are so few that, in any event, no conclusion is justified.

SCHEIDEGGER (1955) has pointed out that the crustal shortening demanded by most tectonic theories could be readily accomplished by strike-slip faulting if dextral and sinistral faulting occurred about equally so that interfingering could take place. Table 2 lists six faults with strong dextral component, five with strong sinistral component. Table 3 gives five dextral and seven sinistral strike–slip faults. It appears that on the average the two systems are equally well developed.

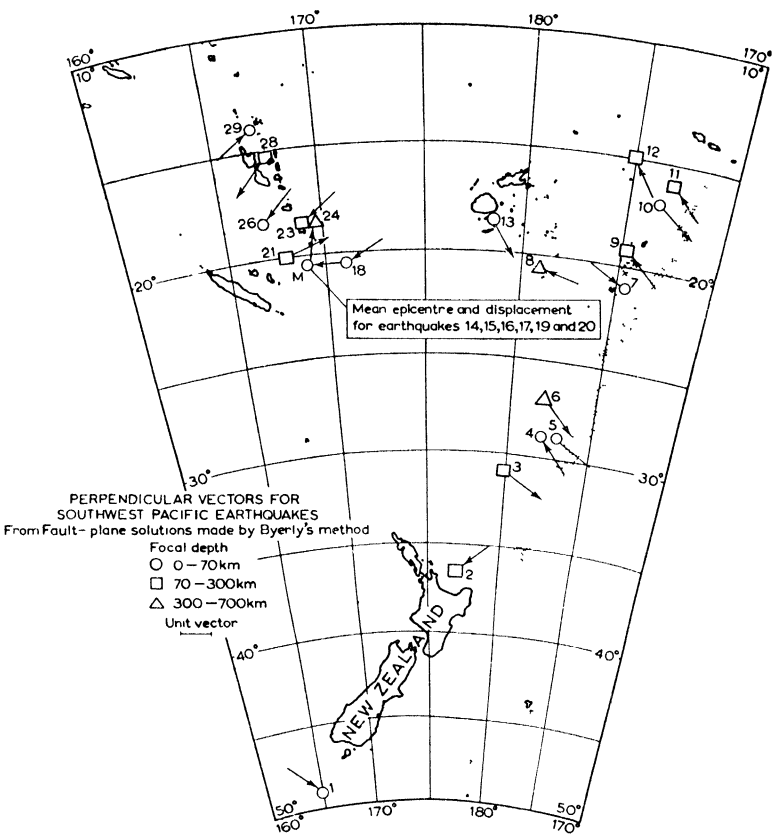

FIG. 4. Displacement directions in the southwest Pacific, selected to be normal to the geographic feature.

Southwestern Pacific. Paper 1 lists twenty-nine earthquakes in the southwest Pacific. Because the Russian work suggests that, while displacement is usually normal to the associated arc, it may be tangential in some instances, and because there is no guide as to which to select in this area, it is necessary to consider both possibilities. This has been done in Figs. 4 and 5, in which the numbers assigned to the earthquakes have been taken from Paper 1. H. W. WELLMAN in a personal communication has suggested to me that the forces on the Northland Peninsula of New Zealand strike northeast while those on the Fiji Islands strike northwest. The normals for earthquakes 2 and 13 have been taken parallel to these directions.

TABLE 5

Direction of displacement and of faulting in the New Zealand–Kermadec–Tonga Sector

(Selected to give displacement normal to the features)

Earthquake	Direction of normal to geographic feature	Direction of displacement	Difference between displacement and normal to feature	Strike direction of fault	Difference between strike and normal to feature	Fault type
			New Zealand			
1	N 41° W	N 47° W	+ 6°	N 46° W	+ 5°	Sinistral strike–slip
			Kermadec Islands			
3	N 69° W	S 57° E	−12°	N 59° W	−10°	Sinistral strike–slip
4	N 70° W	S 41° E	−29°	N 41° W	−29°	Sinistral strike–slip
5	N 72° W	S 57° E	−15°	N 57° W	−15°	Dextral strike–slip
6	N 71° W	S 43° E	−28°	N 43° W	−28°	Dextral strike–slip
			Tonga Islands			
7	N 67° W	N 62° W	− 5°	N 59° W	− 8°	Sinistral strike–slip
8	N 63° W	S 73° E	+10°	N 73° W	+10°	Sinistral strike–slip
9	N 67° W	S 45° E	−22°	N 52° W	−15°	Dextral strike–slip
10	N 73° W	S 53° E	−20°	N 53° W	−20°	Dextral strike–slip
11	N 73° W	S 43° E	−30°	N 42° W	−31°	Sinistral strike–slip
12	N 72° W	S 32° E	−40°	N 32° W	−40°	Dextral strike–slip
			Fiji Islands			
13	N 45° W	S 29° E	−16°	N 29° W	−16°	Dextral strike–slip

Tables 5 and 6 summarize the evidence in Fig. 4, in which the displacements are selected to be normal to the features. In the New Zealand–Kermadec–Tonga sector the mean displacement is inclined to the normal at an angle of $-17° \pm 4°$, the fault strikes make a mean absolute angle with the normal of $19° \pm 3°$, and an algebraic

TABLE 6

Direction of displacement and of faulting in the New Hebrides

(Selected to give displacement normal to the features)

Earthquake	Direction of normal to geographic feature	Direction of displacement	Difference between displacement and normal to feature	Strike direction of fault	Difference between strike and normal to feature	Fault type
			New Zealand			
2	N 54° E	N 54° E	0°	N 54° E	0°	Dextral strike–slip
			New Hebrides			
14	N 68° E	S 87° E	−25°	N 83° W	−29°	Sinistral strike–slip
15	N 68° E	S 59° E	−53°	N 57° W	−55°	Sinistral strike–slip
16	N 68° E	S 88° E	−24°	N 87° W	−25°	Sinistral strike–slip
17	N 68° E	N 87° E	−19°	N 89° E	−21°	Dextral strike–slip
18	N 68° E	N 60° E	+ 8°	N 60° E	+ 8°	Sinistral strike–slip
19	N 68° E	S 80° E	−32°	N 75° W	−37°	Sinistral strike–slip
20	N 68° E	S 80° E	−32°	N 76° W	−36°	Sinistral strike–slip
21	N 68° E	N 72° E	− 4°	N 72° E	− 4°	Dextral strike–slip
22	N 68° E	N 43° E	+25°	N 47° E	+21°	Dextral strike–slip
23	N 68° E	N 50° E	+18°	N 49° E	+19°	Dextral strike–slip
24	N 68° E	S 9° W	+59°	N 17° E	+51°	Sinistral strike–slip
26	N 68° E	N 46° E	+22°	N 45° E	+23°	Dextral strike–slip
28	N 68° E	S 42° W	+26°	N 41° E	+27°	Sinistral strike–slip
29	N 68° E	S 57° W	+11°	N 57° E	+11°	Dextral strike–slip

mean angle of $-16° \pm 5°$. Again it is clear that the strike direction of the faults is controlling the displacements. The faults are equally divided between sinistral and dextral. In the New Hebrides system the situation is more complicated. Seven of the faults indicate dextral faulting, eight sinistral, and the mean angle between the displacement and the normal to the feature is $-1° \pm 8°$. However

this is accomplished by the more southerly earthquakes making negative angles and the more northerly ones making positive angles. The same thing is observed in the angles made by the fault strikes. The mean algebraic value is $-3° \pm 7°$, whereas the mean absolute value is $24° \pm 4°$. This is the first instance in which there has been a change of sign along the arc, and it suggests that the earthquakes at the southern end of the New Hebrides differ in their mechanics from those at the northern end. Despite these anomalies, Tables 5 and 6 would support the hypothesis of displacement normal to the arcs.

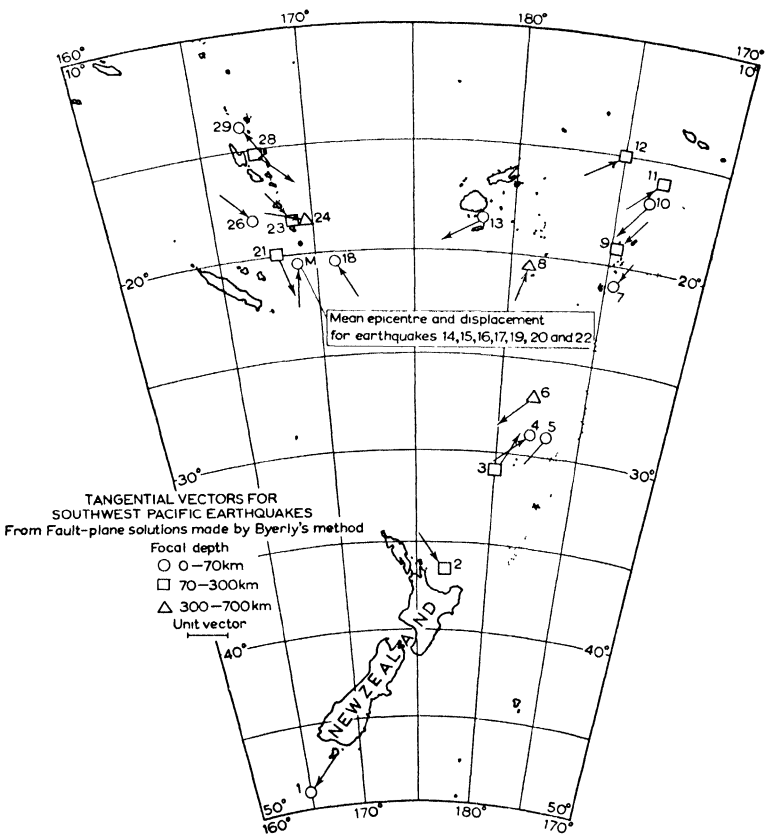

FIG. 5. Displacement directions in the southwest Pacific, selected to be parallel to the geographic feature.

Evidence for the other hypothesis, that displacement is parallel to the arcs, is presented in Tables 7 and 8. Because the displacements are controlled by the fault strikes, these tables may also be used to investigate whether the fault strikes are parallel to the associated features. In the New Zealand–Kermadec–Tonga sector both the

TABLE 7

Direction of displacement and of faulting in the New Zealand–Kermadec–Tonga Sector

(Selected to give displacement parallel to the features)

Earthquake	Direction of normal to geographic feature	Direction of displacement	Difference between displacement and normal to feature	Strike direction of fault	Difference between strike and normal to feature	Fault type
			New Zealand			
1	N 41° W	N 45° E	−86°	N 44° E	−85°	Dextral strike-slip
			Kermadec Islands			
3	N 69° W	N 31° E	+80°	N 33° E	+78°	Dextral strike-slip
4	N 70° W	S 50° W	+60°	N 50° E	+60°	Dextral strike-slip
5	N 72° W	S 33° W	+75°	N 33° E	+75°	Sinistral strike-slip
6	N 71° W	S 48° W	+61°	N 48° E	+61°	Sinistral strike-slip
			Tonga Islands			
7	N 67° W	N 31° E	+82°	N 28° E	+85°	Dextral strike-slip
8	N 63° W	S 17° W	−80°	N 17° E	−80°	Dextral strike-slip
9	N 67° W	N 38° E	+75°	N 45° E	+68°	Sinistral strike-slip
10	N 73° W	S 38° W	+69°	N 38° E	+69°	Sinistral strike-slip
11	N 73° W	S 48° W	+59°	N 47° E	+60°	Dextral strike-slip
12	N 72° W	N 58° E	+50°	N 58° E	+50°	Sinistral strike-slip
			Fiji Islands			
13	N 45° W	S 61° W	+74°	N 61° E	+74°	Sinistral strike-slip

displacements and the fault strikes make the same mean angle, $+ 73° \pm 4°$, with the normal to the arc. This value of displacement is very close, in absolute value, to the angle found by the Russians in the Marianas; parallel displacement must be regarded as a definite possibility. In this case the fault strikes make a mean absolute angle of 20° with the direction of the feature. These are the data already

TABLE 8

Direction of displacement and of faulting in the New Hebrides

(Selected to give displacement parallel to the features)

Earthquake	Direction of normal to geographic feature	Direction of displacement	Difference between displacement and normal to feature	Strike direction of fault	Difference between strike and normal to feature	Fault type
			New Zealand			
2	N 54° E	N 36° W	90°	N 36° W	90°	Sinistral strike–slip
			New Hebrides			
14	N 68° E	S 8° W	+60°	N 4° E	+64°	Dextral strike–slip
15	N 68° E	S 34° W	+34°	N 32° E	+36°	Dextral strike–slip
16	N 68° E	S 4° W	+64°	N 2° E	+66°	Dextral strike–slip
17	N 68° E	S 2° E	+70°	N 4° W	+72°	Sinistral strike–slip
18	N 68° E	S 30° E	−82°	N 30° W	−82°	Dextral strike–slip
19	N 68° E	S 16° W	+52°	N 10° E	+58°	Dextral strike–slip
20	N 68° E	S 15° W	+53°	N 11° E	+57°	Dextral strike–slip
21	N 68° E	S 18° E	+86°	N 18° W	+86°	Sinistral strike–slip
22	N 68° E	S 43° E	−69°	N 43° W	−69°	Sinistral strike–slip
23	N 68° E	N 41° W	−71°	N 40° W	−72°	Sinistral strike–slip
24	N 68° E	N 74° W	−38°	N 81° W	−31°	Dextral strike–slip
26	N 68° E	N 45° W	−67°	N 44° W	−68°	Sinistral strike–slip
28	N 68° E	S 49° E	−63°	N 48° W	−64°	Dextral strike–slip
29	N 68° E	S 33° E	−79°	N 33° W	−79°	Sinistral strike–slip

treated in greater detail by MCINTYRE and CHRISTIE (1957). In the New Hebrides (Table 8), although the mean absolute value of the angle between the displacements and the strike of the feature is 24°, the sign of the displacement is different at the two ends of the arc, so that the mean direction of displacement and of faulting lies within 2° of the direction of the feature. Again this indicates a possibility that the strike directions are parallel to the feature.

Conclusions

The results of this study lend support to MCINTYRE's thesis that, where the null vectors lie parallel to a plane having the strike of the associated geographic feature, either the displacements are perpendicular to the associated feature or the fault strikes are parallel

to it. Only in the northern Marianas does neither of these possibilities apply, and no null vector pattern has yet been found in that area. The Russian solutions show no instances of faults which strike parallel to the associated feature, and, except in the Marianas, do support the idea of displacement perpendicular to the feature. The solutions derived from Paper I may be selected to give consistent results, both in the northwest and in the southwest Pacific, but because of the ambiguity which exists neither of McIntyre's solutions should be ruled out.

The fact that the fault plane results may logically be interpreted to give displacements inclined at small angles to the normal is encouraging to those who feel that island arcs must be the result of forces normal to themselves. It is only necessary to conclude that these forces have usually caused strike-slip faulting, rather than the thrust or gravity faulting that most authorities had anticipated. The small angle between the fault strikes and the postulated force is in agreement with the known properties of strike-slip faulting. The fact that this angle has a consistent sign over most arcs could be interpreted as an indication that only one set of the possible conjugate systems is being developed. Faults on this one system are not uniformly sinistral or dextral, but are about equally divided between the two. This is difficult to explain in terms of failure theory, but it does allow for the necessary amount of crustal shortening.

The concept of displacement and its relation to the normal has been a valuable one. While no final conclusion may yet be drawn the analysis has shown that the fault plane results are not radically inconsistent with other evidence bearing on the problem of island arcs.

REFERENCES

Hodgson, J. H. (1957) Nature of faulting in large earthquakes, *Geol. Soc. Amer. Bull.* **68,** 611–643.

Kogan, S. D. (1954) K voprosu ob izuchenii mekhanizma glubokikh zemletryaseniĭ, *Dokl. Akad. Nauk SSSR* **99**, 385–388.

McIntyre, D. B. and J. M. Christie (1957) Discussion of 'Nature of faulting in large earthquakes', *Geol. Soc. Amer. Bull.* **68,** 645–652.

Scheidegger, A. E. (1955) The physics of orogenesis in the light of new seismological evidence, *Trans. Roy. Soc. Can.*, **49**, Sect. IV, 65–93.

—— (1957) Table of Russian fault plane solutions, *Publ. Dominion Obs.* **19,** 99–109.

7

ON SEISMIC ACTIVITIES IN AND NEAR JAPAN

CHUJI TSUBOI

1

JAPAN and its adjacent areas are noted for their high seismic activities. In the richness of authentic historical documents in the country, dependable earthquake descriptions are abundantly found, of which the oldest dates back to that of A.D. 416. Beginning with this one, nearly 10,000 earthquakes have been put on record, prior to the commencement of routine seismological observations.

Some 420 'destructive' earthquakes are known to have taken place within this area, including those of recent occurrence. Destructiveness is of course not always a good measure of the physical size of an earthquake. There might have been many earthquakes which, in spite of their large size, are not ranked as destructive, because they took place in thinly inhabited areas causing little destruction to be recorded. Also it may very well be that some of the 'destructive' earthquakes were not very large ones actually, and are ranked as such only because they took place in those thickly inhabited areas where there were necessarily some weak establishments to be destroyed by them.

But if we plot the probable epicenters of these 'destructive' earthquakes, largely depending on the historical descriptions concerning the distribution of damages wrought by them, the circumstance stated above is likely to cause no drastic alteration of the general picture of the large earthquake activities which have taken place in this area in the last fifteen centuries.

The epicenters of these historical destructive earthquakes are of course hard to locate, but Fig. 1, which was originally drawn by the late Prof. A. IMAMURA on the basis of his prolonged investigations, will represent an approximate picture of their distribution. In

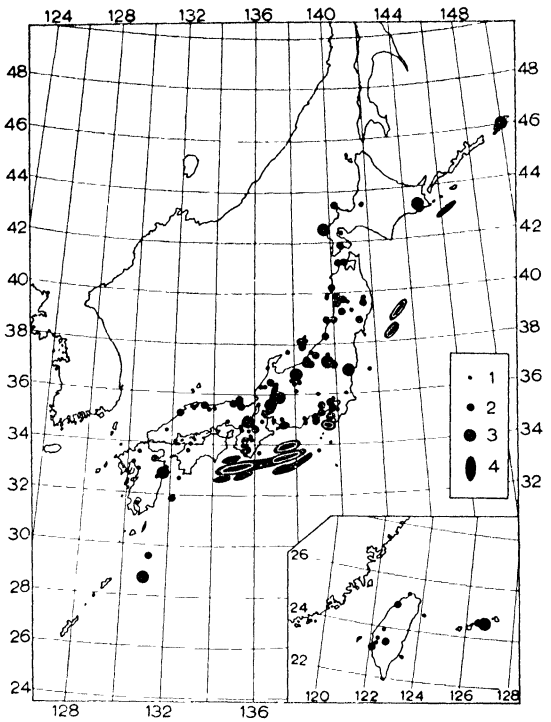

FIG. 1. Epicenters of historical destructive earthquakes in and near Japan.
1. No house completely damaged beyond 20 km from the origin.
2. No house completely damaged beyond 40 km from the origin.
3. No house completely damaged beyond 60 km from the origin.
4. Larger than (3).

drawing this map, IMAMURA classified the earthquakes into four classes (1), (2), (3), and (4) according to their degree of destructiveness as follows:

(1) No house completely damaged beyond 20 km from the origin.
(2) No house completely damaged beyond 40 km from the origin.
(3) No house completely damaged beyond 60 km from the origin.
(4) Larger than (3).

TABLE 1

Magnitudes of historical destructive earthquakes in Japan

Year	Magnitude							
	5.5–6.0	6.1–6.5	6.6–7.0	7.1–7.5	7.6–8.0	8.1–8.5	8.6–9.0	Total
501–600			1					1
601–700			1			1		2
701–800		2	3	1	1			7
801–900		3	6	4	1		2	16
901–1000		1	3					4
1001–1100		4	1			1		6
1101–1200		2		1				3
1201–1300		3	2	1				6
1301–1400		1	4			1		6
1401–1500		4	3	1			1	9
1501–1600		1	7		1			9
1601–1700	3	9	13	7	5	2		39
1701–1800		8	13	5	1	2		29
1801–1900	13	21	14	10	7	4		69
1901–	9	16	14	8	9	5		61
Total	25	75	85	38	25	16	3	267

TABLE 2

Historical destructive earthquakes with magnitudes larger than 8

Year	Month	Day	Magnitude
684	11	29	8.4
869	7	13	8.6
887	8	26	8.6
1096	12	17	8.4
1361	8	3	8.4
1498	9	20	8.6
1611	12	2	8.1
1677	4	13	8.1
1703	12	31	8.2
1707	10	28	8.4
1843	4	25	8.4
1854	12	23	8.4
1854	12	24	8.4
1891	10	28	8.4
1911	6	15	8.2
1933	3	3	8.5
1944	12	7	8.3
1946	12	21	8.1
1952	3	4	8.2

(Japanese Standard Time)

Larger and smaller dots in Fig. 1 correspond to these four classes as indicated in the legend.

By investigating the recorded distributions of damages wrought by these earthquakes, KAWASUMI (1951) elaborately estimated the magnitudes of many of them. Table 1 has been compiled on the basis of his magnitude determinations.

Nineteen earthquakes of which the magnitudes have been estimated by KAWASUMI to be larger than 8.0 are listed in Table 2.

2

Since instrumental routine observations of earthquakes were commenced, the epicenter determination has naturally become more accurate and reliable. Japan Meteorological Agency (formerly Central Meteorological Observatory) is now operating nearly 100 local seismological stations throughout the country and is responsible for routine determination of epicenters. Seismologists in the Agency have been used to classify earthquakes into the following four classes (a), (b), (c), and (d), according as the extent of human perceptibility of the ground motions due to them is:

(a) Larger than 300 km
(b) Between 300 km and 200 km
(c) Between 200 km and 100 km
(d) Smaller than 100 km

from the origins respectively. In some reports, these four classes have been designated as remarkable, rather remarkable, small and local, or conspicuous, rather conspicuous, small and local, respectively, although some insist these are awkward expressions.

The annual numbers of earthquakes belonging to the four classes reported by the Agency are reproduced here in Table 3.

Obviously, this classification of earthquakes into the four classes on the basis of the extent of human perceptibility of the ground motions has its own merits, such as simplicity, abundance of data and so on. The four classes are not uniformly apart, however, in the instrumental magnitude scale, which was introduced comparatively recently by RICHTER (1935) to represent the objective size of an earthquake.

If we plot the logarithms of the earthquake numbers N belonging

to the four classes given in Table 3 against the logarithms of the corresponding limits of perceptibility R, taking 50, 150, 250, and 350 km as their representative values, an almost linear relation is obtained as shown in Fig. 2. This linearity could have been expected from the formulas already deduced by GUTENBERG and RICHTER (1942), for

TABLE 3

Annual numbers of earthquakes belonging to the four classes (a), (b), (c), and (d)

Year	(a)	(b)	(c)	(d)
1923	20	106	—	2660
1924	14	81	129	976
1925	18	60	180	1628
1926	17	36	107	1112
1927	13	51	138	1868
1928	7	22	114	1307
1929	12	20	60	1349
1930	20	31	97	5626
1931	27	25	97	1592
1932	22	22	64	1137
1933	50	40	91	1330
1934	10	12	57	1229
1935	17	23	75	1469
1936	13	12	48	1364
1937	15	21	50	1309
1938	31	36	95	1906
1939	12	17	60	1180
1940	9	16	43	924
1941	10	22	42	1209
1942	12	18	41	1092
1943	22	22	104	2931
1944	20	11	55	1425
1945	22	31	60	804
1946	18	24	79	785
1947	19	29	90	806
1948	26	27	99	1289
1949	18	28	71	733
1950	18	28	73	873
1951	31	18	68	1023
1952	53	56	128	1240
1953	31	59	120	1061
1954	47	35	95	931
1955	38	31	96	912
Total N	712	1070	2726	47080
log N	2.85	3.03	3.44	4.63

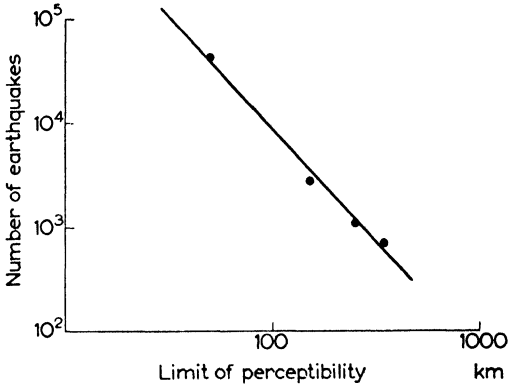

FIG. 2. Number of earthquakes of (a), (b), (c) and (d) classes against the corresponding limits of perceptibility (1923–1955).

they assumed linear relations between log E and log R, log E and M, and M and log N, which when combined will finally lead to a linear relation between log N and log R. M is of course the magnitude and E the energy of an earthquake.

3

In 1951, the present writer (TSUBOI, 1951) derived a formula by means of which the magnitude M of an earthquake can be determined from the maximum ground amplitude due to it and from the epicentral distance of the station at which the amplitude is observed. This formula is useful in that the magnitude can be determined from

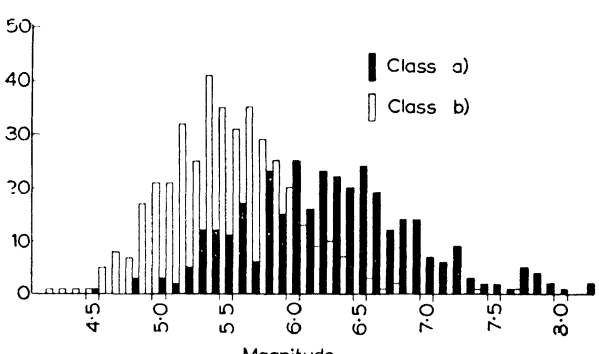

FIG. 3. Number of earthquakes of (a) and (b) classes against their magnitudes.

TABLE 4

Annual numbers of earthquakes according to magnitude

Year	*M*																			
	4.2	4.3	4.4	4.5	4.6	4.7	4.8	4.9	5.0	5.1	5.2	5.3	5.4	5.5	5.6	5.7	5.8	5.9	6.0	6.1	6.2
1931						1		1	4		2	4	6	2	5	2	3	4	2	1	5
1932					1		1	2	2	1	3	2	3	2	4	1	3	2	4	1	3
1933			1		1		1	1	4	2	2	4	2	3	2	1	2	3	3	4	
1934								1	2			2	1	2	1	2	1	2	1	1	2
1935								1			1		2	4	6	2	1	2	1		1
1936								1			4	1	1	3	3			1	1	3	1
1937								1			5	2	1	1	2	2	3	1	2	2	1
1938							1	1	1			1	2	2	4	2	5	6	4	4	4
1939								1			2	1	2	3	1	3	1		1		2
1940												1	2	2	1	2	2	1	1	2	
1941							1	1					4		2	1		3	6	1	2
1942						1				1	2	1	1	1	2	3	4	1		1	
1943						1						1	2	4	4	1	2	3	1	1	6
1944					1	1	1			2				3		3	4	1	3		3
1945							1		4	1	4		2	3	1	5	5	1	2	1	
1946						1		2	1	1	2	2	2	2	4	1	3	3	4		
1947			1	1	1	1	1		2	4	1	1	5	4	1	1	4	1	5	2	
1948				1			3	2		3	3	3	5	3	2	3	5	2	2	2	1
1949						1		1	2	6	5	5	2	1		1	2	1	1		2
1950	1	1			1	1		2	3	2	2	3	5	4	4	5	3	1	1	3	1
Total	1	1	2	2	5	8	10	18	25	23	38	34	50	49	49	41	53	39	45	29	34

M																			Total
6.3	6.4	6.5	6.6	6.7	6.8	6.9	7.0	7.1	7.2	7.3	7.4	7.5	7.6	7.7	7.8	7.9	8.0	8.1	8.2	
1	1	2		1	1	1			1	1				1						52
1	1	1		1	1			1												41
3	3	2	1		1	3		1		1									1	52
3								1												22
4	1	1	3	2	1	1		1	2						1					38
2	1				1										1					24
2	2	2	1	1	2				1								1			35
	6	4	4	1	1	1	1	3	2	1			1	2		1				65
		1	1		1		1		1											22
1	1	1	1			1								1						20
	1	1												1	1					25
1		2		2	2	1														26
3	3	2	5		1						1			1						42
3		1		1		2			1							1				31
1	1	3		1			3		1		2									42
1	2				1	1													1	34
2	1	1	3				1													44
				2	2	1	1					2								48
4			1	1																36
	1	1	1	1	1	1									1					50
32	25	25	21	14	16	13	7	7	9	3	3	2	1	6	4	2	1	0	2	749

observations that are not made by the standard torsion seismometer to which the RICHTER's magnitude scale is originally related. The details of the derivation of the formula will be described later. By means of the formula, the magnitudes of 749 shallow earthquakes of

the classes (a) and (b) which took place in and near Japan during 20 years from 1931 through 1950 have been determined. The annual numbers of earthquakes which belong to the two classes and of which the magnitudes were determined are given in Table 4.

Figure 3 shows graphically how many of the earthquakes in a given magnitude range have been designated as (a) and (b) according to the human perceptibility. Although earthquakes of (a) class are relatively numerous at a little over $M = 6.0$ and those of (b) class at about $M = 5.5$, no sharp boundary can be seen between the distributions of the earthquakes belonging to each of the two classes and the numbers are extremely widely scattered on both sides of the maxima. This shows that the human perceptibility is affected by many other factors than the magnitude.

4

In order to be able to determine the instrumental magnitudes of Japanese earthquakes which are observed by seismographs other than the standard torsion seismometer, a formula is needed in which the magnitude M is expressed in terms of the maximum ground amplitude A observed at a seismological station and of the epicentral

TABLE 5

Values of the constant 'a'

Station	a	Station	a
Nemuro	1.14	Hamamatsu	1.84
Asahikawa	1.37	Matsumoto	1.81
Sapporo	2.04	Wajima	2.22
Urakawa	1.63	Hikone	1.67
Hakodate	1.07	Wakayama	1.56
Aomori	1.62	Shionomisaki	1.74
Morioka	1.59	Toyooka	2.24
Miyako	1.11	Hamada	0.75
Akita	2.47	Hiroshima	1.28
Mizusawa	1.73	Matsuyama	1.40
Sendai	1.02	Murotomisaki	0.78
Yamagata	1.54	Shimizu	0.71
Niigata	1.71	Ooita	0.49
Maebashi	1.76	Fukuoka	1.29
Tsukubasan	1.20	Nagasaki	1.50
Tokyo	1.43	Kumamoto	1.83
Mishima	2.41	Kagoshima	1.50

distance Δ of that station. In 1951, the present writer (TSUBOI, 1951) attempted to deduce a formula for this purpose. Seventy-eight Japanese earthquakes listed in GUTENBERG and RICHTER's *Seismicity of the Earth* were selected, of which the magnitudes had been determined by the authors by their own method. At first the formula:

$$M = a\Delta + \beta \log A + \gamma$$

was assumed; and the constants in it were determined by the least squares method in such a way that, with the values of A and Δ observed at Japanese stations for the seventy-eight earthquakes, the formula will give magnitudes as close as possible to those assigned

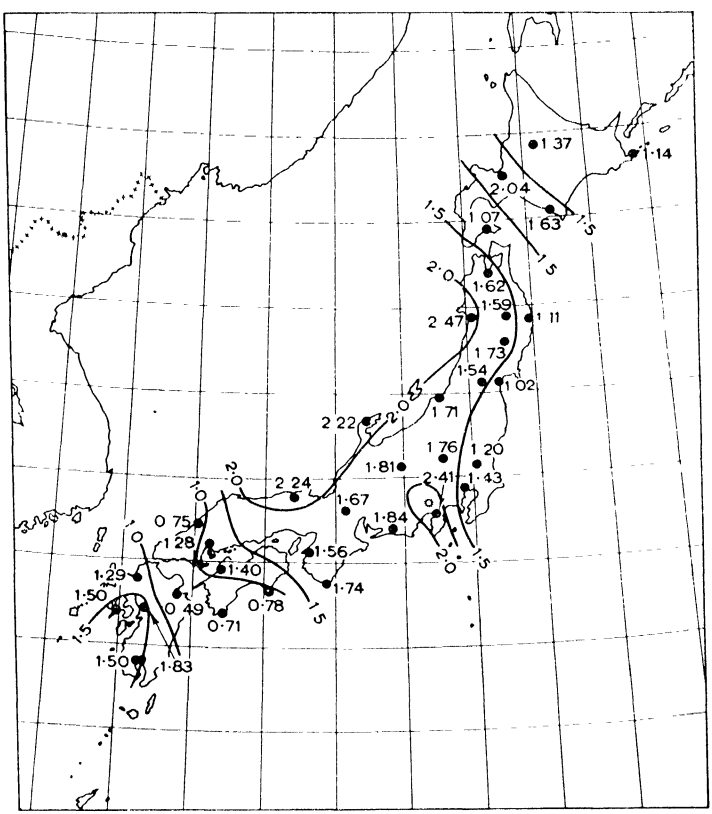

FIG. 4. Geographical distribution of the constant a in the formula $M = a \log \Delta + \log A + c$.

to them by the two authors. Soon it became evident (TSUBOI, 1954) that the formula

$$M = a \log \Delta + \log A + c$$

is better and more reasonable than the first one. The numerical values of the constants of a and c in the formula were determined also by the least squares method for six selected seismological stations in Japan.

HAYATU (1955) extended the study and he determined the numerical values of the constants a and c for 34 Japanese stations. His results are summarized in Table 5, where the epicentral distance Δ is expressed in km and the maximum ground amplitude A in microns. The constant a varies considerably from one station to another, ranging from 2.47 for Akita to 0.49 for Ooita. That the constant a is large in its numerical value for a certain station means that seismic waves approaching that station are more strongly dissipated than those approaching other stations for which a is small. Geographical distribution of the values of this constant which is shown on the map in Fig. 4 appears to be in some way related to the large tectonic structure of the Japanese islands.

5

The relation between the mean annual number of earthquakes in the area in question and their magnitudes was found formerly (TSUBOI, 1952) to be expressed by

$$\log N = -1.33 + 1.01\,(8 - M),$$

the class interval for M being taken as 0.1. But with revised data, the relation has been found to be

$$\log N = -1.08 + 0.71\,(8 - M).$$

It is interesting to compare this formula with the corresponding one for the whole world

$$\log N = -0.48 + 0.90\,(8 - M),$$

which was derived by GUTENBERG and RICHTER (1954). For the magnitude range $M = 8.0 \sim 8.1$, we get $N = 0.083$ for the Japanese area while $N = 0.33$ for the whole world. This will mean that the number of occurrences of earthquakes of this magnitude in the Japanese area is about a quarter of that in the whole world.

Although the formula of this form, giving $\log N$ as a linear function of M, has proved itself to be competent, the present writer is a little sceptical as to its theoretical validity. The reason is that this formula does not permit superposition as it should. That is, if we know

$$\log N = p + qM$$

applies for a certain area and

$$\log N' = p' + q'M$$

for another, and if we combine the two areas together into one set of statistics, $\log (N + N')$ cannot be expressed by a relation which is linear with respect to M any more.

6

Once the magnitudes of earthquakes are determined, the computation of the cumulative sum of released energies is a matter of simple arithmetic. In doing this, however, the final result depends very much upon which formula is used for connecting M and E. Fig. 5 shows the cumulative sum of the released energy with time as calculated by the new formula by GUTENBERG and RICHTER (1956)

$$\log E = 11.8 + 1.5M.$$

The increase of energy with time is beautifully uniform. The final value reached is about 10^{25} ergs in 20 years, so that the annual release of energy is

$$\frac{10^{25}}{20} = 0.5 \times 10^{24} \text{ erg/year.}$$

If the total area concerned is taken to be 3.5×10^{15} cm^2, then the average annual rate of release of energy per unit area will be

$$\frac{10^{25}}{3.5 \times 10^{15} \times 20} = 1.5 \times 10^{8} \text{ erg/cm}^2 \text{ year}.$$

GUTENBERG's value (1956) for the annual release of energy in shallow earthquakes is about 10^{25} ergs for the whole world. As compared with this value, ours for Japan is only one-twentieth of it and appears a little too low. But considering the uncertainties of the numerical

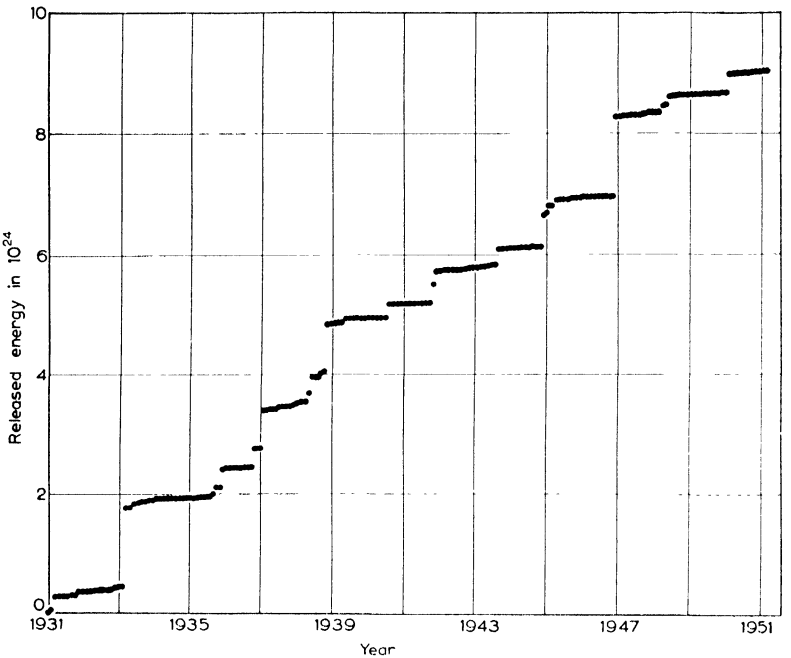

FIG. 5. Cumulative sum of released energy.

values involved in the computations, possibly by a factor 5, perhaps we might be satisfied with this result for the time being (TSUBOI, 1957).

7

In Fig. 6 is shown the epicentral distribution of 3,147 earthquakes which belong to the classes (a) and (b) and which occurred from 1900 through 1950 in the area concerned. In the figure it is to be noted that although Japan is known to be an earthquake country, not

all parts of it are equally active seismically. There are several well-defined areas in which the activity is particularly high as compared with other areas. In these seismic areas, BOUGUER gravity anomalies are conspicuous, whether positive or negative (TSUBOI, 1953–1956).

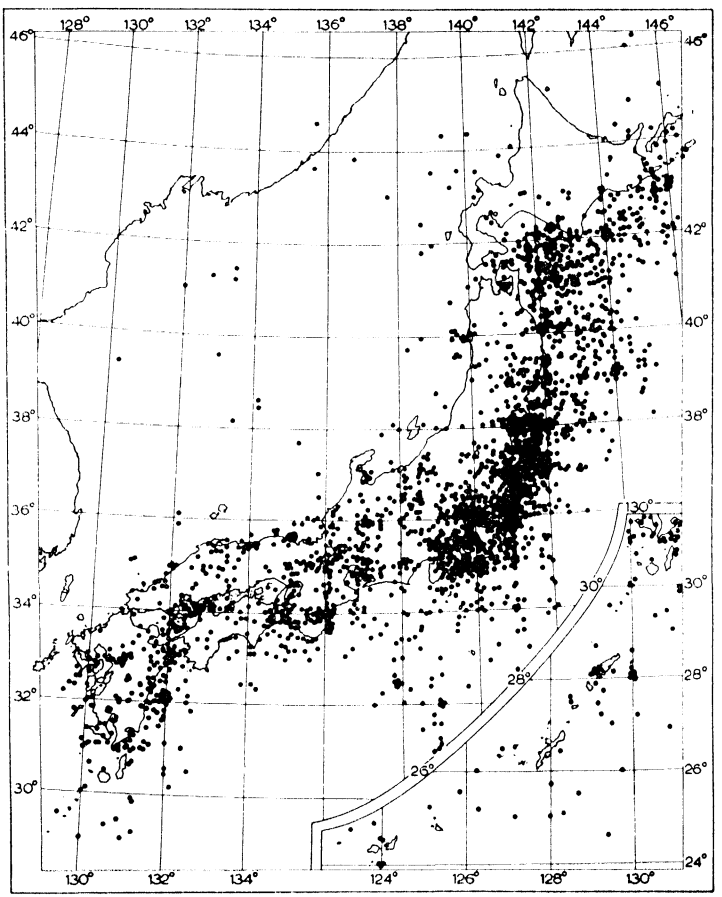

FIG. 6. Distribution of epicenters of 3147 earthquakes of (a) and (b) classes (1900–1950).

It is interesting to compare the two distributions shown in Figs. 1 and 6, the former for the historical destructive earthquakes and the latter for the recent large ones. They show quite different distribution

patterns. More than that, the two distributions may well be said to be nearly complementary, which may have been caused partly by the following circumstance. If an earthquake having the magnitude similar to that of any one of the many large earthquakes off the Pacific coast of northern Japan should have happened on land, it may have caused damage and may have well been ranked as 'destructive'. As already stated, it may well be that some of the 'destructive' earthquakes shown in Fig. 1 are ranked as such not so much because of their size in magnitude as because of their occurrence on land. But the complementarity of the two distributions is so remarkable that the above considerations alone cannot explain it and there is likely something more in it. For instance, in the Pacific offshore area of southwestern Japan which is known to be the site of occurrence of very destructive earthquakes, rather few earthquakes of the classes (a) and (b) have taken place. Also, the area between 39° N-40° N off the Pacific coast of northern Japan is the site of occurrence of very destructive earthquakes such as the one of 1933, but this is exactly the place where the earthquakes of (a) and (b) classes are of relatively less frequent occurrence.

These facts have led the present writer to suspect that the magnitude of an earthquake which occurs at a particular part of an area may be intrinsically determined to a certain extent largely by the mechanical nature of that part of the earth's crust. By the mechanical nature is meant the capacity of that part of the earth's crust for storing stress energy within it which, after the accumulation to a certain critical state, will be released as seismic waves.

There are many reasons for believing that the ultimate strain that the crustal material can reach without breakdown does not differ very much from one part to another and the total energy released in the form of an earthquake is mainly determined by the volume in which it has been stored. Let us call this volume the *earthquake volume*. From this standpoint, the energy E of an earthquake is given by

$$E = \tfrac{1}{2}\mu x^2 V,$$

provided that the whole of the stored energy is released at the time of earthquake occurrence (Tsuboi, 1940). In the formula, μ is the effective elastic constant, x the ultimate strain of the crustal material,

while V is the earthquake volume. μ and x may be taken approximately to be

$$\mu = 5 \times 10^{11} \sim 10^{12} \text{ C.G.S.},$$
$$x = 10^{-4} \sim 2 \times 10^{-4}.$$

This value of x has been derived from the study of the deformation of the earth's crust as disclosed by geodetic measurements, especially by those carried out in epicentral areas of several destructive earthquakes (TSUBOI, 1939). The stress energy $\frac{1}{2}\mu x^2$ that can be stored up in a unit volume of the crustal material will be of the order of $3 \times 10^3 \sim 2 \times 10^4$ ergs. For shallow earthquakes, the volume V cannot extend vertically deeper than the thickness of the earth's crust d, which will be taken approximately as 40–50 km. As to its horizontal extent, the writer has concluded before that it cannot exceed three times the thickness, that is about 120–150 km (TSUBOI, 1939). This conclusion has been reached by the study of regional versus local isostasy. Thus the energy of the largest conceivable earthquake will be

$$\begin{aligned} E &= \tfrac{1}{2}\mu x^2 V \\ &= \tfrac{9}{2}\mu x^2 d^3 \\ &= 1.4 \times 10^{24} \sim 2.3 \times 10^{25} \text{ ergs.} \end{aligned}$$

On the other hand, with the 1955 formula by GUTENBERG and RICHTER

$$\log E = 11.8 + 1.5M$$

and with $M = 8.6$ which is the largest magnitude listed in their book *Seismicity of the Earth*, we get

$$E = 5 \times 10^{24} \text{ ergs},$$

the value being just within the range of our estimated values. BULLEN (1955) states that the volume may reach the order of 500,000 km^3 and this corresponds to the volume in case when the thickness d of the earth's crust is taken to be 38 km in the present writer's model.

In 1954 UTSU and SEKI (1954), on the other hand, studied the relation between the horizontal area A in which aftershocks of a large

earthquake take place and the magnitude of the main shock. Using 30 large Japanese earthquakes as data, they obtained a statistical relation

$$\log A = M + 6.$$

From the assumption of voluminal storage of stress energy in the earth's crust, this relation can very naturally be understood as follows (TSUBOI, 1956). It has already been stated that E is given by

$$E = \tfrac{9}{2}\mu x^2 d^3.$$

If we assume that aftershocks take place only within the earthquake volume of the main shock, and also if we interpret the aftershock area A to be the volume projected on the earth's surface, A may be written as

$$A = 9d^2$$

or

$$d^3 = \tfrac{1}{27}A^{1.5},$$

where d in this case represents the thickness of the earthquake volume, not the thickness of the earth's crust as before. Thus E becomes

$$E = \tfrac{1}{6}\mu x^2 A^{1.5}$$

or

$$\log E = \log(\tfrac{1}{6}\mu x^2) + 1.5 \log A. \tag{1}$$

As already stated, GUTENBERG and RICHTER deduced a formula

$$\log E = 11.8 + 1.5M. \tag{2}$$

Equating $\log E$ in (1) and (2), we get

$$\log A = (M + 5.9) \sim (M + 5.3),$$

and this relation is almost exactly the same as that found by UTSU and SEKI. It is thus very likely that the assumption regarding the voluminal extent of the seismic energy storage is not far from the truth.

8

Statistical studies which follow about the sympathetic occurrences of earthquakes in neighbouring areas also indicate that one continuous

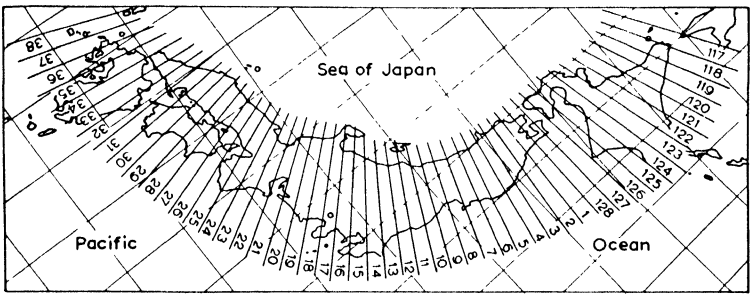

FIG. 7. Division into compartments.

seismic stress field has a certain upper limit in its horizontal extent, so far as Japanese earthquakes are concerned.

The Japanese islands, which are roughly circular in distribution,

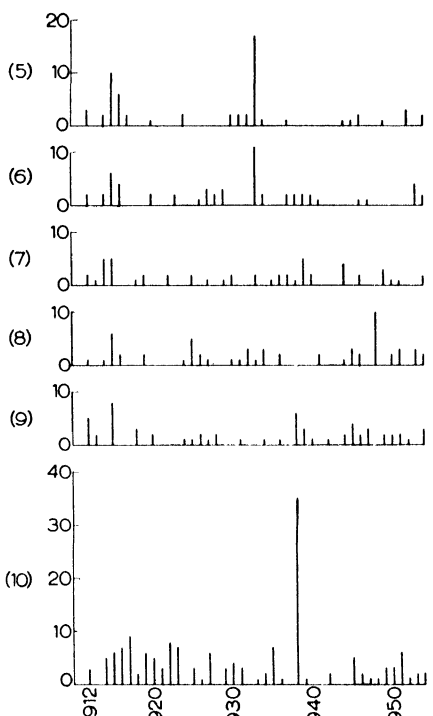

FIG. 8. Number of earthquakes of (a) and (b) classes in the compartments (5), (6), (7), (8), (9), (10).

have been divided into a number of compartments by means of radii radiating from the approximate centre of the circle as shown in Fig. 7. 2π has been divided into 128 equal sectors and each sector has been numbered, starting with (1), which is toward due east, up to (128) in a clockwise sense. Each compartment is 40 km wide along the Japanese islands. In the area concerned, the compartments (122)–(128), (1)–(37) come into question. The annual numbers of earthquakes of the classes (a) and (b) in the compartments have been counted. Table 6 gives the annual numbers of earthquakes

TABLE 6

Annual numbers of earthquakes in the compartments (5), (6), (7), (8), (9) *and* (10)

Year	Compartment						Total
	5	6	7	8	9	10	
1912	3	2	2	1	5	3	16
1913	0	0	1	0	2	0	3
1914	2	2	5	1	0	5	15
1915	10	6	5	6	8	6	41
1916	6	4	0	2	0	7	19
1917	2	0	0	0	0	9	11
1918	0	0	1	0	3	2	6
1919	0	0	2	2	0	6	10
1920	1	2	0	0	2	5	10
1921	0	0	0	0	0	3	3
1922	0	0	2	0	0	8	10
1923	0	2	0	0	0	7	9
1924	2	0	0	1	1	0	4
1925	0	0	2	5	1	3	11
1926	0	1	0	2	2	1	6
1927	0	3	1	1	1	6	12
1928	0	2	0	0	2	0	4
1929	0	3	1	0	0	3	7
1930	2	0	2	1	0	4	9
1931	2	0	0	1	1	3	7
1932	2	0	0	3	0	0	5
1933	17	11	2	1	0	1	32
1934	1	2	0	3	1	2	9
1935	0	0	1	0	0	7	8
1936	0	0	2	2	1	1	6
1937	1	2	2	0	0	0	5
1938	0	2	1	0	6	35	44
1939	0	2	5	0	3	1	11
1940	0	2	2	0	1	0	5

1941	0	1	0	2	0	0	3
1942	0	0	0	0	1	2	3
1943	0	0	0	0	0	0	0
1944	1	0	4	1	2	0	8
1945	1	0	0	3	4	5	13
1946	2	1	2	2	2	2	11
1947	0	1	0	0	3	1	5
1948	0	0	0	10	0	1	11
1949	1	0	3	0	2	3	9
1950	0	0	1	2	2	3	8
1951	0	0	1	3	2	6	12
1952	3	0	0	0	1	1	5
1953	0	4	0	3	0	2	9
1954	2	2	2	2	3	2	13
Total	61	57	52	60	62	156	448

in the compartments (5), (6), (7), (8), (9) and (10), for example. Fig. 8 shows the same thing diagrammatically. Looking at this figure, we notice that the earthquake numbers in the compartments (5) and (6) vary similarly, while those in (5) and (7) vary with less similarity, and those in (5) and (8) still less, until no appreciable similarity in variance can be seen between those in (5) and (10). The correlation coefficients expressing these similarities of seismic activities in the various pairs of compartments are as follows:

Compartment pair	Correlation coefficient
(5) ~ (6)	0.80
(5) ~ (7)	0.25
(5) ~ (8)	0.14
(5) ~ (9)	0.15
(5) ~ (10)	− 0.04

The correlation coefficient is seen to decrease regularly with the distance between the two compartments compared.

The correlation coefficients for all other pairs of the compartments have similarly been computed. If N_m represents the year-to-year numbers of earthquakes in the m-th compartment, the correlation coefficient between N_m and N_{m+1} could be obtained for 43 pairs of adjoining compartments, for there are 44 compartments altogether. The weighted mean of these 43 correlation coefficients will be

TABLE 7

Correlation coefficients of earthquake numbers compared against the distance between the compartments

Distance	Correl. Coef.
0	1.00
1	0.34
2	0.19
3	0.13
4	0.06
5	0.04
6	— 0.02
7	— 0.01
8	— 0.02
9	— 0.06
10	— 0.02
11	— 0.03
12	— 0.04
13	— 0.02
14	0.00
15	0.08
16	0.06
17	0.01
18	0.05
19	0.09
20	0.08
21	— 0.01
22	— 0.05
23	— 0.03
24	0.02
25	0.04
26	— 0.03
27	— 0.04
28	— 0.06
29	— 0.00
30	— 0.00
31	— 0.04
32	0.08
33	— 0.00
34	— 0.05
35	0.03
36	— 0.06
37	— 0.00
38	0.01
39	0.01
40	0.00
41	— 0.06
42	— 0.05
43	0.40

denoted by $r(1)$. Similarly $r(2)$ will represent the weighted mean of the 42 correlation coefficients between N_m and N_{m+2}, $r(3)$ the weighted mean of the 41 correlation coefficients between N_m and N_{m+3}, and so on. In taking the weighted means of the correlation coefficients, the weight proportional to the earthquake numbers involved in the computation was given to each of them. The correlation coefficients r calculated in this way are given in Table 7 and shown in Fig. 9 graphically as a function of the distance between

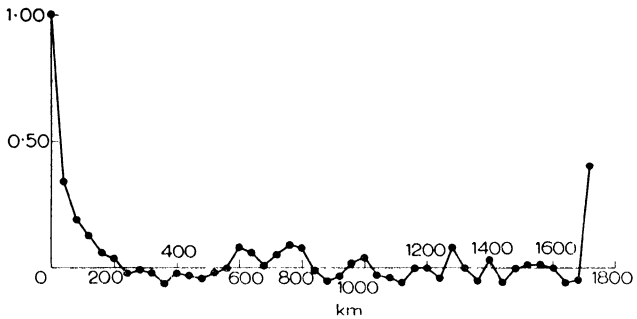

FIG. 9. Correlation coefficient of earthquake numbers against the distance between the compartments compared.

the paired compartments. The coefficient decreases very regularly with the distance until it is almost zero at about the distance of 4 or 5. Since the compartments are each 40 km wide, this means that the similarity in seismic activity sequence in various compartments is appreciable up to the distance of 160–200 km, but not beyond that. This may be taken to be another fact which strongly supports the view that the extent of one continuous earthquake stress field cannot be unlimited (TSUBOI, 1949).

9

Looking into more detail, however, the correlation coefficient is not a function of distance alone. In Fig. 10, $r(1)$ is plotted on a deformed map of Japan at the corresponding locations. It is seen, for example, that the coefficients are high between the compartments (17) and (16), but are almost zero between (17) and (18), although they are equally apart horizontally. This would mean that the earthquake stress field of which the compartment (17) occupies a part

does not extend southward from (17) any further across its boundary with (18), but does extend northward.

In Fig. 11, the correlation coefficients between various pairs of the compartments are shown by symbols at the corresponding positions in a square lattice. Relatively high positive correlation coefficients ($\geqslant 0.3$) are marked by black circles. At several places,

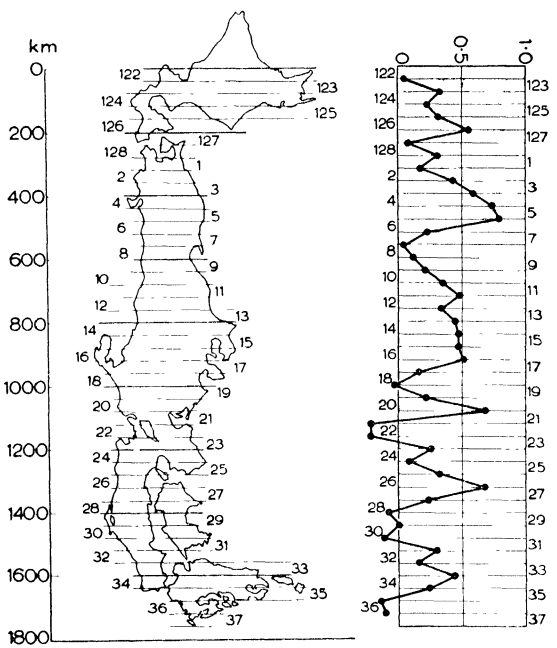

FIG. 10. Geographical distribution of $r(1)$.

black circles are seen to be clustered in square forms as shown diagrammatically in Fig. 12. In this example there must be a certain kind of discontinuity of the seismic field across the boundary between the compartments (o) and (p) and also across that between (t) and (u). The compartments (p), (q), (r), (s), (t) show sympathetic earthquake activity sequence, thus forming what will be called an *earthquake province*. From this standpoint, the following six earthquake provinces may be established in Japan; although one of the six is doubtful.

Earthquake province	Compartments
A	125 126 127
B	2 3 4 5 6
C	11 12 13 14 15 16
D	20 21 doubtful
E	25 26 27
F	31 32 33 34

On the average, the earthquake province is 150 km wide. The grouping into these provinces is not necessarily parallel with that

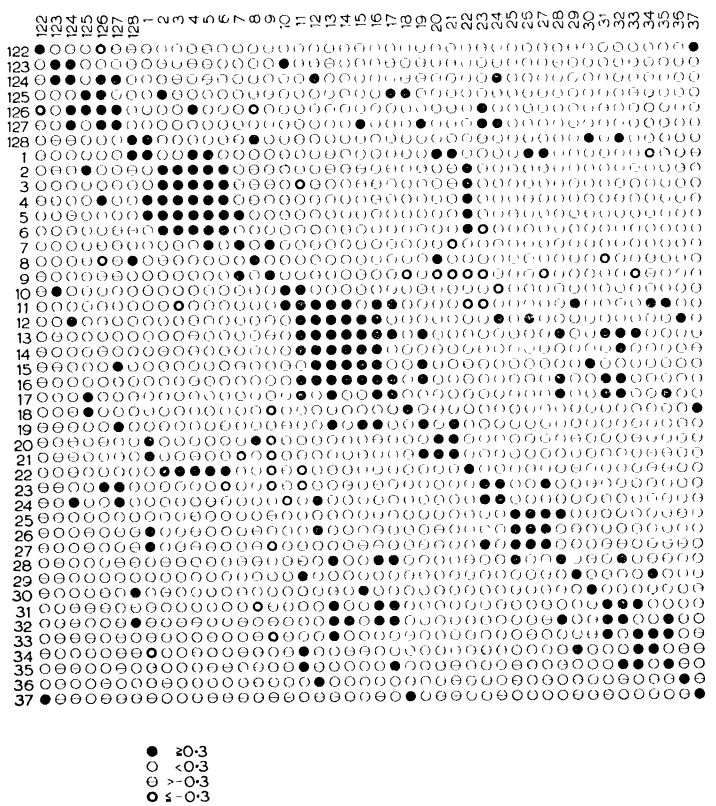

FIG. 11. Diagram of correlation coefficients of earthquake numbers in various compartments.

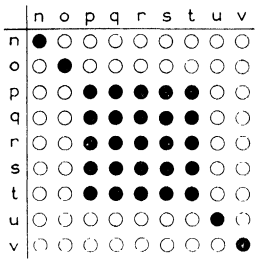

FIG. 12. Diagrammatic distribution of relatively high correlation coefficients.

of the earthquake number itself as will be seen in Fig. 13. Even if several adjoining compartments are similarly high in seismic activities, this does not necessarily mean that these activities are in some way correlated, varying in a similar way.

The mutual correlation coefficients of earthquake numbers in these provinces are very low as Table 8 shows. Therefore it must be

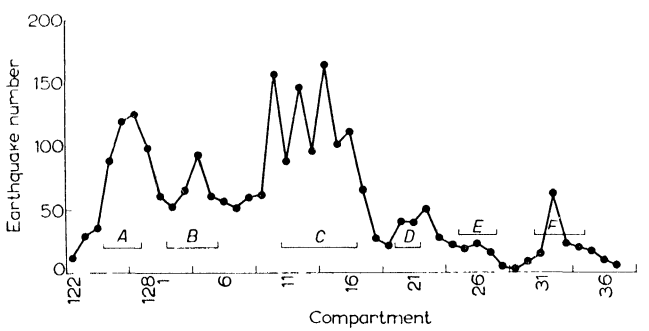

FIG. 13. Earthquake numbers (32 years) in various compartments and earthquake provinces.

TABLE 8

Correlation coefficients of earthquake numbers in various earthquake provinces

	A	B	C	D	E	F
A	1.00	0.16	0.13	− 0.11	− 0.11	− 0.04
B	0.16	1.00	− 0.07	− 0.02	− 0.14	− 0.14
C	0.13	− 0.07	1.00	− 0.05	− 0.08	0.38
D	− 0.11	− 0.02	− 0.05	1.00	0.05	− 0.03
E	− 0.11	− 0.14	− 0.08	0.05	1.00	− 0.11
F	− 0.04	− 0.14	0.38	− 0.03	− 0.11	1.00

concluded that the seismic activities in various earthquake provinces are independent events.

10

Finally a short remark may be added concerning recent studies on very small earthquakes by T. ASADA and his group (ASADA, 1957). They have built electromagnetic seismometers having magnifications of the order of 10^7 at 20–100 c/sec and, by means of these special seismometers, they could record earthquakes having energies as small as about 10^{10} ergs, which corresponds to $M = -1.0$. On the basis of their observations in a certain area, the annual number of occurrences of these very small earthquakes has been estimated to be several thousand times larger than of earthquakes of $M = 4$ or 5 in the same area, and the linear relation

$$\log N = a + b(8 - M)$$

appears to hold good at least down to such a very small M, if not exactly. Also they claim that in those areas in which few of these very small earthquakes could be recorded within the time span of several tens of hours, earthquakes $M \geqslant 5$ have been also very rare. In fact, earthquakes of these magnitudes have taken place once in 10 years or less in the same area. Thus they believe that the frequency of very small earthquakes in a certain area will provide us with good information as to the seismicity in the area at large, even if they are observed for a relatively short duration of time.

REFERENCES

ASADA, T. (1957) Personal communications.

BENIOFF, H., GUTENBERG, B., PRESS, F. and RICHTER, C. F. (1956) Progress Report, Seismological Laboratory, California Institute of Technology, 1955, *Trans. Amer. Geophys. Un.* **37**, 232–238.

BULLEN, K. E. (1955) On the size of the strained region prior to an extreme earthquake, *Bull. Seism. Soc. Amer.* **45**, 43–46.

GUTENBERG, B. (1956) The energy of earthquakes, *Quart. J. Geol. Soc. London* **112**, 1–14.

—— and RICHTER, C. F. (1942) Earthquake magnitude, intensity, energy and acceleration, *Bull. Seism. Soc. Amer.* **32**, 163–191.

—— —— (1954) *Seismicity of the Earth.* Princeton University Press.

HAYATU, A. (1955) On the decay factor of maximum amplitude of earthquake motions (in Japanese), *J. Seism. Soc. Japan* **8**, 75–79.

KAWASUMI, H. (1951) Measures of earthquake danger and expectancy of maximum intensity throughout Japan as inferred from the seismic activity in historical times, *Bull. Earthq. Res. Inst.* **29**, 469–482.

RICHTER, C. F. (1935) An instrumental earthquake magnitude scale, *Bull. Seism. Soc. Amer.* **25**, 1–32.

TSUBOI, C. (1939) Deformation of the earth's crust as disclosed by geodetic measurements, *Erg. d. kos. Physik* **4**, 106–168.

—— (1940) Isostasy and maximum earthquake energy, *Proc. Imp. Acad. Japan* **16**, 449–454.

—— (1951) Determination of the Richter–Gutenberg's instrumental magnitudes of earthquakes occurring in and near Japan, *Geophys. Notes, Tokyo Univ.* **4**, No. 5.

—— (1952) Magnitude-frequency relations for earthquakes in and near Japan, *J. Phys. Earth* **1**, 47–54.

—— (1954) Determination of the Richter–Gutenberg's instrumental magnitudes of earthquakes occurring in and near Japan (in Japanese), *Zishin (J. Seism. Soc. Japan)* **7**, 185–193.

—— (1956) Earthquake energy, earthquake volume, aftershock area, and strength of the earth's crust, *J. Phys. Earth* **4**, 63–66.

—— *et al.* (1939) Relation between the gravity anomalies and the corresponding subterranean mass distribution (IV), *Bull. Earthq. Res. Inst.* **17**, 385–410.

—— *et al.* (1953–1956) Gravity survey along the lines of precise levels throughout Japan by means of a Worden gravimeter, *Bull. Earthq. Res. Inst., Suppl.* **4**, 1–552.

—— (1957) Energy accounts of earthquakes in and near Japan, *J. Phys. Earth* **5**, 1–7.

8

SOLIDITY OF THE INNER CORE

K. E. BULLEN

THIS article is intended as a summary of the present state of evidence on the solidity of the earth's inner core.

The first accurate determination of the mean radius R of the whole core was made by Professor GUTENBERG in 1914. The estimate by JEFFREYS in 1939 gives $R = 3473 \pm 3$ km. The core was shown to be composite when Miss LEHMANN (1936) adduced evidence for the presence of an inner core in interpreting seismic P readings at distances less than 142°. GUTENBERG and RICHTER (1938) supported Miss LEHMANN's proposal with detailed travel-time evidence, and JEFFREYS (1939a) applied AIRY's theory of diffraction near a caustic to refute the hypothesis of diffraction of waves round the outer core boundary as a cause of certain of the readings in question. The matter has been further discussed by SCHOLTE (1956).

A crucial point in Miss LEHMANN's investigation was that the inner core is characterized by values α of the P velocity which markedly exceed the outer core values. This is now a well-accepted feature of the earth's P velocity distribution, although the details of the velocity changes between outer and inner core are not yet known precisely.

Let z denote the depth of a point below the outer core boundary, and r the distance from the earth's centre, so that $z + r = R \approx 3473$ km. In the Jeffreys velocity solution (1939b), α increases fairly steadily from 8.10 km/sec at $r = R$ to 10.44 km/sec at $r = 0.40R$ (≈ 1390 km). Jeffreys found evidence that below this last level, α decreases with z for a range of depth. He *postulated* that α is proportional to r in this range, and was able to fit the travel-time data on this hypothesis on taking the range to be $0.40R > r > 0.36R$. Jeffreys has referred to this calculation as being essentially an 'existence theorem', and has been at pains to point out that, since α

is an indeterminate function of r when $\mathrm{d}\alpha/\mathrm{d}r > \alpha/r$, the solution is not unique. At $r = 0.36R$ ($\approx$ 1250 km), the solution gave a sudden jump in α from 9.47 to 11.16 km/sec. From here downwards, α increases slowly to 11.31 km/sec at the center.

(In a previous paper (1953), the writer used 9.7, in place of 9.47 km/sec, for the lower value of the velocity at $r = 0.36R$. This arose from a misprint (p. 211) in the first edition of his textbook (1947). The value 9.47 km/sec, which is correctly given in the second edition (1953a), is used in the present paper and is responsible for some minor numerical changes from previous work.)

The regions $R > r > 0.40R$, $0.40R > r > 0.36R$, and $0.36R > r \geqslant 0$ have been called by the writer (1942) the regions E, F and G, respectively. The region E is commonly referred to as the outer core, and G as the inner core. In contexts where only a two-layer core is envisaged, it has been the custom to include F as part of the outer core.

The original evidence for the existence of the region F rested on readings of the deep-focus Solomon Islands earthquake of 9 January 1932. JEFFREYS (1942) subsequently found supporting evidence from readings of the Celebes Sea earthquake of 29 June 1934.

In the Gutenberg velocity solution, α increases steadily from 8.0 km/sec at $r = R$ to 10.1 km/sec near $r = 1250$ km. Gutenberg has not found a region resembling F, but considers that, in view of the accompanying uncertainties, the existence of such a region is not precluded. Near $r = 1250$ km, his solution gives a sharp increase in the gradient $\mathrm{d}\alpha/\mathrm{d}z$, the value of α reaching 11.2 km/sec near $r =$ 1100 km. From here to the center, α is nearly constant.

The notation *PKIKP* denotes a phase corresponding to a ray which enters the inner core and is of P type throughout its whole length. The Gutenberg solution gives the type of P velocity variation which deviates from a smooth curve to the least extent that could be compatible with observations of the phase *PKIKP*. The solution differs from the formal Jeffreys solution essentially in showing no negative values of $\mathrm{d}\alpha/\mathrm{d}z$ and no discontinuous jump in α. It gives an increase of 1.1 km/sec in α spread over the range 1250 km $> r >$ 1100 km, as against the sudden increase of 1.7 km/sec at $r = 1250$ km/sec on the Jeffreys solution. With respect to changes in the vicinity of the boundary between the outer and inner core, the two solutions may be taken to represent fairly extreme opposite cases.

In 1946, the writer drew attention to the smallness of the changes of the incompressibility k and its pressure gradient dk/dp across the boundary between mantle and core of his Model A (1947). Taken in conjunction with the experimental data then available, this led to the postulate (1946) that k is a smooth function of pressure throughout the whole earth below a depth of 1000 km. The word 'smooth' is here understood to mean in effect that the curvature of the p–k curve is, at all points, of the same order of magnitude as that say in the interior of the region D' or E.

On both the Gutenberg and Jeffreys solutions, the P velocity in the vicinity of $r = 1250$ km ceases to be a smooth function of pressure in the sense just defined. This is an essential feature of Miss LEHMANN's original work from which the existence of the inner core was first inferred. For present purposes, it is sufficiently accurate to write

$$\alpha^2 = (k + 4\mu/3)/\rho, \tag{1}$$

where μ and ρ denote rigidity and density. By (1), the seismic data therefore imply at least one of k and μ must cease to be a smooth function of p near $r = 1250$ km, since lack of smoothness in ρ cannot cause α or $d\alpha/dz$ to *increase* with the depth.

The Gutenberg solution formally implies (BULLEN, 1953) that $d\alpha^2/dz$ jumps by a factor of order 10 at $r = 1250$ km. It gives an average value of 0.14 km/sec^2 of $d\alpha^2/dz$ in the range 1250 km $> r >$ 1100 km, as against 0.02 km/sec^2 for $r > 1250$ km. By (1), this entails either that dk/dp fluctuates by a factor of at least 7 in this vicinity, or else that there is a significant increase in rigidity. The formal Jeffreys solution implies either that k jumps discontinuously by nearly 40%, or else that there is a discontinuous jump in μ. On the seismic evidence, there is thus no alternative between the existence of drastic departure from smooth variation of k in the core, and the presence of significant rigidity in the inner core.

The writer (1949), following his compressibility hypothesis, selected the second alternative as giving by far the more likely interpretation of the changes in α. His conclusion (1953) was that, in the region $r < 1100$ km, the rigidity is not less than 1.5×10^{12} dyn/cm^2, and may be as high as 4×10^{12} dyn/cm^2 if the Jeffreys trial curve for α is near the truth.

The attempt has been made to reach greater precision by seeking direct seismic evidence on the presence of S waves in the inner core. Theoretical travel-time and amplitude tables were calculated (BULLEN, 1950 and 1951) for a phase $PK\jmath KP$, where $\jmath$ corresponds to S rays in the inner core. The tables were based on the Jeffreys solution for α, in conjunction with the assumed continuity of k throughout the whole core. The computed travel-times are uncertain by the order of a minute (see BULLEN, 1953, for details), because of the uncertainties in the data on α. The calculations give the maximum amplitudes to be expected since they are based on the assumption of first-order discontinuities in α and β (the S velocity) at the inner core boundary. In the event of there being sudden changes in only the gradients of α and β, corresponding to the Gutenberg solution, the actual amplitudes would be much smaller than those computed.

The calculations formally imply that, at any given epicentral distance Δ, the amplitude of $PK\jmath KP$ could be at most one-fifth of that of the comparison phase $PKIKP$. The factor of one-fifth applies when $130° < \Delta < 150°$ (or $210° < \Delta < 230°$), approximately, and the value falls away fairly rapidly on both sides of this range.

At a number of centres, searches have been made for the phase $PK\jmath KP$, the most comprehensive known to the writer being that of BURKE-GAFFNEY (1953). BURKE-GAFFNEY's work made it clear that the number of seismograms which may show the phase is very limited. Several centres have informed the writer of recorded movements which would be compatible with the arrival of the phase. HUTCHINSON (1955), on the other hand, refers to a case where a phase of amplitude one-fifth that of the observed $PKIKP$ should have been readable on a Tucson record, but was not recorded at the expected time for $PK\jmath KP$. The writer (1956) has made a further investigation, however, and it appears that the $PKIKP$ amplitude was freakishly large in this instance, and so does not provide a suitable basis for estimating the $PK\jmath KP$ amplitude; thus the question of the existence of $PK\jmath KP$ is not affected by this case. But the occurrence of such freakish readings of $PKIKP$ makes it clear, conversely, that a small number of apparent observations of $PK\jmath KP$ at the expected times might also be freakish, so that the existence of $PK\jmath KP$ can be established only by a critical statistical analysis of readings from many suitable records.

A further point is the well-known fact that near $\Delta = 142°$, P'

readings often have large amplitudes, and the particular amplitude which belongs to the branch *PKIKP* cannot always be reliably assessed. Thus the anticipated *PKJKP* amplitude is not always predictable in practice from *P'* readings. When direct comparison is made with *PKIKP* amplitudes, the most suitable range of distance to look for *PKJKP* is therefore about $130° < \Delta < 140°$.

The experience which the writer has accumulated to date indicates that *PKJKP* is not normally likely to be detectable except in earthquakes of magnitude 8.0 or more on the Gutenberg–Richter 1954 scale. At the favourable range of distance, the maximum ground amplitude to be expected for *PKJKP* in earthquakes of magnitude 8.0 is about 4μ.

It needs to be repeated that the quoted amplitude calculations have assumed a discontinuous change in α, which is the most favourable boundary condition for the generation of *S* waves in the inner core. If the changes of property between the outer and inner cores are nowhere discontinuous (as for example on the Gutenberg solution), then observable *S* waves in a solid inner core will probably not be excited. Thus even should efforts to find the phase *PKJKP* fail when a sufficient number of suitable cases has been examined, this will in no wise refute the conclusion that the inner core is solid.

There is in fact good supporting evidence for the solidity of the inner core from other sources. JENSEN (1938), FEYNMAN (1949) and others have considered the connection between compressibility, pressure and atomic number for Thomas–Fermi–Dirac matter at pressures beyond 10^7 atm. ELSASSER (1951) sought to construct interpolated curves between these results and data from the experiments of BRIDGMAN at 10^5 atm. ELSASSER'S curves were modified (BULLEN, 1952) by taking account of certain geophysical data, which help to guide the curves through the difficult 'intermediate' pressure range of order 10^6 atm. The curves give k as a function of p for a series of representative atomic numbers Z. They indicate the likely extent of departure inside the whole core from the postulate that k varies smoothly with p, although of course allowance has to be made for some uncertainties in the interpolations.

Should the outer and inner cores be of different composition, the evidence (BULLEN, 1952) makes it unlikely that Z changes by more than 7 units in the transition region where the variation of α is not smooth. For a change of 7 units in Z, the interpolated curves imply

that k changes by not more than 5 per cent as against nearly 40 per cent required on the Jeffreys solution if the inner core is not solid. The possibility of a 5 per cent change in k has been allowed for in assessing the minimum likely value of the rigidity in the inner core as 1.5×10^{12} dyn/cm^2.

If, on the other hand, as many investigators believe, the inner and outer cores are of nearly the same chemical composition, then there is practically no change in the value of Z between them. In that case, it may well be that k is indeed nearly a smooth function of p throughout the core. And it would follow that μ is not less than 2.0×10^{12} dyn/cm^2 in the inner core.

A number of physical explanations for the presence of a solid inner core have been put forward. BIRCH (1940) had suggested that the velocity changes in the central core might be connected with a solid inner core. SIMON (1953) has estimated the melting point of iron at very high pressures, using experimental data on the change of melting point with pressure for substances such as helium which can be examined over a wide range of pressure. On the assumption that the transition between the inner and outer core is from liquid to solid iron, SIMON'S calculations yield a temperature of about 3900°K where the transition occurs.

JACOBS (1953), also assuming a core of fairly constant composition, has suggested that the earth started solidifying at the centre, a solid inner core growing until a curve representing the adiabatic temperature distribution in the earth intersected the melting point curve at two points corresponding to the base of the mantle and the top of the inner core. As the Earth cooled further the mantle would start to solidify from the bottom upward leaving a fluid outer core trapped in between.

The work of JACOBS and SIMON fits together as a satisfactory explanation of the solidity of the inner core if the whole core is composed largely of iron. LUBIMOVA (1956) has also carried out temperature calculations which imply that the inner core is below melting point.

The summary then is that all the available evidence supports the solidity of the inner core in the sense that the inner core is capable of transmitting S waves, should these be excited in it. It will be some time before seismic data on $PKJKP$ can be used as a definite test. If $PKJKP$ can be shown to exist, the solidity of the inner core will be

definitely established. If, on the other hand, the phase fails to be detected in a sufficient number of appropriate cases, then it will follow either that the inner core is not solid, or, more probably, that the transition between outer and inner core is a gradual one. In the meantime, more direct evidence may be forthcoming from considerations of theoretical physics.

REFERENCES

BIRCH, F. (1940) The alpha-gamma transformation of iron at high pressures, and the problem of the Earth's magnetism, *Amer. J. Sci.* **238**, 192–211.

BULLEN, K. E. (1942) The density variation of the Earth's central core, *Bull. Seism. Soc. Amer.* **32**, 19–29.

—— (1946) A hypothesis on compressibility at pressures of the order of a million atmospheres, *Nature* **157**, 405.

—— (1947) *An Introduction to the Theory of Seismology*, 1st ed. Cambridge University Press.

—— (1949) Compressibility-pressure hypothesis and the Earth's interior, *Mon. Not. Roy. Astr. Soc., Geophys. Suppl.* **5**, 355–368.

—— (1950) Theoretical travel-times of *S* waves in the Earth's inner core, *Mon. Not. Roy. Astr. Soc., Geophys. Suppl.* **6**, 125–128.

—— (1951) Theoretical amplitudes of the seismic phase *PKJKP*, *Mon. Not. Roy. Astr. Soc., Geophys. Suppl.* **6**, 163–167.

—— (1952) On density and compressibility at pressures up to thirty million atmospheres, *Mon. Not. Roy. Astr. Soc., Geophys. Suppl.* **6**, 383–401.

—— (1953) The rigidity of the Earth's inner core, *Roma, Ann. Geofis.* **6**, 1–10.

—— (1953a) *An Introduction to the Theory of Seismology*, 2nd ed. Cambridge University Press.

—— (1955) Physical properties of the Earth's core, *Ann. Géophys.* **11**, 5–12.

—— (1954) *Seismology*, Methuen and Co., London.

—— (1956) Note on the phase *PKJKP*, *Bull. Seism. Soc. Amer.* **46**, 333–334.

BURKE-GAFFNEY, T. N. (1953) A search for the phase *PKJKP*, *Bull. Seism. Soc. Amer.* **43**, 331–334.

ELSASSER, W. M. (1951) Quantum-theoretical densities of solids at extreme compression, *Science* **113**, 105–107.

FEYNMAN, R. P., METROPOLIS, N. and TELLER, E. (1949) Equations of state of elements based on the generalized Fermi-Thomas theory, *Phys. Rev.* **75**, 1561–1572.

GUTENBERG, B. (1914) Über Erdbebenwellen, VII A. *Nachr. Ges. Wiss. Göttingen, Math. Phys. Klasse*, 125–176.

—— (1951) *PKKP*, *P'P'* and the Earth's core, *Trans. Amer. Geophys. Un.* **32**, 373–390.

—— and RICHTER, C. F. (1938) *P'* and the Earth's core, *Mon. Not. Roy. Astr. Soc., Geophys. Suppl.* **4**, 363–372.

—— —— (1954) *Seismicity of the Earth*, 2nd ed. Princeton University Press.

HUTCHINSON, R. O. (1955) The core phase *PKJKP*, Earthquake Notes, Eastern Section, *Seism. Soc. Amer.* **36**, 45–46.

JACOBS, J. A. (1953) The Earth's inner core, *Nature* **172**, 297.

JEFFREYS, H. (1939) The times of *PcP* and *ScS*, *Mon. Not. Roy. Astr. Soc., Geophys. Suppl.* **4**, 537–547.

—— (1939a) The times of the core waves, *Mon. Not. Roy. Astr. Soc., Geophys. Suppl.* **4**, 548–561.

—— (1939b) The times of the core waves (second paper), *Mon. Not. Roy. Astr. Soc., Geophys. Suppl.* **4**, 594–615.

—— (1942) The deep earthquake of 1934 June 29, *Mon. Not. Roy. Astr. Soc., Geophys. Suppl.* **5**, 33–36.

—— (1952) *The Earth*, 3rd ed. Cambridge University Press.

JENSEN, H. (1938) Das Druck-Dichte Diagramm der Elemente bei höheren Drucken am Temperaturnullpunkt, *Z. Physik* **111**, 373–385.

LEHMANN, I. (1936) *P′*, *Publ. Bur. Centr. Séism. Internat.*, série A, **14**, 3–31.

LUBIMOVA, E. (1956) *C.R. Acad. Sci. U.S.S.R.* **1**, 107.

SCHOLTE, J. G. J. (1956) On seismic waves in a spherical Earth, *Konink. Ned. Meteorol. Inst.* **65**, 1–55.

SIMON, F. E. (1953) The melting of iron at high pressures, *Nature* **172**, 746.

9

ON PHASES IN EARTHQUAKE RECORDS AT EPICENTRAL DISTANCES OF 105° TO 115°

I. LEHMANN

MANY phases can be distinguished in earthquake records obtained at epicentral distances between 105° and 115°. Fig. 1 shows characteristic records as obtained on Galitzin–Wilip instruments at Scoresby-Sund at an epicentral distance of 108°. *P* and *P'* are small, but all the other phases marked in the records are quite large and conspicuous. *PP*, *SKS* and *PS* rise from relatively small background movement and have well defined onsets. *PPP* and *PPS* are in one or two of the records well separated from the preceding phases, but the onsets of *SKKS*, *S*, *SS* and *SSS* are masked by the movement that precedes them. There are other phases due at these distances. Of these *PKKP* should be mentioned, but it is not well recorded on long-period seismographs.

The phases *P* and *S* have been considered in an earlier investigation (LEHMANN, 1953). Here we shall deal chiefly with the phases *PP*, *SKS* and *PS* the arrival times of which are usually observable with greater precision than those of the others. Tables of travel times for them were constructed by GUTENBERG and RICHTER (1934, 1939) and by JEFFREYS and BULLEN (1940). Both sets of tables rest on a great number of earthquake data. GUTENBERG and RICHTER constructed time-curves for all the phases directly from observation, but for the Jeffreys–Bullen (J–B) tables the travel times of the reflected waves were calculated from the empirically determined times of the direct waves.

Since these tables were constructed, a great many, and in part, better data have accumulated in the International Seismological Summary (I.S.S.) and we shall here compare some recent data with

them. We shall use only series of observations of the three phases and no isolated observations. It is found that large earthquakes in the Celebes region, No. 23 (GUTENBERG and RICHTER, 1954) yield series containing numerous observations; European as well as North American observatories are at the required distances. Useful series are also obtained from the adjacent regions 22 and 16 and smaller series from regions 12–15. The South American region 8 and the Southern Antilles region 10 yield good series.

In the latest issues of the I.S.S. there are some large and well observed earthquakes from the Celebes region. The earthquake of 1 March 1948, 1*h* was recorded by 51 stations at distances from 105° to 115° and there are many entrances of the phases due at these distances, especially of *P*, *PKP*, *PP*, *SKS* and *PS*. Fig. 1 is the Scoresby-Sund record of this earthquake. When comparison is made with the J–B tables the residuals are found to have considerable scatter, indeed so much scatter that sampling by seconds yields a distribution which is inconvenient to handle and seems unnecessarily wide. I therefore took the numbers of residuals in 5 sec groups, picking out first the central group in which the number of residuals was greatest. Indicating each 5 sec group by the residual at its centre we obtain for the earthquake of 1 March 1948 the distributions as indicated on page 123. The numbers in parentheses are the numbers of residuals outside the ranges indicated.

The *PP*, *SKS* and *PS* distributions are symmetrical and determine their central values with fair accuracy. The m_2's are the 'standard errors' calculated from the distributions as they stand with the numbers in parentheses left out. They are not truly standard errors, unless the distributions are normal, but they provide us with a rough measure of the uncertainties, which is all that is desired. If the frequencies of the single residuals are taken instead of those of 5 sec groups, somewhat different m_2's are found, but the difference is not significant. For *SKS*, for example, we find 0.74^s instead of 0.8^s.

The distribution of the *P* residuals is asymmetrical owing to a preponderance of late readings. This is quite usual at these distances where *P* often is marked by small, increasing oscillations. There is sufficient concentration of residuals to show that the *P* onset is not indefinite in good records. Comparison was made with the extrapolated J–B table.

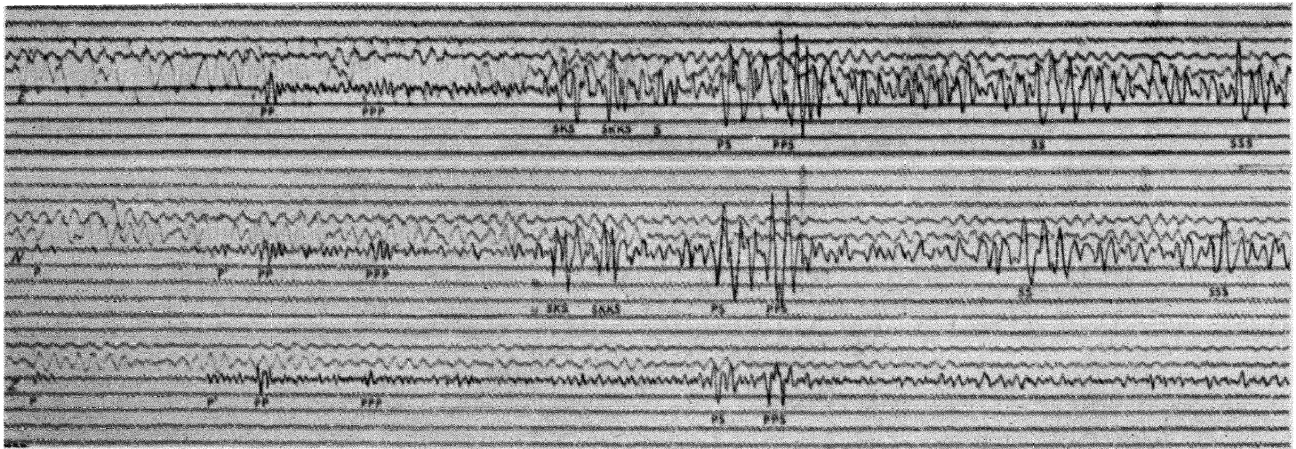

FIG. 1. 1 March 1948. Off West Coast of New Guinea, Scoresby-Sund G–W E, N, Z. $\triangle = 108°$.

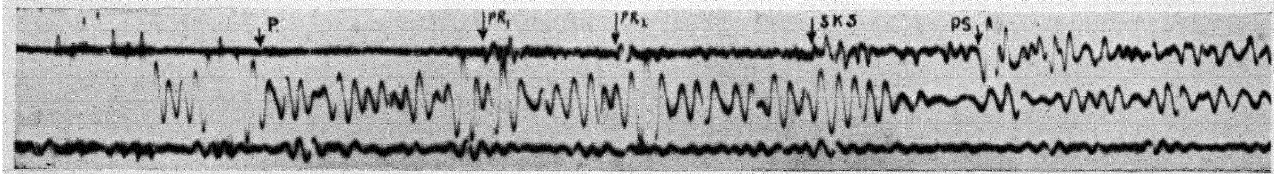

FIG. 2. 1 December 1928. Chile, Stonyhurst M–S E, $\triangle = 107°$.

1 March 1948

P	32 obs.	Centr. res. sec.		− 10	− 5	0	5	10		
		No. of observ.		1	1	12	9	6	(3)	
PKP	29 obs.	Centr. res. sec.		− 10	− 5	0	5	10		
		No. of observ.	(13)	2	4	5	3		(2)	
PP	44 obs.	Centr. res. sec.		− 8	− 3	2	7	12		
		No. of observ.	(2)	1	10	15	10	1	(5)	$m_2 = 0.7^s$
SKS	39 obs.	Centr. res. sec.		− 9	− 4	1	6	11		
		No. of observ.	(2)	2	8	15	9	1	(2)	$m_2 = 0.8^s$
SKKS	16 obs.	Centr. res. sec.		− 6	− 1	4	9	14		
		No. of observ.		1	1	7	1	2	(4)	
S	13 obs.	Centr. res. sec.		− 7	− 2	3	8	13		
		No. of observ.		1	3	4	4	1		
PS	33 obs.	Centr. res. sec.		− 14	− 9	− 4	1	6		
		No. of observ.	(1)	5	4	13	6	1	(3)	$m_2 = 1.0^s$

PKP residuals show no good concentration. There are, as is often the case, many very early readings; their residuals scatter greatly.

There are not so many *SKKS* and *S* readings, probably partly because it is not usual to read the diagrams to great detail and partly because they follow so closely upon foregoing phases that their onsets are not clear. In view of this difficulty *SKKS* shows remarkably good concentration.

There are entrances of other phases than those here taken but not a great many of each and their residuals scatter greatly. The phases are: *PPP*, *PPS*, *PKKP*, *PKKS*, *SS*, *SSS* and a few others.

The central values of *PP*, *SKS* and *PS*, being 2^s, 1^s and -4^s respectively, indicate slight deviations from the tables. It has to be considered, however, that the residuals may be affected by errors in the elements of the earthquakes. The earthquake is very large ($M = 8$) and recorded by a great many stations (145 stations reported to the I.S.S.), but nevertheless an error in the epicenter is not excluded. The nearest station is at an epicentral distance of 20° and the majority of the stations at the shorter as well as at great distances are in a sector 100° wide between azimuth 310° and 50°. Since the time-curves of *P* and *SKS* are parallel at the distances considered, errors in the epicenter and the time of occurrence would not show in *SKS* if *P* were adapted to the tables, but they would show in *PP* and *PS*, rendering their residuals positive if the epicenter had been taken too near the recording stations and negative if it had been taken too far away. There are in this case two sets of recording stations, the European and the North American, but they are both in the said sector and a shift of the epicenter to the north or the south would affect them in the same way. The central residuals of *PP* and *PS* having different signs they could not, however, both be reduced to zero. The tables for a surface focus were used. Actually a large earthquake recorded to great distances is not likely to have, strictly, a surface focus. It is more likely to be at 'normal' depth, i.e. at about half the depth to the Mohorovičič discontinuity. This would not show in the *P* residuals since the *P* curves for a surface focus and for $h = 0.00$ are very nearly parallel from 20° upwards. It would not show in *PP* either, but the residuals of *PS* and *SKS* should be negative, about -2^s or -3^s. Our *PS*, having the central residual $-4^s \pm 1.0^s$ corresponds approximately to normal depth, but *SKS* corresponds to a surface focus, and if greater depth were assumed the

residual would be increased. Thus neither change of epicenter nor of focal depth would bring the travel times of our three phases as here determined into perfect agreement with the tables. There are small deviations, but the single deviations cannot be determined owing to the uncertainty of the elements of the earthquake.

SKS is the most important of the phases considered because its travel times are used when the travel times in the core are determined. The J–B times here used do not depart very much from those of GUTENBERG and RICHTER (1939, p. 118). At 110° the travel times are equal, but the slopes of the time-curves differ so that at 105° that of Gutenberg and Richter is 1^s below and at 115° $1\frac{1}{2}^s$ above the J–B curve. The travel times of NELSON (1954) are from $2\frac{1}{2}^s$ to 1^s smaller than the J–B times at these distances. The large California earthquake of 21 July 1952, the epicenter of which was exceptionally well determined, had only two observations of *SKS* between 105° and 115°; their residuals were -2^s and -8^s. The mean of nine *SKS* observations at distances between 95° and 105° was -5^s. The depth of the earthquake could not be accurately determined but it is supposed to be normal.

For the two large earthquakes of 12 June 1947 (9*h*) and 13 March 1948 (20*h*) the central values of the *PP*, *SKS*, and *PS* residuals were also determined. Both epicentres were approximately at $1\frac{1}{2}°$ N $106\frac{1}{2}°$ E (region 23) and the I.S.S. took the depths to be 0.00 and 0.01 respectively. The magnitudes were 7.2 and 7.1 and the number of reporting stations at epicentral distances between 105° and 115° were 42 and 40 respectively. We find:

12 June 1947:

PP: $-2^s \pm 1.0^s$ *SKS*: $0^s \pm 1.1^s$ *PS*: $-5^s \pm 1.7^s$

13 March 1948:

PP: $-4^s \pm 1.1^s$ *SKS*: (7^s) *PS*: $0^s \pm 1.1^s$

SKS of the first earthquake agrees approximately with the tables and the *PP* and *PS* residuals could be reduced nearly to 0^s by a shift of the epicenter to the north. It should be mentioned that *P* of this shock was very well observed between 105° and 115°. Twenty-five out of 42 observing stations reported *P* and 20 of the observations were in the 5 sec group centring on 0^s. This is a clear indication of the fact that there is not a definite boundary of the shadow zone at

105°. *SKS* of the second shock evidently was poorly recorded for it was read only by 16 of the 40 reporting stations and the residuals scatter widely, from -21^s to $+36^s$. There are seven residuals in the 5 sec group centring on 7^s, but this is not a well determined central value. However, except for three rather large negative residuals all the residuals are positive and this indicates that the focus has been taken too deep. It also shows in *S*, the residuals being positive at all distances, and in distant *P*'s. The depth of GUTENBERG and RICHTER (1954) is 60 km or close to 0.05. If this depth is assumed and the epicenter shifted somewhat to the north the residuals of all three phases are reduced, but complete agreement with the tables is not obtained.

Several other earthquakes from region 23 and other western Pacific regions were taken, but the results for our three phases were not very satisfactory. In only one of the earthquakes, the one of 5 October 1936, were the central residuals for all three phases well determined. They were large and negative, but the depth was evidently greater than assumed and a shift of the epicenter was required. For the other earthquakes one or more of the central residuals had great uncertainty and sometimes the residuals scattered widely and had no concentration anywhere.

Some earthquakes from the South American region 8 were also considered. For the following three central values could be determined:

1 December 1928, $4h$:
PP: $1^s \pm 1.1^s$ *SKS*: ? *PS*: $12^s \pm 0.6^s$
18 March 1931, $8h$:
PP: $-2^s \pm 1.6^s$ *SKS*: (-1^s) *PS*: $8^s \pm 1.0^s$
26 January 1939, $3h$:
PP: ? *SKS*: $-2^s \pm 0.6^s$ *PS*: $-6^s \pm 0.6^s$

We notice the large, positive, well determined central *PS* residuals of the first two earthquakes. The epicenters of these earthquakes are not well determined, but no shift of epicenter would reduce the large *PS–PP*. The earthquakes have been taken to be shallow and assumption of greater depth would increase the *PS* residual. There is, therefore, actually a considerable deviation from the tables. The third earthquake is possibly slightly deeper than the other two. The *PS* residual could be brought nearer to zero by a shift of the epicenter,

so there is not in this case any sure indication of a departure from the tables. The *SKS* residuals of the first shock do not concentrate on a central value; those of the second show good concentration on -1^s, but the distribution is asymmetrical. While the *SKS* and *PS* residuals of the third shock have unusually well determined central values the *PP* residuals scatter from -25^s to $+26^s$ and do not concentrate anywhere.

JEFFREYS as well as GUTENBERG and RICHTER found that *SKS* observations of shallow shocks have no great precision and they therefore made use of observations of deep and intermediate shocks when they constructed their time-curves. There are, however, only a few deep shocks well recorded in the range of distance here considered. There are deep shocks in the South American region 8, but they are further inland than the shallow shocks and therefore at smaller distances from the European observatories. The two shocks of 28 August 1946 and 29 January 1947, both at 26° S 63° W have few but consistent *SKS* observations between 105° and 115°. The mean I.S.S. residuals are $+5^s$ and -2^s respectively. The depths were assumed to be 0.090 and 0.080, but a depth of about 0.082 would fit the observations of both shocks. In the 'Seismicity of the Earth' the depth has been taken to be 580 km. In region 23 we have the earthquake of 11 August 1937 at depth 0.080 the *P*'s of which have great precision up to 111° (LEHMANN, 1953, p. 296). The *SKS* residuals, however, show no good concentration, the distribution being as follows:

11 August 1947:

SKS	Centr. res. sec.	— 9	— 4	1	6	
	No. of observ.	2	6	3	1	(4)

It is thus seen that the *SKS* observations of deep shocks are not always more precise than those of shallow shocks. In the region 12 earthquake of 16 April 1937 there were 18 stations at epicentral distances between 105° and 115°, but only ten of them reported *SKS*. The residuals scattered a great deal and so did those of *S* at all distances. In the I.S.S. the depth is taken to be 0.03 but in the 'Seismicity of the Earth' it is 400 km.

Some intermediate South American earthquakes are quite well observed in Europe, but their *SKS* have no great precision. In the

South Antilles region 10 there are some large intermediate earthquakes very well observed between 105° and 115° as e.g. the earthquake of 8 September 1937. There were 51 reporting stations in this range of distance and 32 observations of *SKS*; 19 of these were in the 5 sec group centring on -4^s. The usefulness of precise observations of region 10 earthquakes is, however, limited by the fact that the elements of the earthquakes cannot be accurately determined. In the 1937 earthquake the nearest station was at a distance of 29.8° and there were only 14 stations at distances smaller than 90°.

We have seen that in the range 105° to 115° the transmission times of the phases read in earthquake records vary a great deal. This applies also to the most clearly marked phases *PP*, *SKS* and *PS*. In a time–distance plot the points marking their transmission times lie on bands of considerable width. Sometimes the majority of the points of an earthquake is restricted to bands about 5 sec wide, but more often only about half the points of a phase or less than half are on a 5 sec band and the remaining points are more or less symmetrically arranged around it on a band of width 25 sec or more. Not unfrequently, however, there is no concentration on a narrow band and the points scatter widely. The heights of the well-determined 5 sec bands are somewhat uncertain because the elements of the earthquakes that are well recorded at these great distances cannot be well determined. Nevertheless it has been possible to ascertain that deviations from the tables occur.

It is well known to routine observers that the onsets of phases of distant earthquakes are rarely sharp enough for readings to the second to seem certain, and that quite often the uncertainty is much greater. The large swings of a phase are often preceded by smaller ones and if these are superposed on background movement it may be difficult or impossible to see where the onset is. Background movement is much more severe at some stations than at others, but it also varies from one earthquake to another. In deep earthquakes it is usually small, but in shallow earthquakes it may be strong enough to blur the onsets of most phases. Microseismic movement sometimes seriously increases the disturbing effect. Therefore it is not surprising to find that in some earthquakes the travel times of our three phases *PP*, *SKS* and *PS* have no great precision. However, it seems doubtful that the very great scatter sometimes observed can be attributed wholly to background movement of one kind or another,

especially so because, as we have seen, great scatter may occur in one of the phases while the others have great precision. It seems as if there may be other, contributory causes. In an attempt to throw light on this, a study was made of the phases in the records of an earthquake, and the one that was chosen was the Chile earthquake of 1 December 1928, well recorded at European observatories at epicentral distances between 105° and 115°. The records had previously been used for another study (LEHMANN, 1953).

The earthquake of 1 December 1928 (4*h*) was large and highly destructive. A macroseismic account was published in the Bolletino del Santiago de Chile, XX, 1930. It is shown on a map that the greatest destruction occurred in a long, but comparatively narrow zone extending from the coast about 200 km inland and comprising the Maule valley. The two cities, Talca and Constitucion, situated in the valley, were so seriously damaged that not more than about 20% of their houses remained habitable. The sea was set into motion but there was no tsunami and from this it may safely be concluded that the epicenter was not at sea. Geological considerations caused the Chile seismologists to place it in the eastern part of the area of highest intensity, near the Andes mountain chain.

The epicenter cannot be determined with much accuracy from microseismic data. The I.S.S. placed it at 34.0° S 73.0° W which is at sea and far from the area of highest intensity. The European residuals are negative, indicating that the epicentral distances are too great. JEFFREYS and BULLEN (1935) corrected it to 35.7° S 73.0° W which is also at sea, but JEFFREYS later concluded that it could not be accurately determined (JEFFREYS, 1938, p. 285). For this study it was attempted to find an epicenter reasonably well adapted to microseismic data and not in obvious disagreement with macroseismic evidence. The point 35.3° S 72.3° W was found to fulfil these requirements.

Thirty-one European observatories kindly lent their records of the earthquake to the Danish Geodetic Institute where they were copied and thus available for this belated study. Seventeen of the observatories had big Wiechert seismographs and these, when well adjusted, yield very good records of a strong distant earthquake. Four stations had long-period Galitzin instruments and two had Galitzin–Wilip. The other instruments were Mainka, Quervain–Picard and Milne–Shaw seismographs. The Quervain–Picard seismographs are adjusted for

the recording of short-period waves and are not very useful for the phases here studied. It would be preferable to have a more homogeneous material for a collective study, but on the whole the records were useful. Fig. 2 is the Stonyhurst Milne–Shaw record from a distance of 107.2^s. Owing to the slow recording speed a clear picture is obtained; the magnification being only 150 it is undisturbed by overlapping swings from the succeeding lines. The three phases *PP*, *SKS* and *PS* stand out very clearly in the record. It is an *E* component record and the azimuth of the epicenter being nearly WSW in Europe most phases except *S* are more clearly recorded in the European *E* than in the *N* component records.

All the records were first read to great detail, independently by two observers. The common phases were kept and a few others that seemed equally clear and the transmission times were plotted against epicentral distance. Many of the points arranged themselves so as to indicate time-curves while others scattered over the plot. The readings were carefully revised and particular attention given to those found to belong to time-curves. They were on the whole more pronounced phases than the others read. Although some of the phases were indicated by rather broad bands they were easily identified. No attempt was made to identify the phases of the scattered points. They are much more frequent in some records than in others and are evidently partly of local origin. The phases marked in Fig. 1 were all present except *SKKS* which could not be identified at distances between 105° and 115°, whereas at København (115.8°) and at Uppsala (119.8°) there are clear phases where *SKKS* is due. Searching the I.S.S. for entrances of *SKKS* we find that in some earthquakes there are many at the distances in question whereas in others there are few or none. Search was made for the phase *ScSP* the time-curve of which should cross the *PS* curve at 117° and at 112° have a focal point 19^s after *PS*. The phase was not traceable where it is due after *PS*. At Uppsala, at 119.8°, a reading which was at first taken to be an early *PS* is possibly due to *ScSP*.

The travel times of the phases *P*, *PP*, *SKS* and *PS* have been tabulated. The residuals are against the J–B tables for a surface focus. All the readings made are included, also those from a few stations at distances greater than 115°. With a few exceptions the readings here given do not differ by more than a few seconds from those of the I.S.S.

1 December 1928, 4 : 06 : 03 35.°3 *S* 72.°3 *W*

Station	Δ	P	$O-C$	PP_1	PP_2	$O-C_1$	$O-C_2$	SKS_1	SKS_2	$O-C_1$	$O-C_2$	PS	$O-C$
	°	m s	m s	m s	m s	s	s	m s	m s	s	s	m s	s
Liverpool	106.8	14 35	16	!18 54	19 21	7	34		!25 22		23	28 14	11
Kew	106.9	21	2	! 52	19	4	31	25 5		6		! 17	13
Paris	106.9	33	14	! 53	8	5	20	!24 57	! 21	−2	22	! 14	10
Stonyhurst	107.2	29	9	! 52	13	2	23	25 11	23	11	23	! 16	10
Edinburgh	108.2	35	11	! 57	31	0	34	! 10	24	5	19	! 26	9
Neuchatel	108.4	28	3	19.1	15	(7)	16		26		21	32	13
Uccle	109.0	28	0	!19 3		−1		10	23	2	15	! 36	12
Zürich	109.5	42	12		26		18					! 40	11
Strasbourg	109.7	31	0	17	32	8	23		! 33		22	! 44	13
Chur	109.8	32	0		25		15	25.3		(7)		43	11
De Bilt	110.1	35	2	! 10	33	−2	21		29		16	! 49	14
Karlsruhe	110.3			19.4	! 37	(11)	24	!25 14		1		! 59	22
Ravensburg	110.3	14.7	0.1		19.5		(17)	! 26	37	13	24	! 46	9
Hohenheim	110.6			19 29	19 39	14	24	! 25		10		59	19
Frankfurt	110.9	59	23	12	47	−5	30						
Nördlingen	111.4				36		15	25.5		(12)		! 58	10
Scoresby-S	111.5	59	21	! 32		10			36		18	!29 1	12
München	111.7	14.9	0.2	19.4		(1)						! 3	13
Göttingen	112.4	15 7	24	!19 23	51	−5	23		! 45		23	! 10	13
Jena	113.0	14 48	2	24	20.1	−9	(33)		! 46		22	! 9	6
Zagreb	113.2	14.8	0.0	32		−2			! 46		21	! 18	13
Hamburg	113.3	14 53	6	! 38	21.0	3	(25)	!25 29	48	3	22	! 17	11
Graz	113.5	14.9	0.1	! 29		−8		! 28		2		! 13	5
Leipzig	113.6	14.9	0.1	! 38		1			! 50		23	! 8	−1
Potsdam	114.5			! 45	20 10	1	26		! 44		14	! 28	11
Wien	114.5			! 46	13	2	29					! 30	13
Beograd	115.6				20.5		(39)						
Budapest	115.9			47	20 13	−6	20					! 35	5
Lund	116.0	15.2	0.2	!19 57	10	3	16	!25 47		11		! 46	15
Königsberg	119.5			20 22	35	3	16		!26 3		15	!30 18	15
Uppsala	119.8			! 23	50	3	30	! 55		6		! 4	10

Many of the *P* residuals are large and positive. The phase is nowhere strong and in the records of the most sensitive instruments the first oscillations are quite small and they are evidently lost elsewhere.

There are two sets of readings of the phases *PP* and *SKS*. *PP* is a large phase and in 16 out of the 31 records the onsets are well defined; the readings have been marked by a !. The mean of the PP_1 residuals is + 1^s and the 'standard error' is 1.1^s. There is in most of the records a later increase of the amplitude of *PP*, sometimes combined with a lengthening of the period. The second reading was made where this change seemed to take place but it was rarely at a clear onset and the residuals scatter so much that no second phase can be said to be defined. Some first readings were placed in the second column because their residuals were large and there was no subdivision of the phase so that, apparently, the first part of the phase was missing.

The *SKS* readings were also placed in two columns, but there are only six stations for which there are two readings. The subdivision of the phase is clear at the smallest distances as, for example, at Paris. Where there was only one reading this was placed in the first column if it had a 'small' residual or else in the second column, but at the greatest distances the distinction is rather arbitrary. Nine of the 14 early readings were at clear onsets and so were nine of the 17 late readings. The phase was stronger at the smaller than at the greater distances; at some stations it was not clearly recorded. Eleven of the residuals of the late readings are in a 5 sec group centering on 22^s; those of the early readings are more scattered. When the residuals of the first readings of all the stations are taken there is no concentration on a central value as was indicated on p. 126. Since the existence of two separate phases was indicated the records were examined afresh in an attempt to trace a second phase where only one had been read, but this gave no result. In a few records the background movement is so strong that a small phase could possibly be covered by it, but in most of the records there is obviously not a double phase. The pattern of the movement recorded at the different stations clearly varies so that it is not always quite the same waves that mark the phase. Thus the great scatter of the residuals is due mainly to a variation of the phase itself and not to disturbing background movement. With all the recording stations in Europe the

paths should not differ much, but it seems as if we shall have to admit the possibility of irregularities in them. *SKS* waves are refracted at the Mohorovičič discontinuity and at the core boundary and if there are irregularities in the paths they are likely to arise on the one or the other of these two surfaces or in the bordering regions of the mantle. However, evidence that could help to elucidate this matter is not easily obtained. In the Chile earthquake of 25 January 1939 with its epicenter only 1° south of that of 1928 *SKS* had great precision.

PS is the most conspicuous phase in the records. The amplitudes are large and the onsets are usually clear. The central residual is $+ 12^s \pm 0.6^s$. There is quite likely to be an error in the epicenter and this will affect the *PS* residual, but it will also affect that of *PP* and the difference, 11^s, of the residuals of *PS* and *PP* could not be reduced by more than about 2^s by a shift of the epicenter of 1°. There is, therefore, unmistakably a departure of the *PS* travel times from those of the tables. The well determined positive central residual of *PS* as well as the scattered, but mainly positive residuals of *SKS* indicate 'high focus'. It has sometimes been possible to explain seemingly too long transmission times by the occurrence of a later and stronger shock the phases of which are taken for those of the first shock at great distances. We observe in this earthquake increase of movement in the phases *P*, *PP* and *SKS*, but we have not succeeded in determining distinct later phases, and the large and sharp *PS* phase does not fit in with the late readings of the other phases.

It is not easy to see how so great a delay in *PS* could arise. It might be expected to be regionally conditioned and we actually find that *PS* is also late in the earthquake of 18 March 1931, having its epicenter about 3° north of that of the 1928 shock. However, the 1939 shock, only 1° to the south of it, had not a late *PS*.

The study of the records of the earthquake of 1 December 1928 has made it probable that the great uncertainty of the *SKS* travel times of that earthquake is due mainly to a variation of the phase itself and only to a small degree to ordinary errors of observation or to the disturbing effect of background movement. Similar uncertainty has been observed in the phases *PP*, *SKS* and *PS* of various earthquakes. When there is very great scatter and no concentration on a central value it seems on the face of it unlikely that it should be one and the same wave that is recorded everywhere, and our result for *SKS* of the 1928 earthquake has confirmed us in the idea that in such cases

the phase varies and is not marked by identical waves everywhere. How the variation is effected cannot be said. It is most likely to be connected with the discontinuity surfaces in which the waves are refracted or reflected or with the bordering regions. The constitution and depth of the Earth's surface layers vary and the constitution of the upper mantle is not everywhere the same (LEHMANN, 1955, 1956). Variations of the depth of the core boundary and of the constitution of the bordering region of the mantle seem to be indicated (LEHMANN, 1953). More fruitful studies of these questions could possibly be made at shorter epicentral distances where well recorded earthquakes are more frequent and where the results from various regions could be compared.

REFERENCES

GUTENBERG, B. and RICHTER, C. F. (1934) On seismic waves I, *Gerl. Beitr. Geophys.* **43**, 56–133.

—— —— (1939) On seismic waves IV, *Gerl. Beitr. Geophys.* **54**, 94–136.

—— —— (1954) *Seismicity of the Earth and associated phenomena*, Princeton University Press.

JEFFREYS, H. (1938) Southern earthquakes and the core waves, *Mon. Not. Roy. Astr. Soc., Geophys. Suppl.* **4**, 281–308.

—— and BULLEN, K. E. (1935) Times of transmission of earthquake waves, *Publ. Bur. Centr. Séism. Intern.*, série A, **11**.

—— —— (1940) *Seismological Tables*, London.

LEHMANN, I. (1953) On the shadow of the Earth's core, *Bull. Seism. Soc. Amer.* **43**, 291–306.

—— (1955) The times of *P* and *S* in northeastern America, *Ann. Geofisica* **8**, 353–370.

—— (1956) The velocity of *P* and *S* waves in the upper part of the Earth's mantle, *Publ. Bur. Centr. Séism. Intern.*, série A, **19**, 115–123.

NELSON, R. L. (1954) A study of the seismic waves *SKS* and *SKKS*, *Bull. Seism. Soc. Amer.* **44**, 39–55.

10

QUELQUES EXPÉRIENCES SUR LA STRUCTURE DE LA CROÛTE TERRESTRE EN EUROPE OCCIDENTALE

J. P. ROTHÉ

EN hommage à l'ancien Président de l'Association internationale de Séismologie et de Physique de l'Intérieur de la Terre et au pionnier qui commença ses recherches en Europe occidentale, je voudrais rassembler et comparer quelques résultats obtenus en Allemagne et en France dans l'étude de la croûte terrestre par l'enregistrement d'explosions provoquées. Plusieurs de ces expériences ont amené des équipes de pays voisins à travailler ensemble dans un esprit de parfaite collaboration scientifique; ainsi se trouvait confirmé, une fois de plus, le caractère international de la science séismologique.

Les expériences de Haslach (1948)

Ces expériences, organisées par l'Institut de Physique du Globe de Strasbourg, avec la collaboration d'équipes de l'Institut géophysique de Goettingen, utilisèrent lors de la destruction d'une usine souterraine, dans la Forêt-Noire, près de Haslach (48° 16′ N, 8° 07′ E) l'énergie mise en jeu par l'explosion de 73 tonnes d'explosifs (Fig. 1). Plusieurs travaux détaillés ont été publiés et les résultats de ces expériences sont aujourd'hui classiques (REICH *et al.*, 1948; FÖRTSCH, 1951; ROTHÉ et PETERSCHMITT, 1950). L'interprétation présentée par J. P. ROTHÉ et E. PETERSCHMITT tient compte de l'ensemble des dépouillements des enregistrements obtenus par les équipes allemandes et françaises.

Rappelons les 4 équations des temps de propagation des ondes longitudinales:

$$t_1 = 0{,}14 + \frac{\Delta}{5{,}63}; \qquad t_2 = 0{,}42 + \frac{\Delta}{5{,}97}; \qquad t_3 = 2{,}85 + \frac{\Delta}{6{,}54};$$

$$t_4 = 6{,}5 + \frac{\Delta}{8{,}15}$$

Les deux interprétations géologiques suivantes ont été proposées indépendamment:

	I. J. P. Rothé et E. Peterschmitt				II. O. Förtsch		
	épaisseur h(km)	v km/s	nature	Ondes	épaisseur h(km)	v km/s	nature
	2,4	5,63	granito-gneiss		4–6	5,88	granit
	17,7	5,97	granit profond	Pg, Sg	11,5	6,005	diorite
	10,1	6,54	gabbro-basalte	Pb, Sb	17–18	6,55	gabbro
Total	30,2				32–34		
	—	8,15	péridotite	Pn, Sn	—	8,34	péridotite

On notera que l'interprétation II n'a pas tenu compte des premières arrivées dans les stations françaises à des distances comprises entre 10 et 30 km, arrivées qui définissent une vitesse voisine de 5,6 km.

Quelles que soient les divergences de détail les expériences de Haslach ont permis d'établir que les surfaces de discontinuité de Conrad et de Mohorovičič se trouvaient sous la Forêt-Noire et sous le Plateau Souabe, respectivement vers 20 et 30 km de profondeur.

A partir d'une stratification inspirée directement des expériences d'Haslach, nous avons calculé des tables de propagation des ondes Pg, Sg, Pb, Sb et Pn, Sn en fonction de la distance et en supposant un foyer situé, soit à la surface, soit à 10, 20 ou 30 km de profondeur.

Nous avons adopté les valeurs numériques suivantes:

Profondeur	Onde	Vitesse	Onde	Vitesse
de 0 à 20 km	Pg	5,9 km/s	Sg	3,4 km/s
de 20 à 30 km	Pb	6,5 km/s	Sb	3,7 km/s
au delà de 30 km	Pn	8,2 km/s	Sn	4,4 km/s

Les tableaux I et II sont extraits de ces tables jusqu'ici inédites et qui, utilisées de façon constante par nos collaborateurs de l'Institut de Physique du Globe de Strasbourg, ont permis de dépouiller avec succès les enregistrements de nombreux séismes naturels, originaires en particulier de France et du Sud de l'Allemagne.

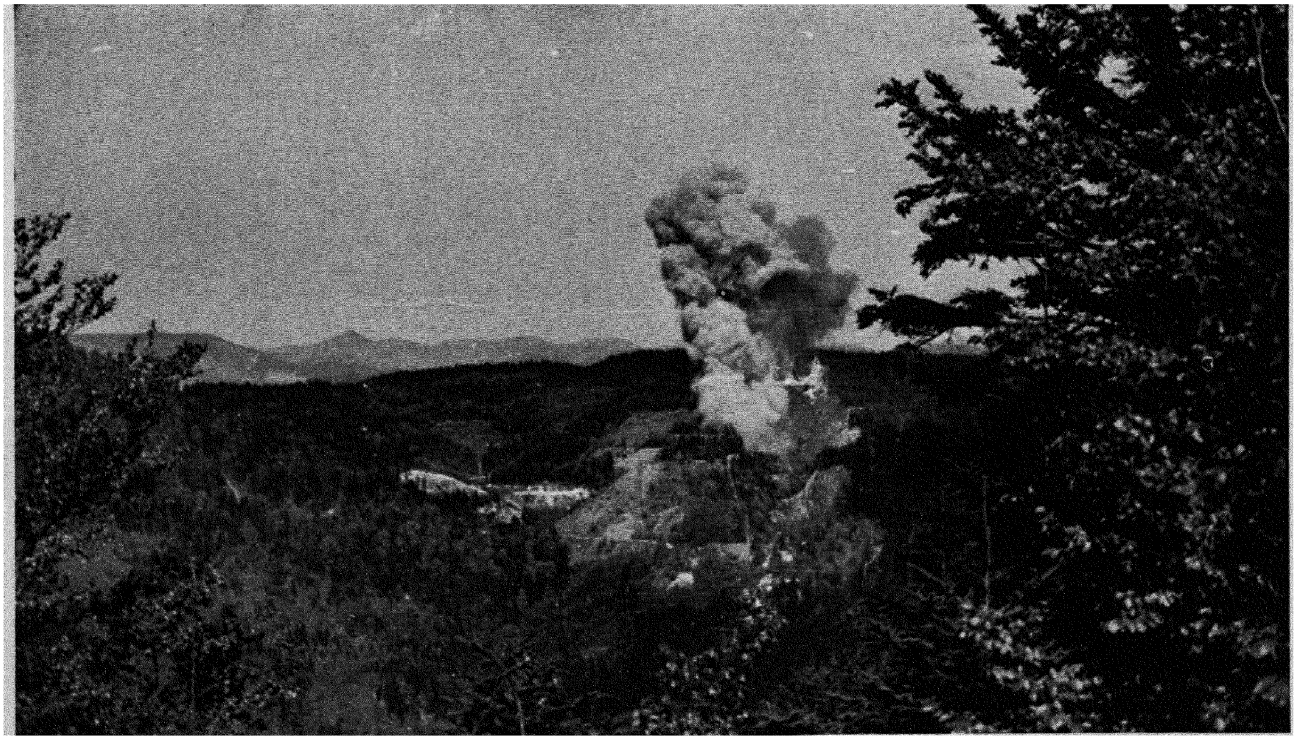

FIG. 1. Explosion de 73 tonnes de bombes dans la carrière souterraine de Haslach (28 avril 1948).

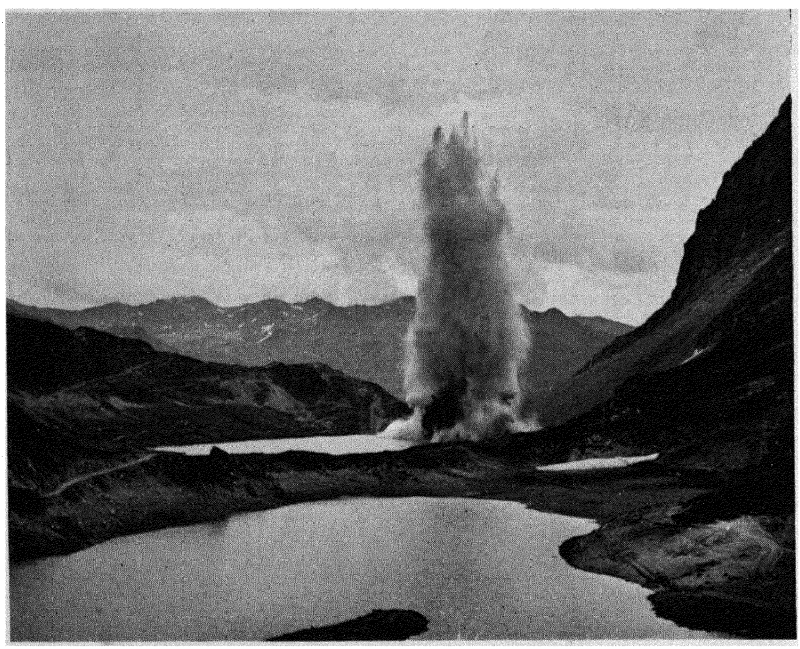

Fig. 2. Explosion de 10 tonnes de mélinite dans le lac Rond des Rochilles (6 septembre 1956).

TABLES DE HASLACH

Profondeur du foyer $h = 0$ km

Δ km	Phases					
	Pn	Pb	Pg	Sn	Sb	Sg
20	—	—	03,4s	—	—	05,9s
40	—	—	06,8	—	—	11,8
60	—	—	10,2	—	—	17,6
80	16,3s	15,1s	13,6	28,6s	26,3s	23,5
100	18,8	18,2	16,9	33,1	31,7	29,4
120	21,2	21,3	20,3	37,7	37,1	35,3
140	23,7	24,4	23,7	42,2	42,5	41,2
160	26,1	27,5	27,1	46,8	47,9	47,0
180	28,5	30,5	30,5	51,3	53,3	52,9
200	31,0	33,6	33,9	55,8	58,7	58,8
220	33,4	36,7	37,3	60,4	64,1	64,7
240	35,8	39,7	40,7	64,9	69,5	70,6
260	38,3	42,8	44,1	69,5	74,9	76,5
280	40,7	45,9	47,5	74,0	80,3	82,4
300	43,2	49,0	50,9	78,6	85,7	88,2
320	45,6	52,1	54,2	83,1	91,1	94,1
340	48,0	55,1	57,6	87,7	96,5	100,0
360	50,5	58,2	61,0	92,2	101,9	105,9
380	52,9	61,3	64,4	96,8	107,4	111,8
400	55,4	64,4	67,8	101,3	112,8	117,6
420	57,8	67,4	71,2	105,8	118,2	123,5
440	60,2	70,5	74,6	110,4	123,6	129,4
460	62,7	73,6	78,0	114,9	129,0	135,3
480	65,1	76,7	81,4	119,5	134,4	141,2
500	67,6	79,7	84,7	124,0	139,8	147,0

Expériences de Camargue (1949)

En septembre 1949 des mesures ont été faites sur un profil de réfraction long de 26 km et s'étendant des environs d'Arles à la mer en direction NW–SE à travers la Camargue. Toutes les stations se trouvaient sensiblement au niveau de la mer (BEAUFILS *et al.*, 1956).

Six arrivées d'ondes longitudinales ont été reconnues; leurs équations de propagation sont les suivantes:

$$t_0 = \frac{\Delta}{1{,}0}\ ; \quad t_1 = 0{,}23 + \frac{\Delta}{2{,}3}\ ; \quad t_2 = 0{,}45 + \frac{\Delta}{3{,}6}\ ;$$

$$t_3 = 0{,}70 + \frac{\Delta}{5{,}0}\ ; \quad t_4 = 0{,}80 + \frac{\Delta}{5{,}6}\ ; \quad t_5 = 0{,}87 + \frac{\Delta}{6{,}0}$$

TABLES DE HASLACH
Profondeur du foyer $h = 10$ km

Δ km	Phases					
	Pn	Pb	Pg	Sn	Sb	Sg
20	—	—	03,8^s	—	—	06,6^s
40	—	—	07,0	—	—	12,1
60	—	—	10,3	—	—	17,9
80	15,2^s	14,4^s	13,7	26,7^s	25,1^s	23,7
100	17,6	17,5	17,0	31,2	30,5	29,5
120	20,0	20,6	20,4	35,8	35,9	35,4
140	22,5	23,7	23,8	40,3	41,3	41,3
160	24,9	26,7	27,2	44,9	46,7	47,1
180	27,4	29,8	30,5	49,4	52,1	53,0
200	29,8	32,9	33,9	54,0	57,5	58,9
220	32,2	36,0	37,3	58,5	62,9	64,8
240	34,7	39,1	40,7	63,1	68,3	70,6
260	37,1	42,1	44,1	67,6	73,8	76,5
280	39,6	45,2	47,5	72,2	79,2	82,4
300	42,0	48,3	50,9	76,7	84,6	88,3
320	44,4	51,4	54,3	81,2	90,0	94,1
340	46,9	54,4	57,7	85,8	95,4	100,0
360	49,3	57,5	61,0	90,3	100,8	105,9
380	51,8	60,6	64,4	94,9	106,2	111,8
400	54,2	63,7	67,8	99,4	111,6	117,6
420	56,6	66,7	71,2	104,0	117,0	123,5
440	59,1	69,8	74,6	108,5	122,4	129,4
460	61,5	72,9	78,0	113,1	127,8	135,3
480	63,9	76,0	81,4	117,6	133,2	141,2
500	66,4	79,1	84,7	122,2	138,6	147,0

Le résultat le plus caractéristique est l'existence d'une couche où la vitesse de propagation atteint 6,0 km/s: l'hodochrone est définie par les arrivées des premiers impetus aux stations situées à des distances comprises entre 4 et 16 km du point d'explosion. La profondeur à laquelle se trouve cette couche à forte vitesse est relativement faible (de l'ordre de 2000 mètres). L'interprétation géologique de cette couche à grande vitesse est délicate, faute de forages profonds. On sait seulement que dans la Vaunage, au nord-ouest du profil de Camargue, on a pu par carottage séismique, mesurer des vitesses dépassant 5000 m/s à 1500 m de profondeur, dans des terrains calcaires du Jurassique supérieur. Au point de vue géologique la région occupée actuellement par le delta du Rhône se trouve d'une part dans l'axe probable d'un fossé plus ou moins

affaissé (c'est ce fossé qui a orienté le cours du Rhône), et d'autre part dans la partie méridionale d'une zone qu'on peut appeler l'*isthme durancien* dont l'existence fut particulièrement nette au crétacé supérieur: cet isthme émergé reliait alors le Massif des Maures au Massif Central, séparant le Golfe de Basse-Provence de la zone alpine profonde. La réalité de cet isthme permettrait d'expliquer la présence à une profondeur relativement faible de couches à grande vitesse, couches qui pourraient appartenir au socle paléozoïque.

Lorsqu'on se rapproche de la côte, aux distances supérieures à 24 km, les premiers impetus présentent des retards croissants: ces retards doivent s'expliquer par un épaississement rapide des formations alluviales du delta du Rhône.

Un autre résultat à signaler est relatif aux ondes de Rayleigh: la propagation d'un train d'ondes de surface—facilement identifiable car il correspond aux maxima d'amplitude—a pu être suivi sur toute l'étendue du profil; la vitesse de propagation était seulement de 500 m/s. Les terrains de surface sont constitués par des alluvions (cailloutis et sables gorgés d'eau).

Expériences de Blaubeuren (1952)

Utilisant deux fortes explosions (2975 et 3625 kg de Donarit) effectuées en mars et mai 1952 dans les carrières de Blaubeuren, H. REICH chercha à enregistrer avec un appareillage de prospection séismique moderne (PRAKLA) des réflexions sur les surfaces de discontinuité de la croûte, comme celles que A. JUNGER venait d'obtenir aux Etats-Unis. Les résultats furent présentés à la réunion de la Commission Séismologique Européenne tenue en septembre 1952 à Stuttgart (REICH, 1953).

Les carrières de Blaubeuren (48° 23′ N, 9° 49′ E) sont situées sur le plateau souabe à proximité du profil séismique étudié à l'occasion des expériences d'Haslach.

Une première série de réflexions ($t = 0{,}59^s$ à $0{,}89^s$ pour des distances au point d'explosion comprises entre 150 et 2315 mètres) peut-être mise en relation avec la surface supérieure du socle cristallin. En admettant une vitesse moyenne de 3500 m/s dans les terrains sédimentaires (Malm, jurassique moyen, lias, keuper), on peut calculer que le socle se trouve à environ 1040 m de profondeur (soit 400 m au-dessous du niveau de la mer). Cette profondeur est tout à fait compatible avec les données des forages profonds.

Des réflexions particulièrement nettes apparaissent sur les séismogrammes à 7,075^{s} et 9,20^{s} après le moment de l'explosion (Fig. 3).

Pour interpréter ces réflexions, H. REICH a fait appel aux résultats des expériences d'Haslach rappelés plus haut. En adoptant une vitesse moyenne de 5750 m/s la profondeur de la première surface réfléchissante serait d'environ 20,3 km; avec une vitesse moyenne de 6000 m/s la profondeur de la deuxième surface serait d'environ 27,6 km. Les résultats sont tout à fait du même ordre de grandeur que ceux trouvés par réfraction dans les expériences d'Haslach. Notons

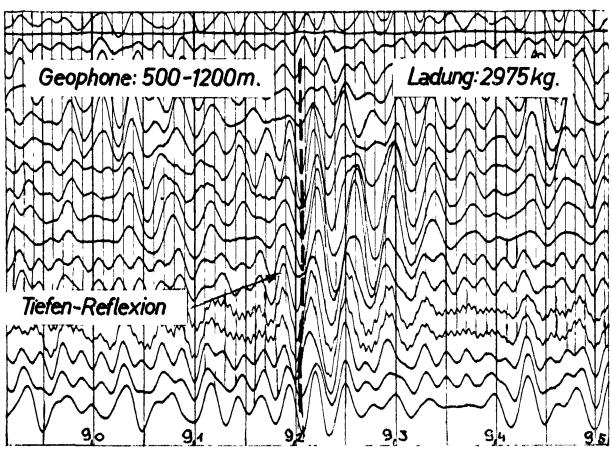

FIG. 3. Réflexions profondes : Plateau Souabe (Document Prakla, H. Reich).

que le schéma donné par J. P. ROTHÉ et E. PETERSCHMITT conduirait à prendre une vitesse moyenne un peu supérieure à celle adoptée par H. REICH. On trouverait pour les surfaces de discontinuité des profondeurs un peu plus grandes, mais en accord avec celles indiquées par ces auteurs d'après les mesures de réfraction.

Les expériences d'Haslach (*par réfraction*) et de Blaubeuren (*par réflexion*) confirment l'existence dans le Sud-Ouest de l'Allemagne de deux surfaces de discontinuité, l'une à 20 km de profondeur (surface de Conrad), l'autre à 30 km environ (surface de Mohorovičič).

Expériences de Champagne (1952)

En octobre 1952 des mesures ont été effectuées en Champagne (BEAUFILS, *et al.*, 1956) par les instituts de Physique du globe de Paris et de Strasbourg. Les points d'explosion étaient situés aux

environs de Suippes (49° 08′ N, 4° 32′ E), à 160 km environ à l'E de Paris; les charges utilisées variaient entre une et dix tonnes d'explosifs. Des stations d'enregistrements furent réparties sur un profil de réfraction long de 70 km orienté Est-Ouest en direction de Paris et passant par Epernay. Il a été possible de contrôler les valeurs des vitesses par un tir inverse jusqu'à une distance de 25 km.

Six arrivées d'ondes longitudinales ont été identifiées. Les équations de propagation sont les suivantes:

$$t_1 = \frac{\Delta}{1{,}8}\ ; \quad t_2 = 0{,}047 + \frac{\Delta}{2{,}92}; \quad t_3 = 0{,}191 + \frac{\Delta}{3{,}80};$$

$$t_4 = 0{,}325 + \frac{\Delta}{4{,}50}; \quad t_5 = 0{,}745 + \frac{\Delta}{5{,}20}; \quad t_6 = 0{,}985 + \frac{\Delta}{6{,}00}$$

Les cinq premières équations sont relatives à la propagation des ondes séismiques dans les terrains sédimentaires: Sénonien supérieur (1800 m/s); Sénonien inférieur, Turonien, Cénomanien (2920 m/s); Crétacé inférieur (3800 m/s); Portlandien, Jurassique supérieur et moyen, Lias (4500 m/s); Trias et Permien (5200 m/s).

La vitesse $V_6 = 6000$ m/s est identique à celle déjà trouvée en Camargue; *elle peut ici être attribuée sans ambiguïté au socle paléozoïque.* Deux forages profonds effectués dans le Bassin Parisien ont en effet rencontré le socle: l'un, au voisinage de Verdun a touché des schistes métamorphiques à 2170 m de profondeur; l'autre aux environs d'Esternay a touché du granite vers 3180 m. Ces deux forages sont distants d'environ 140 km et encadrent la région étudiée par le profil de réfraction. Le pendage des couches est faible; en première approximation la profondeur calculée pour le socle en Champagne, d'après les équations de réfraction, est voisine de 2900 m, valeur qui est en accord avec les données géologiques.

Signalons encore que la vitesse de propagation, très constante, de la phase donnant les maxima d'amplitudes des ondes de Rayleigh est ici de 0,9 km/s, chiffre notablement plus élevé que celui trouvé en Camargue (0,5 km/s). Enfin l'interprétation est compliquée par l'apparition de réfractions multiples très nombreuses et qui sont encore très nettement visibles 30 secondes après le début de l'enregistrement (LABROUSTE et BEAUFILS, 1956).

Par ailleurs devant l'intérêt des résultats obtenus par le Professeur Reich, j'avais demandé à la *Compagnie Générale de Géophysique* de

procéder à des enregistrements de réflexions au voisinage des points d'explosion au moyen d'un laboratoire mobile de prospection séismique. De nombreuses réflexions ont été effectivement obtenues (GENESLAY, *et al.*, 1956). Certaines d'entre elles sont des réflexions simples et multiples sur les discontinuités dans les terrains sédimentaires. Un groupe de réflexions arrivant 1,412^{s} à 1,416^{s} après l'instant de l'explosion (pour une distance des géophones comprises entre 1170 et 1460 m) peut-être attribué à la surface supérieure du socle paléozoïque. Plusieurs autres réflexions indiquent de grandes

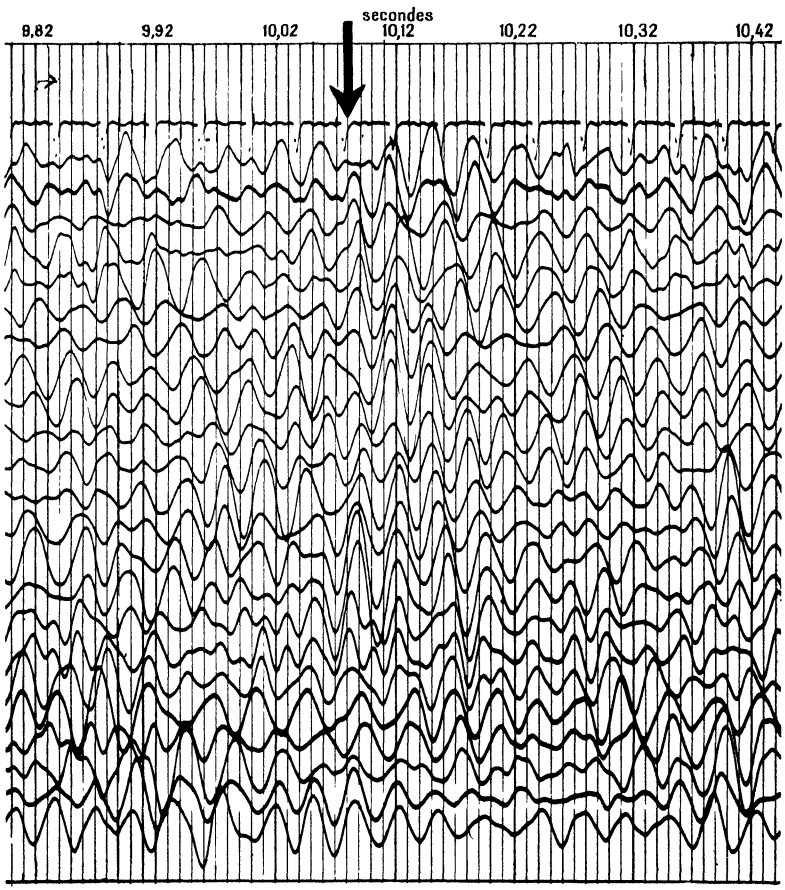

FIG. 4. Réflexions profondes : Champagne (Document C.G.G.).

valeurs de la vitesse moyenne et paraissent constituer des réflexions profondes (5 km, 8 km, 11 km). Il n'est pas possible de dire si l'une de ces réflexions peut être attribuée à la discontinuité de Conrad.

Enfin sur le film 9 (obtenu avec une charge de 10 tonnes) on peut lire 10,08^{s} après le moment de l'explosion, une arrivée simultanée d'ondes aux différents géophones (à des distances variant de 1960 à 2292 m). On peut considérer qu'il s'agit d'ondes réfléchies à grande profondeur: en admettant une vitesse moyenne de 7 km/s dans la partie inférieure de l'écorce, on en déduit pour l'épaisseur de cette dernière une valeur de 30 km environ. La réflexion profonde se produit 0,9^{s} plus tard en Champagne qu'en Souabe (Fig. 4).

Expériences dans les Alpes françaises (1956)

La Commission Séismologique Européenne réunie à Rome en septembre 1954 après avoir pris connaissance des résultats que nous venons de rappeler, adopta un voeu recommandant l'organisation dans la zone alpine d'expériences systématiques mettant en jeu de fortes charges explosives.

Sous l'active présidence de Madame LABROUSTE, la section de séismologie du comité national français de géodésie et géophysique se préoccupa de la réalisation du voeu de la Commission Séismologique Européenne. Un projet d'expériences fut soumis à la réunion tenue à Vienne en avril 1956 par cette commission. Le plan de collaboration scientifique internationale établi au cours de cette réunion a pu être réalisé du 25 août au 6 septembre 1956. Des équipes allemandes (Amt für Bodenforschung, institut géophysique de Hambourg et de Munich), italiennes (Observatoire géophysique de Trieste) et françaises (Compagnie générale de Géophysique, Instituts de Physique du Globe de Paris et de Strasbourg) ont pris part aux expériences qui n'ont pu être effectuées que grâce à une importante participation de l'Armée française (Génie et Transmissions).

Il avait été décidé de *choisir un point d'explosion dans la zone interne des Alpes* (zone briançonnaise): le lac Rond des Rochilles (45° 05′ N, 6° 29′ E) à 6 km au NE du Col du Galibier, offrait avec une profondeur d'eau de 7 mètres, suffisante pour assurer le bourrage, de nombreux avantages matériels pour l'exécution des expériences (Fig. 2). Les premiers résultats des mesures ont été résumés dans une note rédigée au nom de tous les participants (TARDI, 1957) et sont présentés dans un mémoire collectif (BALTENBERGER, *et al.*, 1958).

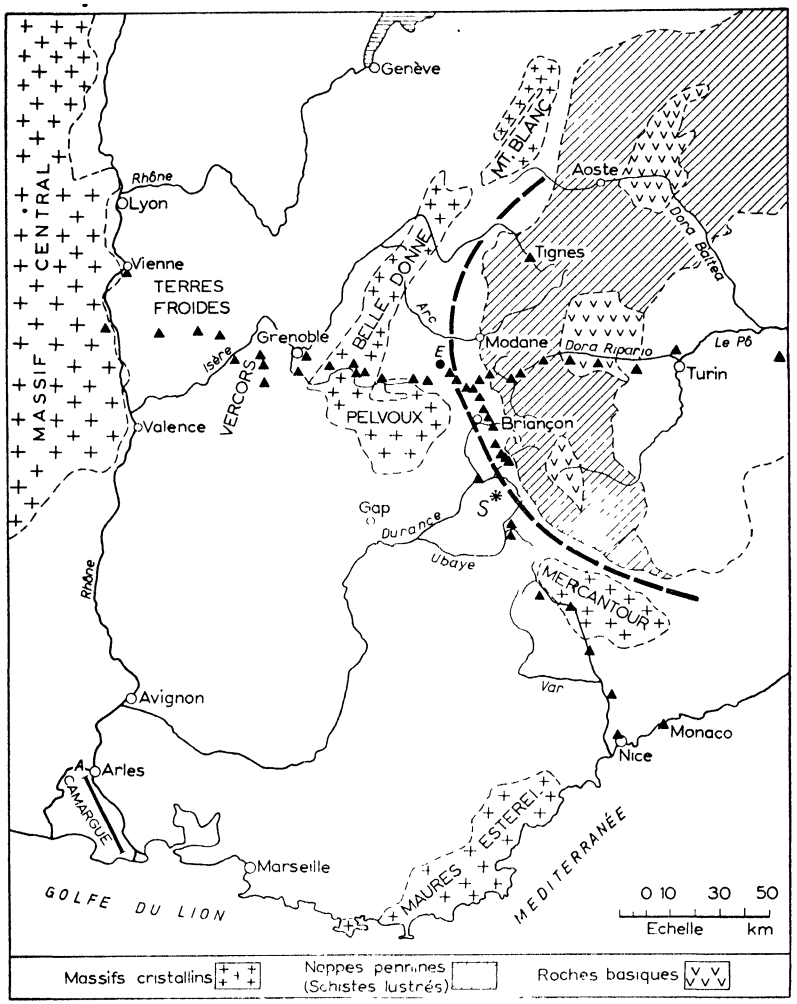

FIG. 5. Carte schématique des Alpes occidentales ▬ ▬ ▬ : Axe de la zone interne briançonnaise; E : point d'explosion; ▲ stations de réfraction; S : épicentre du séisme du 18 juillet 1938.

(a) *Profils de réfraction.* Sur la carte Fig. 5 sont indiqués les emplacements des stations de réfraction.

Sur le profil Sud les enregistrements à faible distance font apparaître deux vitesses de propagation, l'une de 4,5 km/s (terrains houillers de surface), l'autre comprise entre 5,2 et 5,5 km/s. Aux

stations plus éloignées à partir d'une distance de 12 km (Névache) et jusqu'à 150 km (Nice) l'équation s'écrit $t = 0{,}50 + \frac{\Delta}{6{,}07}$. La mise en évidence de nombreuses *réfractions multiples* indique que la limite supérieure du milieu rapide constitue une surface de discontinuité. A une profondeur d'environ 2 km, on retrouve donc ici encore et de façon très nette, un milieu caractérisé par une vitesse d'environ 6 km/s. Il est remarquable que cette surface soit définie aussi bien dans la première partie du profil où *les stations sont situées dans la zone interne briançonnaise*, que dans la deuxième partie où le milieu rapide doit correspondre au socle cristallin, prolongement du Massif du Mercantour. Les résultats séismiques ne confirment donc pas l'hypothèse d'un enfoncement en profondeur des terrains houillers du Briançonnais.

Sur le profil Ouest en direction de Grenoble, les résultats se groupent suivant 2 régions nettement différentes:

Jusqu'à la station du Fort des 4 Seigneurs voisine de Grenoble (55 km du point d'explosion) l'équation de l'hodochrone s'écrit: $t = 0{,}36 + \frac{\Delta}{5{,}86}$. Les ondes semblent s'être propagées au voisinage

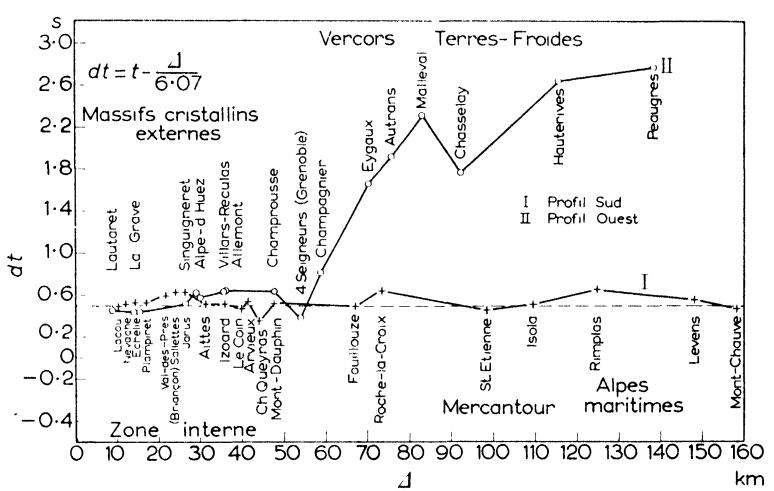

FIG. 6. Comparaison des hodochrones réduites obtenues sur le profil Ouest et sur le profil Sud

$$dt = t - \frac{\Delta}{6{,}07}$$

de la surface du sol à partir d'une distance de 10 km du point d'explosion à travers les gneiss et les roches éruptives.

A l'ouest du massif de Belledonne les temps d'arrivée accusent des retards plus ou moins importants sur ceux qu'on peut calculer par l'équation ci-dessus: ces retards traduisent une plongée vers l'ouest de la limite supérieure du socle et un épaississement des terrains sédimentaires qui doit correspondre, d'une part à l'empilement des plis couchés dus à la tectonique d'écoulement qui constitue le massif du Vercors, et d'autre part à l'existence d'un fossé subsident mis en évidence antérieurement au nord de Romans.

Sur la Fig. 6 nous avons tracé et comparé les hodochrones réduites des profils Sud et Ouest en portant en ordonnées $dt = t - \frac{\Delta}{6{,}07}$. Jusqu'à une distance de 55 km, les deux courbes sont très voisines bien que le profil Sud soit *longitudinal* et le profil Ouest *transversal* par rapport à la direction tectonique; au contraire, au-delà de 55 km, les deux courbes se différencient très nettement.

Enfin, sur le profil Est en direction de Turin, une seule vitesse a pu être mesurée: elle est voisine de 5,3 km/s.

Les ondes Pb n'ont pas été observées clairement, sauf en quelques stations éloignées du profil Ouest. Pour ces stations le report des impetus sur une hodochrone donne à penser qu'il existe une surface de discontinuité à une profondeur d'environ 25 km (au-dessous du niveau de la mer). La vitesse correspondante est d'environ 6,7 km/s. Il est possible qu'il s'agisse de la discontinuité de Conrad; les valeurs correspondantes étaient d'environ 17 à 20 km dans l'expérience d'Haslach et de 9,5 km dans celle d'Heligoland. La discontinuité de Conrad serait donc plus profonde en bordure ouest des Alpes françaises que dans l'Europe septentrionale.

(b) *Réflexions.* Les grands profils de réfraction ne peuvent fournir que des indications moyennes sur la profondeur des surfaces de discontinuités et c'est seulement par l'enregistrement—en des points aussi nombreux que possible—d'ondes réfléchies à peu près verticalement qu'on peut espérer suivre les variations de profondeur de ces surfaces. Au cours des expériences de 1956, deux laboratoires de prospection séismique fournis par la Compagnie Générale de Géophysique et par l'observatoire géophysique de Trieste, ont opéré sur deux bases situées à 3200 m et 5700 m au NW du point de tir. De nombreux

trains d'ondes réfléchies ont été enregistrés et leur dépouillement est encore en cours. Les interprétateurs pensent qu'une partie des trains d'ondes s'expliquent par des *réflexions multiples* se répétant toutes les 900 millisecondes environ. De telles réflexions multiples pourraient se produire entre la surface et un socle à 2 km de profondeur, socle qui pourrait être un prolongement du massif cristallin du Combeynot. Les interprétateurs ajoutent: 'On peut également se demander, *sous toutes réserves*, si les séries réfléchissantes vers 9,8s et 10,7s ne proviennent pas réellement de miroirs profonds' (TARDI, 1957). On notera que les temps indiqués sont voisins de ceux obtenus en Champagne. Il est cependant trop tôt pour fixer avec certitude la profondeur de la surface de Mohorovičič sous les Alpes. De nouvelles expériences sont projetées, cette fois, à l'intérieur du massif cristallin du Pelvoux et on peut espérer éviter ainsi les réflexions multiples.

Il semble, en tout cas, que la zone 'interne' Briançonnaise et les massifs cristallins 'externes' ne se différencient pas au point de vue séismique. Ce résultat est important et il devra en être tenu compte dans la nouvelle synthèse des Alpes occidentales que souhaitait récemment le professeur Goguel, synthèse qui conduira peut-être à modifier l'image que nous nous sommes faite d'empilements de nappes reployées en profondeur.

Comparaison des résultats avec ceux déduits de l'étude de séismes naturels

Les quatre profils de réfraction dont nous venons de résumer rapidement les résultats font apparaître de façon très concordante une vitesse voisine de 6,0 km/s qui doit caractériser le socle cristallin (Fig. 7). Une vitesse de cet ordre a été souvent signalée dans les expériences d'explosions et plusieurs auteurs ont cru constater que les vitesses des ondes P et des ondes S dans les couches supérieures des continents, calculées à partir d'explosions, étaient notablement plus élevées que celles déterminées précédemment à partir de l'étude des séismes naturels (GUTENBERG, 1955).

Le profil Sud des expériences alpines de 1956 passe à proximité de l'épicentre du séisme naturel du 18 juillet 1938. Ce séisme originaire des environs de Ceillac (44° 37′ N, 6° 47′ E), a fait l'objet d'une étude approfondie et j'ai publié en 1941 le dépouillement détaillé des enregistrements. Or le tracé des hodochrones avait montré que les ondes Pg s'étaient propagées avec *une vitesse bien constante*,

voisine de 6,0 km/s (ROTHÉ, 1941) pour des distances épicentrales comprises entre 180 et 500 km. Ces résultats complètent et prolongent par conséquent parfaitement ceux qui résultent des expériences d'explosions de 1956. Les vitesses de propagation sont les mêmes dans les deux cas.

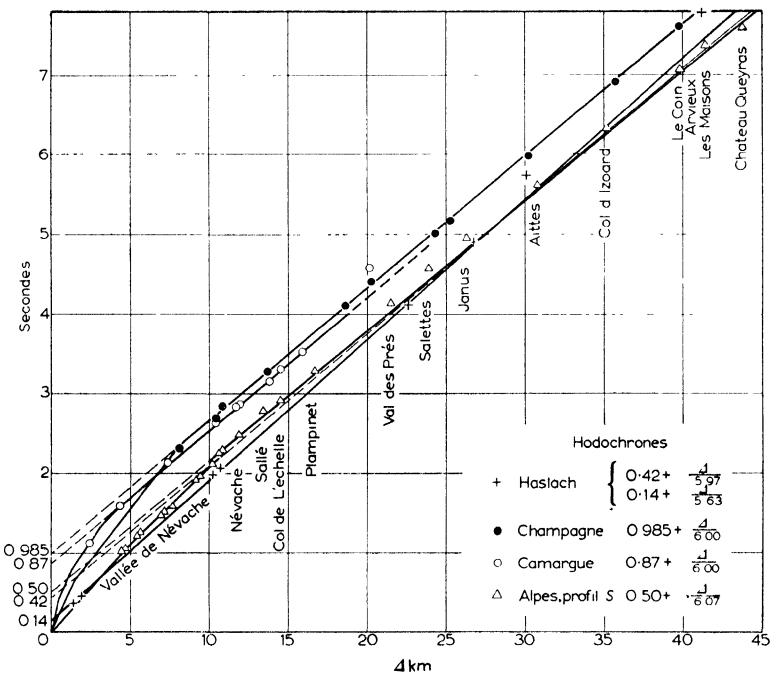

FIG. 7. Hodochrones comparées.

L'étude du séisme alpin de 1938 avait encore montré que les ondes Pb et Sb n'apparaissaient pas nettement; au contraire les ondes Pn étaient parfaitement définies; j'avais établi l'équation $t = 7{,}0 + \frac{\Delta}{8{,}2}$ (ROTHÉ, 1941). La vitesse de 8,2 km/s qui pouvait en 1941 paraître trop élevée, a été reconnue depuis comme étant bien celle qui caractérise les couches supérieures du manteau.

Le séisme belge du 11 juin 1938 offre un autre exemple d'étude ayant conduit pour la vitesse de l'onde Pg à une valeur élevée voisine de 6,0 km/s. O. SOMVILLE (1939) a publié un tableau des

durées de trajet des ondes Pg, Pb, Pn. D'après ce tableau la vitesse des ondes Pg est voisine de 5,95 km/s, celle des Pb de 6,7 km/s et celle des Pn de 8,1 km/s.

Or dans la première partie de son travail l'auteur a sous-estimé la vitesse de propagation de l'onde Pg; considérant les temps d'arrivée de l'onde Pg aux deux stations d'Uccle et de De Bilt, il en a déduit que la profondeur du foyer du séisme se trouvait à 45 km de profondeur en posant $V_1(\mathrm{Pg}) = 5{,}7$ km/s.

Il est facile de voir qu'une faible erreur sur V_1 entraine une erreur considérable sur le calcul de la profondeur h.

Si on désigne par τ la différence des temps d'arrivée aux deux stations et si on pose $\Delta_1 + \Delta_2 = p$, $\Delta_1 - \Delta_2 = q$ (Δ_1 et Δ_2 étant les distances épicentrales), on peut écrire:

$$h = \frac{\sqrt{[(v\tau - p)(v\tau + p)(v\tau - q)(v\tau + q)]}}{2v\tau}$$

formule facilement calculable par logarithmes.

A partir des données utilisées par O. Somville:

Uccle	Pg	10 h. 57 m. 46,3 s.	$\Delta_1 =$ 54 km
De Bilt	Pg	10 h. 58 m. 07,3 s.	$\Delta_2 =$ 184 km

on trouve $h = 28$ km pour $V_1 = 6{,}0$ km/s.

Par ailleurs, l'utilisation des tables de Mohorovičič, en supposant une surface de discontinuité située à 57 km de profondeur, profondeur que nous savons maintenant être beaucoup trop grande, a conduit également O. Somville à calculer une profondeur de foyer trop grande. La valeur indiquée plus haut (28 km) est probablement plus exacte; c'est sensiblement aussi la profondeur à laquelle, d'après les expériences d'Heligoland, doit se trouver la surface de discontinuité de Mohorovičič sous la Belgique.

J'ajouterai que les profondeurs hypocentrales que j'ai moi-même calculées pour certains séismes alpins sont entachées d'erreurs analogues. Le foyer du séisme de Ceillac dont il a été question plus haut serait à une profondeur de 35 km si on utilise les tables de Mohorovičič; c'est une profondeur certainement trop grande. Pour ce même séisme E. Peterschmitt (1952) a calculé une profondeur de 6 km en utilisant une méthode macroséismique. *Une réinterprétation des séismes européens s'impose en profitant des acquisitions auxquelles conduisent les expériences d'explosions.*

J'ai indiqué plus haut que les expériences d'Haslach ont permis de calculer des tables utilisées pour l'interprétation des séismes naturels; nous voyons ici les résultats de l'étude du séisme de Ceillac relayer ceux obtenus dans les expériences alpines de 1956. Expériences d'explosions et études des séismes naturels se complètent pour nous conduire vers une meilleure connaissance de la structure de la croûte terrestre.

BIBLIOGRAPHIE SOMMAIRE

Haslach

FÖRTSCH, O. (1951) Analyse der seismischen Registrierungen der Grosssprengung bei Haslach im Schwarzwald am 28 April 1948, *Geol. Jahrb.* **66**, 65–80.

REICH, H., SCHULZE, G. A. und FÖRTSCH, O. (1948) Das geophysikalische Ergebnis der Sprengung von Haslach in südlichen Schwarzwald am 28 und 29 April 1948, *Geolog. Rundschau* **36**, 85–96.

ROTHÉ, J. P. et PETERSCHMITT, E. (1950) Etude séismique des explosions d'Haslach, *Ann. Inst. de Phys. Globe Met.*, 3è partie, Géophysique, t. V, Strasbourg, 13–38.

Camargue

BEAUFILS, Y., BERNARD, P., COULOMB, J., DUCLAUX, F., LABROUSTE, Y., RICHARD, H., PETERSCHMITT, E., ROTHÉ, J. P. et UTZMANN, R. (1956) Enregistrement des ondes séismiques provoquées par de grosses explosions, I: Camargue, 1949, Publ. *Bureau Central séismologique international*, Série A, Travaux Scientifiques **19**, Toulouse, 325–326.

Blaubeuren

REICH, H. (1953) Uber seismische Beobachtungen der Prakla von Reflexionen aus grossen Tiefen bei der grossen Steinbruch-Sprengungen in Blaubeuren am 4 März und am 10 Mai 1952, *Geol. Jahrb.* **68**, 225–240.

Champagne

BEAUFILS, Y., COULOMB, J., GENESLAY, R., JOBERT, G., LABROUSTE, Y., PETERSCHMITT, E. et ROTHÉ, J. P. (1956) Enregistrement des ondes séismiques provoquées par de grosses explosions, Champagne 1952, Publ. *Bureau Central séismologique international*, Série A, Travaux Scientifiques **19**, Toulouse, 327–329.

GENESLAY, R., LABROUSTE, Y. et ROTHÉ, J. P. (1956) Réflexions à grande profondeur dans les grosses explosions (Champagne, octobre 1952), Publ. *Bureau Central séismologique international*, Série A, Travaux Scientifiques **19**, Toulouse, 331–334.

LABROUSTE, Y. et BEAUFILS, Y. (1956) Réfractions multiples dans les enregistrements séismographiques des explosions de Champagne, Publ. *Bureau Central séismologique International*, Série A, Travaux Scientifiques **19**, Toulouse, 335–338.

Alpes

TARDI, P. (1957) Expériences séismiques dans les Alpes occidentales en 1956; résultats obtenus par le "Groupe d'Etudes des Explosions Alpines", *C. R. Acad. Sci., Paris*, **244**, 1114–1117.

GROUPE D'ETUDE DES EXPLOSIONS ALPINES (M. BALTENBERGER, Melle BEAUFILS, MM. BEHNKE, BENOÎT, BERG, CHOUDHURY, H. CLOSS, GENESLAY, GOGUEL, HUSSMANN, KORSCHUNOV, Mme LABROUSTE, MM. LOUIS, MARY, MORELLI, OTTMANN, PETERSCHMITT, RICHARD, Melle RIMBERT, MM. ROTHÉ, SALAMANNA et VISINTINI). Expériences séismiques dans les Alpes occidentales en 1956, *Ann. de Géophys.* 1958 (sous presse).

Séismes

GUTENBERG, B. (1955) Wave velocities in the Earth's crust, *Geol. Soc. America*, Special Paper No. 62, 19–34.

PETERSCHMITT, E. (1952) Sur la variation de l'intensité macroséismique avec la distance épicentrale, Publ. *Bureau central intern. Séismologie*, Travaux Scientifiques **18**, Toulouse, 183–208.

ROTHÉ, J. P. (1941) Les séismes des Alpes françaises en 1938 et la séismicité des Alpes occidentales, *Ann. Inst. Phys. Globe Mét.*, 3è partie, Géophysique, t. **III**, Mende, 1–17.

SOMVILLE, O. (1939) Le tremblement de terre belge du 11 juin 1938, *Ann. Obs. Belg.*, 3è Série, t. **II**, 1–15.

11

SEISMIC OBSERVATIONS AT ONE KILOMETER DEPTH

HOWARD E. TATEL* and MERLE A. TUVE

Introduction

At distances of 80–150 km from a surface shot, large compressional wave disturbances are observed in many regions one to four seconds after the first observed arrival (TATEL and TUVE, 1955). These abrupt and prominent ground motions, superposed on the earlier wave motions, apparently arise from the reflection or refraction of the explosion generated waves and the velocity discontinuity at a depth of 30–50 km under the earth's surface (Mohorovičič). This discontinuity is considered to be the lower crustal boundary and its properties are of great interest.

The usual observation of total reflected and refracted waves is laborious. Such measurements cannot, furthermore, differentiate between a total reflection at a discontinuity and a refraction through a region with velocity changing rapidly with depth (TUVE, *et al.*, 1954). We have therefore tried many times to observe a vertically reflected wave. We have been uniformly unsuccessful and this we attribute to the large reverberation signal which is always observed in the form of an extensive coda directly following the first arrival (compressional).

The expected amplitude of the vertically reflected wave can be estimated from the critical reflection amplitude observed at 80–120 km from the shot. Taking into account the expected reflection coefficient and difference of ray travel, a vertical reflection should have an amplitude of about 0.2 the critical reflected wave. We have made many observations near shot points looking for such vertical reflections. As an example, consider the 29,000 lb blast in the Potomac River. A critical reflection of 800 Å was observed at 100 km; the vertical reflection should therefore be 200 Å. At 10–12 sec

* Deceased 15 November 1957

after the shot, which is the expected arrival time of the vertical reflection, the reverberation level, 4.5 km from the shot point, was greater than 800 Å. No 200 Å vertical reflection could be identified in such a background. This is typical of our many experiences.

In 1954 we had performed various experiments, the interpretation of which convinced us that there was considerable conversion of body waves to secondary surface waves (TATEL and TUVE, 1954). The question arose as to whether or not we could eliminate these surface or Rayleigh waves by special observational techniques. One such technique was to observe at depths sufficient to attenuate the secondary Rayleigh waves. However, a subsequent model experiment (TATEL, 1954) indicated that the Rayleigh waves also convert to form body waves and so it could be that, even underground, we would observe the effects of surface conversion.

Experiment

The seismometer-amplifier system utilized in our work has a band-pass of 3–30 c/s. The dominant frequency could be said to be about 10 c/s. For Rayleigh waves of 3 km/sec or 10,000 ft/sec, the observed range of wave lengths is 3000–300 ft, with a characteristic length of say 1000 ft. Thus, with a seismometer at the bottom of a well, at a depth of 3000 ft, the longest wave length component is attenuated by a factor of 10 and the shortest by a factor of 10^4. If Rayleigh waves were an important factor in themselves, a measurement at the depth of 3000 ft would be decisive in their almost complete elimination.

Arrangements were made to make such a test by lowering vertical seismometers into Pennsylvania gas wells 3000 ft deep. An armoured casing was constructed for the seismometers to withstand the full-well water pressure. It turned out that dry gas wells (depleted) were available. We also made a rig to lower and raise our seismometers gently into the well. The seismometer and casing weighed 60 lb while the breaking strength of our (inexpensive) copper-clad steel wire cable was only 200 lb.

Arrangements were made with Mr. Frank Eckert and Mr. John Woods and their associates of Hanly and Bird and with Mr. J. W. Bird of Bird Well Surveys, all of Bradford, Pennsylvania, to use their gas wells. We are grateful to them for their help and consideration.

Three wells, Fig. 1, were used as observation points and we had a surface detector at the shot well and the Cook No. 2 well. We noticed at once that the surface unrest was considerably greater than that in the well. The surface motion due to natural causes such as wind was 40μV or greater, whereas the noise at the 3000-ft level was about 4μV. At the bottom of one well, the Keyes Well, Fig. 2, the unrest recorded was about 1μV and indistinguishable from the amplifier input noise. On our scale, 1μV is approximately 1 Å (10^{-8} cm) unit of

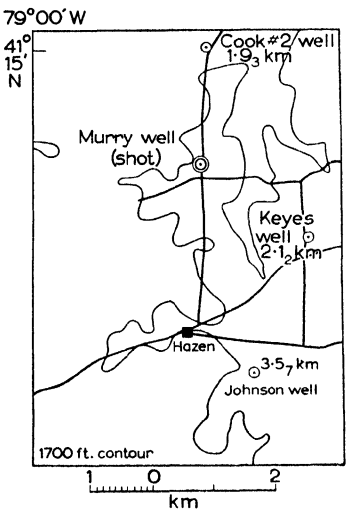

FIG. 1. Map showing the location of 3000 ft deep wells. The shot was at the Murry Well, the distance in kilometers of the others from the Murry Well are shown.

motion. A practical aspect of these low levels is it could enable more distant disturbances to be detected. That the lower level natural ground unrest is less than that at the surface indicates there could be a large component of Rayleigh waves in the surface noise for the portion of the spectrum (3–30 c/s) for which our instruments are most sensitive.

We were able to observe only one shot of 15 quarts of nitroglycerine. No other shooting occurred during the time available for our field station (June 1954). This shot was set off at a 3000 ft depth in the Murry Well. The amplitude of ground motion was less than we anticipated and we were unable to obtain a very good record at the

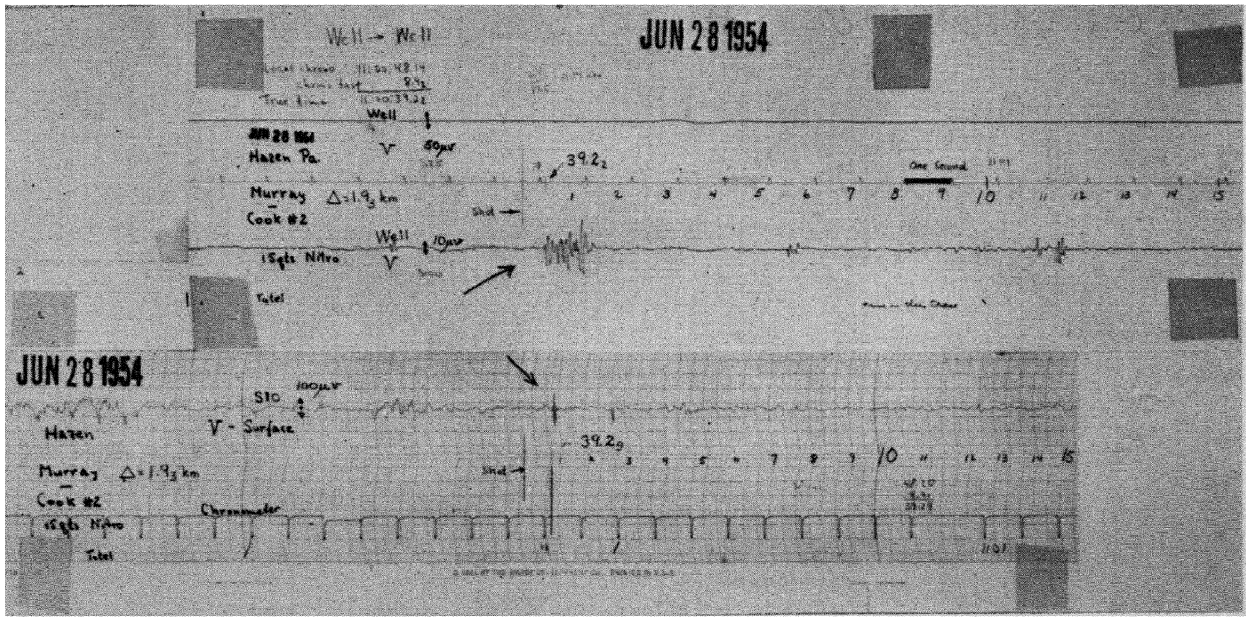

FIG. 2. Upper record of unrest at depth and lower record is of the surface unrest at Cook No. 2 Well. Upper record has seismogram on lower trace and chronometer seconds ticks on central trace. Lower record contains surface seismogram on upper trace and chronometer record showing seconds ticks on lower trace. Shot instant marked by vertical line, arrows indicate onset of motion.

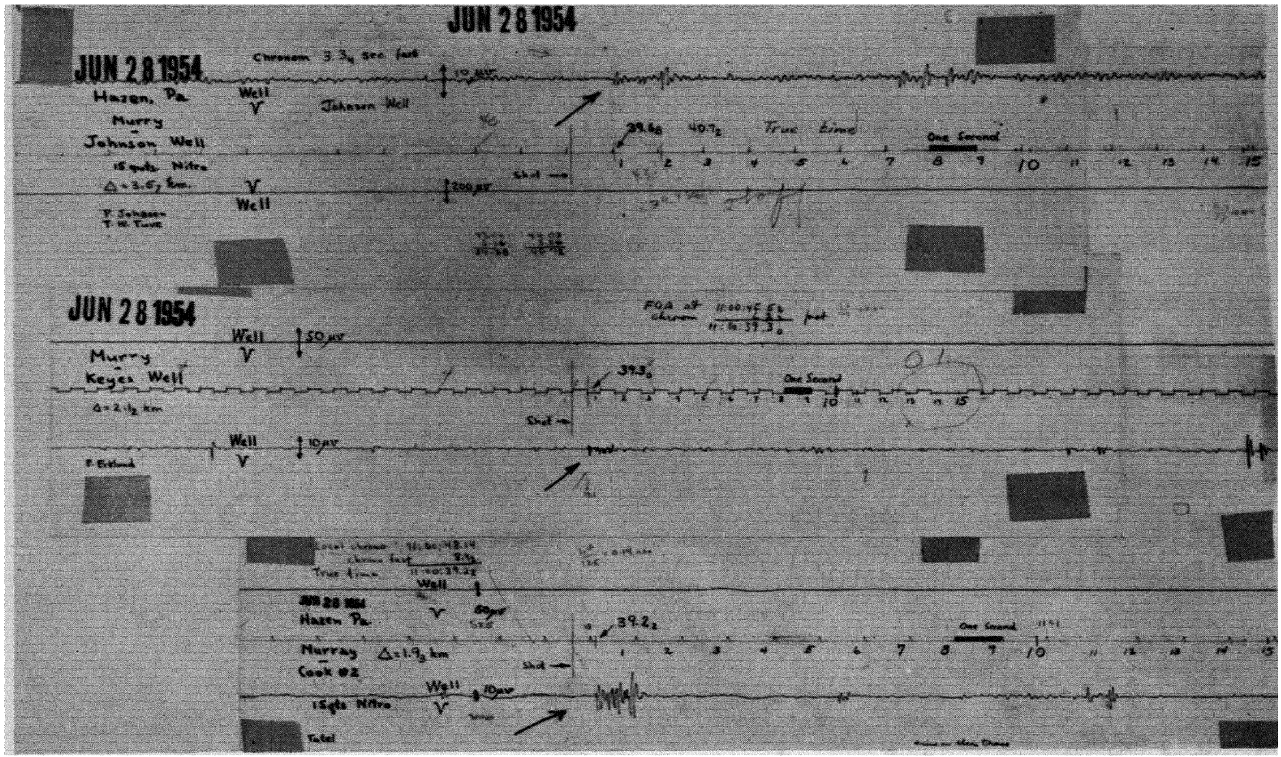

FIG. 3. Shot records at Hazen, Murry, and Cook No. 2. Onset of first motion shown by arrows. Central trace records seconds ticks of chronometer.

epicenter. The shot records are shown in Fig. 3 and Table 1 lists the arrival time, distance, and apparent velocities.

The strongest pulse was received at the Cook No. 2 well. The surface seismometer was also at this well. The first observed surface arrival amplitude was 100μV compared to the amplitude at depth of 20μV. Apparently, the wave front was curving upwards and the

TABLE 1

Showing the differences in distance, arrival time, and apparent velocities

Well	Distance from Murry Well (km)	First observed motion (sec)
Johnson	3.57	39.68
Cook No. 2	1.93	39.22
	difference 1.64	difference 0.46
	velocity 3.6 km/sec	
Keyes	2.12	39.30
Cook No. 2	1.93	39.22
	difference 0.19	difference 0.08
	velocity 2.4 km/sec	
Johnson	3.57	39.68
Keyes	2.12	39.22
	difference 1.45	difference 0.46
	velocity 3.8 km/sec	

seismometer at the surface received a stronger pulse. This effect is not as large as it might seem as there is probably a velocity gradient enhancing the surface motion. In addition, conservation of momentum forces the surface particles to move with twice the amplitude of the interior particles.

Assume that the radial amplitude at the bottom of the Cook well was 50μV. The observed amplitude was less because we used a vertical seismometer whose direction of major sensitivity was almost perpendicular to the major radial motion. The distance from shot to receiver direct is 2 km. To the deep discontinuity and return it could be about 70 km. The echo amplitude from a reflecting plane at this distance would be about 1μV, assuming 100 per cent reflection

(20 per cent would be more realistic) at the surface, and the echo would arrive about 12 sec after the shot. There is no coherent agreement between records at this time; we did not detect any echo. The shot amplitude was too small and this part of the experiment is inconclusive. The small irregular bursts evident in the seismograms were characteristic of all three records. The gas emitted at the well bottom bubbled spasmodically. This activity diminished with time.

Discussion

While we were unsuccessful in obtaining a shot of sufficient amplitude to obtain a vertical reflection from the lower crustal discontinuity, two interesting observations may be made concerning the seismograms themselves. These seismograms are surprisingly similar to surface seismograms. However, the surface seismograms owe a considerable portion of their complexity to wave conversion and scattering at the surface. In the interior, under conditions such as were tried for this experiment, the surface cannot play such an important part. For example, just after the *P* (compression) wave arrival, the motion could not possibly originate from a surface scattering; it would not have time to go up to the surface and then down.

Other means by which secondary energy can be generated must then be of importance in the interior.

Interior conversion scattering with shear instead of Rayleigh waves as secondaries can account for the time delays seen. Normal mode propagation in stratified layers can give some delay and a limited coda. Later portions of the record could be influenced by the surface and near-surface conversion scattering. However, in any such scheme, the interior motions directly after the *P* wave arrival must come from interior wave interaction. Whether or not the interior scattering background diminishes more rapidly with elapsed time after the shot than the reverberation we observe at the surface, thus possibly yielding a better signal to reverberation-background ratio for possible observation of vertical reflections, cannot be settled until observations are made with larger shots. Shots at least 20 times as great would be necessary.

The lesser natural background (no shot energy present) of the seismograms compared to the surface background level is quite interesting. Since *R* waves at the surface convert to *P* waves, it

would be expected that there should be a considerable interior ground unrest. However, there is a considerable gradient in propagation velocity near the surface. Thus, waves generated at the surface would tend to be refracted back to the surface. The surface and near-surface velocity gradients form a trapping system which tends to keep the surface energy tied to the surface, either in the form of surface waves or refracted body waves. If this is so, a surface shot observed at great distances would be expected to show a smaller conversion scattering background for a well observation than for a surface observation at the same distant point.

Conclusion

Earth motion at depths of 3000 ft have been observed. The ground motion is considerably less than the surface motion, which indicates that the surface waves are surface bound either as Rayleigh waves or upwardly refracted secondary *P* waves. A shot at depth was also observed and the seismogram indicates considerable interior wave interaction in the form of scattering.

The lesser ground motion in the interior holds promise for better signal to background ratio for observation of distant shots.

The authors wish to acknowledge their gratitude to Prof. Gutenberg. Besides his direct contributions to the subject, and his generous discussions of many points, his contagious enthusiasm and interest in the study of the earth has led us to share similar interests and satisfactions.

REFERENCES

TATEL, H. E. and TUVE, M. A. (1954) Note on the nature of a seismogram—I, *J. Geophys. Res.* **59**, 287–288.

—— (1954) Note on the nature of a seismogram—II, *J. Geophys. Res.* **59**, 289–294.

—— and TUVE, M. A. (1955) Seismic exploration of a continental crust, *Geol. Soc. Amer.* Special paper 62, 35–50.

TUVE, M. A., TATEL, H. E. and HART, P. J. (1954) Crustal structure from seismic exploration, *J. Geophys. Res.* **59**, 415–422.

12

INTERPRETATION OF THE SEISMIC STRUCTURE OF THE CRUST IN THE LIGHT OF EXPERIMENTAL STUDIES OF WAVE VELOCITIES IN ROCKS

FRANCIS BIRCH

THE experimental data on the velocities of elastic waves in granites and gabbros at high pressures are summarized, corrected for temperature, and compared with several recent studies of the variation of seismic velocity within the continental crust. The seismic velocities fall in most cases between the values for average granite and average gabbro. Distributions showing a gradual increase of velocity with depth are easily interpreted in terms of an increasing gabbroic component; difficulties arise in attempting to account for low-velocity layers within the crust. Solutions in terms of granite and gabbro are not unique, since the same velocities are exhibited by rocks, especially metamorphic rocks, of different composition.

RECENT studies of the variation of velocity within the continental crust, and an accumulation of new laboratory measurements of the effects of pressure and temperature on velocities, open the way for a new attack on the basic problem of accounting for the observed seismic velocities in terms of observed properties of accessible types of rock. The diversity of the suggested seismic velocity distributions lends especial interest to this attempt, since there is some hope that confrontation of these distributions with simple schemes based on laboratory data may aid in selecting the most reasonable, or at worst, in rejecting the least plausible.

GUTENBERG (1955a, b, c) has given velocity-depth profiles for southern California; WILLMORE, *et al.* (1952) for the Transvaal; TUVE, TATEL, and HART (1954); TATEL and TUVE (1955); HART (1954) principally for eastern Maryland and Virginia. Several alternative schemes have usually been offered, any of which would account for

the principal features of the seismic observations. The difficulty or impossibility of making a unique choice based on the available seismic data has been emphasized by Tuve, Tatel and Hart, who have made the most complete investigation of seismically equivalent distributions.

The laboratory studies now available include the older work on the shear velocity (V_S) to as much as 600°C and 9000 kg/cm² for some rocks (BIRCH and BANCROFT, 1938, 1940; BIRCH, 1943, 1955 and unpublished); new measurements on the compressional velocity (V_P) at room temperature to 10,000 kg/cm² (BIRCH, unpublished); and measurements on both compressional and shear velocities to 300° or 400° and 5000 to 8000 kg/cm² (HUGHES and CROSS, 1951; HUGHES and MAURETTE, 1956, 1957). Little or no extrapolation of either pressure or temperature is required to reach the combinations of pressure and temperature to be expected in a 'normal' continental crust. On the other hand, there remain difficulties arising from the irreversible behavior of rocks when exposed to changes, especially of temperature, so that some of the coefficients required for the present purpose are relatively uncertain.

The greatest number of samples is included in the new measurements of compressional velocity, and since this velocity is also the one most satisfactorily determined by the seismic work, the following discussion will be restricted to it in the main. The details of the measurements of V_P to 10,000 kg/cm² will be published elsewhere; the technique is generally similar to that used by HUGHES and his collaborators, except for the use of barium titanate transducers in place of quartz, and a variable mercury delay line for time measurement. The velocities are believed to be accurate to a few parts in one thousand.

With a few exceptions, there are three mutually perpendicular samples for each of our rocks. The differences of velocity in three such samples are small for granites, seldom exceeding 2 per cent at pressures above 1000 kg/cm². Gabbros and diabases are slightly more anisotropic, but the greatest departures from isotropy have been found for dunites and certain schists. For the present discussion, we shall concentrate upon granites, including a few samples of granodiorite, and gabbro, including diabase and anorthosite. On the average, these two types are distinctive in their properties, though their distribution curves overlap slightly. All of the new measurements for

each of these types have been averaged to give composite velocity-pressure curves, summarized in Table 1. The corresponding averages from the measurements of HUGHES are also tabulated. The agreement between means at any given pressure is good, the difference scarcely exceeding 1 per cent for the granites or 2 per cent for the gabbro–

TABLE 1

Compressional velocity as function of pressure, at room temperature

P, kg/cm^2	1	500	1,000	2,000	4,000	6,000	10,000
				km/sec			
Granite							
9 rocks, 22 samples	5.22	6.00 ±0.05	6.15	6.23	6.31	6.35	6.41 ±0.02
Standard deviation		0.24					0.08
6 rocks, 6 samples (HUGHES and CROSS, 1951; HUGHES and MAURETTE, 1956)		6.09	6.20	6.27	6.34	(6.42)*	
Gabbro–diabase–anorthosite							
6 rocks, 18 samples	6.26	6.80 ±0.06	6.87	6.91	6.97	7.00	7.04 ±0.06
Standard deviation		0.24					0.24
3 rocks, 3 samples (HUGHES and MAURETTE, 1957)		6.69	6.77	6.84	6.89	6.93	

* 2 samples

diabase group. Two of the granites studied by Hughes (Quincy, Barriefield) are also represented in our group, by a total of five samples.

The dispersion among the samples of granite is notably reduced on passing from 500 kg/cm^2 to 10,000, while that of the gabbro–diabase group remains unchanged. In all of these rocks, the velocities at one atmosphere are considerably below those at 500 kg/cm^2, with much greater dispersion. The effect of the initial porosity is nearly exhausted at 500 kg/cm^2 for the diabases and gabbros, but continues to decrease up to several thousand bars for the granites. The range of V_P for individual samples is as follows: for granites at 500 kg/cm^2, from 5.33 to 6.34 km/sec, at 10,000 kg/cm^2, from 6.31 to 6.62 km/sec;

for gabbros at 500 kg/cm², from 6.37 to 7.20 km/sec, and at 10,000 from 6.61 to 7.36 km/sec. Thus the values for the 'slowest' diabase (Holyoke, Mass.) coincide with those for the 'fastest' granite (biotite granite or granodiorite, Englehart, Ont.). The two curves, for average granite and for average gabbro, at room temperature, have been plotted as solid curves in Fig. 1, where the pressure scale has also been marked off in depths, according to a hydrostatic increase with a density of 2.7 to 10 km, and thereafter a density of 2.9.

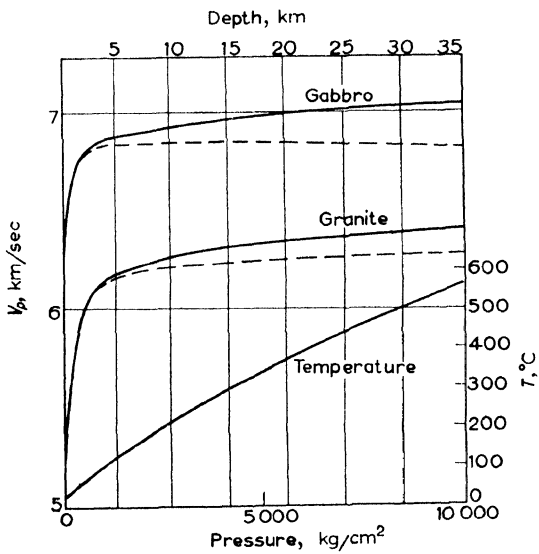

FIG. 1. The velocity V_P for average granite and average gabbro as function of pressure and depth.
The solid curves give velocity versus pressure at 20°C. The broken curves give velocity versus depth after correction for the assumed temperatures shown by the bottom curve.

We have next to estimate the effect of temperature. This raises two questions, both difficult: first, the rate of increase of temperature with depth; second, the rate of change of velocity with temperature. The former is not a fixed quantity; variations from place to place are to be expected, and we can do little more than assess the effect of some representative distribution. For definiteness, let us take curve B of a former discussion (BIRCH, 1955, p. 114); this curve,

plotted in the lower part of Fig. 1, has as its chief merit that it is intermediate between two distributions which are probably near the outer limits for non-volcanic continental areas of normal elevation. The effect of temperature upon velocity requires a new discussion.

Measurements of velocity (both V_P and V_S) up to several hundred degrees at pressures of 500 kg/cm^2 and upward by Hughes and Maurette indicate maxima for both granites and gabbros at shallow depths; the temperatures adopted were not greatly different from those of curve B. There is a question as to whether the technique employed by these investigators was suitable for establishing a true temperature effect. It has been known since the work of IDE (1937) that the consequence of heating rocks at ordinary pressure is a progressive loosening of structure which leads to irreversible decreases of velocity. Hughes and Maurette endeavoured to avoid this by keeping the pressure at 500 kg/cm^2 or above while heating to temperatures above 100°C, or at 200 kg/cm^2 or more for heating to 100°. In our experience, this is not enough pressure to prevent damage, and in high-temperature studies of V_S (BIRCH, 1943 and unpublished) the practice has been to raise the pressure to 4000 kg/cm^2 or more before heating. Even then, it is often necessary to carry out several cycles of heating and cooling in order to obtain a linear, reversible effect. In a number of cases, linear, reversible curves to as much as 500°C have been obtained; beyond this point, most rocks begin to exhibit an accelerated rate of decrease of velocity with temperature, which may sometimes be 'real', sometimes an effect of damage which presumably would not occur under the relatively steady conditions of the crust.

Under these conditions, the smallest temperature effects (aside from the illusory constancy often found at low pressures up to 100°C) are probably most nearly correct as intrinsic properties of the compact aggregates; another helpful criterion is linearity. By these tests, most of the temperature change shown by the rocks of Hughes and Maurette seems likely to be the result of damage caused by heating at low pressure. We then have recourse to the temperature coefficients for V_S, which are unlikely to differ greatly from those for V_P at the relatively low temperatures within the crust.

In addition to the early measurements to 100°C (BIRCH and BANCROFT, 1938) there are now a number to 200° or higher, which are shown in Table 2. Here the primary observation is the frequency

TABLE 2

Temperature variation of frequency, under pressure

Sample		$-10^6 \frac{1}{f}\frac{\Delta f}{\Delta T}$	Maximum temperature (°C)	Pressure kg/cm²
Granites				
Quincy, Mass.	10	34	200	4000
	11	42	180	4000
		43	180	8000
Rockport, Mass.		71	200	4000
Barre, Vt.	1	46	500	3500
	2	34 mean to	400	4500
		43 mean to	500	4500
Chelmsford, Mass.		65 mean to	200	5000
		82 mean to	300	5000
Barriefield, Ont.	1	53	200	3000
		57	200	7000
		41	500	4500
Lynnfield, Mass.	1	38	180	5000
	3	39	180	5000
	3	56	300	3000
Latchford, Ont.	3	53	500	4500
	3	52	180	5000
Englehart, Ont.	1	60	180	5000
	2	49	180	5000
	3	53	180	5000
Weston, Mass.		30	150	4300
Gabbro, diabase, anorthosite				
Diabase (Keweenaw) Michigan	1	57	180	4500
		51	180	9000
	2	68	400	8000
	3	48	180	9000
Diabase, Frederick, Maryland	2	47	180	8000
	3	49	100	4000
Diabase, Cobalt, Ont. (Nippissing)	1	50	180	5000
	3	57	180	5000
Gabbro, Mellen, Wis.	2	116	100	4000
	3	53	120	5000
	4	62	180	5000
		150 mean to	500	5000
Gabbro, French Creek, Pa.	2	87	100	4000
Anorthosite, Stillwater Complex, Mont.	2	50	500	7500
Anorthosite, New Glasgow, Ont.	1	38	180	4000
Coefficients for V_P, after Hughes and Maurette				
Gabbro, Duluth Minn.		160	300	4000
Gabbro, San Marcos Cal.		14	300	6000

of resonance of a cylinder of rock in the torsional mode; the relative change of this frequency with temperature, at constant pressure, has been tabulated. Since the velocity is equal to the frequency (f) times the wave length (L), the velocity coefficient is given by

$$\frac{1}{V}\frac{dV}{dT} = \frac{1}{f}\frac{df}{dT} + \frac{1}{L}\frac{dL}{dT}.$$

The frequency coefficient, intrinsically negative, must be added to the linear thermal expansion coefficient to give the velocity coefficient. The linear thermal expansion has been taken as 10.10^{-6}/deg for the granites, 7.10^{-6}/deg for the gabbros. These figures are based on the thermal expansions of the minerals rather than on measured values for rocks, which are affected by the same troubles with irreversibility as are the velocities, but the differences are not important for this correction. The mean frequency coefficient for the granites is $-\ 50.10^{-6}$/deg, for the gabbros, $-\ 66.10^{-6}$/deg. The corresponding figures for the velocity coefficients are then, in round numbers, $-\ 40.10^{-6}$ for the granites, $-\ 60.10^{-6}$ for the gabbros, as found earlier for a much smaller range of temperature and smaller groups of samples. The figures for gabbro include two exceptionally high values; if these were omitted, the velocity coefficient for the gabbro would be $-\ 50.10^{-6}$/deg. Keeping in mind the possibility that even these apparently reversible changes may not characterize the conditions in the crust, and that we are applying the coefficient for V_S in what follows to a discussion of V_P, we may guess that the real uncertainty as to the velocity coefficients might be as much as 50 per cent.

Table 2 includes several coefficients derived from the measurements of Hughes and Maurette; the large coefficient for V_P for the Duluth gabbro of these investigators is close to that which we have found for V_S in the gabbro from Mellen, Wisconsin. The San Marcos gabbro shows almost no change. Most of the other rocks studied by Hughes and Maurette show so much curvature in velocity–temperature plots that coefficients cannot be determined. The intrinsic changes are small and easily obscured by the irreversible processes.

I take this opportunity to correct an error in an earlier paper. In Tables 5 and 6 (BIRCH, 1943), the 'new measurements' have not been corrected for thermal expansion, contrary to the statement in

the text. The correction will make all of the coefficients smaller in absolute magnitude. Only for the quartzite is the change relatively important; for quartzite, with an average linear expansion of 12.10^{-6} the two velocity coefficients will be reduced to -8.10^{-6} and -13.10^{-6}, in good agreement with an earlier value which had been so corrected.

We now apply temperature corrections to the curves of Fig. 1 with the velocity coefficients just obtained and the temperature distribution shown on this figure. The corrected curves are shown in broken lines. Several values on these curves are shown in Table 3. With the figures which have been adopted, the velocity always increases with depth in a uniform layer of average granite, and decreases slightly, for depths greater than about 10 km, in a uniform layer of average gabbro.

TABLE 3

V_P, corrected for pressure and temperature, in km/sec

Depth km approx.	T (°C)	Granite uncorrected	Granite corrected	Gabbro uncorrected	Gabbro corrected
11	220	6.27	6.22	6.93	6.85
23	420	6.36	6.26	7.01	6.84
32	520	6.40	6.27	7.04	6.83

Since these conclusions are evidently sensitive to changes of assumptions about gradients of temperature and coefficients, a more general treatment which was applied to the earlier measurements (BIRCH and BANCROFT, 1938, p. 134) may be repeated here. The maximum gradient of temperature $(\Delta T/\Delta z)_m$ consistent with upward refraction in a uniform spherical layer of radius r is given by

$$\left(\frac{\Delta T}{\Delta z}\right)_m = -\left[\frac{1}{r} + \left(\frac{1}{V}\frac{dV}{dP}\right)_T \frac{\Delta P}{\Delta z}\right] \div \frac{1}{V}\left(\frac{dV}{dT}\right)_P$$

Here z is the depth. The figures for this calculation are shown in Table 4.

We have also the materials for deriving an estimate of the effect of a gradual change of composition with depth. For example, let us

TABLE 4

Coefficients, and maximum gradients of temperature for upward refraction

Rock	Pressure interval in 10^3 kg/cm^2	$10^6 \frac{1}{V}\left(\frac{dV}{dP}\right)_T$ per kg/cm^2	$-10^6 \frac{1}{V}\left(\frac{dV}{dT}\right)_P$ per deg	$\left(\frac{\Delta T}{\Delta z}\right)_m$ deg/km
Average granite	2– 4	6.5	40	48
	4– 6	3.0	40	24
	6–10	2.2	40	19
Average gabbro	2– 4	3.9	60	21
	4– 6	2.4	60	14
	6–10	1.5	60	10

consider a crust in which the fraction of gabbro at any depth is x; then we need the partial derivative of the velocity with respect to x at constant pressure and temperature, $\frac{1}{V}\left(\frac{dV}{dx}\right)_{P,T}$. At room temperature and 6000 kg/cm^2, this is 0.65/6.7 or about 0.10. The maximum gradient of temperature consistent with upward refraction in a layer in which x as well as P and T vary may now be found by adding to the values of Table 4 the term,

$$-\frac{1}{V}\left(\frac{dV}{dx}\right)_{T,P}\frac{\Delta x}{\Delta z} \div \frac{1}{V}\left(\frac{dV}{dT}\right)_{P,z}$$

Suppose that the composition changes linearly from granite to gabbro over the depth of 35 km, so that $\Delta x/\Delta z = 1/35$ per km. With a mean temperature coefficient of -50.10^{-6}/deg, the correction term is 57°/km, and upward refraction would occur everywhere in the crust for any plausible temperature rise. Even a much smaller change of composition makes an appreciable difference; a linear increase in the amount of gabbro to 10 per cent at the base of the crust would give a correction term of about 6°/km.

This calculation is evidently oversimplified, failing to take account of the real course of variation of velocity with composition. In the sequence of igneous rocks from granites toward gabbros, there is at first little change of velocity (BIRCH, 1955, p. 104); most of the rise takes place between diorite and olivine gabbro. Thus the 'partial

derivative' $\frac{1}{V}\left(\frac{dV}{dx}\right)_{P,T}$ is not constant through this sequence, but increases with x. This would mean that there would be little correction for small x, but a larger one for deeper levels. This would increase the likelihood of upward refraction in a crust with a gabbroic component gradually increasing with depth.

Let us now turn to the seismic results. In Fig. 2, these are super-

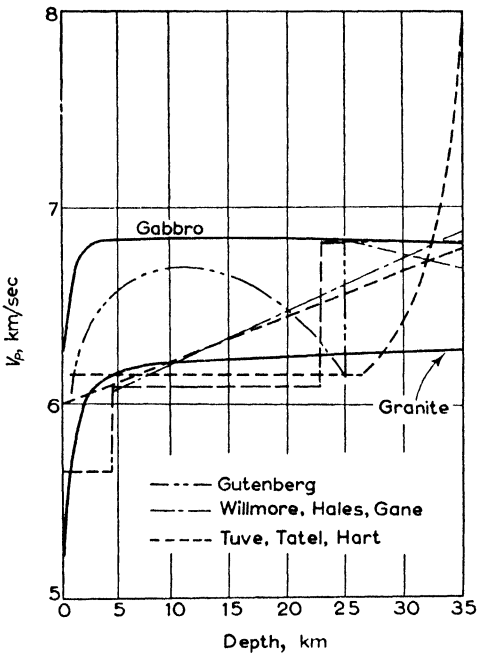

FIG. 2. Experimental velocities compared with seismic velocities, as function of depth.

The solid curves are the corrected (broken) curves of Fig. 1. The other curves show the distribution of seismic velocity according to the authors indicated.

imposed on the two corrected curves for average granite and for average gabbro, the dashed curves of Fig. 1. Disregarding the details for the moment, we readily reach a major conclusion: the 'observed' velocities lie everywhere between the two laboratory curves for granite and gabbro, except for one variant given by TUVE, TATEL and HART (Model D) which would require an increasing

proportion of ultramafic rock near the base of the crust. Model B of TUVE, TATEL and HART, and the continuous distribution of WILLMORE, HALES and GANE, are easily consistent with a simple increase of basic component, from something close to average granite near the top to gabbro or nearly gabbro at the base. The two-layer solution of WILLMORE, HALES and GANE corresponds closely to layers of granite and gabbro. None of these distributions raises any special difficulty of interpretation in terms of the laboratory measurements; they all suggest a generally increasing velocity toward the base of the crust, within the range between granite and gabbro. Further work in the Transvaal (GANE, *et al.*, 1956) has led to a loss of confidence in the reality of the phases P_2 and S_2 formerly associated with the second layer, and indeed, to scepticism regarding the evidence for any systematic variation of velocity with depth. Their best mean value for V_P in the crust is 6.18 km/sec; a possible linear variation according to $V_P = 6.00 + 0.011z$, with z in km, leads to 6.39 km/sec at 35 km. This work became available too late to be included in Fig. 2, but these new values produce no particular difficulty of interpretation.

This is not the case for the distribution given by GUTENBERG, although even here the range of velocity is about the same. This curve rises rapidly in the first 10 km to about 6.7 km/sec, or almost to the velocity for average gabbro at this depth; this is definitely higher than can be ascribed to granitic rocks at this pressure, and in order to account for such a change, it would be necessary to postulate the presence of predominantly gabbroic material at depths of from 5 to 10 km. The variation below this level must be problematic, but the curve as given would demand either (a) a return toward granitic composition as the depth increases, or (b) a rate of rise of temperature much above the usual rate. If (a), having reached granitic composition at about 25 km, we then must postulate a discontinuous change to another gabbroic layer. If (b), then the discontinuity at 25 km must be to a material with a higher velocity than gabbro, with still another transition at the base of the crust. While regional differences are certainly to be sought, either of these schemes is so much more complex than those demanded for the other regions that we may well reserve acceptance if other alternatives provide equally good seismic solutions. In view of the considerable differences of detail consistent with the close seismic coverage in the Transvaal and the

Maryland–Virginia studies, it seems possible that a more readily intelligible distribution of velocity might also account for the observations in southern California.

As a caution in the use of velocities for interpretation, it must be understood that velocities intermediate between those for the granites and gabbros are found for a great variety of rocks, including not only representatives of the igneous sequence such as granodiorites, quartz diorites, and diorites, but also metamorphics such as granitic gneisses and schists, quartzites, limestones and marbles, serpentines, talc and chlorite schists. Within the range between 6 and 7 km/sec, the existence of rocks of entirely different chemical and mineralogical compositions with indistinguishable velocities has two important consequences: on the one hand, it will not be possible to determine the chemical composition of the crust uniquely on the basis of seismology, however detailed; on the other hand, it becomes possible to reconcile the extraordinary uniformity of the seismic velocities from region to region with the great variety of the exposed basement rocks.

The last remark has a bearing on the significance of the *Lg* phase. This is most readily interpreted as a shear wave refracted by the steep near-surface velocity gradient and reflected, perhaps several times, at the surface. Calculations (BIRCH, 1938) based on the experimental studies of V_S in granites showed that rays reaching depths of from 6 to 14 km in an average uniform granitic layer would have mean surface velocities of from 3.45 to 3.52 km/sec. The most recent discussion (PRESS, 1956) gives 3.54 km/sec for the average velocity of *Lg* in California, the range being from 3.32 to 3.71. The agreement with expectation for a predominantly granitic layer is good. But with the further demonstration (BIRCH, 1955, p. 106) that V_S is very nearly the same in a great variety of common metamorphic rocks as in average granite, and that all of these rocks exhibit much the same kind of rapid initial rise of velocity with pressure, the remarkable constancy of the *Lg* velocity for long continental paths becomes intelligible.

Acknowledgment

My thanks are due to DARRELL S. HUGHES and CHRISTIAN MAURETTE for their kindness in furnishing me with a copy of their paper on the velocity in basic igneous rocks in advance of publication.

REFERENCES

BIRCH, Francis and BANCROFT, Dennison (1938) The effect of pressure on the rigidity of rocks, *J. Geol.* **46**, 59–87 and 113–141.

—— —— (1940) New measurements of the rigidity of rocks at high pressure, *J. Geol.* **48**, 752–766.

—— (1938) Travel times for shear waves in a granitic layer, *Seism. Soc. Amer., Bull.* **28**, 49–56.

—— (1943) Elasticity of igneous rocks at high temperatures and pressures, *Geol. Soc. Amer., Bull.* **54**, 263–286.

—— (1955) Physics of the crust, *Geol. Soc. Amer.* Special Paper No. 62, 101–117.

GANE, P. G., ATKINS, A. R., SELLSCHOP, J. P. F. and SELIGMAN, P. (1956) Crustal structure in the Transvaal, *Seism. Soc. Amer., Bull.* **46**, 293–316.

GUTENBERG, B. (1955a) Channel waves in the Earth's crust, *Geophysics*, **20**, 283–294.

—— (1955b) Wave velocities in the Earth's crust, *Geol. Soc. Amer.* Special Paper No. 62, 19–34.

—— (1955c) Low velocity lithosphere channel, *Geol. Soc. Amer., Bull.* **66**, 1203–1204.

HART, P. J. (1954) Variation of velocity near the Mohorovičič discontinuity under Maryland and northeastern Virginia. Harvard University thesis. 83 pp. plus appendix and seismic records.

HUGHES, D. S. and CROSS, J. H. (1951) Elastic wave velocities at high pressures and temperatures, *Geophysics* **16**, 577–593.

—— and MAURETTE, C. (1956) Elastic wave velocities in granites, *Geophysics* **21**, 277–284.

—— —— (1957) Variation of elastic wave velocities in basic igneous rocks with pressure and temperature, *Geophysics* **22**, 23–31.

IDE, J. M. (1937) The velocity of sound in rocks and glasses as a function of temperature, *J. Geol.* **45**, 689–716.

PRESS, Frank (1956) Velocity of Lg waves in California, *Trans. Amer. Geophys. Union* **37**, 615–618.

TATEL, H. E. and TUVE, M. A. (1955) Seismic exploration of a continental crust, *Geol. Soc. Amer.* Special Paper No. 62, 35–50.

TUVE, M. A., TATEL, H. E. and HART, P. J. (1954) Crustal structure from seismic exploration, *J. Geophys. Res.* **59**, 415–422.

WILLMORE, P. L., HALES, A. L. and GANE, P. G. (1952) A seismic investigation of crustal structure in the western Transvaal, *Seism. Soc. Amer., Bull.* **42**, 53–80.

13

THE FREE OSCILLATIONS OF THE EARTH

C. L. PEKERIS and H. JAROSCH*

A SYSTEMATIC study is made of the free oscillations of the earth. Three methods of approach are followed. In the first, the periods of free oscillation of a uniform earth possessing the average properties of the real earth (the 'average model') are investigated. The periods are then determined for the real earth by the use of a variational method. In the third method an exact solution is obtained for the real earth by integrating the differential equations numerically on the electronic computer (WEIZAC).

The periods determined for the uniform model by the variational method were found to be very close to those obtained from the exact solution. Similarly, the fundamental period of radial oscillations for the real earth obtained from the variational method agrees well with the exact value derived on the electronic computer. The results for radial oscillations are shown in Table 1, and some preliminary results for oscillations of the spheroidal type are shown in Table 2. In the case of radial oscillations, the fundamental period for the average model is larger by 30 per cent than the period for the real earth, while for spheroidal oscillations the fundamental period for the average model is 44.3 min, as against a period of 53 min derived from the variational method for the real earth. Should the latter period be substantiated by an exact numerical solution now in progress, then such a result would lend support to BENIOFF's identification of the observed 57 min oscillation with the free oscillation of spheroidal type of the earth.

1. Introduction

This investigation was undertaken at the instigation of Professor H. Benioff in connection with his observation (BENIOFF, 1954) of an oscillation of a period of 57 min in the records of the Kamchatka earthquake of 1952. BENIOFF attributes this oscillation to the free mode of vibration of the earth of the spheroidal type, which

* Research supported by the Office of Naval Research under Contract Nonr-1823(00).

according to a calculation made by LOVE (1911, p. 143) has a period close to 60 min. Since this is the first time that natural oscillations of the whole globe have been detected observationally, it was considered to be of interest to determine whether a free period of 60 min is still valid for the earth in the light of the seismic evidence on the internal constitution of the earth which has accumulated since LOVE's investigation.

LOVE assumed in his calculation that both the density and elastic constants of the earth are constant, and that the mean rigidity $\bar{\mu}$ is equal to that of steel, which he took to be equal to 8.9×10^{11} dyn/cm^2. The information which we now have on the internal constitution of the earth (BULLEN, 1950), derived mainly from seismic data, suggests a structure which is quite different from LOVE's assumed uniform model. Halfway up from the center, in the so-called core of the earth, the rigidity is zero, whereas in the outer mantle the rigidity is many times that of steel. The mass-average value of the rigidity $\bar{\mu}$ is 1.463×10^{12} even allowing for the liquidity of the core, whereas $\bar{\lambda}/\bar{\mu}$ is 2.402, as against a value of 1 assumed for this quantity by LOVE. In addition, we have some indirect evidence on the variation of density with depth.

Besides the problem of the free period of spheroidal oscillation of the real earth, BENIOFF's observation raises other questions which cannot be overlooked. Among these is the magnitude of the periods of other modes of free oscillation of the earth, with a view to detecting them also in earthquake records. We have therefore undertaken a systematic study of the free vibrations of the earth, beginning with the radial pulsations, which are mathematically of the simplest type. Since in the case of non-radial oscillations the problem involves the solution of a system of three simultaneous differential equations of the second order with empirically determined variable coefficients, it was thought necessary to provide an independent method of solution in addition to the direct method of numerical integration. We have adopted for this purpose the *variational method.* Again, partly for the purpose of checking the accuracy of the periods deduced from the variational method, we have derived by a different procedure LOVE's solution for the free oscillations of a uniform earth. The solution for a uniform earth was also needed for the purpose of serving as a guide in the coding on the electronic computer of the problem for the real earth.

Our method of attack on the problem of free oscillations of the earth has, therefore, been undertaken in three stages. First we seek to ascertain the extent to which the dynamical behavior of the earth in its natural oscillations can be approximated by that of a uniform model possessing the average properties of the real earth. Next, we apply the variational method to determine the periods of free oscillation of the real earth. Lastly, we obtain an exact solution of the problem for the real earth by carrying out the numerical integration of the differential equations on the electronic computer.

2. The equations of motion

In treating the free oscillations of the earth we may neglect the effects of the earth's rotation, since the free periods turn out to be of the order of one hour, and are therefore small in comparison with the period of the earth's rotation. We shall also neglect the ellipticity of the earth. Adopting a spherical system of co-ordinates with the origin at the centre of the earth, the equations of elastic vibrations of the gravitating sphere are (LOVE, 1927, p. 91):

$$\rho \frac{\partial^2 u}{\partial t^2} = \rho F_r + \frac{\partial \widehat{rr}}{\partial r} + \frac{1}{r} \frac{\partial \widehat{r\theta}}{\partial \theta} + \frac{1}{r \sin \theta} \frac{\partial \widehat{r\phi}}{\partial \phi} + \frac{1}{r} (2\widehat{rr} - \widehat{\theta\theta} - \widehat{\phi\phi} + \widehat{r\theta} \cot \theta), \quad (1)$$

$$\rho \frac{\partial^2 v}{\partial t^2} = \rho F_\theta + \frac{\partial \widehat{r\theta}}{\partial r} + \frac{1}{r} \frac{\partial \widehat{\theta\theta}}{\partial \theta} + \frac{1}{r \sin \theta} \frac{\partial \widehat{\theta\phi}}{\partial \phi} + \frac{1}{r} \left[(\widehat{\theta\theta} - \widehat{\phi\phi}) \cot \theta + 3\widehat{r\theta} \right], \quad (2)$$

$$\rho \frac{\partial^2 w}{\partial t^2} = \rho F_\phi + \frac{\partial \widehat{r\phi}}{\partial r} + \frac{1}{r} \frac{\partial \widehat{\theta\phi}}{\partial \theta} + \frac{1}{r \sin \theta} \frac{\partial \widehat{\phi\phi}}{\partial \phi} + \frac{1}{r} (3\widehat{r\phi} + 2\widehat{\theta\phi} \cot \theta). \quad (3)$$

Here u, v and w denote the components of displacement in the r, θ and ϕ directions respectively; $\widehat{rr}$, $\widehat{r\theta}$, etc. denote the components of stress, ρ is the density and F the body-force per unit mass.

The usual stress–strain relations have to be modified in our problem, since in the equilibrium position the earth is already under initial stress. We shall assume that this *initial stress* is given by a hydrostatic pressure p_o balancing the gravitational force

$$\frac{\partial p_o}{\partial r} = -g_o\rho_o, \tag{4}$$

where the subscripts refer to the equilibrium values. Following a method proposed by RAYLEIGH (1906), it is assumed that in the disturbed state the stress consists of the *initial stress* and of an *additional stress* which is related to the strain, measured from the equilibrium state, by the usual stress–strain relations holding for an isotropic elastic body. With LOVE (1911, p. 89) we further assume that in this scheme we are to take for the initial stress at a point (x, y, z), the value of the initial stress which was obtained at the point where the particle now at (x, y, z) originated. On the basis of these assumptions the stress–strain relations take the following form

$$\widehat{rr} = -p_o + u\frac{\partial p_o}{\partial r} + \lambda\Delta + 2\mu e_{rr}, \tag{5}$$

$$\widehat{\theta\theta} = -p_o + u\frac{\partial p_o}{\partial r} + \lambda\Delta + 2\mu e_{\theta\theta}, \tag{6}$$

$$\widehat{\phi\phi} = -p_o + u\frac{\partial p_o}{\partial r} + \lambda\Delta + 2\mu e_{\phi\phi}, \tag{7}$$

$$\widehat{r\theta} = \mu e_{r\theta}, \qquad \widehat{r\phi} = \mu e_{r\phi}, \qquad \widehat{\phi\theta} = \mu e_{\phi}\theta, \tag{8}$$

where λ and μ denote the elastic constants and (LOVE, 1927, p. 56)

$$e_{rr} = \frac{\partial u}{\partial r}, \qquad e\theta_\theta = \frac{1}{r}\frac{\partial v}{\partial \theta} + \frac{u}{r}, \tag{9}$$

$$e_{\phi\phi} = \frac{1}{r\sin\theta}\frac{\partial w}{\partial \phi} + \frac{v}{r}\cot\theta + \frac{u}{r}, \qquad e_{r\theta} = \frac{\partial v}{\partial r} - \frac{v}{r} + \frac{1}{r}\frac{\partial u}{\partial \theta}, \tag{10}$$

$$e_{r\phi} = \frac{1}{r\sin\theta}\frac{\partial u}{\partial \phi} + \frac{\partial w}{\partial r} - \frac{w}{r},$$

$$e_{\theta\phi} = \frac{1}{r}\frac{\partial w}{\partial \theta} - \frac{w}{r}\cot\theta + \frac{1}{r\sin\theta}\frac{\partial v}{\partial \phi}, \tag{11}$$

$$\Delta = \frac{\partial u}{\partial r} + \frac{2u}{r} + \frac{1}{r\sin\theta}\frac{\partial}{\partial\theta}(v\sin\theta) + \frac{1}{r\sin\theta}\frac{\partial w}{\partial\phi}. \tag{12}$$

The equation of continuity yields

$$\rho = \rho_o + \rho', \qquad \rho' = -\rho_o\Delta - u\frac{\partial\rho_o}{\partial r}. \tag{13}$$

The gravitational potential Ψ can be written as

$$\Psi = \psi_o(r) + \psi, \tag{14}$$

ψ denoting the perturbation of the gravitational potential arising from the attraction of the density-field ρ' and from the corrugations of the surface. We have

$$\mathbf{F} = \nabla\Psi, \tag{15}$$

$$\nabla^2\psi_o = -4\pi G\rho_o, \qquad \frac{dg_o}{dr} + \frac{2}{r}g_o = 4\pi G\rho_o, \tag{16}$$

$$\nabla^2\psi = 4\pi G(\rho_o\Delta + u\dot{\rho}_o). \tag{17}$$

Here G denotes the gravitational constant and the dot signifies differentiation with respect to r.

By substituting from Eqs. (5), (6), (7), (13) and (15) into Eqs. (1), (2) and (3), we get for the equations of motion

$$\rho_o\frac{\partial^2 u}{\partial t^2} = \rho_o g_o\Delta + \rho_o\frac{\partial\psi}{\partial r} - \rho_o\frac{\partial}{\partial r}(g_o u) + \frac{\partial}{\partial r}\left(\lambda\Delta + 2\mu\frac{\partial u}{\partial r}\right) +$$

$$\frac{\mu}{r}\frac{\partial e_{r\theta}}{\partial\theta} + \frac{\mu}{r\sin\theta}\frac{\partial e_{r\phi}}{\partial\phi} + \frac{\mu}{r}(4e_{rr} - 2e_{\theta\theta} - 2e_{\phi\phi} + \cot\theta e_{r\theta}), \tag{18}$$

$$\rho_o \frac{\partial^2 v}{\partial t^2} = \frac{\rho_o}{r}\frac{\partial \psi}{\partial \theta} + \frac{\partial}{\partial r}(\mu e_{r\theta}) + \frac{1}{r}\frac{\partial}{\partial \theta}(-g_o\rho_o u + \lambda\Delta + 2\mu e_{\theta\theta}) + \frac{\mu}{r\sin\theta}\frac{\partial e_{\theta\phi}}{\partial \phi} + \frac{\mu}{r}\left[2\cot\theta\left(\frac{1}{r}\frac{\partial v}{\partial \theta} - \frac{v}{r}\cot\theta - \frac{1}{r\sin\theta}\frac{\partial w}{\partial \phi}\right) + 3e_{r\theta}\right], \tag{19}$$

$$\rho_o \frac{\partial^2 w}{\partial t^2} = \frac{\rho_o}{r\sin\theta}\frac{\partial \psi}{\partial \phi} + \frac{\partial}{\partial r}(\mu e_{r\phi}) + \frac{\mu}{r}\frac{\partial e_{\theta\phi}}{\partial \theta} + \frac{1}{r\sin\theta}\frac{\partial}{\partial \phi}(-g_o\rho_o u + \lambda\Delta + 2\mu e_{\phi\phi}) + \frac{3\mu}{r}e_{r\phi} + \frac{2\mu}{r}\cot\theta e_{\theta\phi}. \tag{20}$$

3. Boundary conditions

The above equations are to be solved under the conditions of:

(1) Regularity at the origin.

(2) Vanishing of the stresses on the *deformed* surface of the earth, and

(3) Equality at the *deformed* surface of the earth of the values of the internal and external gravitational potentials, and of their respective gradients.

Let a denote the mean radius of the earth. Then we have for the value of the stress $\widehat{rr}$ at the surface $r = a + u$,

$$\widehat{rr}(a+u) = \widehat{rr}(a) + u\frac{\partial \widehat{rr}}{\partial r} = \left[-p_o + u\frac{\partial p_o}{\partial r} + \lambda\Delta + 2\mu\frac{\partial u}{\partial r}\right]_a -$$
$$u\frac{\partial p_o}{\partial r} = \lambda\Delta + 2\mu\frac{\partial u}{\partial r} = 0, \qquad \text{at } r = a, \tag{21}$$

to within quantities of the first order in u. Similarly, the conditions of the vanishing of $\widehat{r\theta}$ and of $\widehat{r\phi}$ at the deformed surface are met by putting

$$e_{r\theta} = e_{r\phi} = 0, \qquad \text{at } r = a. \tag{22}$$

Let ψ_e denote the gravitational potential outside the sphere. Then the matching of ψ and ψ_e on the deformed surface can be accomplished by putting

$$\psi = \psi_e, \qquad r = a, \tag{23}$$

$$\frac{\partial \psi}{\partial r} - \frac{\partial \psi_e}{\partial r} = 4\pi G \rho_o u, \qquad r = a, \tag{24}$$

again to within quantities of the first order in u. Since, moreover, each spherical harmonic component ψ_{en} of order n satisfies the relation

$$\frac{\partial \psi_{en}}{\partial r} = -\frac{(n+1)}{r}\psi_{en}, \tag{25}$$

Eq. (24) can be written as

$$\frac{\partial \psi_n}{\partial r} + \frac{(n+1)}{a}\psi_n = 4\pi G \rho_o u_n, \tag{26}$$

in which only quantities pertaining to the interior of the earth appear.

4. Radial oscillations

A. *The equation of motion.* Eqs. (17), (18), (19), and (20) represent a differential system of the eighth order for the four variables u, v, w and ψ, in which enter as coefficients the empirical functions of r, ρ_o, g_o, λ and μ, representing the equilibrium characteristics of the internal constitution of the earth. We shall confine our discussion to the special cases of:

(1) Radial oscillations.

(2) Non-radial oscillations, in which the radial component of the curl of the displacement vanishes.

In the case of purely radial pulsations, we have

$$v = w = 0, \qquad u = u(r), \qquad \Delta = \dot{u} + \frac{2u}{r}, \tag{27}$$

and, on adopting a time factor $e^{i\sigma t}$, Eq. (18) reduces to

$$\rho_o \sigma^2 u + \rho_o g_o \Delta + \rho_o \dot{\psi} - \rho_o \frac{d}{dr}(g_o u) + \frac{d}{dr}(\lambda \Delta + 2\mu \dot{u}) + \frac{\mu}{r}\left(4\dot{u} - \frac{4u}{r}\right) = 0. \tag{28}$$

Eq. (17) takes the form

$$\frac{1}{r^2}\frac{d}{dr}\left(r^2\frac{d\psi}{dr}\right)=\frac{4\pi G}{r^2}\frac{d}{dr}(r^2\rho_o u), \tag{29}$$

which integrates into

$$\frac{d\psi}{dr}=4\pi G\rho_o u, \tag{30}$$

under the condition of regularity at the origin. By the use of Eqs. (30) and (16), Eq. (28) reduces to

$$\rho_o\sigma^2 u+\frac{4}{r}\rho_o g_o u+\frac{d}{dr}\left[\lambda\left(\dot{u}+\frac{2u}{r}\right)+2\mu\dot{u}\right]+\frac{\mu}{r}\left(4\dot{u}-\frac{4u}{r}\right)=0. \tag{31}$$

This is an equation involving u only and is to be solved subject to the boundary condition (21):

$$(\lambda+2\mu)\dot{u}+\frac{2}{r}\lambda u=0, \qquad r=a. \tag{32}$$

From the boundary condition (26) on ψ, it follows that ψ vanishes at $r=a$, a result which can also be derived from elementary considerations.

B. *Radial oscillations of a uniform earth.* In the case of a uniform earth in which ρ_o, λ and μ are constant, the gravitational force increases linearly with the distance from the center

$$g_o=Ar, \qquad A=4\pi G\rho_o/3, \tag{33}$$

and (31) yields

$$\ddot{u}+\frac{2\dot{u}}{r}-\frac{2u}{r^2}+k^2u=0, \tag{34}$$

where

$$k^2=\frac{\rho_o(\sigma^2+4A)}{(\lambda+2\mu)}. \tag{35}$$

An appropriate solution of (34) is

$$u = \frac{\sin kr}{k^2r^2} - \frac{\cos kr}{kr}. \tag{36}$$

The boundary condition (32) yields a relation determining the period of free radial oscillations of the uniform earth

$$\frac{\tan x}{x} = \frac{1}{\left[1 - \frac{x^2}{4}\left(2 + \frac{\lambda}{\mu}\right)\right]}, \qquad x = ka. \tag{37}$$

The solution (36) and the frequency relation (37) are identical in form with the corresponding expressions for the case of radial oscillations of a non-gravitating uniform elastic sphere (LOVE, 1911, p. 103, 113; 1927, p. 285), except for the fact that in the latter case the term $4A$ in expression (35) for k^2 is missing. The fact that gravity appears only in the expression for k^2, and there only in the combination of $(\sigma^2 + 4A)$, exhibits clearly the *destabilizing effect of gravity*. Indeed, if x_1 denote the lowest root of (37), for a given value of (λ/μ), then σ^2 will become negative, or *gravitational instability will ensue*, if the density or radius is big enough, or the elastic constants are small enough for the following relation to hold

$$\frac{16\pi G\rho_o^2 a^2}{3(\lambda + 2\mu)} > x_1^2. \tag{38}$$

If we adopt BULLEN's (1950) model B for the earth, we find that the mass-average values of the elastic constants λ and μ and of the density ρ_o are

$$\bar{\mu} = 1.463 \times 10^{12}, \qquad (\bar{\lambda}/\bar{\mu}) = 2.402, \qquad \bar{\rho} = 5.52, \tag{39}$$

in C.G.S. units. We shall refer to a uniform earth characterized by the above constants as the *average model*. For this average model the lowest two roots of (37) are

$$x_1 = 2.788, \quad \text{and } x_2 = 6.132,$$

yielding, by (35), the periods of

$$T_1 = 26.7\text{m}, \quad T_2 = 10.6\text{m}, \tag{40}$$

for the fundamental mode and for the second mode, respectively, of radial oscillations of the average model. It will be seen in the next section that the period of the fundamental mode for the average model is about 30% higher than for the real earth. Thus, for the purpose of determining the period of the fundamental mode of radial oscillations, the average model is not a proper substitute for the real earth.

C. *Radial oscillations of the real earth.* By the term 'real earth' we shall mean in the sequel BULLEN'S (1950) model B for the earth. Two methods of attack were used to determine the period of free radial oscillations for the real earth:

(1) A variational method, and
(2) Numerical integration of Eq. (31) on the electronic computer of the Weizmann Institute (WEIZAC).

Eq. (31) is the Eulerian equation for the minimization of I, where

$$I = \int_0^a dr[\sigma^2\rho_0 r^2u^2 + 4g_0\rho_0 ru^2 - \lambda(r\dot{u} + 2u)^2 - \mu(2r^2\dot{u}^2 + 4u^2)]. \tag{41}$$

Furthermore, (32) is the corresponding free boundary condition. With $\rho_0(r)$, $g_0(r)$, $\lambda(r)$ and $\mu(r)$ given as in BULLEN'S model B, and adopting a polynomial expression for $u(r)$, the minimization of I can be reduced, in the usual manner, to a condition for the vanishing of a determinant, and the roots of this determinant give the natural frequencies. The values of the first two periods obtained thus from the variational method are

$$T_1 = 20.7\text{m}, \quad T_2 = 9.8\text{m}. \tag{42}$$

One practical advantage of the variational method is that the derivatives of μ and λ do not appear in the integrand of I in (41), in contrast to the differential equation (31) where they appear explicitly. Now, if we know the density $\rho_0(r)$, we can then compute μ and λ from the seismically determined values of the compressional velocity c_p and the shear velocity c_s, by using the relations

$$\mu = \rho_0 c_s^2, \quad \lambda = \rho_0(c_p^2 - 2c_s^2). \tag{43}$$

On the other hand, an explicit evaluation of the derivatives of the empirically determined functions $\mu(r)$ and $\lambda(r)$ is subject to considerable uncertainty, and should be avoided. One way of accomplishing this formally is to transform (31) into a system of two first order differential equations, using as a new independent variable the stress $\widehat{rr}$:

$$\dot{u} = -\frac{2\lambda}{r(\lambda + 2\mu)} u + \frac{\widehat{rr}}{(\lambda + 2\mu)}, \tag{44}$$

$$\dot{\widehat{rr}} = u\left[\frac{4\mu(3\lambda + 2\mu)}{r^2(\lambda + 2\mu)} - \rho_0\sigma^2 - \frac{4}{r}\rho_0 g_0\right] - \frac{4\mu\widehat{rr}}{r(\lambda + 2\mu)}. \tag{45}$$

The system of equations (44) and (45) was coded and integrated on the WEIZAC, using the Runge-Kutta method. The values thus obtained for the periods of the fundamental mode and of the second mode in the radial oscillations of the real earth are

$$T_1 = 20.7\text{m}, \qquad T_2 = 10.1\text{m}. \tag{46}$$

The results for the periods of radial oscillations of the earth are summarized in Table 1.

TABLE 1

The periods T_1 of the fundamental mode and T_2 of the second mode of radial oscillations of the earth. The real earth is represented by Bullen's model B. The numerical integration was carried out on the WEIZAC.

Earth Model	Method of Solution	T_1	T_2
Average Model	Exact	26.7m	10.6m
Real Earth	Variational	20.7m	9.8m
Real Earth	Numerical Integration	20.7m	10.1m

It is seen from Table 1 that in the case of the fundamental mode of radial oscillations, the variational method yields an accurate value for the period, whereas the corresponding period for the average model deviates by nearly 30% from the correct value for the real earth.

5. Non-radial oscillations of the earth

A. *The equations of motion.* We shall limit our discussion of the non-radial oscillations of the earth to the class of motions specified by (HOSKINS, 1920)

$$u = U(r)S_n(\theta, \phi), \quad v = V(r)\frac{\partial S_n(\theta, \phi)}{\partial \theta}, \quad w = \frac{V(r)}{\sin\theta}\frac{\partial S_n(\theta, \phi)}{\partial \phi}, \tag{47}$$

where $S_n(\theta, \phi)$ denotes a spherical surface harmonic of order n. This class is characterized by the vanishing of the radial component of the curl of the displacement ω_r, while the components ω_θ and ω_ϕ are different from zero. The dilatation Δ and the perturbation in the gravitational potential ψ are, according to (12) and (17), given by

$$\Delta = X(r)S_n(\theta, \phi), \qquad \psi = P(r)S_n(\theta, \phi), \tag{48}$$

with

$$X = \dot{U} + \frac{2}{r}U - \frac{n(n+1)}{r}V, \tag{49}$$

$$\ddot{P} + \frac{2}{r}\dot{P} - \frac{n(n+1)}{r^2}P = 4\pi G(\dot{\rho}_o U + \rho_o X). \tag{50}$$

Substitution of (47) into Eqs. (18) and (19) leads to

$$\sigma^2\rho_o U + \rho_o\dot{P} + g_o\rho_o X - \rho_o\frac{d}{dr}(g_o U) + \frac{d}{dr}(\lambda X + 2\mu\dot{U}) + \frac{\mu}{r^2}[4\dot{U}r - 4U + n(n+1)(-U - r\dot{V} + 3V)] = 0, \tag{51}$$

$$\rho_o\sigma^2 Vr + \rho_o P - g_o\rho_o U + \lambda X + r\frac{d}{dr}\left[\mu\left(\dot{V} - \frac{V}{r} + \frac{U}{r}\right)\right] + \frac{\mu}{r}[5U + 3r\dot{V} - V - 2n(n+1)V] = 0. \tag{52}$$

Here, we have assumed as before that the time-variation is represented by a factor $e^{i\sigma t}$. The w-equation (20) leads again to Eq. (52).

The boundary conditions (21), (22) and (26) require that at $r = a$,

$$\lambda X + 2\mu U = 0, \tag{53}$$

$$r\dot{V} - V + U = 0, \tag{54}$$

$$\dot{P} + \frac{(n+1)}{r} P - 4\pi G\rho_o U = 0. \tag{55}$$

We note that the conditions of the vanishing at the surface of $e_{r\theta}$ and of $e_{r\phi}$ yield the same relation (54).

Equations (50), (51) and (52) represent three simultaneous second order differential equations for the determination of the three functions P, U and V, or a sixth-order differential equation for each of these variables. Of the three equations, (50) can be integrated immediately to

$$P(r) = \frac{4\pi G}{(2n+1)}\left\{\frac{1}{r^{n+1}}\int_0^r \rho_o[nU + n(n+1)V]r^{n+1}\,dr + r^n\int_r^a \frac{\rho_o}{r^n}[-(n+1)U + n(n+1)V]dr\right\}, \tag{56}$$

enabling us to determine P if U and V are known. The solution (56) was chosen so as to satisfy the boundary condition (55). As for Eqs. (51) and (52) for U and V, they have to be solved numerically in the general case when ρ_o, g_o, λ and μ are given as empirical functions of r. The integration for the real earth is at present being carried out on the WEIZAC.

Another possible approach to the problem of determining the free periods of non-radial oscillation of the real earth is the *variational*

*method.** The appropriate integral I whose extremum is to be sought is

$$I = \int_o^a dr \left\{ \begin{array}{l} \frac{\sigma^2}{2} r^2 \rho_o [U^2 + n(n+1)V^2] - \frac{1}{2}(\lambda + 2\mu)[r\dot{U} + 2U - \\ n(n+1)V]^2 - \frac{1}{2}\mu n(n+1)(r\dot{V} - V + U)^2 + \\ U^2(2\mu + 2rg_o\rho_o - 2\pi G r^2 \rho_o^2) + n(n+1)\mu V^2 - \\ n(n+1)V[2\mu U + 2r\mu\dot{U} + g_o\rho_o rU] + 4\mu r U\dot{U} + \\ r^2\rho_o U\dot{P} + n(n+1)r\rho_o VP - \frac{1}{8\pi G}[r\dot{P} + (n+1)P]^2 \end{array} \right\}. \quad (57)$$

The variations of I with respect to U, V and P yield Eqs. (51), (52) and (50) respectively, while Eqs. (53), (54) and (55) are the corresponding free boundary conditions. The integral (57) refers to the type of motion defined in (47), and therefore applies separately to each spherical harmonic component of such motion.

B. *Exact solution for non-radial oscillations of a uniform earth.* In order to have some guide as to the magnitude of the periods of free non-radial oscillations of the real earth, we shall treat first the case of a uniform earth, where an exact solution can be obtained. This problem was solved by LOVE (1911, Ch. X), but as the analysis is rather involved, we shall give an independent derivation of the solution based on our method, in which spherical co-ordinates are used *ab initio*.

Using (33) in (50), (51) and (52), we get

$$\ddot{P} + \frac{2}{r}\dot{P} - \frac{n(n+1)}{r^2} P = 4\pi G \rho_o X, \quad (58)$$

$$\sigma^2 U + \dot{P} + ArX - Ar\dot{U} - Au + \frac{\lambda}{\rho_o}\dot{X} + \frac{2\mu}{\rho_o}\ddot{U} + \frac{\mu}{r^2\rho_o}[4r\dot{U} - 4U + n(n+1)(3V - U - r\dot{V})] = 0, \quad (59)$$

*The variational method was used in the problem of the bodily tide, by R. STONELEY (1926).

$$\sigma^2 rV + P - ArU + \frac{\lambda}{\rho_o} X + \frac{\mu}{r\rho_o}(r^2\ddot{V} - r\dot{V} + V + r\dot{U} - U) + \frac{\mu}{r\rho_o}[5U + 3r\dot{V} - V - 2n(n+1)V] = 0. \quad (60)$$

If we differentiate (60) and subtract (59) from the result, we obtain the relation

$$\frac{\mu}{\rho_o} \nabla^2 H + \sigma^2 H = AX, \quad (61)$$

where

$$H = \dot{V} + \frac{V}{r} - \frac{U}{r}, \quad (62)$$

and the ∇^2 operator is defined as

$$\nabla^2 = \frac{d^2}{dr^2} + \frac{2}{r}\frac{d}{dr} - \frac{n(n+1)}{r^2}. \quad (63)$$

$H(r)$ represents the radial dependence of each of the two non-vanishing components of the curl of the displacements ω_θ and ω_ϕ. Again, upon differentiating (59) and adding multiples of (59) and (60) so as to give $\sigma^2 X$, we obtain the result

$$\left(\frac{\lambda + 2\mu}{\rho_o}\right) \nabla^2 X + (\sigma^2 + 4A)X = An(n+1)H. \quad (64)$$

It follows now from (61) and (64) that X satisfies the homogeneous equation of the fourth order

$$\left(\sigma^2 + \frac{\mu}{\rho_o}\nabla^2\right)\left[(\sigma^2 + 4A)X + \left(\frac{\lambda + 2\mu}{\rho_o}\right)\nabla^2 X\right] - n(n+1)A^2 X = 0. \quad (65)$$

Similarly H satisfies the same equation.

Let

$$r = ay, \qquad \alpha^2 = \frac{\sigma^2 \rho_o a^2}{\mu}, \qquad \beta^2 = \frac{(\sigma^2 + 4A)a^2\rho_o}{(\lambda + 2\mu)}, \quad (66)$$

$$\gamma^2 = \frac{n(n+1)A^2 a^4 \rho_o^2}{\mu(\lambda + 2\mu)}, \qquad \omega^2 = 3Aa^2, \qquad \nu^2 = \frac{Aa^2\rho_o}{\mu}, \quad (67)$$

$$2k^2 = \alpha^2 + \beta^2 + \sqrt{[(\alpha^2 - \beta^2)^2 + 4\gamma^2]},$$
$$2q^2 = \alpha^2 + \beta^2 - \sqrt{[(\alpha^2 - \beta^2)^2 + 4\gamma^2]}. \tag{68}$$

Then Eq. (65) can be written in the form

$$(\nabla^2 + k^2)(\nabla^2 + q^2)X = 0, \tag{69}$$

where the independent variable in the ∇^2 operator is now y instead of r.

The general solution of (69) can be expressed in terms of spherical wave functions of order n, but in view of our immediate application, we shall confine the discussion to the case $n = 2$. With

$$\phi(x) = \frac{\mathfrak{J}_{5/2}(x)}{\sqrt{x}}, \qquad f(x) = \sqrt{(x)}\mathfrak{J}_{7/2}(x), \tag{70}$$

an appropriate solution of (69) is

$$X = B\phi(ky) + C\phi(qy). \tag{71}$$

Eq. (61) now gives

$$H = \frac{B\nu^2}{(\alpha^2 - k^2)}\phi(ky) + \frac{C\nu^2}{(\alpha^2 - q^2)}\phi(qy), \tag{72}$$

there being no solution for H of the form $\phi(\alpha y)$. With X and H known, we can obtain U, V and P by solving Eqs. (49), (52) and (58) respectively. The result is

$$yU = \frac{aB}{k^2}\left\{ -\left[2 + \frac{6\nu^2}{\alpha^2 - k^2}\right]\phi(ky) + f(ky)\right\} +$$
$$\frac{aC}{q^2}\left\{ -\left[2 + \frac{6\nu^2}{(\alpha^2 - q^2)}\right]\phi(qy) + f(qy)\right\} + 2aEy^2, \tag{73}$$

$$yV = \frac{aB}{k^2}\left\{ -\left[1 + \frac{3\nu^2}{\alpha^2 - k^2}\right]\phi(ky) + \frac{\nu^2}{(\alpha^2 - k^2)}f(ky)\right\} +$$
$$\frac{aC}{q^2}\left\{ -\left[1 + \frac{3\nu^2}{\alpha^2 - q^2}\right]\phi(qy) + \frac{\nu^2}{(\alpha^2 - q^2)}f(qy)\right\} + aEy^2, \tag{74}$$

$$P = -\frac{\omega^2 B}{k^2}\phi(ky) - \frac{\omega^2 C}{q^2}\phi(qy) + \frac{\omega^2 E}{3\nu^2}(2\nu^2 - \alpha^2)y^2, \tag{75}$$

where B, C and E are arbitrary constants. When the above expressions are substituted in the boundary conditions (53), (54) and (55), there result three homogeneous equations in B, C and E. The vanishing of the determinant of these equations gives the required frequency relation for the non-radial oscillations. Let

$$\tau = \frac{\lambda}{\mu}, \qquad s = \frac{\sigma^2}{A}, \tag{76}$$

$$F(x) = -\frac{\mathfrak{J}_{5/2}(x)}{x\mathfrak{J}_{3/2}(x)}, \qquad 2R = \sqrt{[(s+s\tau-4)^2+24\tau+48]}, \tag{77}$$

then we have from (68)

$$\begin{aligned} k^2 &= \frac{\nu^2}{(4+2\tau)}(4+3s+s\tau+2R), \\ q^2 &= \frac{\nu^2}{(4+2\tau)}(4+3s+s\tau-2R), \end{aligned} \tag{78}$$

and the frequency relation can be reduced to the form

$$\begin{aligned} &\frac{\left\{F(k)\left[(2+\tau)k^2-\frac{(20s-25)}{(5s-4)}(12+4\tau-s-s\tau+2R)\right]-\right.}{\left\{F(k)\left[(2+\tau)\left(4-\frac{s}{2}-\frac{s\tau}{2}+R\right)k^2-20\,(12+4\tau-s-\right.\right.} \\ &\qquad\qquad \frac{\left.\left.8-2\tau+s+s\tau-2R\right\}}{\left.s\tau+2R)\right]-48-16\tau+4s+4s\tau-8R\right\}} - \\ &\frac{\left\{F(q)\left[(2+\tau)q^2-\frac{(20s-25)}{(5s-4)}(12+4\tau-s-s\tau-2R)\right]-\right.}{\left\{F(q)\left[(2+\tau)\left(4-\frac{s}{2}-\frac{s\tau}{2}-R\right)q^2-20(12+4\tau-s-\right.\right.} \\ &\qquad\qquad \frac{\left.\left.8-2\tau+s+s\tau+2R\right\}}{\left.s\tau-2R)\right]-48-16\tau+4s+4s\tau+8R\right\}}=0. \end{aligned} \tag{79}$$

For a given value of τ and for an assumed value of s, $-k$, q and R can be computed from (77) and (78), and then (79) evaluated. When a root s of (79) is thus found, the corresponding period T of free non-radial oscillations of the second spherical harmonic type can be obtained from the relation

$$T = \frac{2\pi}{\sqrt{[sA]}} = \frac{2\pi}{\sqrt{[s4\pi G\rho_0/3]}} = \frac{84.3}{\sqrt{s}} \text{ min} \tag{80}$$

Some results of such calculations are given in Table 2, and will be discussed later.

C. *Solution for the non-radial oscillations of a uniform earth by the variational method.* Our purpose in treating the theory of non-radial oscillations of a *uniform earth* was first to determine how the hitherto generally quoted result of LOVE of 60 min for the free period of spheroidal oscillations of the earth is affected if, instead of LOVE'S values of $\lambda = \mu = 8.19 \times 10^{11}$, we use the very different average values given in Eq. (39). The latter are based on our present-day information concerning the interior of the earth. Secondly, we wished to have an exact solution for *some* model in order to be able to test on this model the efficacy of the variational method in determining the period of free non-radial oscillations. The results would be expected to provide an estimate of the accuracy which could be attributed to a variational value for the period of non-radial oscillations of the *real earth*, where an exact solution is difficult to obtain.

With this in mind we have also determined the free period of non-radial oscillations of a uniform earth by the use of the variational method. The normal procedure would be to use (57) with $n = 2$, assume polynomial expressions in the variable r for each of the functions U, V and P chosen so as to satisfy the boundary conditions (53), (54) and (55), and then to equate to zero the derivatives of I in (57) with respect to each of the independent coefficients in the three polynomials. We have, however, adopted a different procedure, which effectively reduces the sixth order differential system to a fourth order one. Instead of assuming an arbitrary polynomial for P, subject only to the boundary condition (55), we have determined the coefficients of P in terms of those of U and V by using the exact solution (56).

The polynomials assumed for U and V were

$$U = 2y + \alpha y^3 + \beta y^5, \qquad V = y + \gamma y^3 + \delta y^5. \tag{81}$$

Here, the coefficients of the y terms were chosen* so as to annul the constant term in the expression for X, since such a term would lead to a term $r^2 \ln r$ in P, which would give a discontinuous value of the gradient of gravity at the origin. The corresponding expression for P resulting from Eq. (56) is

$$P = (aA/420)(By^2 + Cy^4 + Dy^6),$$
$$B = 504 - 378\alpha - 189\beta + 756\gamma + 378\delta, \tag{82}$$

$$C = 450\alpha - 540\gamma, \qquad D = 245\beta - 210\delta. \tag{83}$$

The imposition of the boundary conditions allows us to express γ and δ in terms of α and β:

$$6\tau\gamma = 8 + 6\tau + (12 + 13\tau)\alpha + (20 + 17\tau)\beta, \tag{84}$$

$$-6\tau\delta = 4 + 6\tau + (6 + 8\tau)\alpha + (10 + 10\tau)\beta; \quad \tau = \lambda/\mu. \tag{85}$$

With this scheme, the variational integral I in (57) becomes an inhomogeneous quadratic expression in the two arbitrary coefficients α and β. We then substitute in this expression

$$\alpha = \frac{a}{c}, \qquad \beta = \frac{b}{c}, \tag{86}$$

whereby c^2I becomes a homogeneous quadratic expression in a, b and c. Variation of c^2I with respect to a, b and c leads to three simultaneous linear homogeneous equations in these constants. The condition of the vanishing of the determinant of these equations provides us with a relation to determine the periods of the fundamental mode and of the second and third modes of non-radial oscillations of a uniform earth. Some results obtained in this manner are given in Table 2, and will be discussed presently.

* α, β and γ should not be confused with the quantities defined in Eqs. (66) and (67).

D. *Solution for the non-radial oscillations of the real earth by the variational method.* The solution for the non-radial oscillations of the real earth is complicated not only by the high order (sixth) of the controlling differential system and by the empirical nature of the coefficients appearing in the differential Eqs. (50), (51) and (52), but also by the differing nature of the motion inside the liquid core and in the rigid outer mantle, due to the lack of shear stresses in the former. Even when a numerical solution is achieved, an independent approach is needed to provide some check on the results. For these reasons we have determined the free periods of non-radial oscillations of the real earth by the use of the variational method.

The same general procedure was followed as was described in the preceding section for the uniform earth, but the details are more involved due to the empirical nature of the coefficients. We adopt the forms (81) for U and V, with the arbitrary constants α, β, γ and δ. The boundary conditions again allow us to express γ and δ in terms of α and β through Eqs. (84) and (85), where now however *one has to use for* τ *the value of* λ/μ *at the surface*: $\tau_0 = 1.165$. The function $P(r)$ of (56) has now to be obtained by numerical integration, using the empirical values of $\rho_0(r)$. These integrations were carried out on the WEIZAC using an interval of integration of 1/32 of the radius of the earth. This gives for $P(r)$ a linear expression in terms of α, β, γ and δ, with coefficients which vary from point to point. These expressions were used in the integrand of (57). I was thus obtained by numerical integration, using the empirically determined functions of r of the quantities ρ_0, g_0, λ and μ, as a quadratic expression in α, β, γ and δ. The latter was reduced to a quadratic expression in α and β only, by using Eqs. (84) and (85) with $\tau = 1.165$. The variation of the resulting expression for c^2I with respect to a, b and c, led, as before, to a determinant whose roots gave the periods of free non-radial oscillations of the real earth. These are shown in Table 2.

E. *Discussion of the results to date on the free period of non-radial oscillations of the earth.* The results of the various investigations made to date by LOVE and ourselves on the periods of non-radial oscillations of the earth of the second spherical-harmonic type are summarized in Table 2. The generally quoted value of LOVE (1911, pp. 142, 143) of 60 min is represented in case 1. It is based on the assumption that the mean rigidity of the earth is equal to that of steel, which Love

took to be 8.19×10^{11} dyn/cm^2. In order to provide a guide on the coding of the problem of non-radial oscillations of the real earth, we have coded the corresponding problem for the uniform model and have integrated LOVE's case on the WEIZAC. The result is shown in case 2, where a period identical with LOVE's value was obtained.

Next, we wished to ascertain how LOVE's value for the period will be modified if we use the actual average values of μ and λ for the real earth. This is shown in case 3, where a period of only 44.3m was obtained. An identical value for the period was obtained for this model by the variational method, as stated in case 4. In order to check

TABLE 2

The period T_1 of the fundamental mode of free oscillations of the earth of the second spherical-harmonic type. The exact values were obtained from Eq. (79). *The numerical integration was carried out on the WEIZAC.*

Case	Earth Model	μ	λ/μ	Method of Solution	T_1
1	Uniform	0.819×10^{12}	1	Exact	60.0m*
2	Uniform	0.819×10^{12}	1	Num. Integration	60.0m
3	Uniform	1.463×10^{12}	2.402	Exact	44.3m
4	Uniform	1.463×10^{12}	2.402	Variational	44.3m
5	Uniform	0.91×10^{12}	1	Exact	56.5m*
6	Uniform	0.91×10^{12}	1	Exact	56.7m
7	Uniform	0.91×10^{12}	1	Variational	56.7m
8	Real Earth	Variable	Variable	Variational	52.0m

* LOVE (1911), pp. 142, 143.

further the accuracy to be expected for the periods derived by the use of the variational method, we have treated the model of case 5 by both methods. It is seen that the periods quoted in cases 6 and 7 agree to within a few seconds. The somewhat lower value of case 5 obtained by LOVE is probably due to the rather indirect numerical procedure which he used to obtain the period for a given value of μ.

Finally we applied the variational method to compute the period of spheroidal oscillations of the real earth, following the procedure outlined in the preceding section. The result of 53.0m for the fundamental mode quoted in case 8 is considerably higher than the values of 44.3m given in cases 3 and 4 for the 'average model'. The

exact period for the real earth should be higher than the value of 53.0m obtained by the variational method, but judging by the evidence presented by cases 4 and 6, the difference is probably small.

Pending the substantiation of this result by an exact solution of the problem currently in progress on the WEIZAC, it would seem provisionally that the existence of the liquid core as well as the effect of the constraints imposed by the boundary conditions at the surface, where the rigidity is smaller than the average, tend to make the real earth behave dynamically in spheroidal vibrations as a less rigid body than is represented by the mass-average value of its rigidity.

REFERENCES

BENIOFF, H. (1954) *Trans. Amer. Geoph. Un.* **35**, 985.

BULLEN, K. E. (1950) *Roy. Astr. Soc. Geo. Suppl.* **6**, No. 1, 50.

HOSKINS, L. M. (1920) *Trans. Amer. Math. Soc.* **21**, 10.

LOVE, A. E. H. (1911) *Some Problems of Geodynamics*, Cambridge University Press.

—— (1927) *A Treatise on the Mathematical Theory of Elasticity*, p. 91. Cambridge University Press.

RAYLEIGH, Lord (1906) *Scientific Papers* **5**, 300. Cambridge University Press.

STONELEY, R. (1926) *Roy. Astr. Soc. Geo. Suppl.* **1**, 357.

NOMENCLATURE

Symbol	Meaning	Defined on page	Adopted value in C.G.S. units
G	Gravitational constant	175	6.670×10^{-8}
a	Mean radius of the earth	176	6.37×10^{8}
σ	2π times the frequency of oscillation	177	
A	A constant equal to $4\pi G\rho_0/3$	178	
$\bar{\rho}$	Average density for the earth	179	5.52
$\bar{\mu}$	Average of the rigidity μ for the earth	179	1.463×10^{12}
$\bar{\lambda}$	Average of the elastic constant λ for the earth	179	$2.402\bar{\mu}$
ν^2	$Aa^2\rho_0/\mu$	185	2.450
ω^2	$3Aa^2$	185	
τ	λ/μ	187	
s	σ^2/A	187	
T	Period of non-radial oscillations	188	$\frac{84.3}{\sqrt{s}}$ min
τ_0	Value of λ/μ at the surface	190	1.165

14

THE GEOPHYSICAL HISTORY OF A GEOSYNCLINE

F. A. VENING MEINESZ

IT IS with great pleasure that I contribute to this book, in honour of my good friend Dr. BENO GUTENBERG. In doing so I have chosen the subject of the deformation of the earth's crust in the zones of weakness, commonly indicated as geosynclines, where in the first stage a subsidence occurs, gradually combined with folding of the surface layers, in the second stage a rising, leading to a mountain range, and in the last stage a lowering, partly by subsidence, partly by erosion, but accompanied by the development of lower topographical features in the foreland. This last stage leads finally to the disappearance of the mountains.

This whole series of phenomena can, practically speaking, only be satisfactorily accounted for by assuming episodically occurring periods of uniaxial horizontal compression in the earth's crust. This provides us with a new argument for supposing these stresses to be brought about by currents in the mantle, for which already several other arguments can be given; contraction of the crust by the earth's cooling could hardly cause uniaxial compression in the crust. Other arguments for assuming mantle-currents may be found in the facts, that, in the same period during which geosynclines develop, in other areas graben originate, which must be attributed to tension, while in still other areas relative movements of crustal blocks along faultplanes of considerable length occur, as, for example, we find along the San Andreas fault in California. The simultaneous occurrence of these phenomena points to currents below the crust and not to contraction. The shift of the poles with regard to the crust, which the recent measurements of the direction of magnetization of rocks strongly seems to indicate, are likewise difficult to explain in any other way than by assuming current-systems in the mantle

exerting drag-forces on the crust, of which the resultant moment makes the crust rotate around the earth's interior.

For more arguments in favour of such current-systems the reader may refer to other papers (VENING MEINESZ, 1957). Here we want to mention, that assuming them to be convection-currents caused by the earth's cooling, we may, in a way we shall presently set forth, explain that these currents have an episodic character. We can thus make it clear that the development of geosynclines is likewise episodic. The period of uniaxial compression in the crust and the accompanying folding, i.e. the first stage of that development, lasts some 40–60 million years. It is followed by a period of absence of crustal compression of about 150–300 million years, during which the second and third stages of the geosyncline's history take place. After this period of rest, the phenomenon repeats itself in general elsewhere.

For an explanation of the episodic character of the convection-currents in the mantle, we have to suppose that the rocks of the mantle are plastic or, in other words, that the effect of stresses below the limit of elasticity, working on these rocks, is an elastic deformation, disappearing when the stresses are removed; but that stresses above that limit bring about permanent strain and flow.

It is easy to see that this property entails that the cooling of the mantle, though causing the outer layer to become denser than the inner layer, does not bring about instability, at least if the temperature gradient coincides with the direction of gravity. If, however, it has a sufficiently large horizontal component, or if another disturbance of equilibrium occurs, a convection-current sets in. This current has an accelerating character for the first quarter of a revolution. If, with respect to the duration of this current phenomenon, the temperature conduction may be neglected—as no doubt is the case—the current velocity has, obviously, at that moment a maximum value. This is probably of the order of 1–10 cm/year. During the ensuing quarter of a revolution it slows down till it comes to a stop. At that moment stability in the mantle is readjusted; the surface matter of lower temperature and, consequently, higher density is down, and the matter of higher temperature and lower density is at the top.

Very slowly the temperature radiation at the surface cools down the upper layer and the high temperature of the core transmits heat to the lower part of the mantle. Thus, eventually, the original

downward temperature gradient is restored. A secondary phenomenon can again start a convection-current and the whole process repeats itself. Because of the need of such a secondary phenomenon for setting the current going, we cannot expect these currents to be accurately periodic; they must have an episodic character. The same is true for the tectonic crustal phenomena which these currents bring along.

In passing we may also mention another consequence of the mantle rocks behaving plastically and not like a Newtonian fluid with high viscosity modulus; the current-pattern over the sphere cannot be the same as it would be in the latter case. When the secondary phenomenon has started flow in a certain area and in a certain direction, the limit of elasticity must put a restriction to its spreading over the sphere. The resulting pattern must be less complete and less symmetrical than for the Newtonian fluid.

We shall now take up our main subject and deal successively with the three stages of the history of a geosyncline, its development, its consequences in the shape of a mountain range, and its long last stage, during the first phase of which other ranges and 'Mittelgebirge' originate.

During the first stage we suppose uniaxial compression in the crust. We must assume that this stress exceeds the elastic limit because, if this were not the case, no geosyncline could develop; it can be shown that for elastic downbuckling of the rigid crust a far greater compressional stress is required than the elastic limit—in fact about 3×10^{10} dynes/cm^2—and so, for a stress smaller than this limit, the elastic deformation would be restricted to a small elastic shortening of the dimensions in the direction of the uniaxial stress and, according to Poisson's constant, a still smaller increase of the crustal thickness. These small deformations disappear when the compression vanishes.

If, however, the uniaxial compressional stress exceeds the elastic limit—which we suppose to occur in a belt of weakness of the crust—plastic flow sets in, leading to a thickening of the crust in this belt. As BYLAARD (1936) has shown, this must bring about a downbuckling of the crust of the type the writer of this paper adduced on the evidence of the narrow belts of strong negative gravity anomalies found in the Indonesian and Antillean Archipelagos. This process is identical with the development of a geosyncline and, in the oceans, with the formation of a deep ocean trough.

This downbuckling process is caused by the adjustment of the isostatic equilibrium in the plastically thickened belt. This brings along the subsidence of this belt in such a way that the outward bulge of the crust becomes many times smaller than the inward bulge at the lower boundary of the crust. As a consequence of this, the resultant of the compressional stresses working in a vertical cross-section of this thickened belt of the crust is no longer located in the centre of the cross-section, but above it, and so the plastic compression at the crust's surface must be stronger than at the lower boundary. It is clear that this involves a crustal down-bending and, as this increases the asymmetry of the compressional stress in the cross-section, the down-bending is accelerating. The crustal deformation in the belt must have the character of a downbuckling. At the same time the thickness of the crust increases.

Because of the high value of the modulus of pseudo-viscous flow of the crustal matter—probably of the order of 10^{23} poises—the development of both phenomena is slow. Assuming this value, we find that for the continental crust it takes about 15 million years before at the surface the initial rising, caused by the crust's thickening, has been neutralized by the subsidence, caused by the downbuckling, and that it takes about 10 million years more before a geosyncline of 5000 m depth is formed. For an oceanic crust the first period is smaller, viz. about 5 million years, but the second period of 10 million years is about the same. The difference between both cases is caused by the fact that the mean density of the rigid continental crust differs much more from that of the plastic substratum in which it has to be pushed down, than that of the rigid oceanic crust; in both cases the initial crustal thickness was assumed at the same value of 35 km, but at the time the syncline has a depth of about 5000 metres, this thickness for the continental case has increased by about 27 km and for the oceanic case by about 17 km.* In these computations no allowance was made for possible sedimentation in the geosyncline but it was supposed that it was filled with sea-water; sedimentation must of course change the figures. Two stages of the geosyncline development in a continental crust are represented on true vertical scale in Fig. 1.

* For details about the formulas and computations leading to these figures, the writer may refer to a book which may be expected to appear in 1958: W. HEISKANEN and F. A. VENING MEINESZ, *The Earth and its Gravity Field.*

We must, however, mention that, for the larger values of the subsidence and crustal thickening, the formulas following from the mathematical treatment are no longer precise; the folding together of the geosyncline, of which the five stages of KUENEN'S well known experiments represented in Fig. 2 gives a good illustration, obeys more complicated formulas. The possible filling of the geosyncline by sediments renders the problem still more difficult to handle. Gradually more and more folding and overthrusting will occur at the surface.

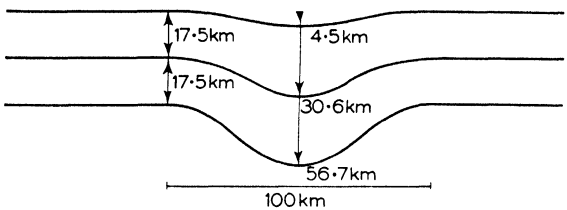

FIG. 1. Plastic downbuckling and thickening of the earth's crust; the crust is assumed to consist of two layers of equal thickness, a granitic and a basaltic one.

We shall now deal with the second stage of the phenomenon, which we suppose to begin at the time that the convection-current comes to a stop. We therefore, assume that the compression in the crust has vanished. The result must be that the isostatic equilibrium of the crust can readjust itself. The geosynclinal zone, in particular, will rise till this equilibrium is re-established. The crustal thickening must cause a positive topography, which in the continental geosynclinal belt must have a considerable elevation; a high mountain-range develops. It depends on the time during which the compression has worked, how high this range will be and whether the sediments at the surface show much folding and overthrusting. Usually the height will be several kilometres.

For the oceanic geosyncline the mean density of the rigid crust, which has been compressed, differs little from that of the subcrustal layer into which it was pressed down. So the elevation of the submarine ridge, which develops during the second stage, must be much lower. If no sediments have been deposited in the ocean trough, it cannot be much more than a few hundred metres. We thus can understand that in the oceans in general, we do not find high folded mountain-ranges.

During the third stage the continental mountain-range must be attacked by two processes. At the surface we have the effect of the erosion by water, ice and wind. This effect must begin already during the second stage. At the lower boundary of the crust we may expect that gradually the downbuckled root, which was lowered to a depth where the subcrustal matter is plastic, because of its higher temperature, also assumes that temperature, and likewise becomes plastic. This root must then flow off along the lower boundary of the crust, and, as a consequencé of this and because of isostatic readjustment, the mountain-range subsides and the foreland rises; 'Mittelgebirge' develop.

We shall examine the second process somewhat more in detail, and apply it to the western part of the Alps. The heating of the root must already begin during the first stage of the phenomenon, i.e. during the downbuckling of the crust and the development of the root. As conduction in the earth is extremely slow, it must take a long time before the flowing off of the root takes place. This must occur towards the side where the resistance is smallest. For the western part of the Alps, this must have been the outside of the arc. Once flow in this direction came into being, the elastic limit towards the inside of the arc could no more be overcome and the flow continued towards the outside.

The process of one-sided flowing away of the root is represented in Fig. 3, in which at the crust's surface one of STAUB'S profiles over the Alps has been added. The hatched line gives the original outline of the downbuckled root, and the drawn line the outline after the flowing away. Examining this figure, we can understand the history of rising as it is revealed by the geomorphological evidence. This evidence shows that originally only the main range of the Alps, south of the Rhône and Rhine valleys, came into being. A. PENCK (1924) dated this rising towards the end of the Oligocene or in the Miocene, i.e. about 25–30 million years ago; during this period the Rhône flowed in a northern direction. In the beginning of the Pliocene, i.e. about 15 million years ago, the range north of the Rhône–Rhine depression started to rise, and this rise is still continuing or, at least, has continued till in the Pliocene.

In Fig. 3 we see that this rising process can be well explained. The outflow of the root must cause a release of horizontal compression in the crust of the geosyncline area, and this favours the local isostatic

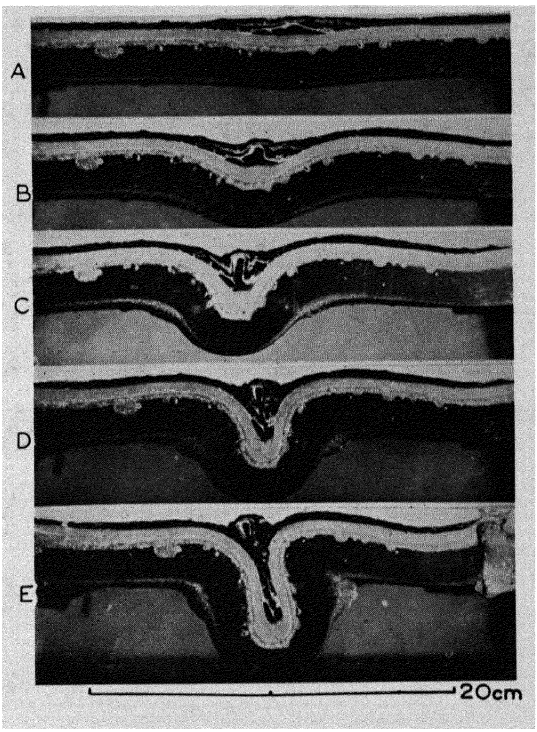

FIG. 2. Five stages of an experiment by Kuenen; horizontal compression of a plastic layer of wax and paraffin floating on water and consisting of three parts of which the rigidity increases downwards.

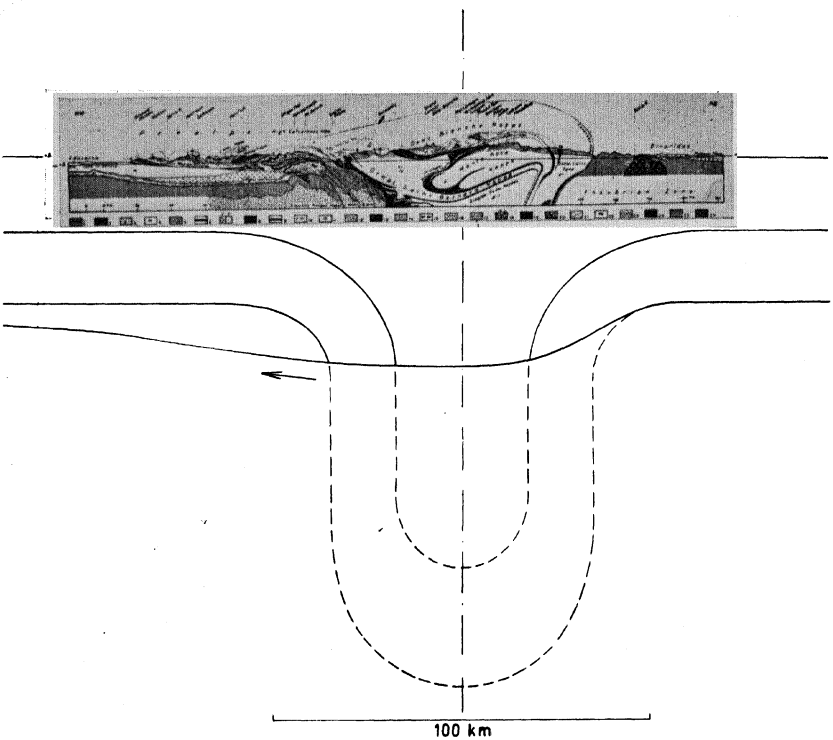

FIG. 3. Melting and flowing off the downbuckled root. At the surface Staub's profile over the St. Bernhard 'nappe'.

adjustment. As Fig. 3 shows, the vertical column in the central part of the geosyncline, i.e. below the main mountain-range, entirely consists of the upper crustal layers, i.e. of sediments and granite with densities of 2.4–2.67, and this corresponds to the high elevation of this range. To the left, i.e. below the Rhône depression, follows a crustal column of nearly the same height but of which a considerable part is basalt of a density of about 3.00, and so we can well understand its lesser elevation. Then follows a large area, where, because of the flow of the molten root matter, the crust is lifted up by a cushion of lighter crustal matter, which gets thinner at greater distance from the original geosyncline belt. This corresponds to the high mountain-range to the north of the Rhône–Rhine depression and to the 'Mittelgebirge', which for greater distances from this range have lower and lower elevation. That in Northwestern Europe these Mittelgebirge extend as far as the Ardennes and Southern Limburg may perhaps be attributed to a furthering of the outflow of the root matter by remnants of the subcrustal mantle-current system which led to the developing of the Alpine geosyncline.

Support of the views given here may be found in the fact that the total excess of crustal mass, represented by the present Alpine ranges and European Mittelgebirge, combined with their corresponding isostatic roots, nearly equals the excess corresponding to the shortening of the rigid crust of a thickness of 35 km in the Alpine geosyncline over a distance of 250 km, which is about the amount derived by the geologists from the folds and overthrusts. A small difference may evidently be accounted for by the river transport to the lowlands and sea of erosion products.

We may finish by remarking that, for oceanic geosynclines, the low submarine ridges can not disappear by erosion nor by root-melting. As the root consists entirely of the olivine of the mantle, the melting has practically no effect on the ridge.

REFERENCES

BYLAARD, P. P. (1936) Théorie des déformations plastiques et locales par rapport aux anomalies négatives, aux fosses océaniennes, aux géosynclinaux, etc., *Rapp. Congrés d'Edimbourg de l'U.G.G.I.*, 6^{e} *Assemb. Gén., Ass. Géod.*

PENCK, A. (1924) Das Antlitz der Alpen, *Naturwiss.* **12** (No. 47).

VENING MEINESZ, F. A. (1957) The geophysical history of a geo-syncline, *Proc. Kon. Ned. Akad. Westenschappen*, B, **60** (No. 21).

15

SOME RECENT STUDIES ON GRAVITY FORMULAS

W. A. HEISKANEN and U. A. UOTILA

SINCE Dr. B. Gutenberg is interested also in the geophysical applications of the gravity anomalies, it might not be too far from his field when we write on the studies concerning the gravity formula carried out during the last few years in the Mapping and Charting Research Laboratory of The Ohio State University, under the sponsorship of the Air Force Cambridge Research Center.

As we know, the gravity formula is of basic significance, because it gives the normal gravity value γ to be used in the gravimetric applications. The gravity anomaly Δg is the difference between the observed gravity value g_o (reduced to sea level) and normal gravity γ, or $\Delta g = g_o - \gamma$. The observed gravity values g_o must be referred everywhere to the same gravimetric system to get Δg-values, which are comparable with one another.

The gravimetric system used now is the Potsdam system, based on the absolute gravity measurements carried out in 1903–1906 in the Pendulum Hall of the Potsdam Geodetic Institute (KÜHNEN and FURTWÄNGLER, 1906).

The principal data of this world gravity base station are: latitude $\phi = 52° 22.86'$, longitude $\lambda = 13° 04.6'$, elevation $h = 87$ m, and the observed gravity $g = 981{,}274$ mgal.

The national gravity base stations like Washington, D.C., Ottawa, Paris, Rome, Pulkova, Dehra Dun, etc., have been connected directly or indirectly with Potsdam to tie the base stations of different countries to the same system. Because the field observations in every country refer to the gravity base station of the respective country, we get thus, also, the field observations of different countries to the same system. If, on the other hand, the base station value of some country is erroneous, all gravity observations of this country are

erroneous too. The best example of this might be India. Still about a decade ago the gravity value, $g = 980{,}073$ mgal, used at the Indian base station Dehra Dun was 10 mgal too high as compared with the latest and most accurate connections carried out by The Wisconsin University Group, which yield the value $g = 980{,}063$ mgal (GULATEE, 1947). Consequently, all gravity values and also the gravity anomalies of India were 10 mgal too high. These errors, brought about by the unfitting base value, have essential significance even in the geophysical applications. And in the geodetic applications they also bring results which are rather far from the truth. For instance, the undulations N of the geoid in India computed in 1948 by Tanni were, because of this fact, 5–15 m too high.

This example shows how important it is to get all base stations to the same system at least with the accuracy of one milligal. It might be strange that this has larger significance in all geodetic and geophysical applications than the *absolute* gravity value in Potsdam. In fact, the latter can be even 30 mgal wrong, and it will not yet interfere at all with the geophysical or geodetic studies. We simply operate with the gravity anomalies; that means, with the differences $g_o - \gamma$. If g_o is everywhere, for instance, 30 mgal high or 30 mgal low, we get also for the normal gravity γ, 30 mgal high or respectively low values. Thus the gravity anomalies $\Delta g = g_o - \gamma$ will be unchanged. Therefore, the geodesists have not paid so much attention to the absolute gravity value itself as to the fact that all countries are brought to the same gravimetric system.

Since astronomy, meteorology, and physics need the *right* gravity values, the Potsdam gravity value has been studied extensively during the last decades. These studies have revealed that the Potsdam value is 10–15 mgal too high and the gravity derived from this absolute value is everywhere also from 10–15 mgal too high. However, because we still do not know exactly what the correction is, neither the system nor the gravity formula has been changed. So far, the geodesists have suggested that other scientists should use 12 mgal smaller gravity values than the International gravity formula gives.

How about the normal gravity γ? It has been derived from the gravity observations made in different parts of the world. The theory as well as the observations have unanimously shown that the gravity will increase from equator to the poles as $\sin^2 \phi$, where ϕ is the latitude.

In addition, there is one small $\sin^2 2\phi$-term. So we can write the gravity formula in the following way:

$$\gamma = \gamma_e (1 + \beta \sin^2 \phi + \epsilon \sin^2 2\phi)$$

This formula has three parameters: γ_e, the gravity value at the equator; β, the coefficient of the term $\sin^2 \phi$; and ϵ, the coefficient of the term $\sin^2 2\phi$. From these parameters ϵ has been derived theoretically by E. Wiechert and G. H. Darwin. The term β is connected by Clairaut's formula with the flattening value α of the meridian of the reference ellipsoid. It can be determined gravimetrically, geodetically, and astronomically. All these methods have been used to get as reliable a value for β as possible. As to the equator value of the gravity formula, that can be obtained only by the aid of gravity observations carried out at the different parts of the world. Very important is that we have gravity observations at as many different latitudes as possible, because the second and third term depend on the latitude ϕ. Quite a few gravity formulas have been derived, particularly during this century. The formulas are the more reliable the more gravity observations are available from different latitudes and longitudes. Until 1930 the mostly used gravity formulas were derived by HELMERT in 1901 and 1915 and by BOWIE in 1917. These formulas are the following:

HELMERT, 1901: $\gamma = 978.030\,(1 + 0.005302 \sin^2 \phi - 0.000007 \sin^2 2\phi)$ cm/sec^2

HELMERT, 1915: $\gamma = 978.052\,(1 + 0.005285 \sin^2 \phi - 0.000007 \sin^2 2\phi)$ cm/sec^2

BOWIE, 1917: $\gamma = 978.039\,(1 + 0.005294 \sin^2 \phi - 0.000007 \sin^2 2\phi)$ cm/sec^2

In 1928 HEISKANEN (1928) derived, on the basis of larger material than was available ever before, the following gravity formula:

$$\gamma = 978.049\,(1 + 0.005289 \sin^2 \phi - 0.000007 \sin^2 2\phi) \text{ cm/sec}^2$$

In this formula the β term was used which agreed with the flattening value $\alpha = 1/297.0$ derived by Hayford and accepted in 1924 as the flattening value of the international ellipsoid.

This formula was accepted in Stockholm, 1930, at the suggestion of G. CASSINIS (1930), with two minor changes as the international gravity formula. The International gravity formula reads:

$$\gamma = 978.0490\,(1 + 0.0052884 \sin^2 \phi - 0.0000059 \sin^2 2\phi)\ \text{cm/sec}^2$$

So we have now five parameters of the earth accepted by the International Association of Geodesy which determine the geometry of the earth and the normal gravity and its change from equator to pole. These parameters are:

$$\begin{aligned} a &= 6{,}378{,}388\ \text{m} \\ \alpha &= 1/297.0 \\ \gamma_e &= 978{,}049.0\ \text{mgal} \\ \beta &= +\ 0.0052884 \\ \epsilon &= -\ 0.0000059 \end{aligned}$$

We shall still emphasize that if we change α we have to change β too and vice versa. Therefore, we must be conservative in changing either of them. We must know accurately how much to change to be able to use the new parameters for at least three decades, as the international parameters have been used.

When the gravity formula was derived by Heiskanen in 1928, he had only 1591 squares of $1^\circ \times 1^\circ$ where at least one gravity observation was done. Since that time a large amount of additional gravity material has been collected around the world, the oceans included. Therefore, we have in Columbus derived new parameters for the gravity formula. The method was the same as in 1928, i.e. we have not used the individual gravity anomalies but only the mean value of $1^\circ \times 1^\circ$ squares. Not to give too high a weight for the relatively small areas of dense gravity station nets, the mean gravity anomaly of each square was given the same weight. Exceptional gravity anomalies, larger than 70 mgal, were omitted.

We got together 6679 squares, the free-air anomalies of which were used, after the elevation correction, in the computations. The corrections $d\gamma$ to the equator value γ_e and $d\beta$ to the coefficient β were computed. As we can understand, the different zones yield quite different gravity formulas and, therefore, cannot be used for the whole earth. Thus we publish the corrections only for the longitude zones of

TABLE 1

Corrections $d\gamma$ and $d\beta$ to the International Gravity Formula in different longitude zones and corrected β and $1/\alpha$
(Using 1° × 1° squares)

Longitude zone	n	$d\gamma$	$d\beta \times 10^3$	$\beta \times 10^3$	$1 : \alpha$
0–45 E	1643	+ 11.6	− 0.0071	5.2813	296.4
45–90 E	1007	− 12.3	+ 0.0173	5.3057	298.5
90–135 E	935	+ 5.9	− 0.0133	5.2751	295.9
135–180 E	287	+ 11.3	− 0.0036	5.2848	296.7
0–45 W	528	+ 3.1	+ 0.0278	5.3162	299.4
45–90 W	1052	− 5.5	+ 0.0107	5.2991	297.9
90–135 W	833	− 2.5	+ 0.0042	5.2926	297.4
135–180 W	192	− 6.9	+ 0.0105	5.2989	297.9
0–90 E	2649	+ 1.8	+ 0.0034	5.2918	297.3
90–180 E	1221	+ 7.2	− 0.0106	5.2778	296.1
0–90 W	1579	− 3.2	+ 0.0188	5.3072	298.6
90–180 W	1024	− 3.3	+ 0.0057	5.2941	297.5
0–180 E	3870	+ 4.5	− 0.0015	5.2869	296.9
0–180 W	2603	− 2.4	+ 0.0105	5.2989	297.9
Northern	5369	− 0.7	+ 0.0063	5.2947	297.5
Southern	1104	+ 5.6	+ 0.0137	5.3021	298.2
Whole earth	6679	+ 0.6	+ 0.0050	5.2934	297.4
	(Using 5° × 5° squares)				
0–90 E	316	+ 1.8	+ 0.0011	5.2895	297.1
90–180 E	247	+ 2.8	− 0.0028	5.2856	296.8
0–90 W	337	− 2.2	+ 0.0075	5.2959	297.6
90–180 W	203	+ 0.9	+ 0.0002	5.2886	297.0
Whole earth	1103	+ 0.7	+ 0.0018	5.2902	297.2

The gravity formulas are:

Northern Hemisphere:

$$\gamma = 978.0483\ (1 + 0.0052947 \sin^2 \phi - 0.0000059 \sin^2 2\phi)\ \text{cm/sec}^2$$

$$\frac{1}{\alpha} = 297.5;\quad n = 5369$$

Southern Hemisphere:

$$\gamma = 978.0546\ (1 + 0.0053021 \sin^2 \phi - 0.0000059 \sin^2 2\phi)\ \text{cm/sec}^2$$

$$\frac{1}{\alpha} = 298.2;\quad n = 1104$$

Whole Earth:

$$\gamma = 978.0496\ (1 + 0.0052934 \sin^2 \phi - 0.0000059 \sin^2 2\phi)\ \text{cm/sec}^2$$

$$\frac{1}{\alpha} = 297.4;\quad n = 6679$$

45°, 90°, and 180° width. The broader the longitude zone is, the more similar the corrections are. Table 1 gives in the first column the longitude zone, in the second column the number, n of the squares $1° \times 1°$, in the third column the correction $d\gamma$ of the equator value, in the fourth column the correction $d\beta$, in the fifth column the corrected β, and finally the corrected flattening value α. The table contains the corrections for eight longitude zones of 45° for the four quarters of the Northern Hemisphere and for the Eastern and Western Hemispheres (longitudes 0°–180° E and 0°–180° W).

Even when we use the squares $1° \times 1°$ the gravimetrically well surveyed areas will have too large weights. Therefore, we made similar computations still using only the mean gravity anomalies of $5° \times 5°$ squares. The results for the four longitude zones of 90° width are also seen in our table. The amount of these squares, total 1103, was fairly evenly distributed; the largest number, 360, was between longitude 0°–90° E and the smallest, 203, between 90°–180° W. The gravity formula for the whole earth, obtained by the aid of $5° \times 5°$ squares is:

$$\gamma = 978.0497\,(1 + 0.0052902 \sin^2 \phi - 0.0000059 \sin^2 2\phi)$$

and the corresponding flattening value $\alpha = 1/297.2$.

In Fig. 1 the heavy circle corresponds to the α-value of 1/297.0; the other two circles to the α-value 1/295 (largest circle) and then to the value 1/299. The staggered, heavy line gives the flattening value for different longitude zones of 10°. For instance, for the zone 40°–50° E the flattening is exactly 1/297.0.

The broken line reveals the correction, in mgals, to the equator value γ_e. The heavy circle corresponds to the correction zero. The largest circle corresponds to the correction + 20 mgal, the smallest zone to the correction − 20 mgal.

The smaller heavy staggered line shows how many squares $1° \times 1°$ were available in different 10°-longitude zones. As it is easy to understand, the material is largest in the longitudes of Europe and North America. In fact, between the longitude 0°–40° E every zone has more than 350 squares. Similarly between the longitudes 60°–100° W every zone has about 300 squares. Also at the longitudes from 100°–130° E we have more than 200 squares.

Our figure shows the known fact that the Pacific is gravimetrically the emptiest area. In fact, between the longitudes 120° W and 150° E,

that means in the longitude zone of 90°, only very few observations exist. A similar relatively empty area is in the Atlantic between the latitudes 20°–60° W.

Our study shows the geodetically important fact that the international gravity formula needs only small corrections $d\gamma$ and $d\beta$, for when we compute gravimetrically the undulations N of the geoid and the deflections of the vertical components ξ and η we must use the gravity anomaly field of the whole earth. In the gravimetrically unsurveyed areas we have to use the gravity anomaly zero, because it corresponds to the complete isostatic equilibrium. If the equator value γ_e of the gravity formula would be, say, 10 mgal too high then all gravity anomalies would be, in average, 10 mgal too small. When we do not know this fact, and use in the empty areas the anomaly zero, it is wrong by 10 mgal; the right value being — 10 mgal. These assumed values, which do not correspond to the reality, will give up to 10 m wrong undulation values. Now when the correction

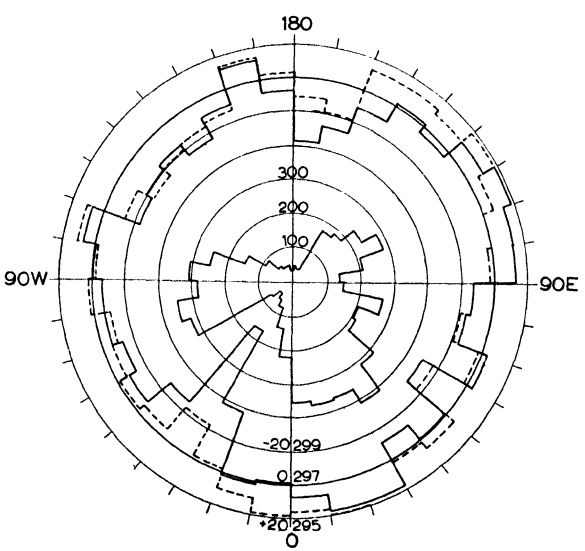

FIG. 1. Diagram giving the corrections to the equator value of the international gravity formula, and the flattening values α in different longitudinal zones of 10° width, and the amount of the squares 1° × 1° available in these zones. Total amount of the squares available in Columbus is 6679, or four times more than in similar computation in 1928.

$d\gamma$ to the equator value is only of the order of 1 mgal its effect will be nearly negligible.

The problem of triaxiality of the earth is geophysically very interesting. Two decades ago, when many fewer gravity observations were available, most observations were done in America, Europe, and India which are about 90° apart from one another. Now it happens to be so that the gravity anomalies in North America are slightly negative, in Europe as well as in the eastern part of the North Atlantic they are strongly positive, and in India strongly negative again. When we compute the gravity formula by the aid of this material we get a striking longitude term.

TABLE 2

Some gravity formulas with longitude term and the corresponding largest and smallest a-values

Author	Year	Gravity Formula	$1/a_1$	$1/a_2$
HELMERT	1915	$= 978.052\,(1 + 0.005285 \sin^2\phi - 0.000007 \sin^2 2\phi + 0.000018 \cos^2\phi \cos 2[\lambda + 17°])$ cm/sec^2	295.2	298.2
HEISKANEN	1924	$= 978.052\,(1 + 0.005285 \sin^2\phi - 0.000007 \sin^2 2\phi + 0.000027 \cos^2\phi \cos 2[\lambda - 18°])$ cm/sec^2	294.3	299.0
HEISKANEN	1928	$= 978.049\,(1 + 0.005293 \sin^2\phi - 0.000007 \sin^2 2\phi + 0.000019 \cos^2\phi \cos 2[\lambda - 0°])$ cm/sec^2	295.3	300.2
HEISKANEN	1938	$= 978.052\,(1 + 0.005297 \sin^2\phi - 0.000007 \sin^2 2\phi + 0.000023 \cos^2\phi \cos 2[\lambda + 25°])$ cm/sec^2	295.3	300.2
NISKANEN	1945	$= 978.047\,(1 + 0.005298 \sin^2\phi - 0.0000059 \sin^2 2\phi + 0.000023 \cos^2\phi \cos 2[\lambda + 4°])$ cm/sec^2	295.7	299.8
UOTILA	1957	$= 978.0516\,(1 + 0.0052910 \sin^2\phi - 0.0000059 \sin^2 2\phi + 0.0000106 \cos^2\phi \cos 2[\lambda + 6°])$	296.3	298.1

The longitude of the long equator axis is according to these solutions: − 17°; + 18°; 0°; − 25°, and − 4°; the average longitude is thus − 6°.

Huge additional material available already does not appear to confirm the triaxiality. In many areas where we had to have negative gravity anomalies they are positive and vice versa.

Fig. 2 shows one striking phenomenon: when we plot the mean gravity anomalies of 5° × 5° on the world map, we realize that the belts of positive and negative gravity anomalies are not in north–south direction but tilt about 45°.

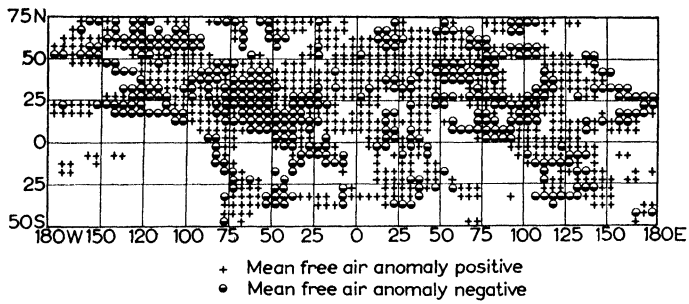

FIG. 2. Diagram showing the striking distribution of the positive (+) and negative (−) free-air anomalies in large belts, which are tilted about 45° from the meridian.

The problem of triaxiality is no more actual, because we can now gravimetrically compute the undulations N of the geoid—in fact, the tentative geoid of the Northern Hemisphere has already been computed in Columbus, Ohio. So the triaxial formulas have been given only from the historical point of view.

The undulations of the geoid seem not to exceed $\pm$ 80 m. After some few years a more detailed geoid will be available.

REFERENCES

BOWIE, William (1917) Investigations of gravity and isostasy, *USCGS*, Spec. Publ. No. 40.

CASSINIS, G. (1930) Sur l'Adoption d'une Formule Internationale pour la Pesanteur Normale, *Bull. Geod.*, No. 26.

GULATEE, B. L. (1947) Value of gravity at Dehra Dun, *Bull. Geod.*, N.S. No. 12.

HAYFORD, J. F. (1910) Supplementary investigation in 1909 of the figure of the Earth and isostasy, *USCGS*.

HEISKANEN, W. A. (1924) Untersuchungen über Schwerkraft und Isostasie, *Veröff. Finn. Geod. Inst.*, No. 4.

—— (1928) Ist die Erde ein dreiachsiges Ellipsoid?, *Gerl. Beitr. z. Geophysik*, B, 19, Heft 4.

—— (1938) Investigations on the gravity formula, *Publ. Isost. Inst. of IAG*, No. 1.

HELMERT, F. R. (1901) Der normale Teil der Schwerkraft im Meeresniveau, *Ber. Kön. Pr. Akad. Wiss.* **XIV**.

—— (1915) Neue Formeln für den Verlauf der Schwerkraft im Meeresniveau beim Festlande, *Ibid.* **XLI**.

KÜHNEN, F. and FURTWÄNGLER, Ph. (1906) Bestimmung der absoluten Grösse der Schwerkraft zu Potsdam, *Veröff. Preuss. Geodät. Inst.* Neue Folge, No. 27.

NISKANEN, E. (1945) Gravity formulas derived by the aid of the level land stations, *Publ. Isost. Inst. of IAG*, No. 14.

16

DATA PROCESSING IN GEOPHYSICS

H. E. LANDSBERG

Introduction

In the geophysical disciplines, the earth as a whole is the scientist's laboratory. The geophysicist has to let nature perform his experiments for him. He has to observe the events diligently. In order to draw valid conclusions from his observations he amasses vast collections of data. These have to be analyzed patiently. Even so, many of the phenomena still elude his grasp. Hence, still more observations have to be added to the stock pile. With the arrival of the International Geophysical Year (IGY) 1957–58 a flood of new data has started.

These new observations have only as much value as the capacity to analyze them keeps pace with the collection. In discussing this problem GUTENBERG (1956b) remarked cogently: 'For the evaluation of observations, it is more important to reduce and analyze well-selected data by the best possible methods than to study all available data by less time-consuming but less accurate methods. . . . Electronic calculators should be used whenever practicable.'

The expenditure for the gathering of geophysical data runs into millions of dollars yearly. Yet it is doubtful if currently more than a fraction, perhaps one-third of the information content of the basic data, is exploited. The reason for this is that man-power for the manual evaluation of the data is either not available or too expensive. New systems of data acquisition and processing have come into existence and are undergoing rapid further development. The revolutionary impact this will have on geophysics justifies a brief review at this time. (For an earlier summary see: BELLAMY, 1952.)

Manual methods

All the geophysical sciences, especially in their applied phases,

have developed and used short-cuts which simplify reduction and interpretation of data. Most common, of course, are tables, nomographs, and special slide rules. These cover a diversity of subjects. Only a few examples will be given here because of their widespread use. Among them are the Smithsonian meteorological tables, the tables in LINKE'S *Meteorologisches Taschenbuch*, the various psychrometric tables and slide rules, the circular slide rules for calculating pilot balloon observations and for solution of the hydrostatic equation of the atmosphere. In another branch of geophysics, seismology, we have various nomographs for determining the magnification of seismographs, the travel-time curves for determining epicentral distances, the graphical methods for obtaining epicentral co-ordinates. In geodesy there are many specialized trigonometric and refraction tables as well as isostatic reduction tables representing various assumptions on the depth of compensation. Numerous graphical and tabular aids exist for geophysical prospecting, particularly for the reduction of gravity and geo-electric measurements.

The various thermo-dynamic diagrams widely used in meteorology (Stüve's adiabatic chart, Shaw's tephigram, the Refsdal and Rossby diagrams, etc.) deserve special mention. These permit primitive but very useful deductions on stability and energy distribution by inspection or simple counting or planimetric methods. In the same category falls the widely used Elsasser radiation chart. This is still a very practical tool for the study of the earth's heat balance, as was shown in recent years by its extensive use for graphical solutions for many levels and latitudes by LONDON (1950). Various statistical probability papers offer a similar simplified approach. These have scales representing the normal and extreme value distributions and permit quick visual analysis of sets of data (COURT, 1952; GUMBEL, 1954; THOM, 1954). Aside from application to extreme floods, winds, temperatures these last mentioned methods were also applied to earthquake magnitudes (NORDQUIST, 1945).

All of these procedures are geared to the still most prevalent outputs of measuring devices. These are usually decimal digital values, read off by eye, or recorded in pen and ink, or photographically by a galvanometer or oscillograph primarily as functions of time.

Other aids to computation in form of schemes for calculation

and common types of analysis were developed gradually. The majority of them applied to the calculation of correlation coefficients and the performance of Fourier analysis (see, e.g. CONRAD and POLLAK, 1950; BROOKS and CARRUTHERS, 1953). Many of these were particularly well adapted to manually operated desk calculators.*

Early machine methods

Actually, geophysical sciences were among the earliest users of mechanized devices for data processing.

Probably a 'first' in geophysics were the mechanical analogue computers for predicting the ocean tides. In these machines the harmonic elements of tidal observations were represented by cog wheels and predictions for each day could be made on the basis of the known components for a number of coasts and harbours. Aperiodic elements influencing sea-level stages, such as wind, constituted a usually minor error for the prediction. The first design was by WILLIAM THOMSON (Lord Kelvin) in 1873. This provided graphically the predicted height of the tide as a function of time. Used were 10 basic parameters which were integrated by the machine. WILLIAM FERREL designed in 1882 another tide predicting machine for the U.S. Coast and Geodetic Survey. It indicated both height and value of tide maxima and minima. In 1910 an improved design (by HARRIS) was developed by the U.S. Coast and Geodetic Survey which, based on 37 constituents, yielded simultaneously the height of the tide as function of time and the times of high and low water (SCHUREMAN, 1941). A still more refined model is now under construction (1956).

The first thought that the just invented punched card might be used for compiling an oceanic climatology from marine weather observations was contained in a report of the U.S. Hydrographer in 1895 (BATES, 1956). Nothing seems to have come of it at the time but in 1920 the British Meteorological Office actually first started punching of marine meteorological observations. Land station weather data and rather sophisticated uses of punched cards in geophysics were pioneered by L. W. POLLAK (see, e.g. CONRAD and POLLAK,

* These will remain useful even for the mechanized aids because tables of functions or constants can be stored in the memory of electronic computers for machine analysis.

1950). The early history of punched card usage in geophysics has been reviewed several times. A good summary appears in CONRAD and POLLAK (1950).*

The computer age in science

Although we could trace the limited use of mechanized summarization and calculation of geophysical data back several decades the widespread use was predicated on the advent of the electronic computer. In the pure sciences this coincides with the period following World War II and has gone hand in hand with the use of computing machines in business. Accounting and inventory control are among their most widespread uses. (For a general, non-mathematical introduction to the principles, see, e.g. CANNING, 1956.) Some of the broad uses of mechanical and electronic data processing have been recently reviewed by HEUMANN (1956).

In many instances the transition from the manual to the automatic data processing system is a painful process, especially if a backlog of valuable old data is to be integrated into the information to be included in the collection. The data must then be coded and entered on a medium suitable for machine processing. Presently the most common forms are five-channel punched tape (produced by use of a Flexowriter), punched cards, or magnetic tape. Other media are under development, as will be pointed out further below.

Among the general scientific problems which can be tackled by machines are several where the term data is used very broadly. For example, the systematic codification of chemical elements which can then be used in the search of analogous compounds in the quest for drugs or pesticides or similar problems. Another example is the codification of technical literature and its contents. This will simplify the compilation of subject matter bibliographies or the search for specific references. Finally, the awkward problem of translations is getting closer to a solution by machine methods. In all these fields things that earlier took days and weeks can be reduced to minutes *once the information is properly coded.*

But at any rate, the availability of many large-scale computers and

* For details see:
H. LANDSBERG, *Bull. Amer. Met. Soc.* 1942, **23**, 34; *idem., ibid.* 1943, **24**, 174; C. S. DURST, *ibid.* 1944, **25**, 221; M. C. GEORGE, *ibid.* 1945, **26**, 76; L. W. POLLAK, *ibid.* 1946, **27**, 195.

the rapid developments in this field make it likely that computer programming and machine data processing procedures will soon be among the elementary devices with which every scientist needs to be familiar.

Geophysical problems

Geophysics in many of its aspects deals with inaccessible areas, such as the depths of the interior of the earth. Even theoretically accessible parts are only incompletely or sporadically covered by observations. This applies, for example, to the extreme heights of the atmosphere and vast expanses of oceans. In those cases the model largely takes the place of observations. There are usually many models imaginable; only some of them can be theoretically justified; only one represents reality. To search out of the multiplicity of possibilities this elusive one which conforms to all available information is one of the tasks of modern methods of machine analysis. The machine can accommodate the observations and can simulate the process as given by the pertinent equations. It can perform these operations within a reasonable time. Incorrect solutions, i.e. those which do not conform to reality, can be improved upon rapidly by amended equations or by new data, or both. By successive approximations optimal solutions can be obtained, representing the best current data and theory permit. Man can free his intellect to improve upon these two elements rather than to spend a lifetime on the calculations.

One of the basic requirements for all the geophysical sciences is a re-design of many of our conventional instruments. The end products now are principally scale values to be read by a human observer, pen and ink recorder curves, or records on film or photographic paper. These can be read and transformed by a number of commercial curve readers into digital or analogue form for input to calculating devices. In many cases, this is an expensive way of doing the job. It would be much preferable if the basic output, be it mechanical or electrical, of the instrument were transferred to punching a tape or card for machine processing. Several such devices are now in their early (and as yet costly) stages but very rapid developments are indicated for the next few years. It is up to the geophysicists to plan for these changes and incorporate them into their own future designs.

Status of Machine Computations in Geophysics

It would seem appropriate to review briefly where we stand in geophysical data processing, primarily by reference to the pertinent literature. *Meteorology* has probably made the greatest strides in mechanized procedures and for this reason we will discuss it first.

The forecast problem in meteorology had long been recognized as a logical target for numerical solutions. Basically, RICHARDSON (1922) had already worked out a system of solving the hydrodynamic equations for numerical processing. Hand computations, however, were hopelessly out-distanced by the rapidly moving weather events. Shortly after World War II VON NEUMANN realized that both in the mathematical solution of functions and the electronic computer developments advances had been accomplished that made a new trial to tackle the weather forecast problem worthwhile. As a proper first, and limited, aim the short-range prediction of the pressure field in the middle latitudes at the surface and aloft was set (CHARNEY and ELLIASSEN, 1949). The first step was to get tooled up for the processing of actual observations and the adoption of a suitable model. Usually the small-scale 'noise' had to be eliminated and two-dimensional barotropic models were used to pre-calculate the 500mb height tendency by manual but machine adaptable procedures (CHARNEY, 1949). Around 1950 results of the first experimental machine forecasts were published (CHARNEY, FJÖRTOFT, and VON NEUMANN, 1950). Trial forecasts for 24 hr were made based on numerical solution of the barotropic vorticity equation. The ENIAC with limited internal memory performed about a million multiplications and divisions and came out with a forecast in 12 hr. Even then it was clear that a better computer could do the job in 30 min.

Since then numerical weather prediction has become a daily practice in the weather services of several countries. New computers and new models have been introduced, such as the BESK in Stockholm (Staff members, Inst. of Met., Univ. of Stockhom, 1954) and the FERUT in Canada (HENRY, 1956). In the U.S. the IBM 701 electronic computer has been extensively used in daily routine since 1955*. From the last volume of the Journal of Meteorology alone the following noteworthy papers can illustrate the development. WHITE (1956) used multiple regression equations for 24-hr predictions

* This has been replaced by the higher capacity machine IBM 704 since July 1957.

of pressure height distribution. The correlations were obtained and inversion of correlation matrices were performed by the computer. BLACKBURN and GATES (1956) accomplished numerical integration of a barotropic model for two-dimensional non-divergent flow with finite differences. It took the computer 4 min to complete the relaxation to a specified accuracy for 1529 internal grid points. For a 24-hr hemispheric barotropic forecast about one hour's time was needed. Later THOMPSON and GATES (1956) reported on a test of 120 forecasts for a 24-hr period by using the iterative method of relaxation with the barotropic and the two-parameter baroclinic method. The IBM 701 computer was given, and stored, 1500 instructions and all the initial data. It took 25 min to produce a 24-hr forecast, $1\frac{1}{2}$ min to load the programme and data into the computer and 3 min to print both a 12 and 24 hr forecast. In the process the computer performed a half million multiplications and followed 15 million other orders. CHARNEY, GILCHRIST and SHUMAN (1956) used the IBM 701 computer for integration of non-linear partial differential equations of elliptic type in predicting general quasigeostrophic motions.

Great strides have also been made in auxiliary use of computer techniques prior to forecasts for the objective analysis (HOLLOWAY, 1956; CRESSMAN, 1956). The ideal of obtaining the data automatically from sounding equipment, transmitting it directly coded for computer use and feeding it into the computer, which performs also a consistency check, is in the early design stages (BIGELOW and GILCHRIST, 1955; Anonymous, 1956b; HALL and HOLLOWAY, 1956; LALLY, MCINNIS and MYERS, 1956). Cost is about the only major obstacle to such an integrated meteorological system.

Of course, the automatic acquisition and processing of data does not guarantee in itself better local weather forecasts (REICHELDERFER, 1954). The computer only performs the multitudinous calculations required by a given theory or model. The improvement of the model in the light of better theoretical insight or empirical analysis of current forecast results remains an important task. The use of the computer for advances in the theory has shown some exceedingly promising results. Thus, PHILLIPS (1956) studied the general atmospheric circulation with aid of the relatively limited computer* of the

* Internal rapid-access memory of 1024 40 binary digit words coupled with a magnetic drum of slow access time of 2048 such words.

Institute for Advanced Study at Princeton, N.J. Using the equations of the 2-level quasi-geostrophic model, starting with the atmosphere at rest, he calculated for 31 days *ab initio*, going through the various energy transformations and adding eddy motions, the state of the atmosphere. This enabled him to show in completely synthetic fashion some of the major features of hemispheric circulation, such as the East–West–East distribution of zonal surface winds, the jet stream, and the net transport of energy toward the pole.

As another approach we have the strictly empirical statistical approach of using orthogonal polynomials to describe the synoptic map and predict the probability of subsequent weather conditions. This approach has been used by MALONE, LORENZ *et al.* (1956), using the high-speed and high-capacity IBM 704 computer.

The exploitation of the potentialities of the electronic computer for the large-scale problems in meteorology has barely begun. Additional opportunities have been pointed out by FRENKIEL (1956b) and WEXLER (1956). The latter advocates its use in an experimental sense in search for solar-terrestrial relations and for pre-evaluation of large-scale interference in atmospheric processes (VON NEUMANN, 1955). NAMIAS (1955) has pointed toward possibilities of using the computer for extended and even long-range forecasts of weather.

On the other end of the scale are the applications of fast data processing systems in studies of atmospheric turbulence. HOWCROFT and SMITH (1956) have used the MIT 'Whirlwind' computer to obtain eddy dimensions from high-frequency recordings of a thermocouple anemometer. This type of analysis by hand methods would be prohibitive in effort. FRENKIEL (1956a) has long been an advocate of using the statistical theory of turbulence to obtain from wind records eddy spectra, turbulence intensities, and a study of the turbulent transfer of energy based on the laws of fluid dynamics by feeding the data into special analogue computers. The direct usefulness of machine methods for the study of atmospheric pollution by applying the theories of diffusion and turbulence has been clear for some time (LANDSBERG, 1952). FRENKIEL (1956a) has used the SEAC electronic computer to obtain probable concentrations of polluting agents from mean air trajectories and diffusion equations. A. V. BLACKADAR (New York University, 1956) has studied the dynamics of air turbulence in the lower layers with data from O'Neill, Nebraska. Using an electronic analogue computer data from

the day and night vertical wind profiles helped in explaining the nocturnal rainfall of the midwestern area.

In the large dimension rapid computation methods have been introduced into the diffusion and fall-out problems connected with nuclear blasts and air pollution from atomic energy installations (U.S. Dept. of Commerce, Weather Bureau, 1955).

In meteorological observing there has been slow progress from early on-station hand punching of observations (L. W. POLLAK, *l.c.*) to the automatic production of cards in a general system. One of these latter is now in use by the National Hurricane Research Project (KIRCHNER, 1956). This General Precision Laboratory data recording system is installed in the TB-50 and B-47 research aircraft. The data* from the various analogue measuring devices are converted to digital form by Librascope code wheels and then directly fed into a compact IBM 523 gang punch. The principles of such data recording systems are now so well established (IBM, 1956) that there remain mainly problems of detailed design (particularly size and weight) and of the always large-looming costs to be solved.

With the increasing expense of manpower it has, however, already been demonstrated in another subfield of meteorology that automatic data processing is the most practical means. *Climatology* has made such use for some time through punched cards. W. C. JACOBS (1956) in a 1954 survey of member nations of the World Meteorological Organization found that twenty-five had started or were about to start punching programmes. At that time non-U.S. members had seventy-six million cards in their archives. The 1956 holdings of the U.S. alone at the National Weather Records Center in Asheville, N.C., are 300 million punched cards.

The uses are manifold. For routine purposes the cards serve for quality control of observations, summarizations, and frequency distributions. The very time-consuming summarizations of marine weather observations, mostly obtained from moving vessels, and hence irregular in space and time, can most conveniently be accomplished by tabulating machines (COPELAND, 1953). However, the cards can also be used for very sophisticated statistical studies, such as fitting maximum likelihood curves to distributions. THOM (1954)

* Time, latitude, longitude, flight number, wind direction, wind speed, pressure altitude, *D*-value (i.e. observed altitude—pressure altitude), temperature from vortex thermometer.

states that such fitting requires an iteration process which can be carried out manually only with difficulty and requires about 3 hr of work. A completely numerical iterated solution has been evolved for the IBM Card Programme Calculator. It fits a curve in about 10 min. Among the other fairly complicated uses of climatological data have been the calculations of fall-out probabilities (using an ALWAC III electronic computer), the determinations of atmospheric refractive indices for radio-wave propagation, and the preparation of vector wind roses (CRUTCHER, 1956).

One look at the stock-pile figures of punched cards stated above makes it immediately clear that even punched cards can become a problem in storage and for real high-speed processing of data. One of the common input media to computers has been magnetic tape. The entire character capacity of a punched card fits on 0.4 in. of magnetic tape. One inch will hold up to 200 characters. The tape can then be used for data processing. At the National Weather Records Center the Air Weather Service presently operates an IBM 705 computer for climatological purposes. It can read data at the rate of 15,000 characters/sec and can perform several thousand computations per second, depending on difficulty.

Although it is an excellent processing medium for data, magnetic tape has yet to be proven as a permanent storage device. This need seems to be better filled by the filming of punched cards in the data processing system dubbed FOSDIC (*F*ilm *O*ptical *S*ensing *D*evice for *I*nput to *C*omputers). This system has been described by GREENOUGH and BOSEN (1956). A filmer places punched cards on 16 mm microfilm at the rate of 420 cards/min, 10½ cards to the inch or about 13,000 images 100/ft roll (Anonymous, 1955b; Anonymous, 1956a). Each inch of film contains 850 characters. The flying spot of a cathode ray tube electron gun scans the microfilm for holes at a rate of 4300 card images per minute for desired data. FOSDIC can then read out the card, feed the information into an IBM punch and reproduce the original card. Future developments foresee that film data can be fed into electronic computers at the speed of 15,000 digits/sec. In storage capacity, weight, unit cost, permanence, and speed for computer input, film has presently the edge on all other processing media.

Film can similarly become the storage medium for data recorded in the unitary incremental notation proposed by BELLAMY (1952;

Cook Research Laboratories, 1955). The use of this system has been primarily demonstrated for radio-sonde data but it is, in principle, applicable to records of any continuous function. The main advantage is that the notation is non-redundant. The dependent variable is recorded from a given base value as + 1, — 1, or 0 elements of minimum (or desirable) unit of resolution by a graphical code. The data together with a suitable comparison scale can be tremendously condensed in scale. Time series or space cross sections can be presented on a film area of a few square inches covering a month of data. The film is readily amenable to automatic scanning and processing.

Climatology has presently in the geophysical field only one rival in data accumulation. This occurs in the upper atmosphere *exploration by rockets*. Thousands of items of information on measured variables as well as flight and aspect data crowd the telemetering channels. Several data recording and processing systems are now available. One of the latest is FLAC (ARDC, 1956), the *Fl*orida *A*utomatic *C*omputer of the U.S. Air Force Long Range Proving Ground. It uses a paper tape input punched from data received from the rocket. This feeds into the computer which has a memory of 4096 4-bit words and can perform 1750 arithmetical computations per second. Presently it reads data at a speed of 300 characters/sec but, according to its developers, a doubling of this speed is readily attainable.

Naturally, most geophysicists' minds are turned at this time toward the most ambitious scheme of IGY: satellite flights. Data from the satellites are received by radio and recorded on the 'Minitrack' system of the U.S. Naval Research Laboratory (HAGEN, 1956). Minitrack can receive six data items simultaneously. Part of these data are used to obtain the position of the satellite by radio-phase comparison methods. The various path element computations are performed by an IBM 704 electronic computer. One of the first geophysical applications of these data will be for geodetic purposes.

In problems involving *geodesy*, gravity and the figure of the earth, machine computations have already become well established. HEISKANEN (1956) mentions that distances between the reference ellipsoid and the geoid are being computed at the rate of 'some 1000 in a few months'. CHOVITZ and FISCHER (1956) have used the U.S. Army Map Service UNIVAC, involving the solution of simultaneous

equations, for a redetermination of the figure of the earth. Rapid calculation methods are also particularly useful for the solution of geodetic networks. The U.S. Coast and Geodetic Survey has successfully employed the IBM 604 calculator for the solution of surveys. In one survey in Alaska this required the solution of 3500 simultaneous equations with 100×100 matrix (WHITTEN, 1956, personal communication). Years of tedious hand computations and checking were once required to handle such data.

In *oceanography* more and more problems with involved computations or large data masses are also finding their way to the modern handling methods. At New York University (1955) an Electronic Associates differential analyzer was used to solve sets of equations to study ship motions as related to wave action. Data collected on wave motion from sea-bottom pressure gauges have been subjected to power spectrum analysis on the IBM 650 computer (MUNK, 1956, personal communication). The complicated differential equations which describe the dynamics of wind-driven currents in the oceans are prime examples of mathematical presentations amenable to handling by computers (NEUMANN, 1955). But, on the whole, oceanography is a field where large-scale data processing can yet make major contributions toward advances (PAQUETTE, 1957).

Hydrology, too, has as yet made only limited use of modern data handling techniques. One of the present ingenious applications in that field is the Flood Routing Machine. This is an analogue computer which handles a series of empirical correlations evolved separately for various river drainage basins. The relations established between rainfall, run-off, and river stages give the basis for input and programme of the computer.

Data in the field of *geomagnetism* are being placed on punched cards by the U.S. Coast and Geodetic Survey. On a current basis, hourly values from the Survey's magnetic observations for declination, horizontal and vertical intensities are being placed on the cards. The base-line corrections are applied and secular change adjustments for grid point intersections are interpolated by machine procedures (ROBERTS and KNAPP, 1956, personal communication).

Some problems in the theoretical approach to the question of the origin of the Earth's magnetic field have also been aided by computers (JACOBS, 1956). Approximate equations for the field produced by hypothetical convection currents were solved by the computers

FERUT (at the University of Toronto), and ACE (at the National Physical Laboratory in England).

Data processing in *seismology* is still largely manually performed. The evaluation of seismograms is primarily an art to discern onset of wave groups in the general motion depicted. It is especially a matter of judgment if the level of microseismic activity—the seismic noise—is high. Curve readers are not yet geared to the level of refinement necessary. It is also questionable whether the amount and type of work justifies automation in this case, when the discriminating human eye can quickly make the necessary decisions and record the results.

It is more likely that the time is becoming ripe for data storage and secondary processing on punched cards for eye-read seismograms (see also: LANDSBERG, 1949). The International Seismological Summary could probably be more readily produced from cards punched at seismograph stations and machine processed at a seismological centre. Each earthquake could be represented on a summary card for other calculations, such as those dealing with earthquake magnitudes, intensities, and energies. The methods given by GUTENBERG and RICHTER (1956) are all easily adapted to computer techniques. The same material could form the basis for seismicity calculations by the measures proposed by ST. AMAND (1956).

Turning to more theoretical work, PEKERIS (1956) states that the period of oscillation of a uniform gravitating sphere, with its mean rigidity, bulk modulus and density conforming to that of the earth, has been computed. He expressed hope that the solid tidal oscillation could be programmed for the electronic computer. His solutions of the pertinent integral equations should make it possible to compute the motion of the ground for specified types of explosions. A check on various layer thicknesses might be obtained by the solution of phase velocity equations which are coded for processing by the SEAC computer of the National Bureau of Standards (STONELEY, 1956). Some numerical solutions for a solid-fluid interface boundary wave have been obtained on the Elecom 120 digital computer by STRICK and GINZBARG (1956).

Considerable help has already been obtained from computers in the development of models of the *interior of the earth* by J. A. JACOBS (1956), who used FERUT, the electronic computer of the University of Toronto, to solve the equation of heat conduction for a radioactive earth. GUTENBERG (1956a) envisages also the inclusion

of heretofore neglected second-order terms in the theories of earth structure. Mass distribution, moments of inertia, rigidity as they affect the nutation could be readily included in an approach that numerically approximates reality better than heretofore.

Conclusions

There are in the various geophysical fields a great many routine and special calculations for which the modern automatic methods of data processing and computations are admirably suited. The following Table 1 lists the operations in which any bulk of data would justify the use of the new devices.

TABLE 1

Problems readily solved by automatic numerical procedures

Means, extremes, arrays (order statistics)
Frequency distributions, standard deviations, other moments
Contingency tables
Correlations, auto correlations (time-lag correlations)
Filtering and smoothing
Harmonic and power spectrum analysis
Vector resultants
Curve fitting, orthogonal polynomials
Calculation of maximum likelihood, least squares
Simultaneous equations, matrices (matrix inversions)
Differential equations
Numerical integrations

Entirely within our grasp are numerical solutions leading to an improved figure of the earth, a more realistic model of the earth's interior, better forecasts of atmospheric flow patterns. Seemingly random phenomena such as atmospheric turbulence and ocean wave motion can be searched for organization in the spectra by electronic data analysis. New insight can similarly be gained into cyclical and quasi-cyclical phenomena of the type represented by pole motions, seismic waves, and the tides of the solid earth, oceans, and atmosphere.

An immediate objective of development should remain the automatic transformation of the output of sensing and measuring devices to media useful as input into computers.

As an aid in future calculations a central library of basic computer programmes for geophysical problems should be established in order

to conserve effort. Although programmes devised for one computer are not immediately applicable to other types, many of the basic routines and steps can still be used as a guide for programming other or newer machines.

The potentials of various automatic data processing equipment for printing results should not be overlooked as devices for preparation of copy for prompt publication of information.

REFERENCES

Anonymous (1955a) Analogues and answers, *N.Y.U. Engng. Res. Rev.* **5** (5), 10.

—— (1955b) Fosdic to the rescue, *Weather Bureau Topics* **14** (2), 24.

—— (1956a) Fosdic, *Weather Bureau Topics* **15**, 175–177.

—— (1956b) Communication errors and JNWP, *Weather Bureau Topics* **15**, 222.

BATES, C. C. (1956) Marine meteorology at the U.S. Navy Hydrographic Office, *Bull. Amer. Met. Soc.* **37**, 519–527.

BELLAMY, J. C. (1952) Automatic processing of geophysical data, *Adv. in Geoph.* **1**, 1–43.

BIGELOW, J. and GILCHRIST, B. (1955) Data transmission for numerical weather prediction, *Bull. Amer. Met. Soc.* **36**, 417–418.

BLACKADAR, A. K. (1956) *Annual Report, NYU College of Engineering*, pp. 8–9.

BLACKBURN, J. F. and GATES, W. L. (1956) Note on hemispheric numerical integration of the barotropic model, *J. Met.* **13**, 59–63.

BROOKS, C. E. P. and CARRUTHERS, N. (1953) *Handbook of Statistical Methods in Meteorology*, Meteorological Office, London, M.O. 538, 412 pp.

CANNING, R. G. (1956) *Electronic Data Processing for Business and Industry*, Wiley and Sons, New York.

CHARNEY, J. G. (1949) On the physical basis for numerical prediction of large-scale motion in the atmosphere, *J. Met.* **6**, 371–385.

—— and ELIASSEN, A. (1949) A numerical method for predicting the perturbations of the middle latitude westerlies, *Tellus* **1**, 38–54.

—— FJÖRTOFT, R. and von NEUMANN, J. (1950) Numerical integration of the barotropic vorticity equation, *Tellus* **2**, 237–254.

—— GILCHRIST, B. and SHUMAN, F. G. (1956) The prediction of general quasi-geostrophic motions, *J. Met.* **13**, 489–499.

CHOVITZ, B. and FISCHER, I. (1956) A new determination of the figure of the Earth from arcs, *Trans. Amer. Geophys. Un.* **37**, 534–545.

CONRAD, V. and POLLAK, L. W. (1950) *Methods in Climatology*, 2nd ed., Harvard University Press, Cambridge, Mass. (See particularly Pt. II, Computing Devices, Periodography, 332–438.)

COOK RESEARCH LABORATORIES (1955) Study of the Usefulness of Unitary Differential Notation for storing and utilizing Meteorological Data, Scientific Report SR 62–1, Chicago.

COPELAND, J. A. (1953) *Climatology by machine methods for naval operations, plans, and research*, U.S. Weather Bureau, Washington.

COURT, A. (1952) Some new statistical techniques in geophysics, *Adv. in Geophys.* **1**, 45–85.

CRESSMAN, G. (1956) Personal communication.

CRUTCHER, H. L. (1956) On the Standard Vector-Deviation Wind Rose, Paper presented at 149th National Meeting Amer. Met. Soc., Asheville, N.C.; preprint, 16 pp.

DEWAR, D. (1949) The Hollerith card system applied to upper air data, *Met. Mag.* **78**, 163–166.

FRENKIEL, F. N. (1956a) Atmospheric pollution and zoning in an urban area, *Scientific Monthly* **82**, 194–203.

—— (1956b) Possibilities and Significance of high-speed computing in Meteorology, *Sci. Proc. Inst. Assoc. Met.*, Rome 1954, pp. 469–475. Butterworth, London.

FRIEDMAN, O. G. (1955) Specification of temperature and precipitation in terms of circulation patterns, *J. Met.* **12**, 428–435.

GREENOUGH, M. S. and BOSEN, J. F. (1956) FOSDIC—A new approach to storage and utilization of digital records. Presented 3 May 1956, at A.M.S. 144th National Meeting, *Bull. Amer. Met. Soc.* **37**, 183.

GUMBEL, E. J. (1954) Statistical Theory of Extreme Values and some Practical Applications, Nat. Bur. Standards, *Appl. Math. Series No.* 33, Washington, 51 pp.

GUTENBERG, B. (1956a) Structure of earth's interior, *J. Geophys. Res.* **61**, 379.

—— (1956b) Uses of International Geophysical Year World-Wide Data in the Solution of Geophysical Problems (Abstr.), *J. Geophys. Res.* **61**, 410–411.

—— and RICHTER, C. F. (1956) Earthquake Magnitude, Energy, and Acceleration (second paper), *Bull. Seism. Soc. Amer.* **46**, 105–145.

HAGEN, J. P. (1956) PROJECT VANGUARD, Paper presented at 12th Annual National Electronics Conference and Exhibition, Chicago, October 1956 (Quoted from news sources).

HALL, F. and HOLLOWAY, L. (1956) Reduction of error in weather communication systems, U.S. Weather Bureau manuscript, 27 pp.

HENRY, T. J. G. (1956) Numerical forecasting on FERUT, *Weather* **11**, 393.

HEUMANN, K. F. (1956) Data processing for scientists, *Science* **124**, 773–777.

HOLLOWAY, L. (1956) Smoothing and filtering of time series and space fields, *Advanc. Geophys.* **4** (in print).

HOWCROFT, J. G. and SMITH, J. R. (1956) A selective analysis of the scale of atmospheric turbulence, *J. Met.* **13**, 75–81.

IBM (1956) Automatic Production Recording Systems, IBM Form No. 33–7083–0 (10-8-56).

IBM, ABCD of IBM Electronic Data Processing, Form No. 32–6757 IBM Co.

JACOBS, J. A. (1956) The interior of the Earth, *Advanc. Geophys.* **3**, 183, 239.

LALLY, V. E., MCINNIS, D. H. and MYERS, R. F. (1956) The transmission of analyzed weather charts. Paper presented at Amer. Met. Soc. Washington Meeting May 1956 (preprint).

LANDSBERG, H. E. (1949) Discussion sur l'I.S.S., *C. R. Séances de la 8ime Conference*, Ass. Séismol. Oslo 17–28 août 1948, p. 33 (Strasbourg).

—— (1952) Discussion Remarks, Meteorology Panel, Air Pollution (*Proc. U.S. Tech. Conf. on Air Pollut.* 1951), pp. 831–833. McGraw-Hill, New York.

LONDON, J. (1950) Study of the Atmospheric Heat Balance, Progress Reports 131.02, 131.03, Contract AF 19(122)–165, N.Y.U. Coll. of Eng.

LORENZ, E. N. (1956) Empirical orthogonal functions and statistical weather prediction, *Bull. Amer. Met. Soc.* **37**, 382–383 (Abstract).

MALONE, T. F. (1956) The role of probability in the communication of weather information, *Bull. Amer. Met. Soc.* **37**, 180 (Abstract).

MUNK, W. (1956) Personal communication, November 1956.

NAMIAS, J. (1955) On the possibility of long range weather forecasting by high-speed computing methods. Remarks presented before the NSF-U. of Cal. Los Angeles Conference on the Significance and the Possibilities of high-speed computing in Meteorology and Oceanography May 13–15, 1955, Abstr. *Met. Abstr. and Bibl.* **7**, 1956, 1076–1077.

NEUMANN, G. (1955) On the Dynamics of Wind-Driven Ocean Currents, Meteorol. Papers, N.Y.U. College of Engineering **2** (4).

NEUMANN, J. von (1955) Can we survive technology? *Fortune* (June), p. 106.

NEWELL, Jr., H. E. (1953) Recovery of Data, *High Altitude Rocket Research*, Chapter III, Academic Press, New York.

NORDQUIST, J. M. (1945) Theory of largest values applied to earthquake magnitudes, *Trans. Amer. Geophys. Un.* **26**, 29–31.

PAQUETTE, R. G. (1957) *Conference on rapid data-handling in Oceanography*, University of Washington, Dept. of Oceanography Tech. Rep. No. 52 (Contract Nonr-477(01) Project NR 083–138, 45 pp.).

PEKERIS, C. L. (1956) Research on the oscillations of the earth and theoretical seismology, *J. Geophys. Res.* **61**, 406–408.

PHILLIPS, N. A. (1956) The general circulation of the atmosphere: a numerical experiment, *Quart. J. R. Met. Soc.* **82**, 123–164.

REICHELDERFER, F. W. (1954) What progress in weather forecasting, *Amer. Petrol. Inst., Refining Sess.* **34**, (I), 52–55.

RICHARDSON, L. F. (1922) *Weather Prediction by Numerical Process*, Cambridge University Press, 236 pp.

ST. AMAND, P. (1956) Two Proposed Measures of Seismicity, *Bull. Seism. Soc. Amer.* **46**, 41–45.

SCHUREMAN, P. (1942) *Manual of Harmonic Analysis and Prediction of Tides*, U.S. Cost & Geodetic Survey Special Publ. 98 (revised) Washington (pp. 126ff.).

STAFF MEMBERS, Institute of Meteorology, University of Stockholm (1954), Results of forecasting with the barotropic model on an electronic computer (Besk) *Tellus* **6**, 139–149.

STONELEY, R. (1956) Surface elastic waves, *J. Geophys. Res.* **61**, 408–409.

STRICK, E. and GINZBARG, A. S. (1956) Stoneley-wave velocities for a fluid-solid interface, *Bull. Seism. Soc. Amer.* **46**, 281–292.

THOM, H. C. S. (1954) Frequency of maximum wind speed, *Proc. Amer. Soc. Civ. Eng.* **80** (Separate No. 53a).

THOMPSON, P. D. and GATES, W. L. (1956) A test of numerical prediction methods based on the barotropic and two-parameter baroclinic model, *J. Met.* **13**, 127–141.

U.S. AIR RESEARCH AND DEVELOPMENT COMMAND (1956) 'Flac' (Florida Automatic Computer), News Release.

(U.S. DEPT. OF COMMERCE WEATHER BUREAU (1955)) *Meteorology and Atomic Energy*, U.S. Atomic Energy Commission, Washington.

WEXLER, H. (1956) *Electronic Computer Applied to Weather Prediction and General Circulation of the Atmosphere*, Unpublished note.

WHITE, R. M. (1956) Pressure height predictability as function of the type and amount of initial data, *J. Met.* **13**, 40–45.

17

GEOMAGNETIC DRIFT AND THE ROTATION OF THE EARTH*

WALTER ELSASSER and WALTER MUNK

THE displacement of the pole of rotation due to motion in the core is negligible.

Introduction

Irregular changes in the rate of rotation of the Earth are known rather precisely since 1890 (JEFFREYS, 1954; BROUWER, 1952). These are superimposed upon a 'secular' decrease in angular velocity usually attributed to tidal friction. The irregular changes might be described as a series of mildly discontinuous changes which persist in each case for an interval of, say, five to fifteen years. To give an idea of the numerical magnitude, let us say that a cumulative gain or loss of time, $\Delta t = 10$ sec, occurring during an interval $T = 10$ years is a rather large change of this type, close to the upper limit of the observed variations. If we assume a uniform angular acceleration $\dot{\omega}$ to act during time T, producing a shift in azimuth $\Delta\phi$, a simple kinematical relation gives (JEFFREYS, 1954)

$$\Delta t = \Delta\phi/\omega = \dot{\omega}T/2\omega^2 \tag{1}$$

and on substituting the above numbers,

$$\dot{\omega} = 1.5 \times 10^{-20}\ \text{sec}^{-2} \tag{2}$$

One need therefore explain variations of the order given by (2).

There appears to be no mechanism having to do with the atmosphere, the ocean, glaciation, or movements of parts of the solid

* Contribution from the Scripps Institution of Oceanography New Series No. 964. The work by MUNK was performed at Cambridge University with the assistance of a Guggenheim Fellowship.

crust that would give effects anywhere near the observed ones (MUNK and REVELLE, 1952). We should perhaps emphasize that the slowing-down process by tidal friction itself cannot be made responsible for the observed variations. The variation of tidal friction from year to year must be extremely small, not in excess of, say 0.1% of the total effect, whereas the observed irregular variations amount to an appreciable fraction of the average rate of slowing down.

In view of this situation it was proposed that a variable magnetic coupling between the earth's mantle and the fluid core might account for the observed irregularities. VESTINE (1953) showed that the so-called westward drift of the geomagnetic secular variation (ELSASSER, 1950; BULLARD, 1950) exhibits an irregular peak during the period where it is well enough known ($\sim$ 1890–1945) and that this irregularity corresponds in shape to the one observed by BROUWER (1952) in the earth's rate of rotation. It has, moreover, the correct sign, exactly what is to be expected if a magnetic torque is interposed between the mantle and core. The evidence consists essentially of a sixty-year pulse starting about 1880 which reduced the westward drift to a very low value in 1910. Of course the inverse-matching of a single pulse is an expedient of desperation (even if it happens only once in fifty years).

ELSASSER and TAKEUCHI (1955; 1954) developed the quantitative theory in terms of the hydromagnetic equations applied to the boundary layer of the core. They were able to show that fluctuations of several gauss of the geomagnetic field at the boundary are of the right order of magnitude to explain the observed variations in the rate of rotation. Furthermore, the time-scale of these changes is of the same general order as that of the geomagnetic secular variation (the main components of the frequency spectrum indicating periods of some decades) and this makes the explanation rather plausible, since significant geophysical phenomena of this time-scale are rare indeed.

Position of the pole

The present note is devoted to a closely allied subject, namely, the question whether changes in the direction of the Earth's axis of rotation relative to the crust (changes in pole position) can be explained by a similar mechanism of variable coupling with the core. If the motion in the core were only zonal (along latitude circles)

then only changes in the rate of rotation would result; if it were purely meridional then the position of the pole would be altered. The drift of the eccentric dipole, as an indicator of motion in the core, indicates that the two components are roughly equal (VESTINE, 1953). There have been three estimates of the polar displacement associated with the meridional component of this 60-year pulse:

VESTINE (1953)	5 ft
ELSASSER and TAKEUCHI (1955)	0.002 cm
MUNK and REVELLE (1952)*	several hundred feet.

The astronomic evidence is that the position of the pole has not moved by more than 15 ft in the interval between 1900 and 1940. There is some indication of a movement by 10 ft towards Greenland between 1900 and 1925 (WANACH, 1927).

These wide discrepancies call for a discussion. It is simplest to give an independent derivation, but a few words concerning the quoted papers may be helpful. In VESTINE'S equation (ELSASSER and TAKEUCHI, 1955) the gyroscopic terms arising from the motion of the core relative to the mantle have been neglected as compared to those arising from time rate of changes of the core's relative angular momentum. The reverse situation appears to be the correct one. This requires that VESTINE'S (1953) solution should be multiplied by $A/(C - A) = 305$, where A,A,C are the moments of inertia of the Earth.

ELSASSER and TAKEUCHI (1955) state that the torque as written in their Eq. (20) refers to axes fixed in space, but in fact they refer to the rotating axes. It happens that this also introduces a factor $A/(C - A)$. They have slipped by a factor 10 at the end of their paper (ELSASSER and TAKEUCHI write $\phi = 3 \times 10^{-12}$ instead of 3×10^{-13}). The modified results are: VESTINE, 1500 ft; ELSASSER and TAKEUCHI, 0.06 cm. The answers are now further apart than they were to start with.

The remaining difference is based on a fundamental difference in the approach taken by ELSASSER and TAKEUCHI (1955) on the one

* 'Under the questionable assumption that the inner and outer core have a *common* axis of rotation so inclined as to account for VESTINE'S observations, we find the computed displacements of the pole of rotation to be an order of magnitude larger than observations of latitude would permit.'

hand, and by VESTINE (1953), MUNK and REVELLE (1952) on the other. ELSASSER and TAKEUCHI base their considerations on the electromagnetic coupling between core and mantle. They have shown that 10^{25} dyne/cm is an upper limit for the electromagnetic torque between the core and the mantle. This requires a torroidal leakage field of 0.1 gauss in the mantle near the boundary. The total torroidal field may amount to a few gauss, but only a fraction is available for variable torques. This torque is barely sufficient to account for the observed change in rate of rotation in terms of electromagnetic coupling to a core, but it is too small by a factor 10^5 to balance the gyroscopic effects arising from a core rotating slowly relative to the mantle about an axis not coincident with that of the mantle. The conclusion is twofold: (1) the meridional component of the magnetic dipole drift is either not real, or not an indication of the movement of the core (except possibly for a thin surface film); and (2) any effect of motion in the core on the position of the pole is negligible. On the other hand, VESTINE (1953), MUNK and REVELLE (1952) computed the displacement of the pole based on the indicated motion of the core simply by assuming conservation of angular momentum of core plus mantle, but without inquiring whether the torque required is available.

One might still ask whether such excursions of the pole, however small, could not be cumulative and hence give rise to pole migration over times of geological length. We may readily show that pole migration is not to be ascribed to such an effect. One should understand that we are not ruling out the possibility of polar wandering, but are here dealing exclusively with the possible effect of the dynamics of the *core* upon the solid mantle and crust. The analysis given here is somewhat broader than would ordinarily seem justified by a purely negative final result; this is owing to the fact that the dynamics of a deformable top has quite recently moved into the focus of geophysical interest, on account of the evidence for pole migration that has been gathered from paleomagnetic data (ELSASSER, 1956).

The Euler equations of a rigid mantle

Since the moment of inertia of the core is only about a tenth of that of the mantle, a method of approach that suggests itself at once is to treat the mantle as a rigid top subject to an imposed variable

torque which represents the coupling with the core. Let A be the moment of inertia of the mantle about any axis in the equatorial plane, C the moment of inertia about the polar axis, and $D = C - A$. We shall treat D/C as a small quantity. Next, let ω_1, ω_2, ω_3 be the angular velocities relative to a system of axes fixed in the body. The Euler equations for such a symmetrical top are

$$\begin{aligned} A\dot{\omega}_1 + D\omega_2\omega_3 &= L \\ A\dot{\omega}_2 - D\omega_1\omega_3 &= M \\ C\dot{\omega}_3 = N & \end{aligned} \tag{3}$$

It should be noted that the components L, M, N of the external torque must also be referred to a system of axes fixed in the top. Clearly, the third equation (3) accounts for the variations in the lengths of the day; using the value (2) for the acceleration we can calculate the variable torque about the axis. To solve the first two equations, we set $\omega_3 = \omega_1$, the undisturbed uniform angular velocity. We then have, in complex notation,

$$A\frac{d}{dt}(\omega_1 + i\omega_2) - iD\omega(\omega_1 + i\omega_2) = L + iM \tag{4}$$

The stationary solution of (4) for a constant torque is

$$\omega_1 + i\omega_2 = i(L + iM)/D\omega$$

If we set

$$| L + iM | = \gamma N = \gamma C\dot{\omega}$$

where γ is some numerical factor, we find

$$| \omega_1 + i\omega_2 | = \frac{\gamma C\dot{\omega}}{D\omega}.$$

The magnitude of the displacement measured at the surface of the earth is

$$d = \frac{R\gamma C\dot{\omega}}{D\omega^2} \tag{5}$$

where R is the radius of the earth. Using (2) and, let us say $\gamma = 0.1$, we obtain $d = 0.055$ cm, small indeed. The smallness of the effect is of course due to the gyroscopic forces. On a non-rotating earth a fixed torque would not produce a fixed displacement, as here, but a steady migration of the pole of a magnitude that could be detected by measurements of latitude.

Next, consider a transient torque. A case that is readily integrated is that of a torque rotating relative to the earth, say

$$L + iM = \gamma N \exp(i\eta t).$$

Substituting this into (4) we find the stationary solution in which the pole migrates in a circle, with

$$|\omega_1 + \omega_2| = \left| \frac{\omega d}{A\eta - D\omega} \right|. \tag{6}$$

We shall not be concerned here with the resonance that occurs when the torque rotates with a period of about 300 days (400 days for an elastic earth), in which case (6) would clearly be invalid. For longer periods, that is smaller values of η, the radius of migration is approximately d; so nothing untoward happens, and the pole is again limited to small excursions.

One might ask whether significant displacements of the pole could occur over periods of geological length by way of a random walk of the pole. It may readily be seen that the mechanism just considered is inadequate for this. Assuming a possible velocity of the pole of 10^{-2} cm/year, we get only 100 km in 10^9 years, but this would correspond to a straight-line displacement for which there is no physical mechanism so far as a variable coupling with the core is concerned. The effects of a succession of random displacements should therefore be altogether negligible.

A rigid mantle with fluid core

We have derived the essential physical result, that the excursions of the pole based on variable coupling with the core are negligible, using the very simple approximation of a rigid mantle where the effect of the core is expressed in terms of an external torque on the mantle. Undoubtedly, the true problem of changes in pole position involves the dynamics of a deformable top. A relatively simple model

is that of a rigid mantle enclosing a liquid core, and we wish to use this occasion to point to some known mathematical developments in the classical literature that are pertinent to this question.

LIOUVILLE (ROUTH, 1905) has considered the problem of a top whose parts may move relative to each other. We shall here confine ourselves to the case where these relative motions are small. To fix our ideas, consider first a system of co-ordinates, $S_o(x_o y_o z_o)$ where the z_o-axis is fixed in space along the invariable axis of the earth's rotation, and the other two axes rotate uniformly about it. The angular velocity vector of this motion, if projected upon the axes of S_o itself, has components O, O, ω. The angular momentum vector of the earth has components O, O, h in S_o. Next, consider a co-ordinate system $S(x,y,z)$ which rotates in an arbitrary, time-dependent fashion. We shall, however, assume that the angular velocity vector describing the motion of S remains always close to the fixed vector describing the motion of S_o. The instantaneous angular velocity of S may be described by the components of the angular velocity vector along the axes of S itself; let these be ω_x, ω_y, $\omega + \omega_z$, where by assumption $\omega_x \omega_y \omega_z$ are small quantities. Again, let the angular momentum vector of the earth if resolved along the instantaneous axes of S have the components h_x, h_y, $h + h_z$. The system S is still quite arbitrary and we can simplify the equations of motion by a proper choice of it. It is advantageous to choose S so that its axes are fixed in the mantle, the z-axis being along the axis of rotational symmetry of the mantle. This makes the moments of inertia, A and C, constants of the motion. With these assumptions, the equations of motion can be transformed into the following form, correct to within first-order terms in the small quantities,

$$\begin{aligned} A\dot{\omega}_x + D\omega\omega_y &= \omega h_y - \dot{h}_y + L \\ A\dot{\omega}_y - D\omega\omega_x &= \omega h_x + \dot{h}_y + M \\ C\dot{\omega}_z &= -\dot{h}_z + N \end{aligned} \tag{7}$$

If we apply these equations to the rigid mantle alone, then h_x, h_y and their time derivatives vanish, and we return to the Euler equations (3). Again, consider the system mantle plus core. The external torques may then be equated to zero; instead, the reaction

of the moving core upon the system is expressed in terms of the angular momentum components h_x, etc., which a circulation in the core appears to possess for an observer fixed in the mantle. Now $\dot{h}_x \sim \omega' h_x$ where $2\pi/\omega'$ designates the time during which h_x changes appreciably. If this time is of the order of years or more, then h_x and h_y in the first two Eqs. (7) are clearly negligible. We thus arrive at a system of equations that is formally completely analogous to (3) except that the external torques acting on the mantle are now replaced by the perturbation terms ωh_y, ωh_x, $-\dot{h}_z$. But now A and C are the moments of inertia of the system mantle plus core, no longer of the mantle alone. Thus we have a more rigorous verification of our previous solution.

To conclude this brief note we should draw attention to a classical investigation by POINCARÉ, since it is so closely related to the problem discussed here. A fairly comprehensive account of this work may be found in LAMB (1932). POINCARÉ considers an ideal incompressible liquid enclosed in a rigid envelope, the whole rotating uniformly about an axis. The question is what internal motions are set up in the fluid if now the envelope is slowly tilted about an axis normal to the axis of rotation. This corresponds to the concrete astronomical case where the earth's mantle is subjected to the precession of the equinoxes. It is clear that in the case of a spherical vessel an inviscid fluid would not follow any forced motion of the envelope. But this is no longer the case for an elliptical envelope. POINCARÉ shows that there is a critical parameter

$$\omega_c = \omega\epsilon \tag{8}$$

where ϵ is the numerical eccentricity of the envelope. For motions whose frequencies are slow compared to ω_c there is no inertial reaction of the fluid to components of rotation normal to the original axis: the fluid follows the motion of the envelope as if solidified. Since, approximately, $\epsilon = D/C$ we see that (8) gives the same critical period of about 300 days that we found in connection with (6). Perhaps POINCARÉ'S problem would be more closely related to a specialization of (7) where the rigid envelope has negligible moment of inertia and A and C are entirely due to the fluid. By virtue of the principle of reciprocity we might try to invert POINCARÉ'S result and conclude that sufficiently slow internal fluid motions will not lead

to a tilt of the rigid envelope relative to the invariable axis of rotation in space. While the two problems considered are patently related, they are not on the face of it identical, since in the one case we introduce explicitly only a difference in the polar and equatorial moments of inertia, in the other an ellipticity of the fluid boundary. Again, however, such an ellipticity leads automatically to a difference in moments of inertia, and so the problem of POINCARÉ is the more general, and the one treated here would probably on closer analysis turn out to be a special case of it.

REFERENCES

BROUWER, D. (1952) *Proc. Nat. Acad. Sci., Wash.* **38**, 1.

BULLARD, *et al.* (1950) The westward drift of the Earth's magnetic field, *Phil. Trans.* **243**, 67.

ELSASSER, W. M. (1950) *Rev. Mod. Phys.* **22**, 1.

—— (1956) *Amer. J. Phys.* **24**, 85.

——and TAKEUCHI, H. (1955) *Trans. Amer. Geophys. Un.* **36**, 584.

JEFFREYS, H. (1954) *The Earth*, 3rd ed. Cambridge University Press.

LAMB, H. (1932) *Hydrodynamics*, 6th ed. Sec. 384. Cambridge University Press.

MUNK, W. and REVELLE, R. (1952) *Mon. Not. Roy. Astr. Soc., Geophys. Suppl.* **6**, 331.

ROUTH, E. J. (1905) *Advanced Dynamics of Rigid Bodies*, 6th ed., Sec. 22. Macmillan.

TAKEUCHI, H. and ELSASSER, W. M. (1954) *J. Phys. Earth* **2**, 39.

VESTINE, E. H. (1953) *J. Geophys. Res.* **58**, 127.

WANACH, B. (1927) Eine fortschreitende Lagenänderung der Erdachse, *Z. Geophys.* **3**, 102–105.

INDEX